

NASA/CR-2011-216880



Damage Arresting Composites for Shaped Vehicles—Phase II Final Report

*Alex Velicki, Nicolette Yovanof, Jaime Baraja, Kim Linton, Victor Li, Authur Hawley,
Patrick Thrash, Steve DeCoux, and Robert Pickell
The Boeing Company, Phantom Works, Huntington Beach, California*

January 2011

NASA STI Program . . . in Profile

Since its founding, NASA has been dedicated to the advancement of aeronautics and space science. The NASA scientific and technical information (STI) program plays a key part in helping NASA maintain this important role.

The NASA STI program operates under the auspices of the Agency Chief Information Officer. It collects, organizes, provides for archiving, and disseminates NASA's STI. The NASA STI program provides access to the NASA Aeronautics and Space Database and its public interface, the NASA Technical Report Server, thus providing one of the largest collections of aeronautical and space science STI in the world. Results are published in both non-NASA channels and by NASA in the NASA STI Report Series, which includes the following report types:

- **TECHNICAL PUBLICATION.** Reports of completed research or a major significant phase of research that present the results of NASA programs and include extensive data or theoretical analysis. Includes compilations of significant scientific and technical data and information deemed to be of continuing reference value. NASA counterpart of peer-reviewed formal professional papers, but having less stringent limitations on manuscript length and extent of graphic presentations.
- **TECHNICAL MEMORANDUM.** Scientific and technical findings that are preliminary or of specialized interest, e.g., quick release reports, working papers, and bibliographies that contain minimal annotation. Does not contain extensive analysis.
- **CONTRACTOR REPORT.** Scientific and technical findings by NASA-sponsored contractors and grantees.
- **CONFERENCE PUBLICATION.** Collected papers from scientific and technical conferences, symposia, seminars, or other meetings sponsored or co-sponsored by NASA.
- **SPECIAL PUBLICATION.** Scientific, technical, or historical information from NASA programs, projects, and missions, often concerned with subjects having substantial public interest.
- **TECHNICAL TRANSLATION.** English-language translations of foreign scientific and technical material pertinent to NASA's mission.

Specialized services also include creating custom thesauri, building customized databases, and organizing and publishing research results.

For more information about the NASA STI program, see the following:

- Access the NASA STI program home page at <http://www.sti.nasa.gov>
- E-mail your question via the Internet to help@sti.nasa.gov
- Fax your question to the NASA STI Help Desk at 443-757-5803
- Phone the NASA STI Help Desk at 443-757-5802
- Write to:
NASA STI Help Desk
NASA Center for AeroSpace Information
7115 Standard Drive
Hanover, MD 21076-1320

NASA/CR-2011-216880



Damage Arresting Composites for Shaped Vehicles—Phase II Final Report

*Alex Velicki, Nicolette Yovanof, Jaime Baraja, Kim Linton, Victor Li, Authur Hawley,
Patrick Thrash, Steve DeCoux, and Robert Pickell
The Boeing Company, Phantom Works, Huntington Beach, California*

National Aeronautics and
Space Administration

Langley Research Center
Hampton, Virginia 23681-2199

Prepared for Langley Research Center
under Contract NNL07AA48C

January 2011

The use of trademarks or names of manufacturers in this report is for accurate reporting and does not constitute an official endorsement, either expressed or implied, of such products or manufacturers by the National Aeronautics and Space Administration.

Available from:

NASA Center for AeroSpace Information
7115 Standard Drive
Hanover, MD 21076-1320
443-757-5802

FOREWORD

This document summarizes the work performed by Boeing Research & Technology, Huntington Beach, California under the NASA Subsonic Fixed Wing Project – Materials and Structures for Wing Components and Non-Circular Fuselage Phase II contract, entitled *Damage Arresting Composites for Shaped Vehicles*. It documents the development work that was performed to support the vehicle-level trade studies and structural testing during the two-year Phase II time span.

The NASA technical monitor was Dawn Jegley of the Mechanics and Durability Branch, Langley Research Center.

This document was written by the following Boeing personnel:

Mr. Alex Velicki	Principal Investigator
Ms. Nicolette Yovanof	Program Manager
Mr. Jaime Baraja	Design Engineering
Mr. Kim Linton	Design Engineering
Mr. Victor Li	Structural Analysis
Mr. Arthur Hawley	Structural Analysis
Mr. Patrick Thrash	Manufacturing Engineering
Mr. Steve DeCoux	Manufacturing Engineering
Mr. Robert Pickell	Manufacturing Engineering

Acknowledgment is also made to the following individuals for their technical contributions to the reporting: Mr. Robert Turley, and Mr. Gary Ferrel of The Boeing Company; Mr. Craig Collier and Mr. Phil Yarrington of Collier Research Corporation for their contribution to the HyperSizer development descriptions; ASC Process Systems, Harbor Patterns Inc. and Process Fab Inc. for their contribution to the specimen tooling and test support structure hardware fabrication; as well as NASA-LaRC researchers, Ms. Dawn Jegley, Mr. Marshall Rouse, and Mr. Andrew Lovejoy for not only conducting the pressure and compression testing, but also for helping document the results of those experiments in this report.

TABLE OF CONTENTS

Introduction.....	1
1.0 Structural Concept Development.....	3
1.1 Design Approach	3
1.2 BWB Configuration Baseline	6
1.3 Test Specimen Sizing Loads.....	7
2.0 Internal Pressure Box (WBS 3.5.1).....	8
2.1 Design	8
2.2 Analysis	16
2.3 Tool Design.....	21
2.4 Panel Fabrication	28
2.5 Pressure Restraint Fixture	39
2.6 Specimen Preparation	45
2.7 Testing.....	53
3.0 Chordwise Tension Panel (WBS 3.5.2)	60
3.1 Design	60
3.2 Analysis	63
3.3 Panel Fabrication	82
3.4 Specimen Preparation	83
3.5 Testing.....	86
4.0 Spanwise Compression Panel (WBS 3.5.3)	97
4.1 Design	97
4.2 Analysis	99
4.3 Panel Fabrication	106
4.4 Specimen Preparation	107
4.5 Testing.....	109
5.0 Panel Sizing Enhancements	120
5.1 Code Change Guidelines.....	120
5.2 PRSEUS Interface Development	121
5.3 Sizing Code Improvements.....	122
5.4 User Documentation	122
5.5 Validation/Checkout	129
6.0 Vehicle Sizing Updates.....	135
6.1 Update BWB FEM.....	135
6.2 Incorporate New HyperSizer	136
6.3 FEM-based Structural Sizing.....	138
6.4 Updated Weights Statement.....	151
6.5 Test Loads.....	152
7.0 Phase II - Metrics and Conclusions	155
7.1 Metrics	155

7.2	Conclusion	157
	References.....	158
	Appendix A – Pressure Box Test Panel	159
	Appendix B – Chordwise Tension Panel	160
	Appendix C – Spanwise Compression Panel.....	176
	Appendix D - HyperSizer User Instructions.....	177
	D.1 Creating the Workspace	180
	D.2 Assigning Sizing Variables.....	180
	D.3 HyperLaminate for Stringer Web and Flange Material/Thickness.....	184
	D.4 HyperLaminate for Frame Web and Flange Material/Thickness	186
	D.5 Mechanical Loads and Panel Dimensions	188
	D.6 Active Failure Modes.....	189
	D.7 Review the Analysis Results.....	190
	D.8 Generate a Local FEM using HyperFEMGen	192
	D.9 Post Buckling Behavior	193

LIST OF FIGURES

Figure 1. Key Elements of Phase II Plan	1
Figure 2. Phase II WBS and Schedule	2
Figure 3. Pressure Cabin Running Loads	3
Figure 4. Pultruded Rod Stitched Efficient Unitized Structure (PRSEUS)	4
Figure 5. Stitched Dry Fabric Used to Create Self-Supporting Preform	5
Figure 6. Resin Infusion and Cured Panel	5
Figure 7. Cured Flat Panel Geometry	5
Figure 8. BWB Baseline for Study	6
Figure 9. Typical Pressure Cabin Cross-Section	6
Figure 10. BWB Baseline Finite Element Model	7
Figure 11. Untrimmed Pressure Panel Preform Geometry	8
Figure 12. Pressure Panel Test Specimen with External Doubler	8
Figure 13. Preliminary Pressure Test Fixture Design from ASC	9
Figure 14. Pressure Box Design Evolution	10
Figure 15. Initial Test Panel Configuration with Stub Frames	10
Figure 16. External Aluminum Skin Doubler	11
Figure 17. Proposed Stringer End Connection	11
Figure 18. External Stringer End Fittings	12
Figure 19. Frame End Fitting	12
Figure 20. Pin-Ended Panel Edge Concept	13
Figure 21. Inflatable Sealing Bag Concept	13
Figure 22. Free Edge Seal Concept	14
Figure 23. Comparison of Stringer Displacements	14
Figure 24. Comparison of Frame Displacements	15
Figure 25. Panel FEM (View from IML)	16
Figure 26. Panel FEM (View from OML)	17
Figure 27. Test Fixture FEM	17
Figure 28. Panel Deflections	18
Figure 29. Principal Strain for Skin under 2P Pressure	18
Figure 30. Principal Strains for Stringers	19
Figure 31. Principal Strains for Frame Wraps	19
Figure 32. Minimum Principal Strain for PRSEUS Rods	20
Figure 33. Von Mises Stress for Aluminum Doubler	20
Figure 34. Typical Fastener Loads under 2P Pressure	21
Figure 35. Conventional Stitching Tool Design	22
Figure 36. Modular Tooling Design Approach	23
Figure 37. Frame Height Adjustment Scheme	23
Figure 38. Modular Prototyping Tool	24
Figure 39. Single Preform Stitching	24
Figure 40. Modified Intersection Block Geometry	25
Figure 41. Stitch Tool Design Model	26
Figure 42. Block Rigging on Completed Stitch Tool	26
Figure 43. Cure Tool Design Model	27
Figure 44. Completed Cure Tool	27

Figure 45. Nested And Cut Flat Patterns for Stringers	28
Figure 46. Stiffener Preform Fabrication.....	29
Figure 47. Stitched Stiffener Preforms With Leader Wire Installed	30
Figure 48. Frame Preform Assembly Sequence	30
Figure 49. Frame and Stiffener Installation into Preform Assembly Fixture	31
Figure 50. Pulling of Rods into Stiffener Preform.....	31
Figure 51. Stiffener Fillet Installation.....	32
Figure 52. Skin Doubler Installation Complete	32
Figure 53. Skin Installation Complete	33
Figure 54. Robotic Stitching of Dry Fiber Preform Assembly.....	34
Figure 55. Lifting of AJ and Preform Using Overhead Crane.....	35
Figure 56. AJ Mated to Mold Tool During Preform Transfer	35
Figure 57. Preform Deposited on Mold Tool After Transfer.....	36
Figure 58. Soft Tooling (Bagging Aids) Installation Over Stiffeners	37
Figure 59. Vacuum Bag Installation Over Dry Fiber Preform	37
Figure 60. Resin Infused Net Molded Panel.....	38
Figure 61. "As Molded" IML Features of PRSEUS Panel	38
Figure 62. Pressure Restraint Fixture During Fabrication	39
Figure 63. Pressure Restraint Fixture as Delivered	40
Figure 64. Fixture Manhole Opening.....	40
Figure 65. Compressible Seal on Fixture Flange.....	41
Figure 66. Wire Harness Provisions	41
Figure 67. Wire Harness Provisions Bench Test	42
Figure 68. Panel Specimen on Pressure Restraint Fixture.....	43
Figure 69. Panel Drilling Using 90-Deg Drill	43
Figure 70. Panel Drilling Using Standard Gun Drill	44
Figure 71. Pressure Restraint Fixture.....	44
Figure 72. As-Fabricated Pressure Panel	45
Figure 73. Trimmed Pressure Panel.....	45
Figure 74. Close-Up of Trimmed Stringer.....	46
Figure 75. Panel Mated to the Pressure Vessel.....	46
Figure 76. Panel Pressure Vessel with Doublers in Place	47
Figure 77. Pilot Holes in Doublers Transferred to Panel.....	48
Figure 78. Completion of Pilot Holes Drilled Through Panel	49
Figure 79. Close-up of Pilot Holes in Doublers.....	49
Figure 80. Panel is Prepared for Cleaning	50
Figure 81. Panel Being Grit-Blasted.....	50
Figure 82. Adhesive Applied to Panel	51
Figure 83. Adhesive Applied to Panel	51
Figure 84. Panel is Mounted to the Drilling Fixture.....	52
Figure 85. Full-Sized Holes Drilled.....	52
Figure 86. Fasteners Installed with Sealant	53
Figure 87. Fastener Installation Complete.....	53
Figure 88. Pressure Panel Test Specimen Assembly	54
Figure 89. Pressure Panel Intended Impact Location (OML Side)	55
Figure 90. Strain at Middle Stringer and Impacted Stringer Show Similar Ranges	56

Figure 91. Actual Impact Locations.....	56
Figure 92. Pressure Panel in COLTS Facility for Testing.....	57
Figure 93. Pressure Panel After 2P Test.....	58
Figure 94. Localized Failure at Impacted Region After 3P.....	58
Figure 95. Damage Arresting by Stitching on Stringer Web.....	59
Figure 96. Displacement Comparison Between FEM and Test VIC Data.....	59
Figure 97. Part 25.571 Damage Tolerance Requirements.....	60
Figure 98. Critical Interfaces are Stitched to Arrest Damage.....	61
Figure 99. Panel Assembly Damage Arrest Sequence Failure.....	62
Figure 100. Finite Element Model.....	63
Figure 101. Phase II Panel (left) and AFRL Panel (right) (Ref. 2).....	64
Figure 102. Damage Progression Comparison.....	64
Figure 103. Panel Response - Damage Initiation – Displacement (in).....	66
Figure 104. Panel Response - Damage Initiation – Principal Strain for Skin.....	67
Figure 105. Panel Response - Crack Growth to Point B – Displacement (in).....	68
Figure 106. Panel Response - Crack Growth to Point B – Principal Strain for Skin.....	69
Figure 107. Panel Response - Fractured to Point B – Principal Strain for Stringers.....	70
Figure 108. Panel Response - Fractured to Point B – Principal Strain for Rods.....	71
Figure 109. Panel Response - Ultimate Panel Failure – Displacement (in).....	72
Figure 110. Panel Response - Ultimate Panel Failure – Principal Strain for Skin.....	73
Figure 111. Panel Response - Ultimate Panel Failure – Principal Strain for Stringers.....	74
Figure 112. Load –Deflection Curve.....	75
Figure 113. Failure Index for Skin Mid-Ply – Crack Growth Initiated.....	76
Figure 114. Failure Index for Skin Mid-Ply – Crack Reached Stringer Flanges.....	77
Figure 115. Failure Index for Skin Mid-Ply – Crack Arrested and Turned.....	78
Figure 116. Failure Index for Skin Mid-Ply – Crack Arrested at Frames, Reached Ult Load.....	79
Figure 117. Failure Index for Skin Mid-Ply – Panel Ruptured.....	80
Figure 118. IML Strain Gages.....	81
Figure 119. OML Strain Gages.....	81
Figure 120. Existing Stitching and Cure Tools Used.....	82
Figure 121. Infused Specimen Blank Prior to Edge Trim.....	82
Figure 122. End Grip Hardware Detail Parts.....	83
Figure 123. Bonded Aluminum Stringer and Skin Doublers.....	83
Figure 124. Steps to End Grip Preparation.....	84
Figure 125. Specimen Strain Gage Placement.....	84
Figure 126. Specimen Delivery to Boeing Hunitington Beach Test Lab.....	85
Figure 127. General Test Arrangement.....	86
Figure 128. Specimen Arrangement and Displacement Gage Placement.....	87
Figure 129. Strain Gage Identification and Locations.....	88
Figure 130. Video Panels Using During Testing.....	89
Figure 131. Key Failure Events During Load.....	89
Figure 132. Load Versus Displacement Measurements.....	90
Figure 133. Damage Progression on IML Surface.....	91
Figure 134. Damage Progression on OML Surface.....	92
Figure 135. Post-Failure OML Surface.....	93
Figure 136. Post-Failure IML Surface.....	94

Figure 137. Specimen Post-Failure Photographs.....	95
Figure 138. Pre-Test Progressive Failure Analysis.....	96
Figure 139. Comparison to Pre-Test Progressive Failure Analysis.....	96
Figure 140. Spanwise Compression Panel Specimen Concept.....	97
Figure 141. Compression Panel Specimen	98
Figure 142. General Features of Specimen Design	98
Figure 143. Design Ultimate Running Load Calculation	99
Figure 144. Compression Panel Finite Element Model.....	100
Figure 145. Skin Buckling of the Compression Panel at 59,000 lbs	100
Figure 146. Skin and Frame Displacements Plots as a Function of Load	101
Figure 147. Global Buckling of the Compression Panel at 207,000 lbs.....	101
Figure 148. Phase I Compression Specimen Failure Strains Used for Phase II	102
Figure 149. Strain Results in the X- and Y-Direction for the Global Panel	102
Figure 150. Y-Direction Strains Shown at Critical Locations.....	103
Figure 151. Minimum Principal Strains Shown At Critical Locations.....	103
Figure 152. Y-Dir and Min Principal Strains on Frame at Critical Locations.....	104
Figure 153. Compression Test Strain Gage Placement – IML Strain Gage Locations	105
Figure 154. Compression Test Strain Gage Placement – OML Strain Gage Locations.....	105
Figure 155. Compression Test Strain Gage Placement – Frame Strain Gage Locations	106
Figure 156. Spanwise Compression Panel After Resin Infusion Processing.....	107
Figure 157. Potting of Ends of Compression Panel.....	108
Figure 158. Potted End of Compression Panel	108
Figure 159. Machining of Potted End Plates	109
Figure 160. Compression Panel Test Set-Up.....	110
Figure 161. Compression Panel in Test Fixture.....	111
Figure 162. Initial Out-of-Plane Displacement Showing Panel Imperfections	112
Figure 163. Out-of-Plane LVDT Measurements and VIC Plots as Load Increases	113
Figure 164. Failure Across Width of Panel	113
Figure 165. IML (Left) and OML (Right) Views of the Panel Failure.....	114
Figure 166. Right IML View of Frame with Initial Failure.....	115
Figure 167. Right IML View of Frame and Skin Failure	115
Figure 168. Left IML View of Frame and Skin Failure	116
Figure 169. Left IML View of Frame Failure.....	116
Figure 170. Upper Delamination After Initial Failure	117
Figure 171. Close-up of Upper Delamination After Initial Failure	117
Figure 172. Out-of-Plane Deflection at Failure with Maximum at Failure Location.....	118
Figure 173. Strain Data from the VIC Results.....	119
Figure 174. Shear Strain Results from VIC Data	119
Figure 175. PRSEUS Interface Screen within HyperSizer	121
Figure 176. Sizing Variables for Stringer	123
Figure 177. Sizing Variables for the Frame.....	124
Figure 178. Sizing Variables for the Panel	125
Figure 179. Example of Hyperlaminates for Stringer Flange Definitions.....	126
Figure 180. Example of Hyperlaminates for Frame Flange Definitions	127
Figure 181. Spacing Span Buckling.....	128
Figure 182. Global ABD Matrix Assessment.....	129

Figure 183. Object Loads.....	131
Figure 184. FEA Buckling Eigenvalue Solution (1st Mode Shape).....	132
Figure 185. Load vs. Strain.....	133
Figure 186. Initial Buckling Mode.....	133
Figure 187. Mode Before Final Collapse (Top View).....	134
Figure 188. Mode Before Final Collapse (Side View).....	134
Figure 189. Upper Skin Panels FEM.....	135
Figure 190. Lower Skin Panels FEM.....	136
Figure 191. FEM Setup Template.....	137
Figure 192. Sizing Form for PRSEUS.....	138
Figure 193. BWB Finite Element Model.....	138
Figure 194. Global-Local Optimization Approach.....	139
Figure 195. Global-Local Process Flow.....	140
Figure 196. 2.5-g Limit Load Streamwise Direction (NX) LBS/IN.....	141
Figure 197. 2.5-g Limit Load Spanwise Direction (NY) LBS/IN.....	142
Figure 198. -1.0-g Limit Load Streamwise Direction (NX) LBS/IN.....	143
Figure 199. -1.0-g Limit Load Spanwise Direction (NY) LBS/IN.....	144
Figure 200. 1.33P Limit Load Streamwise Direction (NX) LBS/IN.....	145
Figure 201. 1.33P Limit Load Spanwise Direction (NY) LBS/IN.....	146
Figure 202. 2.0-g Taxi Bump for Lower Cover LBS/IN.....	147
Figure 203. Upper Skin Design Regions and Number of Skin Stacks.....	149
Figure 204. Lower Skin Design Regions and Number of Skin Stacks.....	150
Figure 205. BWB Pressurized Region.....	151
Figure 206. 1.33P Limit Load Nx (Left) and Ny (Right).....	153
Figure 207. -1.0-g Limit Load Nx (Left) and Ny (Right).....	153
Figure 208. 2.5-g Maneuver Load Case.....	154
Figure 209. Metric Values Established for Phase II Testing.....	155
Figure 210. Metric Target Relationship to Future Development Activities.....	157
Figure 211. Pressure Test Fixture ICD Provided to Vendor.....	159
Figure 212. Chordwise Tension Panel Drawing.....	160
Figure 213. Strain Identification and Locations.....	161
Figure 214. Strain Gage Plot - Top Region.....	162
Figure 215. Strain Gage Plots - Slot Region 1 of 2.....	163
Figure 216. Strain Gage Plots - Slot Region 2 of 2.....	164
Figure 217. Strain Gage Plots - Bottom Region 1 of 2.....	165
Figure 218. Strain Gage Plots - Bottom Region 2 of 2.....	166
Figure 219. OML Strain Gage Placement - 1 of 4.....	167
Figure 220. OML Strain Gage Placement - 2 of 4.....	168
Figure 221. OML Strain Gage Placement - 3 of 4.....	169
Figure 222. OML Strain Gage Placement - 4 of 4.....	170
Figure 223. IML Strain Gage Placement - 1 of 5.....	171
Figure 224. IML Strain Gage Placement - 2 of 5.....	172
Figure 225. IML Strain Gage Placement - 3 of 5.....	173
Figure 226. IML Strain Gage Placement - 4 of 5.....	174
Figure 227. IML Strain Gage Placement - 5 of 5.....	175
Figure 228. Spanwise Compression Panel Drawing.....	176

Figure 229. Seven-Stringer PRSEUS Panel..... 177

LIST OF TABLES

Table 1. Comparison of Strains in Test Region.....	15
Table 2. Pressure Panel Margin of Safety under 2P	21
Table 3. Pressure Panel Test Load Sequence.....	55
Table 4. Test Load Predictions	65
Table 5. Relevant Failure Modes for PRSEUS.....	122
Table 6. Analysis Objects for PRSEUS Design.....	128
Table 7. Load-Strain Comparisons	130
Table 8. Stiffness Comparison.....	130
Table 9. Object Load Comparisons	131
Table 10. Eigenvalue Comparison.....	132
Table 11. Design Limits.....	137
Table 12. Pressurized Center Body Weight.....	152
Table 13. Summary of NRA Phase I and II Metrics.....	156

ACRONYMS

2P	2 times Max Internal Pressure
AFRL	Air Force Research Laboratories
AJ	Assembly Jig
BHD	Bulkhead
BWB	Blended Wing Body
CAI	Compression After Impact
CD	Cold Dry
CAPRI	Controlled Atmospheric Pressure Resin Infusion
CG	Center of Gravity
D&DT	Durability and Damage Tolerance
EVM	Earned Value Management
FAR	Federal Aviation Regulations
FEM	Finite Element Model
H/W	Hot/Wet
HWB	Hybrid Wing Body
ICD	Interface Control Drawing
IML	Inner Moldline
IRAD	Independent Research and Development
IWNG	Inboard Wing
KEAS	Knots Equivalent Airspeed
KIPS	Thousand Pounds
KSI	Thousand Pounds Per Square Inch
L/D	Lift-to-Drag Ratio
MLG	Main Landing Gear
MTOGW	Maximum Takeoff Gross Weight
MZFW	Maximum Zero Fuel Weight
NDE	Nondestructive Evaluation
NDI	Nondestructive Inspection
N_x	Axial Load in x-direction
N_{xy}	Shear Load in xy-plane
N_y	Axial Load in y-direction
OB	Outboard
OEW	Operator Empty Weight
OML	Outer Moldline
OWNG	Outboard Wing
OHC	Open Hole Compression
OML	Outer Moldline
PFA	Progressive Failure Analysis
PRSEUS	Pultruded Rod Stitched Efficient Unitized Structure
PMC	Polymer Matrix Composite
PSE	Principle Structural Element
PSI	Pounds per Square Inch
SQ-IN	Square Inches
VARTM	Vacuum-Assisted Resin Transfer Molding

INTRODUCTION

This work focuses on the development of a novel structural solution that addresses the unique fuselage loading requirements of the Hybrid Wing, or Blended Wing, Body (HWB/BWB) configuration described in the NASA NRA Subtopic A.2.4.3, “Materials & Structures for Wing Components and Non-Circular Fuselage” project solicitation.

The Phase II portion of this contract was a comprehensive Finite Element Model (FEM)-based structural sizing exercise performed using the BWB airplane configuration to generate test loads and fuselage design requirements in support of a three article subcomponent test program (Figure 1). This work maintains the continuity of the Phase I results by extending the building-block development testing plan to encompass more technically demanding analyses and testing tasks. Over the course of Phase II, three large subcomponent specimens were fabricated and tested to understand the structural responses for axial and pressure-type loadings. Further analytical work was then undertaken to improve the panel-level sizing results that were developed during Phase I. All of the Phase I and Phase II data was then compiled in a final vehicle-level trade study to assess the relative benefits during the second year of the Phase II program.

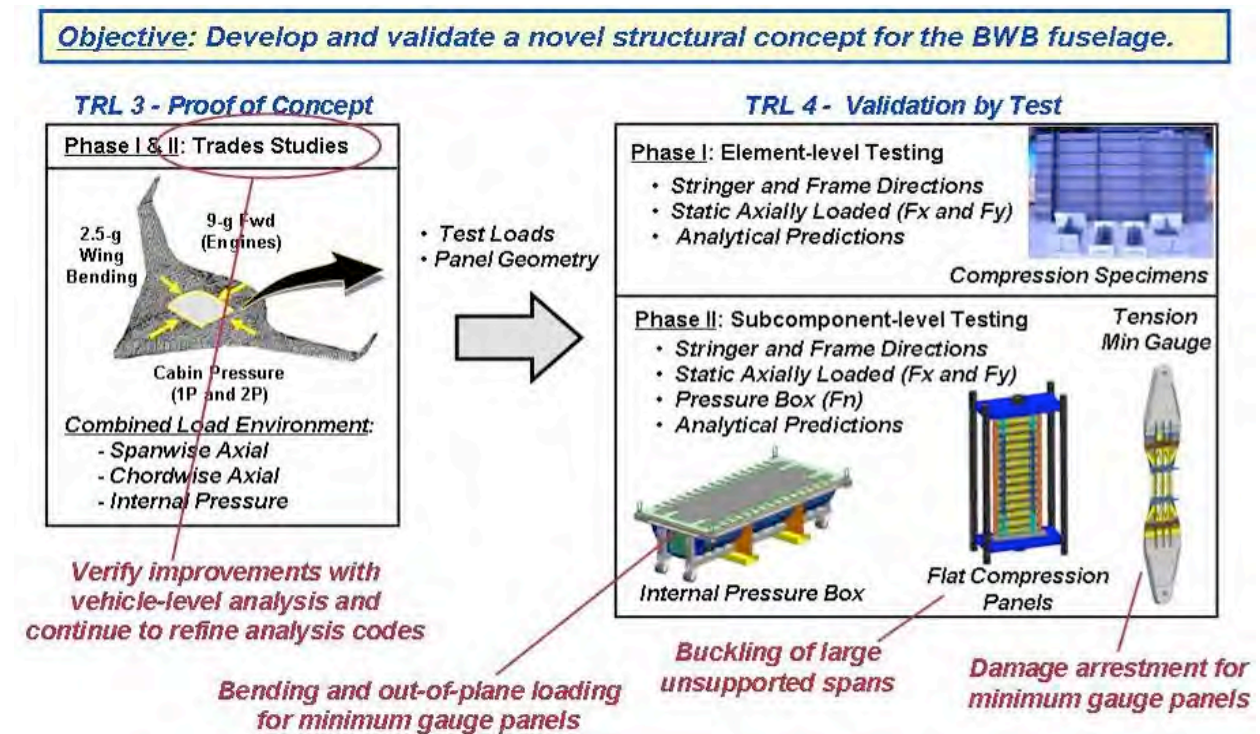


FIGURE 1. KEY ELEMENTS OF PHASE II PLAN

The primary subtasks of the two-year Phase II study are outlined in the schedule in Figure 2. The Test and Validation subtask (WBS 3.5) was comprised of the three subcomponent specimen tests: 1) Internal Pressure Box, 2) Chordwise Tension Panel, and 3) Spanwise Compression Panel, the Panel Sizing Enhancement subtask (WBS 3.6) focuses on improving local PRSEUS panel sizing codes, and the Vehicle Sizing Updates subtask (WBS 3.7) was used to update the global airplane model.

3.0 Statement of Work	Res Group	FY09												FY10											
		CY09												CY10											
		J	F	M	A	M	J	J	A	S	O	N	D	J	F	M	A	M	J	J	A	S	O	N	D
Phase II																									
3.5 Test & Validation																									
3.5.1 Internal Pressure Box																									
3.5.1.1 Design and Analysis	Des/Str																								Design Review, Material POs
3.5.1.2 Panel Tooling	Mfg																								Panel Tooling Built
3.5.1.3 Box & Hardware	Mfg																								Box Built
3.5.1.4 Panel Fab	Mfg																								Panel Complete
3.5.1.5 Specimen Assy	Mfg																								Assembled Box @ LaRC
3.5.1.6 Test Support to NASA	NASA																								Release Test Spec
3.5.2 Chordwise Tension Panel																									
3.5.2.1 Design	Design																								Drawing Release
3.5.2.2 Analyze & Test Spec	Stress																								Analysis & Test Spec Complete
3.5.2.3 Panel Fab	Mfg																								Panel Blank Complete
3.5.2.4 Hardware Fab	Vendor																								Doublers/Shims Ready
3.5.2.5 Specimen Prep	Mfg																								Specimen Prepared
3.5.2.6 Ship to Test Lab	Mfg																								Shipped to test lab
3.5.2.7 Instrumentation	Test																								Gages Installed
3.5.2.8 Specimen Set-up	Test																								Set-up Complete
3.5.2.9 Testing	Test																								Test Complete
3.5.2.10 Prepare Test Report	Stress																								Input for Final Report
3.5.3 Spanwise Compression Panel																									
3.5.3.1 Design	Design																								Drawing Release
3.5.3.2 Analyze & Test spec	Stress																								Analysis & Test Spec Completed
3.5.3.3 Panel Fab	Mfg																								
3.5.3.4 Hardware Fab	Vendor																								End Plates Completed
3.5.3.5 Specimen Prep	Mfg																								Specimen Prepared
3.5.3.6 Ship to Test Lab	Mfg																								Shipped to NASA/Installed at NASA
3.5.3.7 Test Support to NASA	NASA																								Test Complete
3.5.3.8 Prepare Test Report	Stress																								Input for Final Report
3.6 Panel Sizing Enhancements																									
3.6.1 Define Code Changes	Collier																								Code Requirements Complete
3.6.2 PRSEUS Interface Dev't	Collier																								PRSEUS Interface Development Complete
3.6.3 Sizing Code Improvements	Collier																								Sizing Code Improvement Implemented
3.6.4 User Documentation	Collier																								User Documentation Complete
3.6.5 Validation/Checkout	Stress																								HyperSizer Validated
3.7 Vehicle Sizing Updates																									
3.7.1 Update BWB FEM	Stress																								BWB FEM Updated
3.7.2 Incorporate New Hypersizer	Stress																								New HyperSizer Incorporated
3.7.3 FEM-based Structural Sizing	Stress																								Structural Sizing Complete
3.7.4 Develop Wts Statement	Wts																								Wts Statement (reduced scope)
3.7.5 Document Sizing Results	Stress																								Input for Final Report
3.7.6 Breakout Test Loads	Stress																								Test Loads Determined
3.8 Phase II Status Reporting																									
3.8.1 Program Management	Mgr																								
3.8.2 Quarterly Reports	Mgr																								Qtr Rpt
3.8.3 Oral Briefings	Mgr																								Kick-off
3.8.4 Final Written Report	Mgr																								Mid-Yr
																									End of Yr
																									Mid-Yr
																									Final Briefing
																									Phase II Final

FIGURE 2. PHASE II WBS AND SCHEDULE

1.0 STRUCTURAL CONCEPT DEVELOPMENT

To meet the structural challenges presented by the Blended Wing Body (BWB), or Hybrid Wing Body (HWB), aircraft researchers at The Boeing Company in Huntington Beach (Boeing Research & Technology Division) and at NASA Langley Research Center (NASA-LaRC) are developing a highly integrated, stitched composite airframe solution that is tailored and optimized for the HWB airframe. This is done by exploiting the unique processing advantages inherent in dry carbon fabrics and the damage-arrest characteristics of stitched structures. This new design and manufacturing concept is called the Pultruded Rod Stitched Efficient Unitized Structure (PRSEUS). It is a disruptive technology that is a conscious departure from conventional laminated composite design practices developed to meet the demanding structural performance and producibility requirements of the HWB design space.

1.1 Design Approach

An essential feature of the BWB structural approach must be the capability to react the unusual bi-axial loading pattern in the shell (Figure 3). Here the load magnitudes are more nearly equal in each direction (N_x and N_y) than what is normally found on conventional tube-and-wing fuselage arrangements where the cantilevered fuselage is more highly loaded in the N_x direction, along the stringer, than in the N_y direction, along the frame. This single difference has a profound effect on the structural concept selection because it dictates that the optimum panel geometry should have efficient load paths in both the N_x and N_y directions, in addition to transmitting internal pressure loads (N_z) for the near-flat panel geometry. This represents a problem for conventional skin-stringer-frame built up panels, because the frame shear clip is discontinuous to allow the stringer to pass through uninterrupted in the primary longitudinal loading direction. If such an arrangement were used for the HWB, then the frame member (attached by a discontinuous shear clip to the skin) would be less effective in spanwise bending/axial loading, ultimately resulting in an uncompetitive solution.

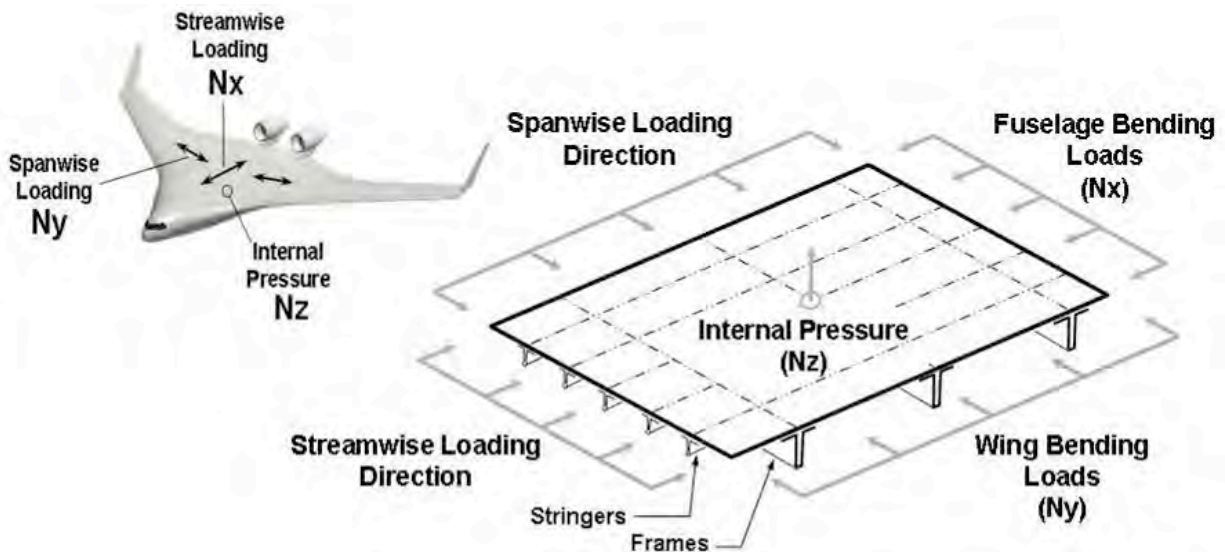


FIGURE 3. PRESSURE CABIN RUNNING LOADS

To combat this problem, the HWB PRSEUS fuselage panel has been designed as a bi-directionally stiffened panel design, where the spanwise wing bending loads are carried by the frame members and the longitudinal fuselage bending loads are carried by the stringers. The

resulting panel design is extremely effective in meeting the unique loading requirements of the HWB, thereby eliminating the weight penalty normally associated with a non-circular pressure cabin. (Reference 1)

The highly integrated nature of PRSEUS is evident in the strategic placement of the carbon fibers (Figure 4). The dry warp-knit fabric, pre-cured rods, and foam-core materials are assembled and then stitched together to create the optimal structural geometry for the HWB fuselage loading. Load path continuity at the stringer-frame intersection is maintained in both directions. The 0-degree fiber dominated pultruded rod increases local strength/stability of the stringer section while simultaneously shifting the neutral axis away from the skin to further enhance the overall panel bending capability. Frame elements are placed directly on the IML skin surface and are designed to take advantage of carbon fiber tailoring by placing bending and shear-conductive lay-ups where they are most effective. The stitching is used to suppress out-of-plane failure modes, which enables a higher degree of tailoring than would be possible using conventional laminated materials.

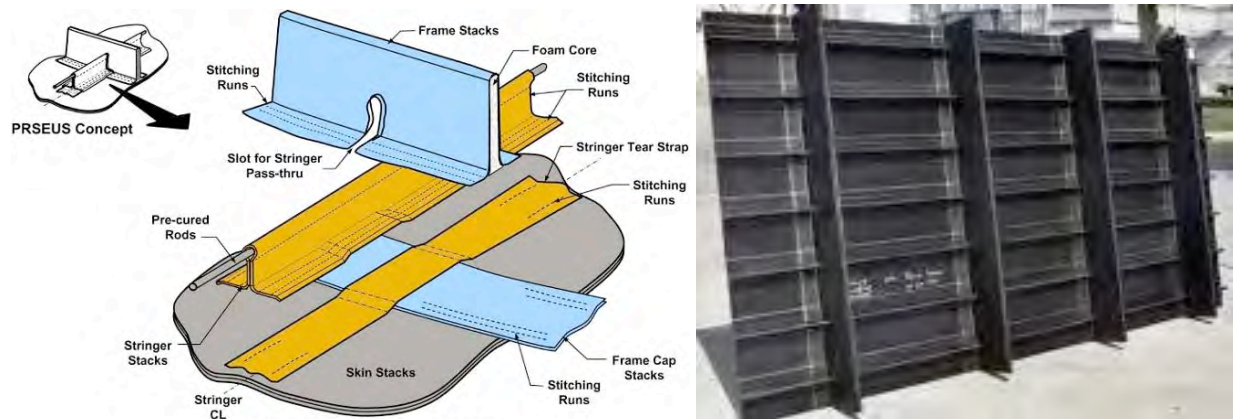


FIGURE 4. PULTRUDED ROD STITCHED EFFICIENT UNITIZED STRUCTURE (PRSEUS)

The resulting integral structure is ideal for the HWB pressure cabin because it is a highly efficient stiffened panel geometry in three directions that is also damage tolerant, stitched to react pull-off loads, and capable of operating well into the post-buckled design regime. This enables the thin gauge skin-stringer designs to be lighter than non-buckled sandwich panels. The PRSEUS HWB airframe design with its continuous load paths, higher notched design properties, and larger allowable damage levels represents a substantially improved level of performance and survivability beyond what would be possible using unstitched materials and designs. (Reference 2)

In addition to enhanced structural performance, the PRSEUS fabrication approach is also ideally suited to the compound curvatures found on the HWB airframe. The self-supporting stitched preform assembly feature that can be fabricated without exacting tolerances and then accurately net molded in a single oven-cure operation using high-precision outer moldline (OML) tooling is an enabler for low cost fabrication (Figure 5). Since all of the materials in the stitched assembly are dry, there are no out-time, or autoclave limitations as in prepreg systems, which can restrict the size of an assembly as it must be cured within a limited processing envelope.



FIGURE 5. STITCHED DRY FABRIC USED TO CREATE SELF-SUPPORTING PREFORM

Resin infusion is accomplished using a soft-tooled fabrication method where the bagging film conforms to the inner moldline (IML) surface of the preform geometry and seals against a rigid OML tool, thus eliminating costly internal tooling that would normally be required to form net-molded details (Figure 6). The manufacture of multiple PRSEUS panels (Reference 3) proved that the essential feature of this concept – the self-supporting preform that eliminates interior mold tooling – is feasible for the near-flat geometry of the BWB airframe (Figure 7). This accomplishment represents a fundamental breakthrough in addressing the producibility needs for the BWB airframe (Figure 7).



FIGURE 6. RESIN INFUSION AND CURED PANEL



FIGURE 7. CURED FLAT PANEL GEOMETRY

All detail parts were built using stacks of preassembled AS4 standard modulus (33 million psi) carbon fibers (DMS 2436 Type, 1 Class 72, Grade A). Each stack has 7 plies in a +45, -45, 0, 90, 0, -45, +45 pattern knitted together. Percentage of fiber by area weight is (44/44/12) using a (0/45/90) nomenclature. A 1200 denier Vectran thread was used to stitch the preform together. DMS2479 Type 2, Class1 (VRM-34) epoxy resin was used to infuse the preforms. All parts were visually inspected per DPS 4.738 for surface defects.

1.2 BWB Configuration Baseline

The BWB aircraft employs advanced technologies to achieve a highly integrated airframe that is capable of substantial aerodynamic performance improvements. Airframe weights are kept low through the extensive use of the PRSEUS structural concept resulting in primary wing and fuselage structures that are appreciably lighter than comparable sandwich designs (Figure 8).

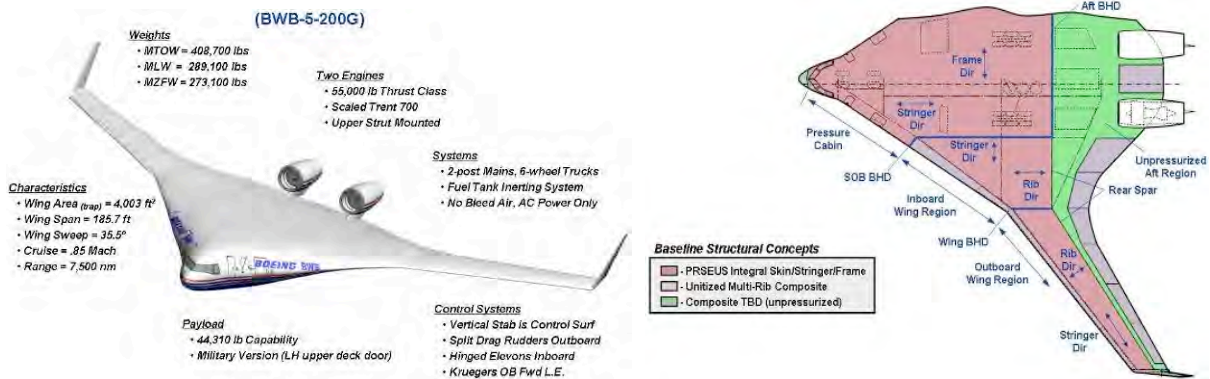


FIGURE 8. BWB BASELINE FOR STUDY

The extensive use of stitching and resin infusion also provides a cost-competitive, damage tolerant airframe that is capable of meeting the performance and producibility challenges of the BWB airframe. Deep frame sections support the frames at each longitudinal rib/bulkhead to reduce the bending moments in the covers (Figure 9). A basic frame depth of 6 inches was used. In the lower cargo region, the frames extend the entire depth between the skin and the cargo floor. Deeper frames or support bracing are used in regions of the lower shell not housing cargo containers, and where landing gear and systems geometries permit.

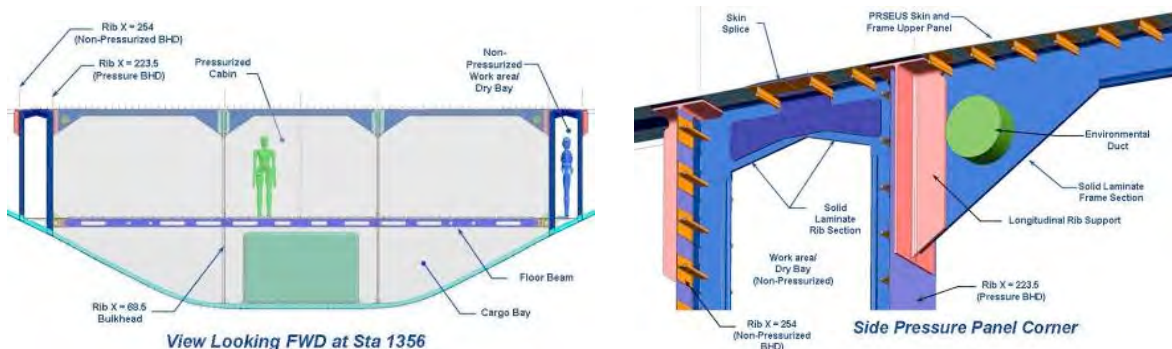


FIGURE 9. TYPICAL PRESSURE CABIN CROSS-SECTION

The passenger floor performs the same functions as other floors, but to keep the space in the under-floor cargo bays as clear as possible, there will be no intermediate struts for the floor beams between the ribs. The beams run continuously across and through the ribs and are attached

to the end pressure bulkheads with some degree of fixity. These end attachments assist the bulkheads in carrying the lateral pressure loads, and in doing so, the beams themselves are subjected to a tension load from the spanwise pressure loads induced at the sidewalls. Additional structural definition along with a more detailed description can be found in the Phase I final report. (Reference 1)

1.3 Test Specimen Sizing Loads

The test specimen sizing loads were derived from the vehicle-level BWB-5-200G finite element model originally developed using Boeing IRAD funding and then modified for the Phase I study. The major changes include implementation of the PRSEUS concept on the upper and lower fuselage skin panels and the new frame design. The final FEM model (Figure 10) features the vehicle's fuselage skins, frames, ribs, spars and floors, wing skins, spars and ribs, vertical stabilizer, movable control surfaces and high-lift devices, and bulkheads. Structural cutouts were included for landing gear doors and cargo doors. The total number of elements in the vehicle model is approximately 44,000, representing more than 142,000 degrees of freedom.

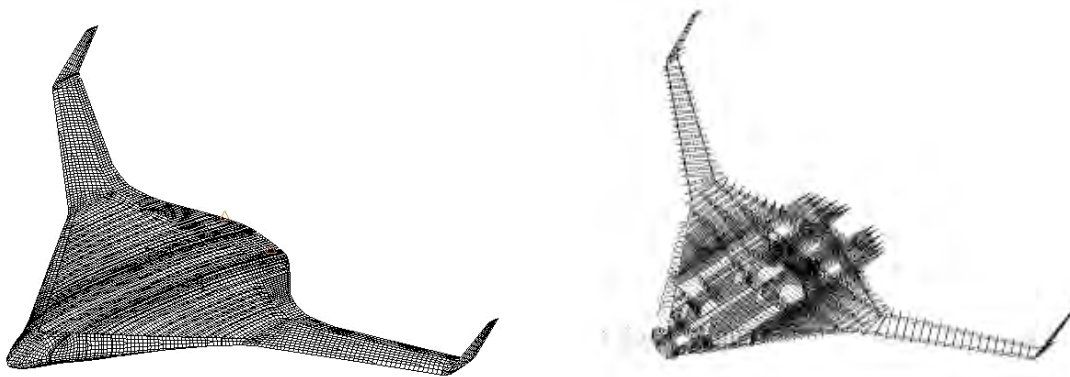


FIGURE 10. BWB BASELINE FINITE ELEMENT MODEL

Three- and four-node bending plate elements are used for skin, spar, and rib webs. Bending bar elements are used to represent frames, and floor beams. Axial rod elements are used to represent spar and rib caps. Stringers in PRESUS panels are not discretely modeled but instead are smeared as equivalent properties for the stiffened panel simulations (PSHELL/MAT2 in NASTRAN), which are then locally sized in HyperSizer as true skin-stringer geometries.

Principal concentrated masses, including landing gear, engines, and major systems, are included to account for internal and external subsystems. The weight of furnishings and payload is applied to passenger and cargo floors/beams as distributed non-structural masses.

The critical load cases are summarized in the Phase I final report (Reference 1). Fourteen cases were determined to be critical for structural sizing. Phase I studies show that the critical maneuver loads (2.5 and -1.0-g) are dominant in the shell region adjacent to the wing, but less so moving forward, whereas the forward portion of the fuselage shell is dominated by the 2P pressure loading ($2P = 1.33P \times 1.5$).

2.0 INTERNAL PRESSURE BOX (WBS 3.5.1)

The large pressure box subcomponent represented the first step in isolating the secondary-bending effects experienced in the BWB pressure shell. It was, in fact, the first time that a PRSEUS test panel was subjected to internal pressure loading. Because the 2P loading condition drives much of the BWB minimum gauge skin and stringer spacing design requirements for the shell region, this is a critical test in establishing the overall structural viability of the airframe design approach. A FEM-based analysis was used to predict failure loads and structural deformations for the test panel and pressure box test fixture.

2.1 Design

A 108-inch by 48-inch BWB minimum gauge fuselage test panel (Figure 11) was manufactured for the pressure test per drawing ZJ153443 (Appendix A). The panel contains two frame members, 20-inches apart, and fifteen stringers at 6-inch spacing.

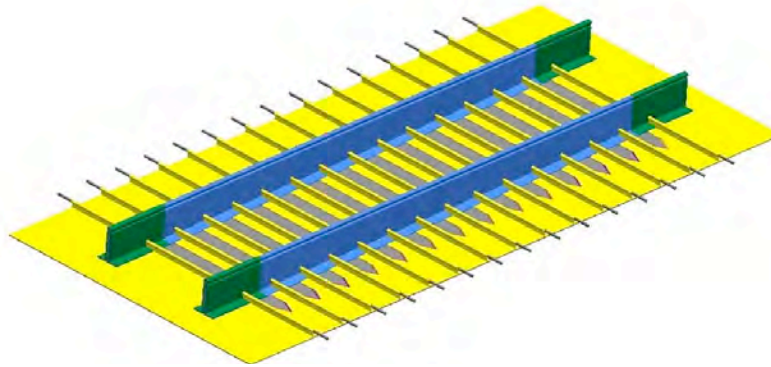


FIGURE 11. UNTRIMMED PRESSURE PANEL PREFORM GEOMETRY

The trimmed panel has a 4-inch flat boundary around the entire perimeter. Aluminum doublers were bonded and bolted on the OML surface of the panel per drawing ZJ153447 (Figure 12). The external stiffeners transition the load out of the internal stiffeners to the pressure vessel by reducing the local bending. Without these external stiffeners, a close-out fitting at each stringer would be needed, which would have increased the difficulty of assembling the panel onto the pressure fixture. This design approach minimizes the amount of time a technician is required to be inside the vessel for final assembly. To ensure the bending continuity of the frame members, internal fittings were added at the ends of both frames.

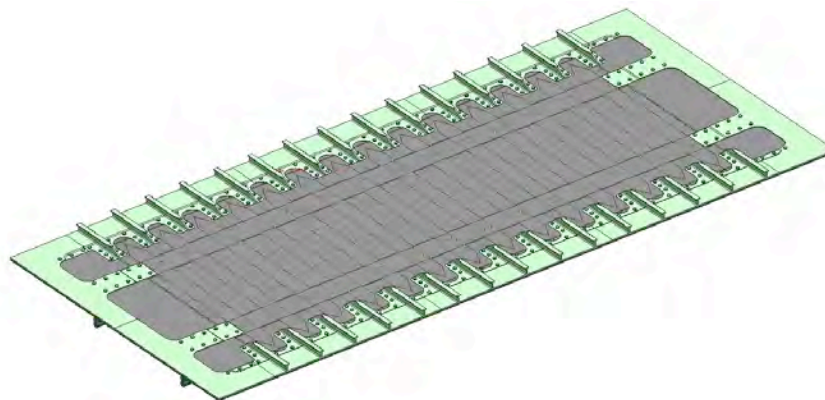


FIGURE 12. PRESSURE PANEL TEST SPECIMEN WITH EXTERNAL DOUBLER

The pressure vessel was designed and manufactured by ASC Process Systems in Sylmar, Ca. The pressure vessel is an all-steel welded assembly shown in Figure 13. A semi-circular shell with end plates is supported by a 7.75-inch by 1-inch upper flange. Several 0.50-inch stiffening plates are added to the sides, ends, and underneath the pressure vessel to reduce local deflections. They were welded to four 0.25-inch thick lower box beams. The pressure vessel is designed to deflect less than 0.05-inches at 30-psi of pressure without support from the test panel. This minimizes the interaction between the test panel and the pressure vessel permitting better model correlation. The fixture is also designed to withstand a maximum internal pressure of 40 psi with a margin of safety greater than two. The panel is attached to the pressure vessel by two rows of .25-inch bolts along each edge effectively constraining the panel edges to be fixed-ended in bending with help from the external stiffeners. Each frame end is attached by an internal fitting using a bolted connection.

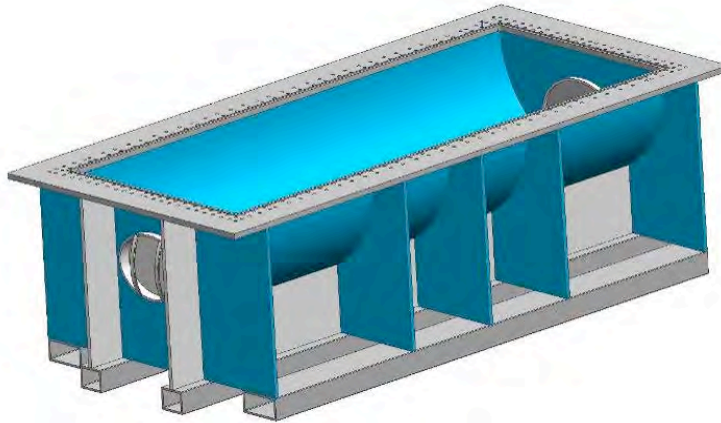


FIGURE 13. PRELIMINARY PRESSURE TEST FIXTURE DESIGN FROM ASC

A large elliptical 18-by-14-inch access door allows access into the pressure vessel after the test panel is installed. The small access door on the opposite side wall acts as a vent port so air can be pumped through the pressure vessel during sealing operations. An over-pressure relief valve is set at 40-psi to prevent any permanent damage to the pressure vessel. The relief valve is sized for a 1-inch inlet hose supplying a maximum of 100-psi inlet pressure at a maximum flow rate of 10 psi per minute. A pressure gage and transmitter port is located on the large door side. The gage permits technicians working on the pressure vessel a visual check that all of the pressure has been evacuated before working on it. The .50-inch pipe threaded nipple transmitter port allows the pressure inside the pressure vessel to be monitored from the control room during the test. A wire port and inlet fitting are located on the vent access cover sidewall. The wire port is sized for a maximum 100 strain gage wires. The wires are sandwiched between foam and sealed with RTV. The inlet fitting is a 1-inch pipe threaded union fitting that will be connected to the house pressure line. A silicon finger seal is located around the entire inner flange perimeter to prevent air leaks between the panel and the flange.

Drain plugs are located at both ends of the shell. When the pressure vessel is stored in the shipping and storage container at a slight angle, any moisture that collects inside the pressure vessel will drain out. Fork lift tubes are designed to load and unload the pressure vessel. Hoist fittings at the four corners allow for lifting by an overhead crane. They are designed with a minimum 3.5 margin-of-safety. Lockable casters are also added to facilitate handling on the ground.

Evolution of the Design - The box fixture has evolved from the initial rectangular cross-section assembly, which consisted of individual panels machined from aluminum plate material, to a welded steel construction having a semi-circular cross-section (Figure 14).

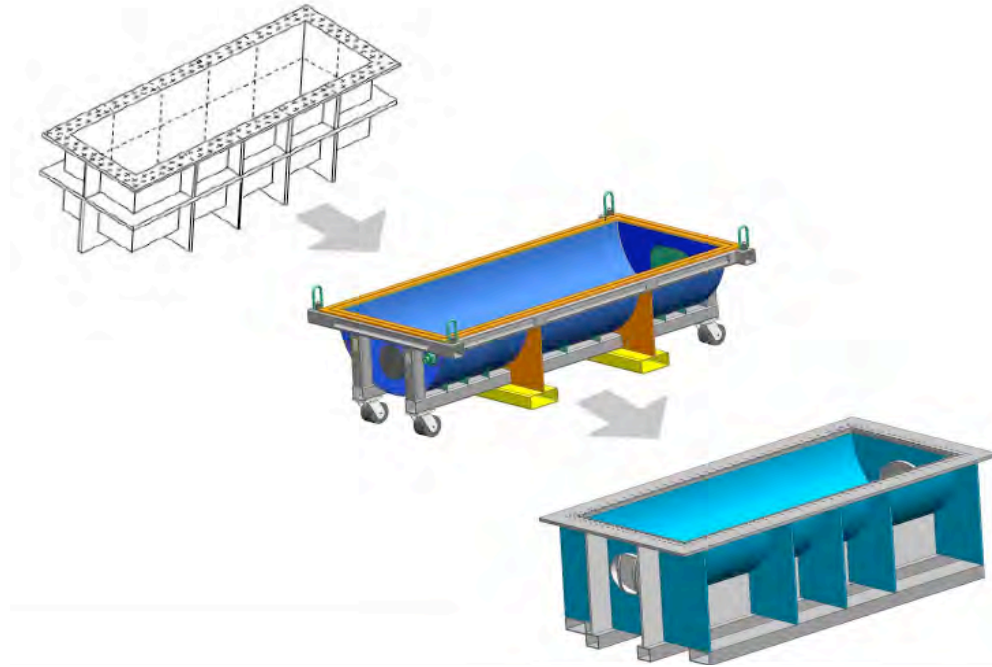


FIGURE 14. PRESSURE BOX DESIGN EVOLUTION

The initial test panel design had two full depth frames with two edge stub frame members to support the ends of the stringers (Figure 15). It soon became evident that the proposed terminations of the stringers presented some problems. The stub frames themselves could not easily be made substantial enough to transfer the loads out of the ends of stringers. Furthermore, the transition from rigid stringers to a lone thin skin in a region where the transverse shears and bending moments are at their peaks was not a satisfactory structural arrangement.

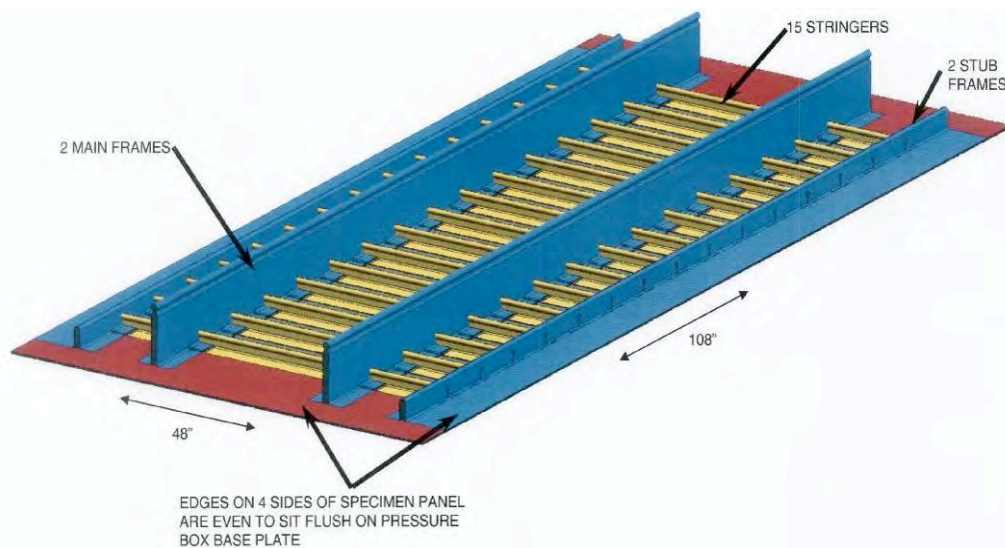


FIGURE 15. INITIAL TEST PANEL CONFIGURATION WITH STUB FRAMES

A number of alternative arrangements for attaching the stringers more directly to the fixture edge were also considered. An external aluminum doubler shown in Figure 16 was added to support the skin and to help transfer the load from the frames and stringers along with internal fittings. Figure 17 indicates how a stringer might be built up to transfer its load into a fitting that is then bolted directly to the fixture. The type of fitting for flight hardware for this approach involves costly end-mill machining. However, for test purposes the fittings were simplified by relocating them to the outside of the panel, as shown in Figure 18. These exterior fittings are bolted rigidly to the fixture and provide a reaction point at their inner tips to constrain the deflection of the stringers, while the frame members are rigidly attached at the ends.

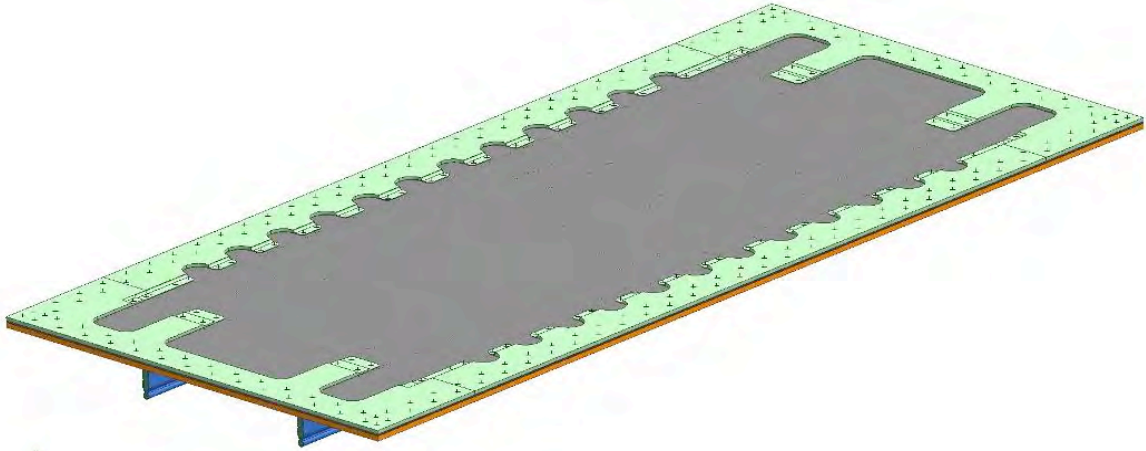


FIGURE 16. EXTERNAL ALUMINUM SKIN DOUBLER

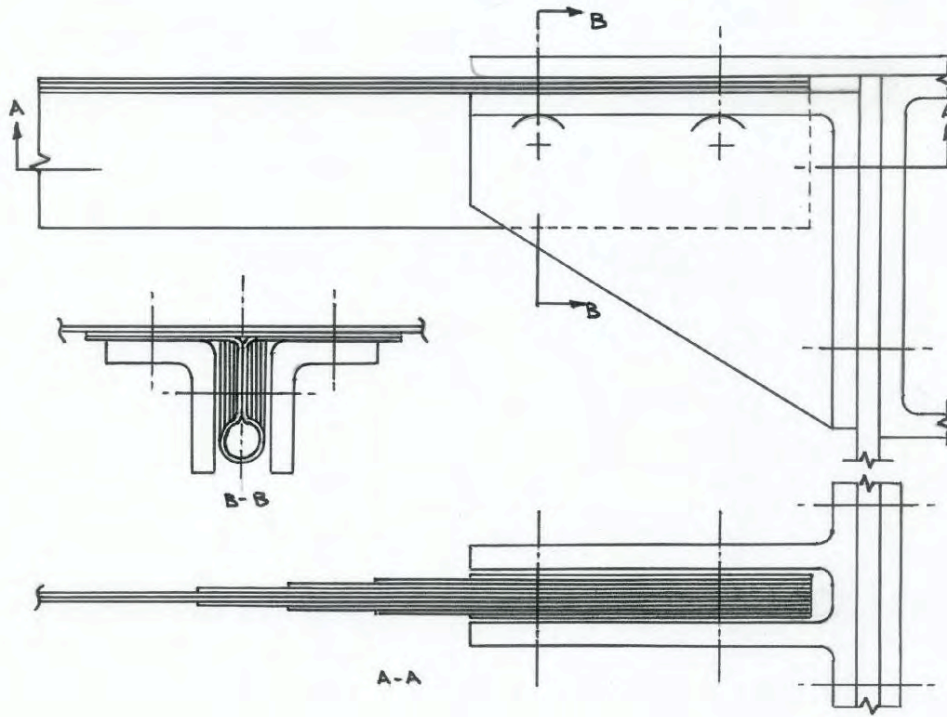


FIGURE 17. PROPOSED STRINGER END CONNECTION

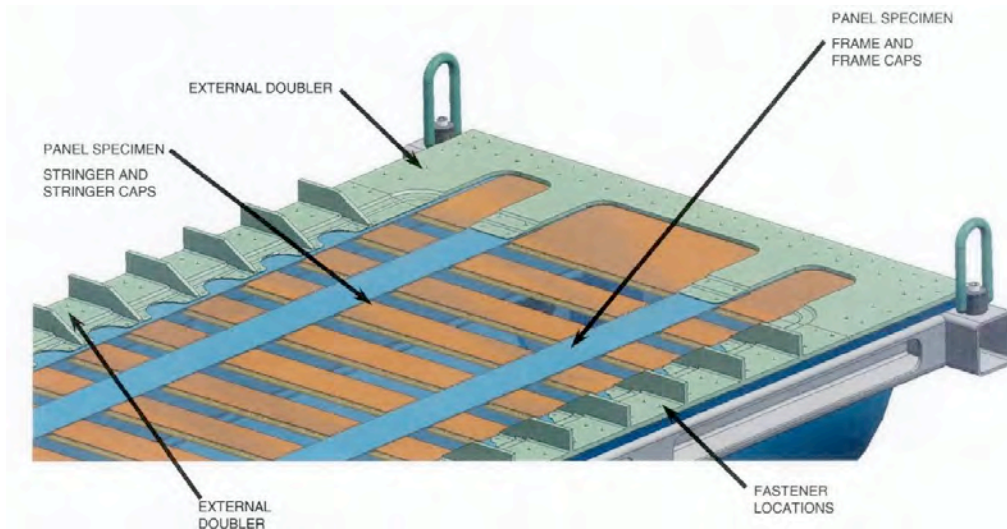


FIGURE 18. EXTERNAL STRINGER END FITTINGS

The attachment of the fitting to the fixture is shown in Figure 19. Although the frames were originally conceived as being pin-ended, they are essentially fixed because the rigid connection of the panel skin to the fixture inhibits free rotation of the frame ends.

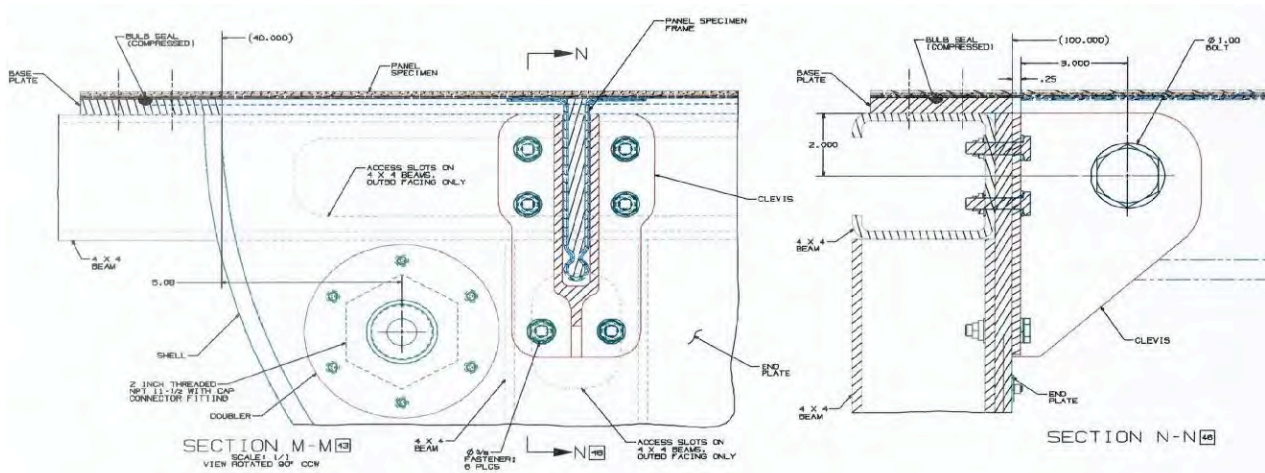


FIGURE 19. FRAME END FITTING

At this point, there was some concern that the concept of rigidly attaching the panel to the fixture was introducing a level of complexity into the design and forcing the panel to deform into shapes that were not consistent with typical aircraft behavior. One proposed alternative approach was to eliminate the direct attachment of the panel to the fixture and to allow the panel edges to rotate freely in a true pin-ended fashion. To accomplish this goal, it was necessary to incorporate a flexible sheet sealing material that extends between the panel and the fixture. External plates hold the sheet material firmly in place to ensure a seal to both the panel and the fixture. The plates attached to the fixture overlap the edges of the panel to form reaction points about which the panel edges are free to rotate. Since this reduces the bending moments around the panel edges to zero, it is now possible to simply run out the stringers at the panel edges and to eliminate the need for end fittings. By extending this arrangement around the panel ends, the frames now also behave in a truly pin-ended fashion. The simplicity of this approach is illustrated in Figure 20.

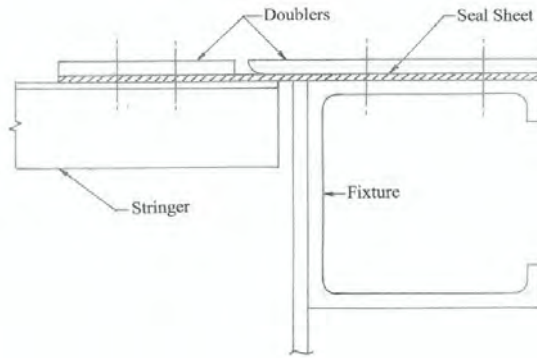


FIGURE 20. PIN-ENDED PANEL EDGE CONCEPT

For both the fixed and the pinned edge conditions, the deformed shape of the stringers results in the frames being twisted along their lengths. This is not desirable and a closer approximation to aircraft deformation behavior could be achieved if the side edges of the panel are to be completely disconnected from the fixture and allowed to move freely in a vertical direction. To accomplish this, it would be necessary to devise a seal material with sufficient extensibility to accommodate the panel deflections or to have a seal with an excess of available length to make stretching unnecessary. In both cases, it would be necessary to extend the sides of the fixture upwards to react pressure when the panel is deflected.

One approach considered, to achieve a free-edge condition, is the use of an extensible inflatable bag shaped to cover the entire inside surface of the pressure shell, as shown in Figure 21. This concept is not strongly favored because of the high probability of bag failure. Figure 22 shows an alternative approach that avoids the need to have a stretchable bag by providing extra sheet sealing material within the pressure shell. The seal would extend around all four panel edges and would be cut from a single sheet of sealing material.

It should be noted that, unlike a panel that is attached rigidly to the fixture, the pinned- and free-edged panel concepts are unable to develop any axial membrane tension loads in the stringer direction.

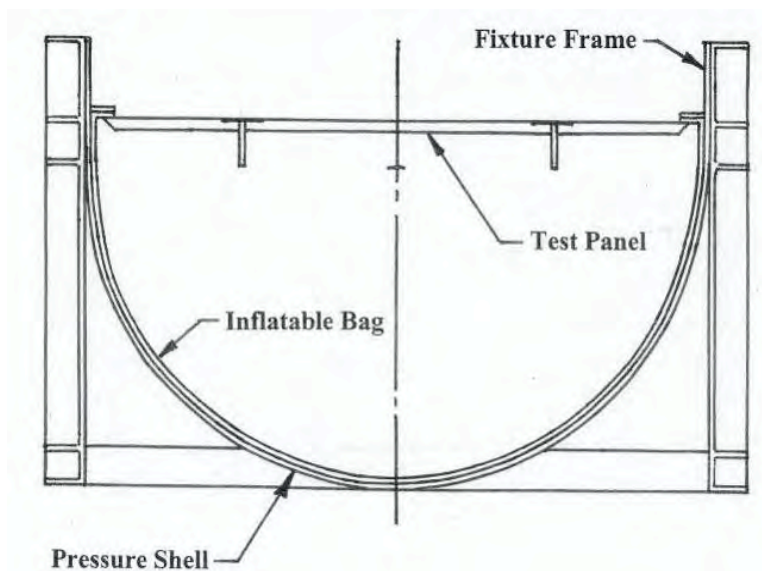


FIGURE 21. INFLATABLE SEALING BAG CONCEPT

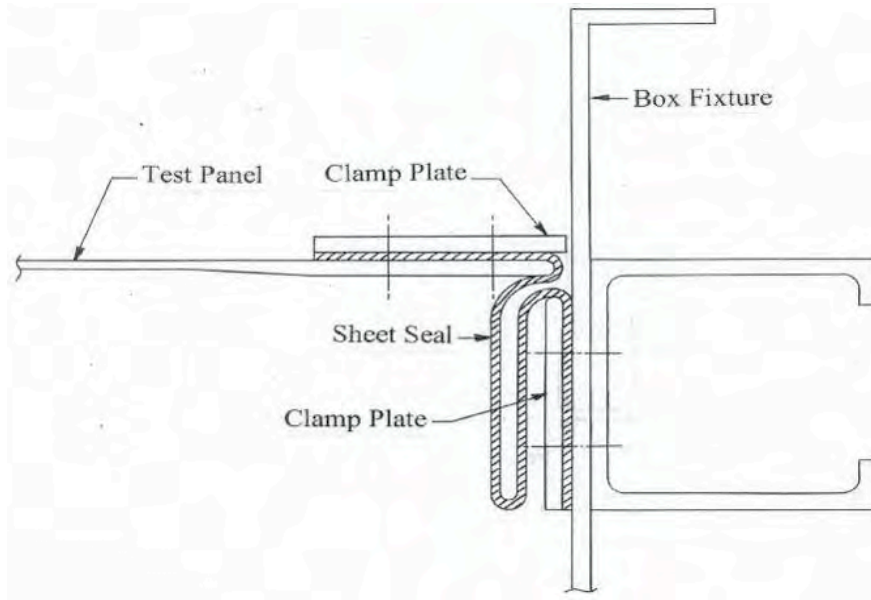


FIGURE 22. FREE EDGE SEAL CONCEPT

Preliminary finite element analyses of the panels, when subjected to the 2P loading condition, illustrate the manner in which the deflected shapes of the central stringers are affected by the different edge conditions, as shown in Figure 23. In the analysis for fixed edges, no fittings are included at the ends of the stringers, leaving only a thin laminate to carry the edge fixing moments. This is clearly evident in the sharp curvature of the skin at the attachment to the fixture. Ongoing analysis studies are developing the design of satisfactory end fittings to alleviate this situation. In the case of the pinned- and free-edge conditions, the panels terminate at the inner sides of the fixture where panel bending moments and curvatures are zero.

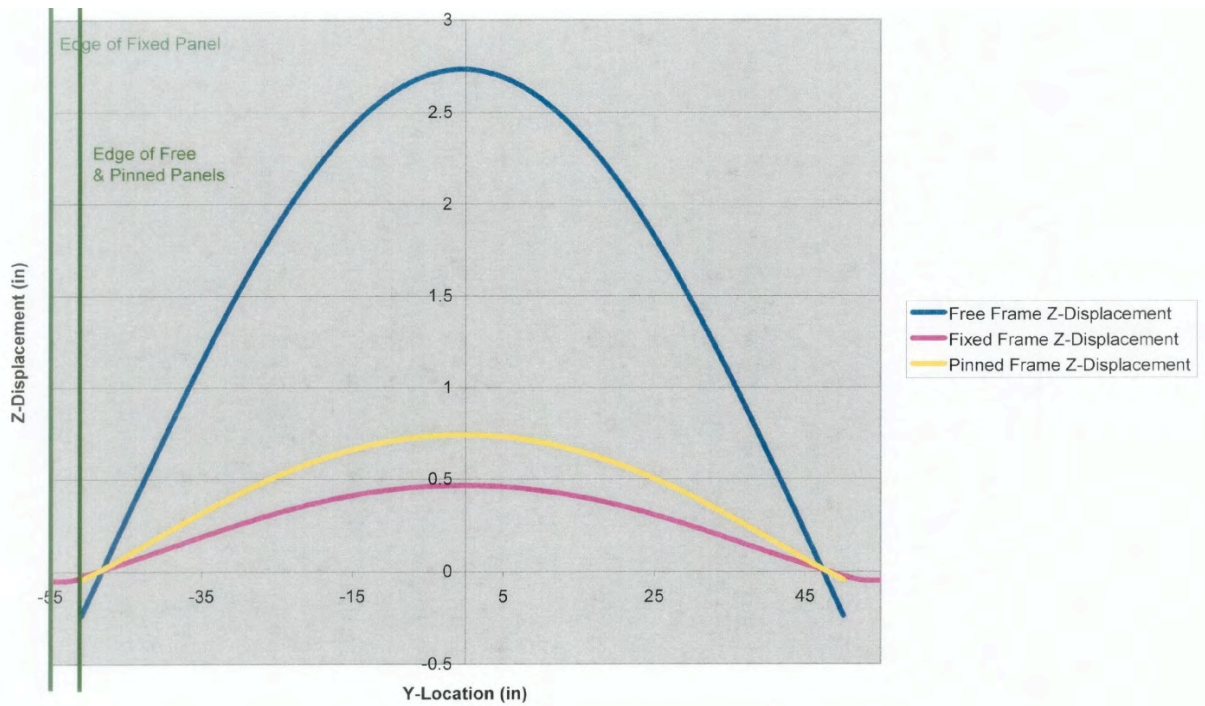


FIGURE 23. COMPARISON OF STRINGER DISPLACEMENTS

The corresponding displacements along the frames are shown in Figure 24. It can be seen that the deflections of the frames in the fixed-and free-edged conditions are severely constrained when no vertical movement is permitted at the ends of the stringers. In each of the conditions, the ends of the frames are assumed to be pinned. This is true for the pinned- and free-edge conditions but not so for fixed edges. In this case, as noted for Figure 24, rotation of the frame about the pin is constrained by the fact that the panel skin is rigidly attached to the fixture. For this condition only, consideration is being given to achieving a more positively fixed-ended condition by replacing the single pin with two or more bolts.

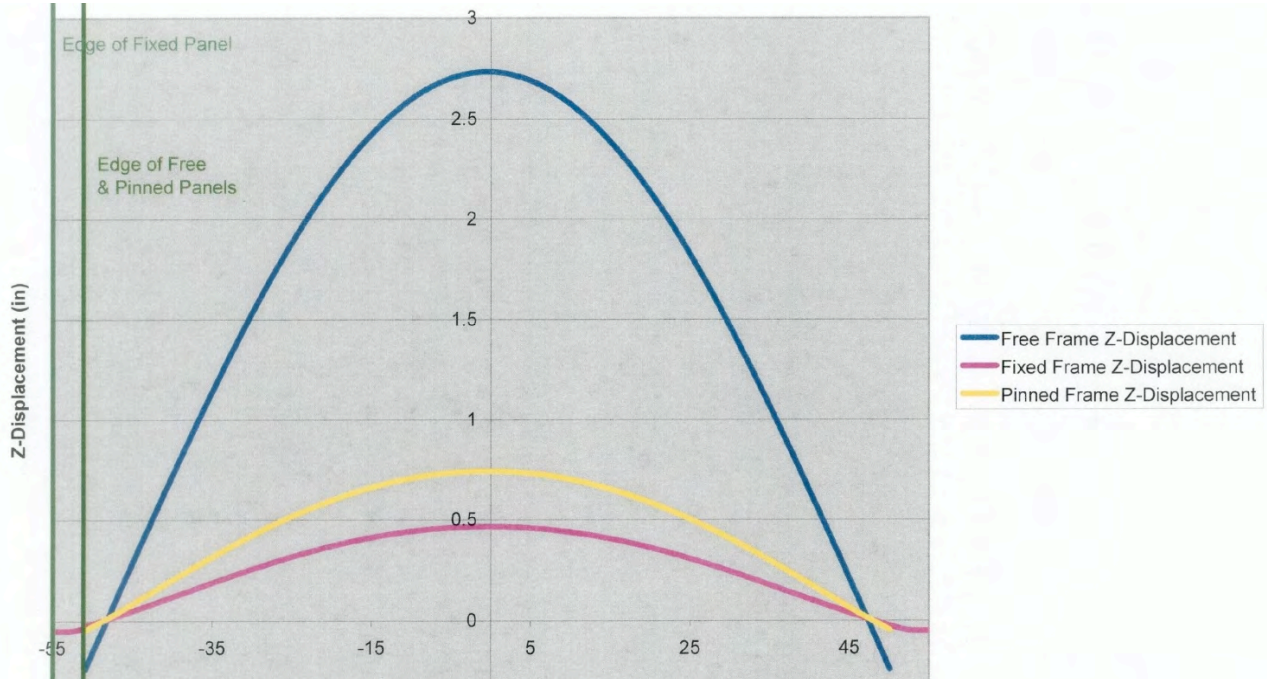


FIGURE 24. COMPARISON OF FRAME DISPLACEMENTS

Many of the peak panel principal strains derived from the analyses for the fixed-ended condition are isolated local conditions at the frame end pins, or along regions of severe curvature at the panel edges. Since it is preferred that the panel will fail in the central test region, it will be necessary to reinforce the laminates in other regions where failures could possibly occur. A summary of principal strains in the test region for the fixed, pinned and free conditions is given in Table 1. Blank entries indicate that no high strains exist in these regions.

TABLE 1. COMPARISON OF STRAINS IN TEST REGION

			Edge Conditions		
			Free	Pinned	Fixed
Principle Microstrain	Skin	Maximum		4,460	2,860
		Minimum		-4760	
	Frame	Maximum	11,600		
		Minimum	-11,900		
	Stringer Rod	Maximum		4,090	
		Minimum		-6,650	-5,610

The free-edged test condition yields the best representation of the actual structural deformations that exist in the selected critical region of the baseline aircraft. The strains in the frames are excessively high but this is just an indication that the frames are under strength and need to be reinforced. The skins and stringers, on the other hand, are not heavily loaded and this is a disadvantage since a main objective of the test program will be to investigate the behavior of these particular elements.

An opposite state of affairs exists for the panels with pinned or fixed edges. For these, the frames are not heavily loaded but strains in the skins and stringers are in a region that should yield useful test results. The desirability of the pinned-edge configuration will depend on being able to ensure the successful behavior of the seal, and this would need to be fully investigated. Based on this concern, a decision was made to concentrate on the fixed-ended configuration. This concept is the easiest to seal and its success will be assured when more detailed analyses verify that panel failure will not occur away from the test region.

Preliminary analyses of the test panels assume that the fixture is infinitely rigid. It is now proposed to make a new finite element model that includes the flexibility of both the test panel and the fixture therefore a new FEM that includes the flexibility of both the test panel and the fixture was created. This provides a better understanding of panel behavior and permits more accurate predictions of test strains and failure modes to be made.

2.2 Analysis

This 100-inch by 40-inch pressure panel was modeled and analyzed in detail to simulate the structural responses under 2P (18.4-psi) internal pressure. Figure 25 through Figure 27 show the finite element models for both the test panel and the proposed fixture. Plate elements (CQUAD4) were used to model the skin, frames & stringers. Bar elements (CBAR) were used for PRSEUS Rods. Structural element stacking (skin, strap, flange, etc.) and layups are characterized by PCOMP members.

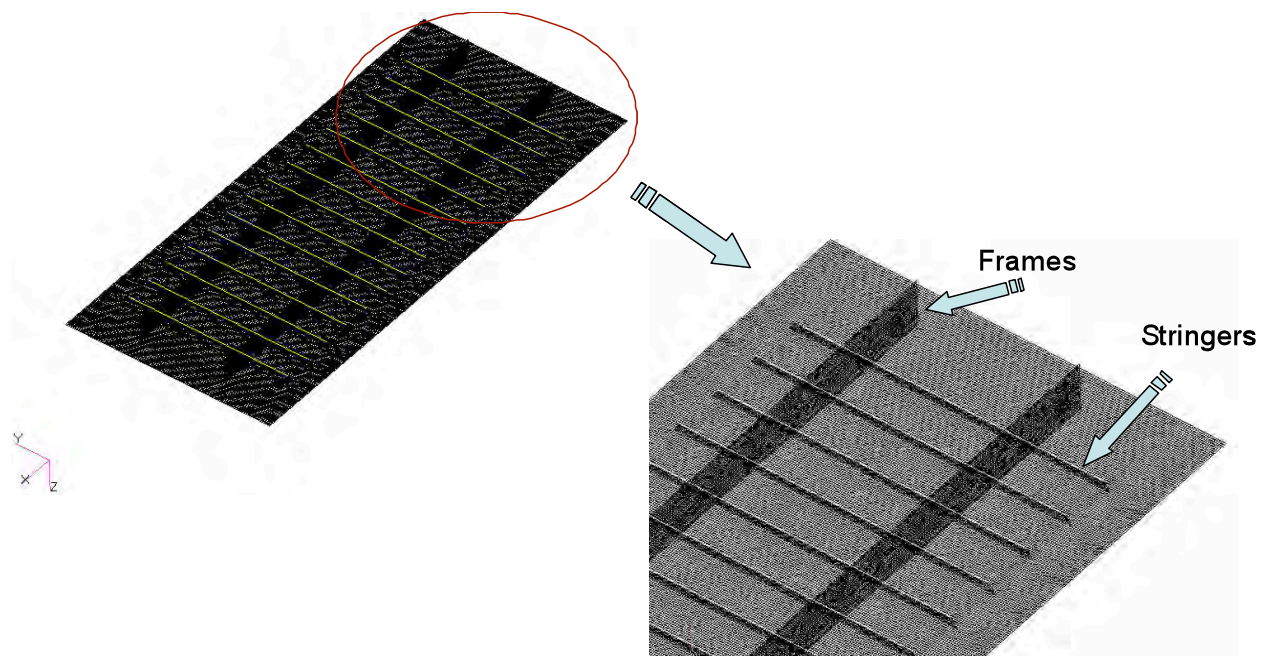


FIGURE 25. PANEL FEM (VIEW FROM IML)

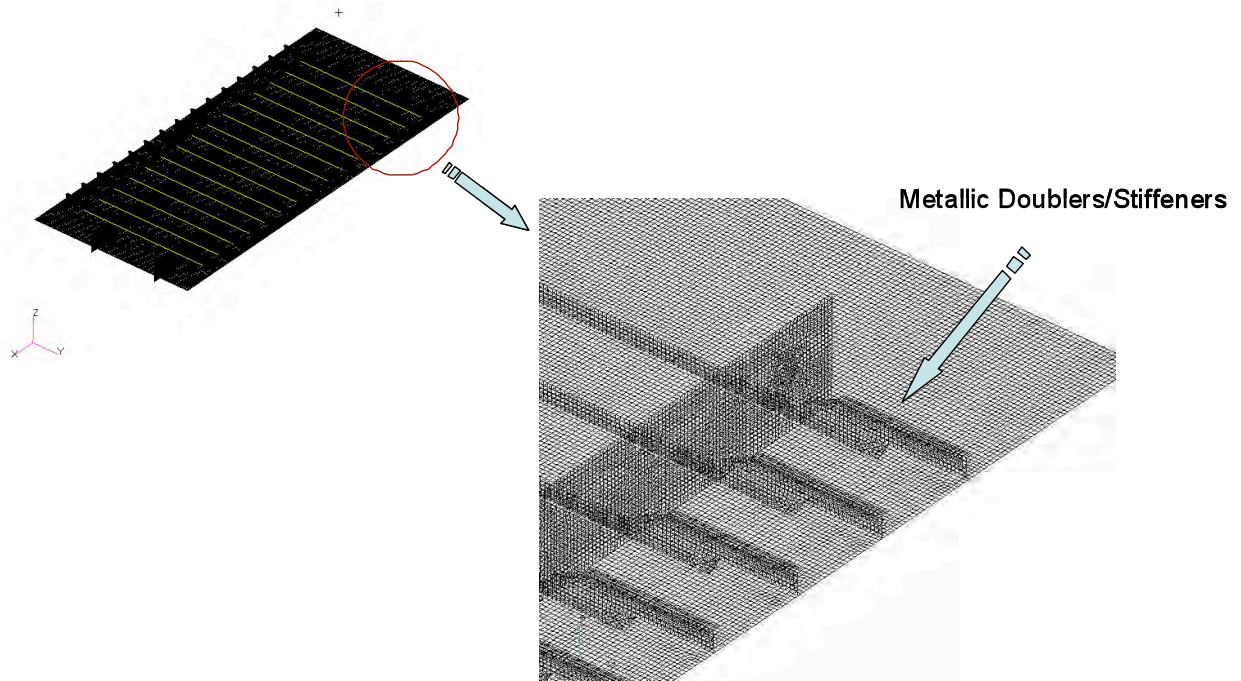


FIGURE 26. PANEL FEM (VIEW FROM OML)

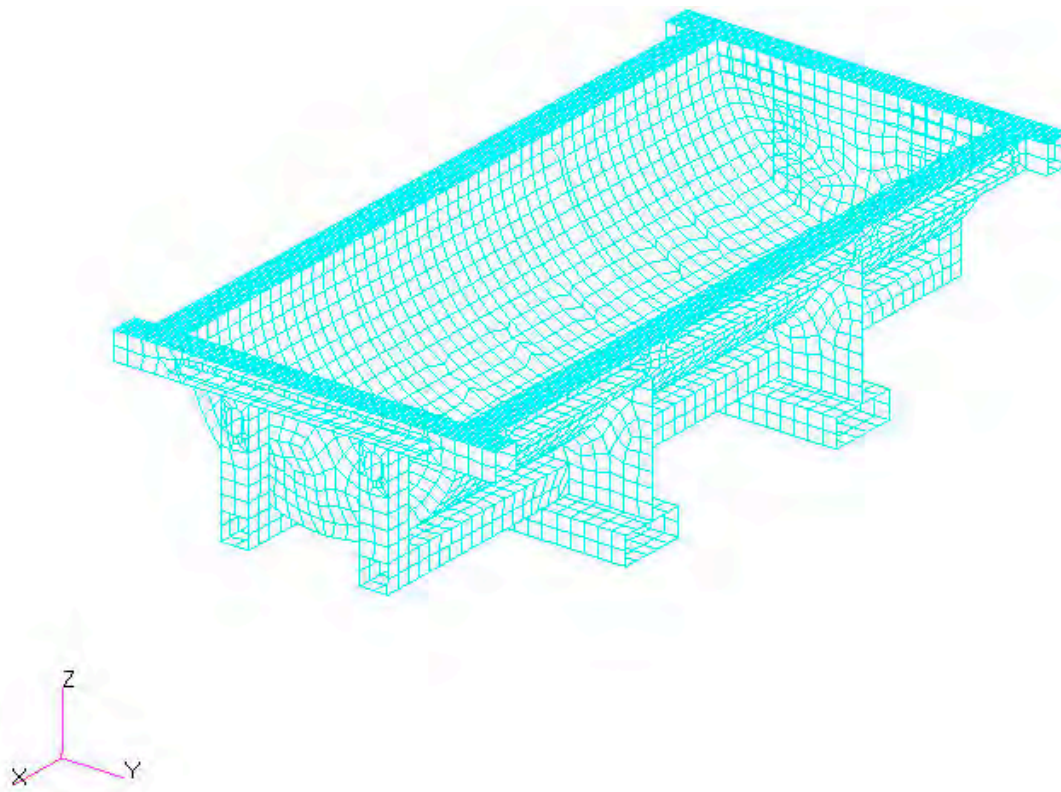
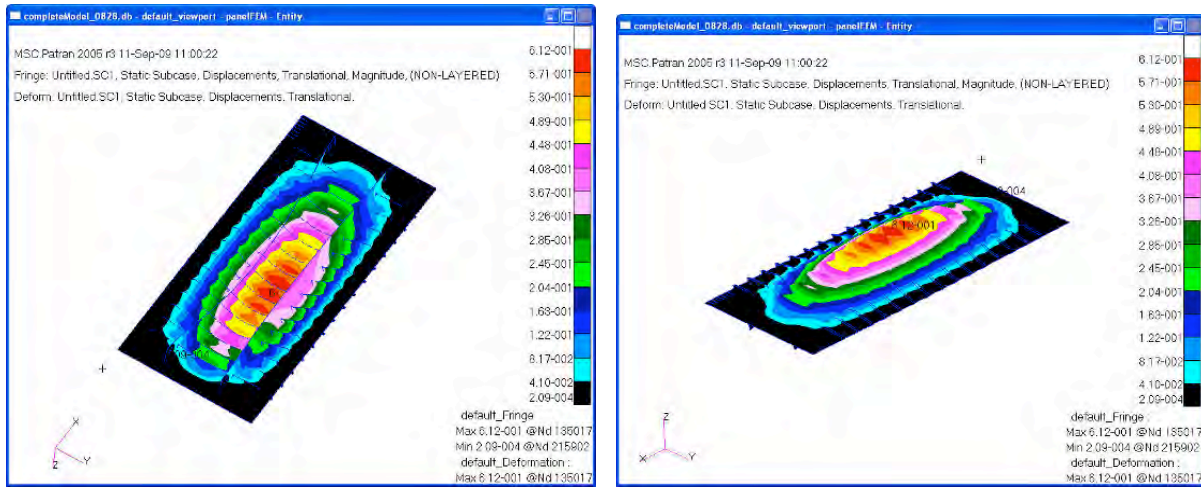


FIGURE 27. TEST FIXTURE FEM

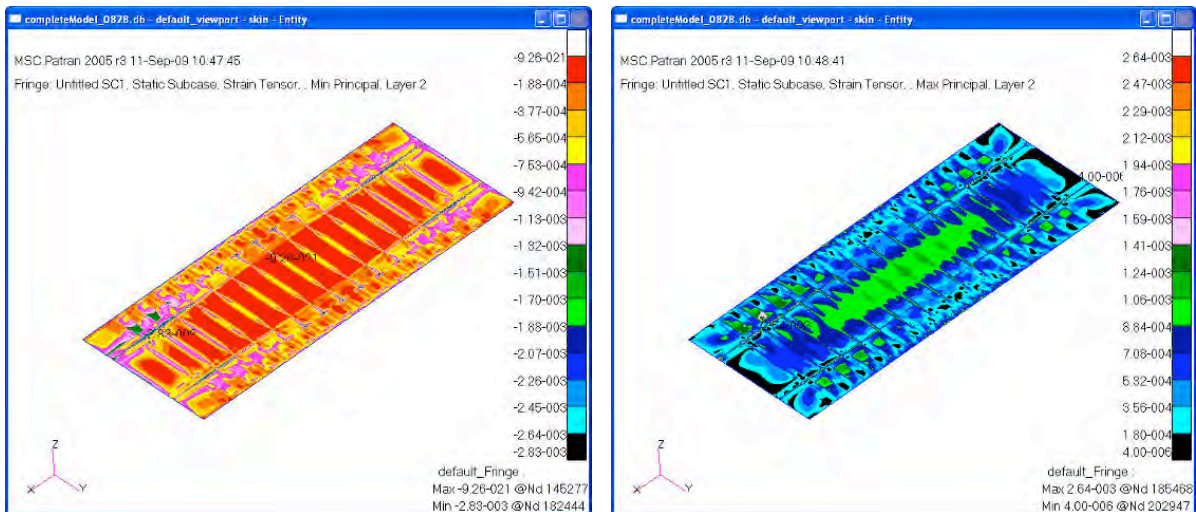
Figure 28 through Figure 34 show general structural responses for 2P pressure. Figure 28 shows the panel deflections. Figure 29 shows max/min principal strain for the skin.



a) View from OML

(b) View from IML

FIGURE 28. PANEL DEFLECTIONS

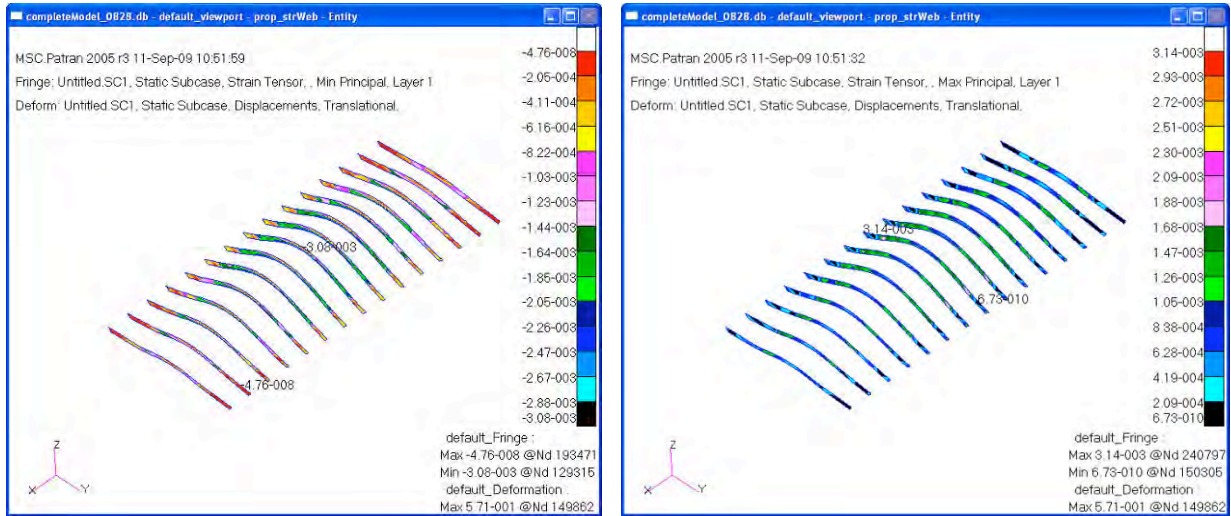


(a) Min Principal Strain

(b) Max Principal Strain

FIGURE 29. PRINCIPAL STRAIN FOR SKIN UNDER 2P PRESSURE

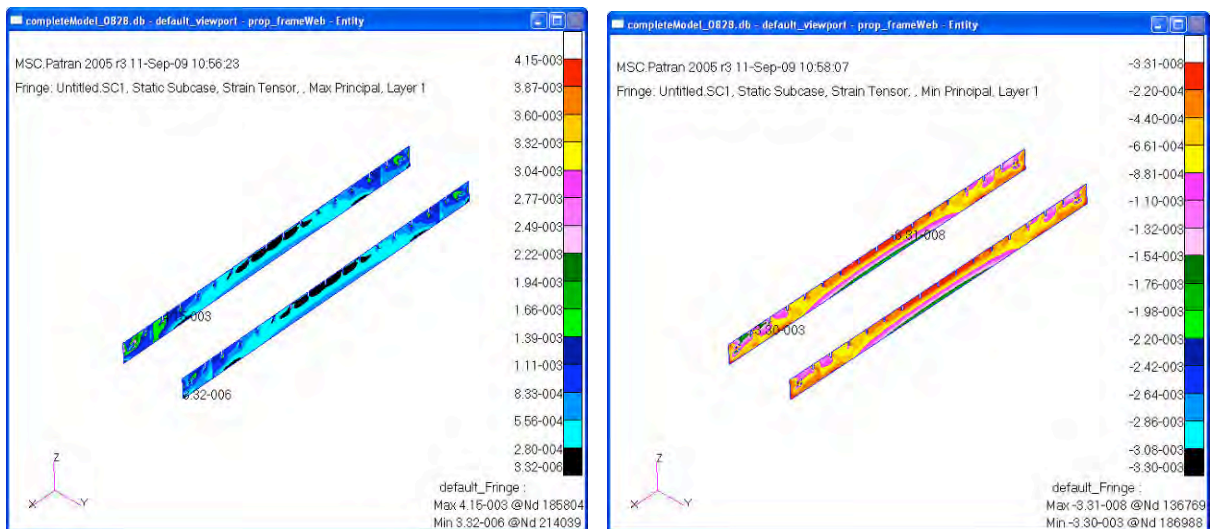
Figure 30 and Figure 31 show maximum and minimum strain for stringers and frames. The max/min principal strains are at approximately 3100 micro-strain for stringers and 4100 micro-strain for frames:



(a) Min Principal Strain

(b) Max Principal Strain

FIGURE 30. PRINCIPAL STRAINS FOR STRINGERS



(a) Max Principal Strain

(b) Min Principal Strain

FIGURE 31. PRINCIPAL STRAINS FOR FRAME WRAPS

Figure 32 shows the minimum principal strain for the PRSEUS rods. Figure 33 shows Von Mises stress for the aluminum doubler blade. The max stress is approximately 38.9 ksi, which is below the 7075-T3 material allowable of 59 ksi for the doublers.

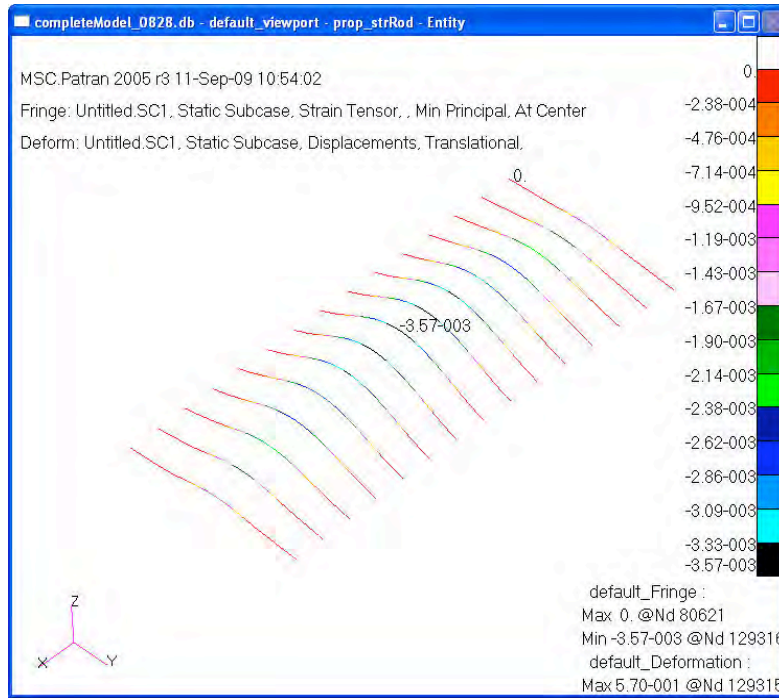


FIGURE 32. MINIMUM PRINCIPAL STRAIN FOR PRSEUS RODS

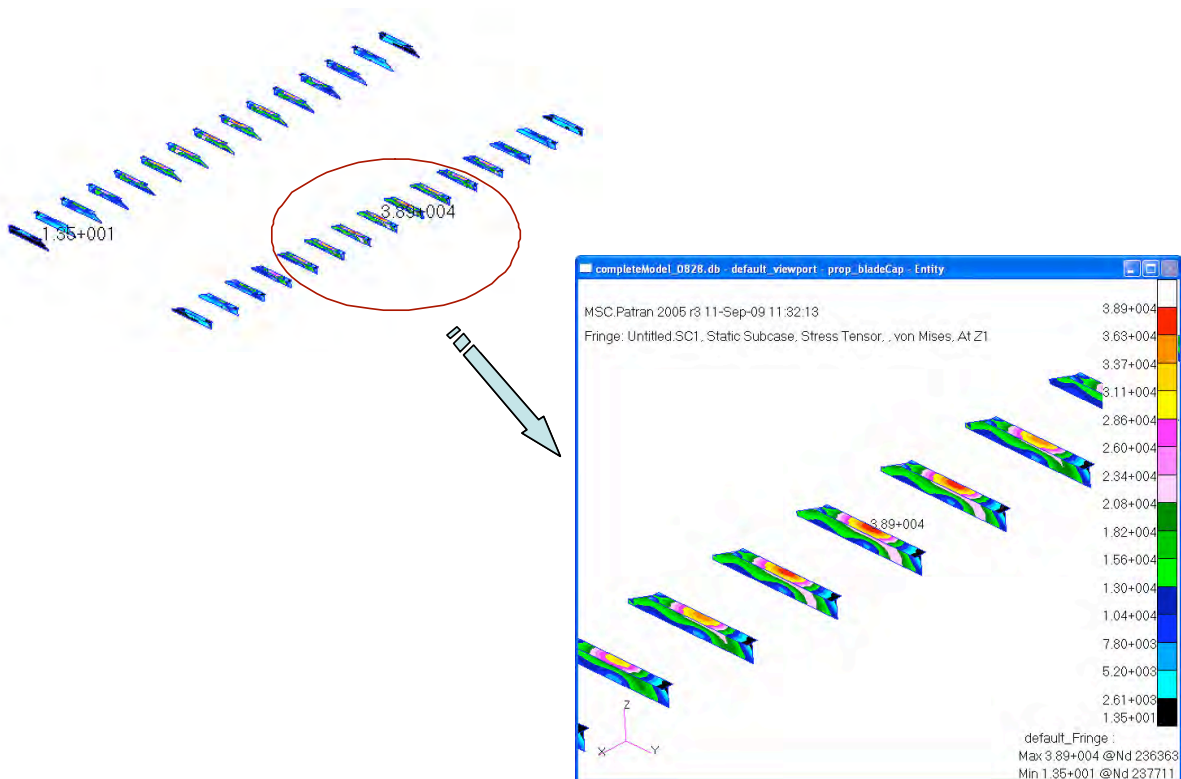


FIGURE 33. VON MISES STRESS FOR ALUMINUM DOUBLER

accommodate different preform geometries in much the same manner as the cure tool can be. To meet this challenge, a prototyping subtask was added to the stitching tool development task to study whether a modular tooling methodology could be developed and implemented for the full-sized stitch tool.

Modular Stitch Tool Development - The primary objective of the modular tool design development activity was to validate whether a flexible stitching tool could be developed that would accommodate variable panel geometries without requiring extensive modifications to the tooling. While such a premise is fairly simple to implement for the cure tool, because the IML tooling has been eliminated, it is not obvious how a variable geometry panel could be accommodated in the rigid indexing approach commonly used for the stitch tool; where stringer placements are held by the machined edges of the base plate, which locate the split polyurethane mandrels (Figure 35), and frames members that contact the base plate directly.

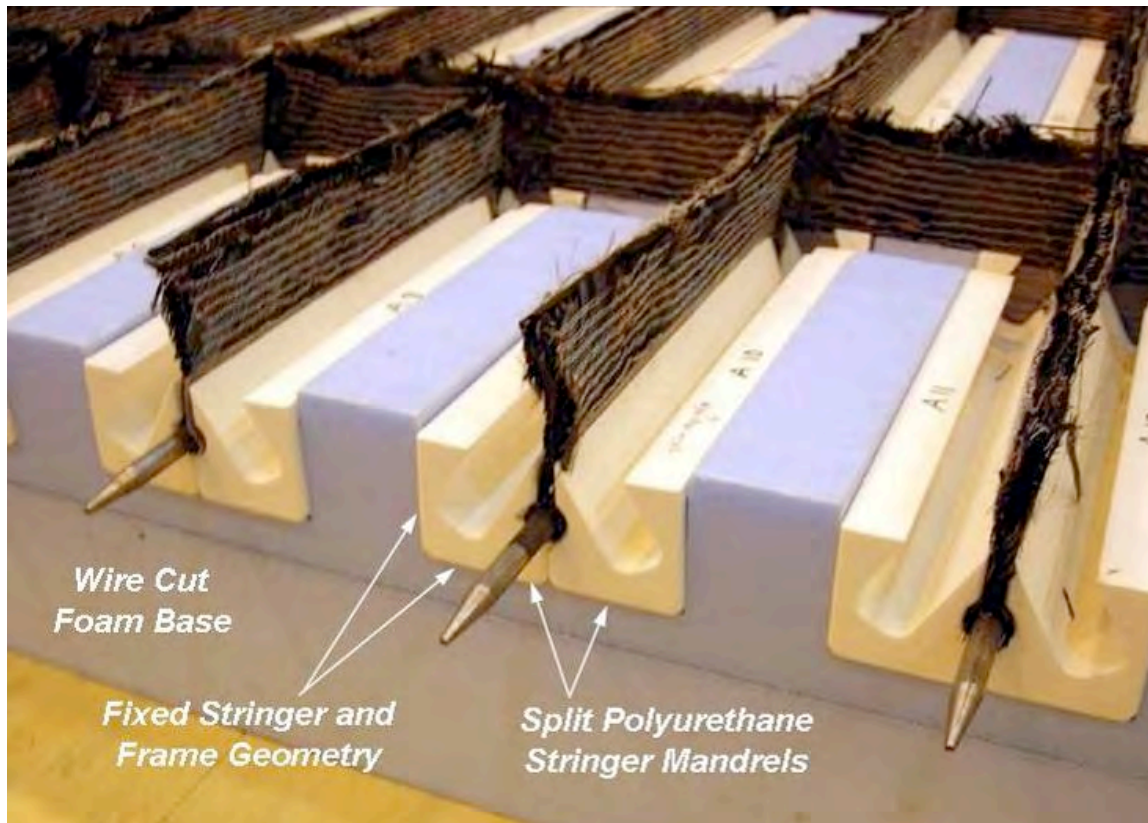


FIGURE 35. CONVENTIONAL STITCHING TOOL DESIGN

As long as the stringer and frame spacing remains constant, this conventional approach works well, and even permits some flexibility to change skin gauges and/or add doubler stacks to the preform without affecting the tooling. While this is more flexible than most composite molding processes, more could be done to get closer to the inherent advantages realized in the tool-less IML cure tool. Thus, if the preform tool could be adjustable, then a new realm of design and fabrication flexibility could be realized across the fabrication spectrum. Such thinking led to the modular tooling approach depicted in Figure 36. By using a common block design at the intersection points, between the frames and stringers, and by filling in the distance between those blocks with spacers, then a new method of adjustment would be capable of supporting changes in stringer or frame placement without expensive modifications to the tooling.

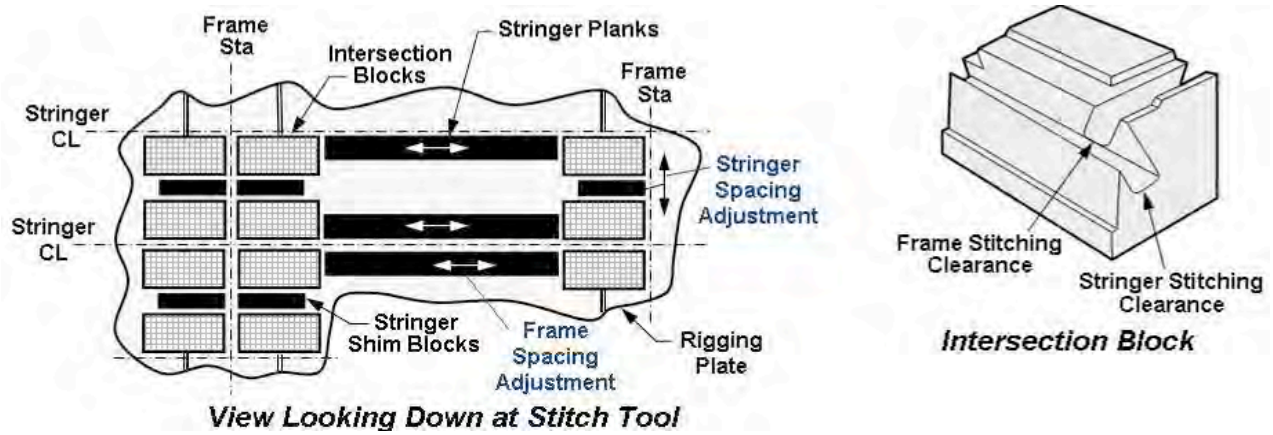


FIGURE 36. MODULAR TOOLING DESIGN APPROACH

This modular tooling scheme also supports changes in the z direction, as frame height changes could be accommodated using the height blocks depicted in Figure 37. The blocks and spacer plates would all be fastened down to a rigging plate to hold their true position before ultimately being flipped upside-down to transfer the stitched preform to the cure tool.

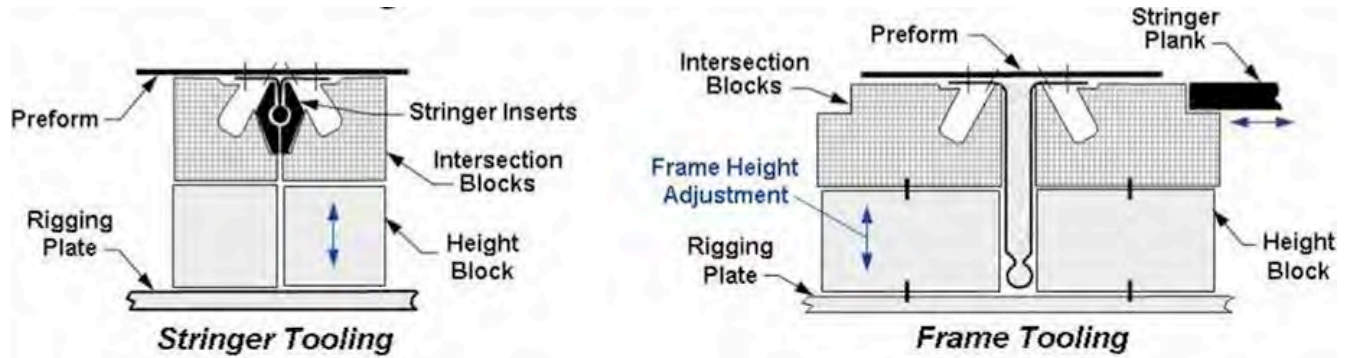


FIGURE 37. FRAME HEIGHT ADJUSTMENT SCHEME

To demonstrate this new tooling approach, a wooden mock-up tool for a single stringer-and-frame panel was created (Figure 38) where all the essential features of the new modular approach were included. The intersection blocks are indexed to grooves in the rigging plate and able to slide along those grooves to permit changes in stringer pitch, while different length stringer planks would be added to accommodate changing frame pitch. Many of the fundamental stitching tool features, such as split fall-away stringer inserts, and channels for needle penetration are carried over from the original design (Figure 35).

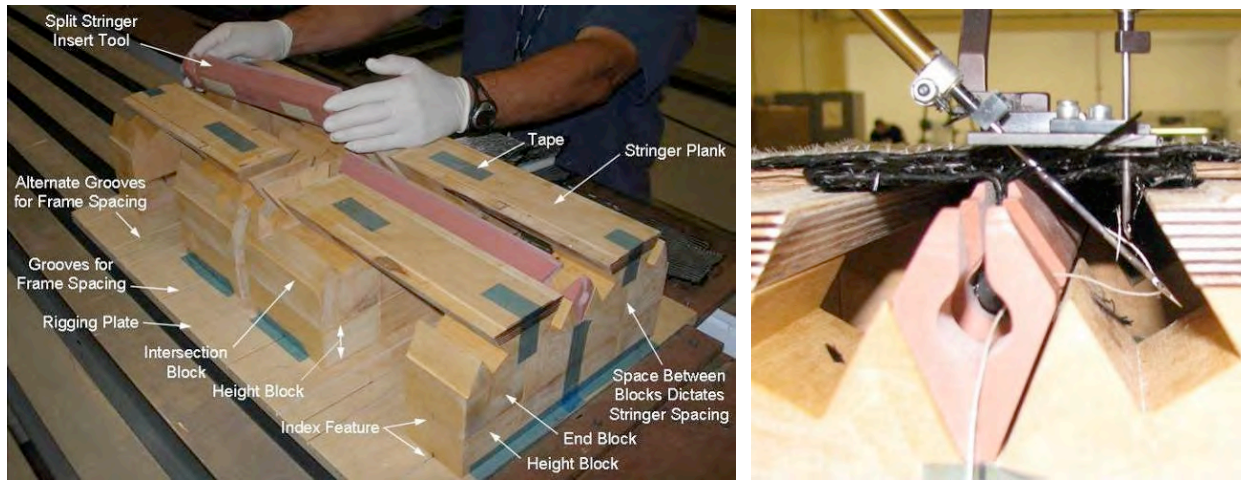


FIGURE 38. MODULAR PROTOTYPING TOOL

Once the modular blocks were located on the rigging plate and taped in place, the dry fabric frame and stringer elements of the PRSEUS panel were loaded into the slots, covered with tear straps and skin stacks, and then stitched together to build the prototype preform (Figure 39).

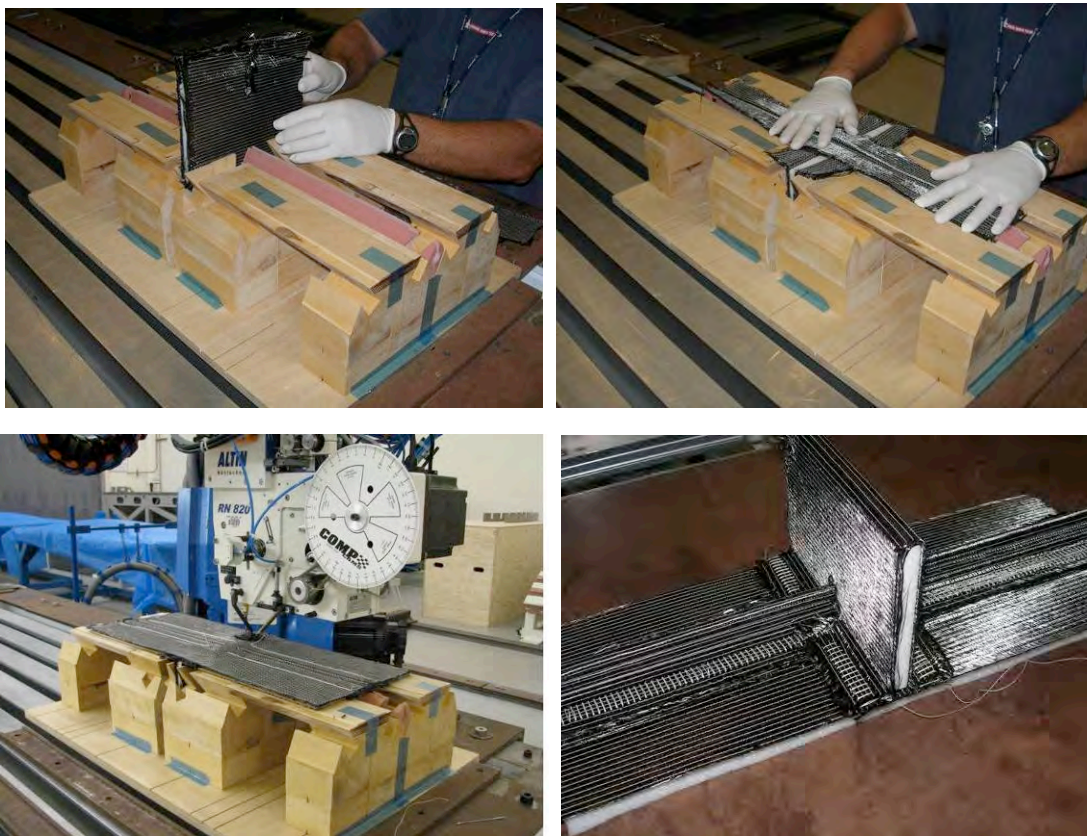


FIGURE 39. SINGLE PREFORM STITCHING

The overall results of the modular stitching tool were very encouraging. The study demonstrated that changes in frame and stringer pitch, thickness changes (skin, stringer, frame), and frame height could be accommodated without requiring extensive modification of the tooling. This simple demonstration validated that the modular approach would work, but more importantly it

identified some of the important scale-up issues that had to be addressed for the larger panel stitching tool:

1. Revise stringer plank surface to flat; add shims to support the skin IML between stringers.
2. Eliminate stitching grooves in stringer insert tools at ends; clearance not required.
3. Account for the frame flange joggle at the stringer intersection.
4. Add tooling block lock-down features.
5. Make the block height block constant; shim intersection blocks if required.
6. Improve frame flange support near stringer web if possible.
7. Incorporate a cut-away foam frame to support the stringer rods during infusion.
8. Add thread tie-down features to the edge of rigging base.
9. Add an alignment point on the assembly jig (AJ) to index the stitching head.
10. Longitudinal tool edges need to support tie down strapping.
11. Add swivel points to each end of the AJ for preform transfer.
12. Add index locators to align block segments so the stringer inserts are aligned.
13. Frame slot depth in AJ should be sized to bottom out foam and remove fiber bulk.
14. Identify all blocks so the tool can be reassembled the same way every time.

Stitch Tool Design and Fabrication - Incorporating the lessons learned from the prototyping exercise, led to a further evolution in the intersection block design. The primary differences being a combination of the left and right-hand blocks into a single unit, modifications to the step arrangement to simplify the stringer plank design, and finally incorporation of the bolt, or hold-down feature into the block design (Figure 40).

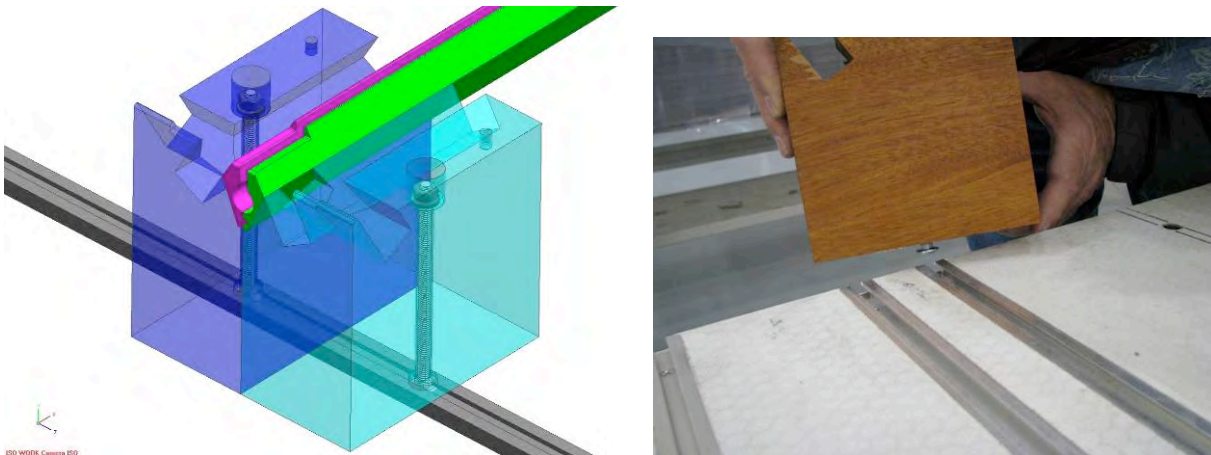


FIGURE 40. MODIFIED INTERSECTION BLOCK GEOMETRY

Although the mechanical aspects of the stitching tool mirror those of the prototype design, some new features were added to facilitate the handling of larger preforms. The rigging plate is now supported by a table constructed of lightweight honeycomb sandwich panels assembled in an egg-crate configuration (Figure 41). Lift rings, a swivel axis, and locating pins were added to facilitate preform transfer onto the cure tool using a production-like scheme.

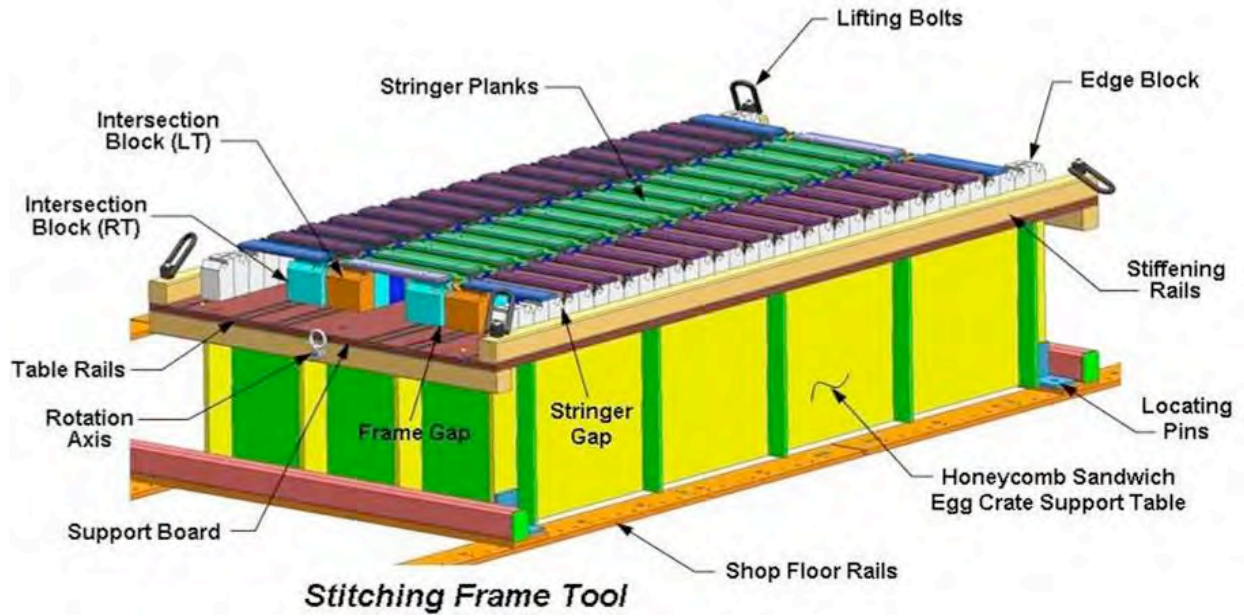


FIGURE 41. STITCH TOOL DESIGN MODEL

The completed stitching frame tool (Figure 42) was fabricated by Harbor Patterns Inc., Los Alamitos, CA.



FIGURE 42. BLOCK RIGGING ON COMPLETED STITCH TOOL

Cure Tool Design and Fabrication - The cure tool establishes the OML of the part and locates the stringer and frame members around the perimeter of the panel. Because the PRSEUS process utilizes a self-supporting preform fabrication method that is devoid of interior moldline tooling the actual cure tool is relatively simple (Figure 43). Resin grooves and inlet/outlet ports are machined into the table surface, as are tooling holes for locating the frame and stringer support bars. Two sets of location holes are added, one for the compression panel, and one for the pressure panel.

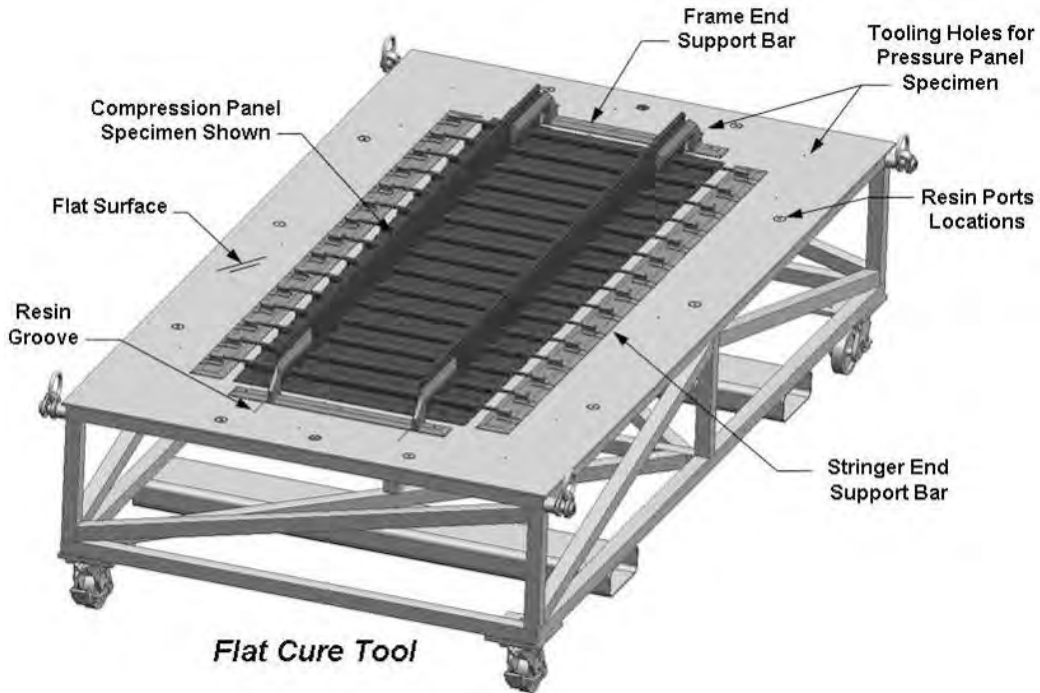


FIGURE 43. CURE TOOL DESIGN MODEL

The cure tooling was fabricated by Process Fab Inc., Santa Fe Springs, CA and delivered to Boeing Huntington Beach in November 2009. The rolling flat table surface with the rigged tooling details for locating the frame and stringer elements is shown in Figure 44.

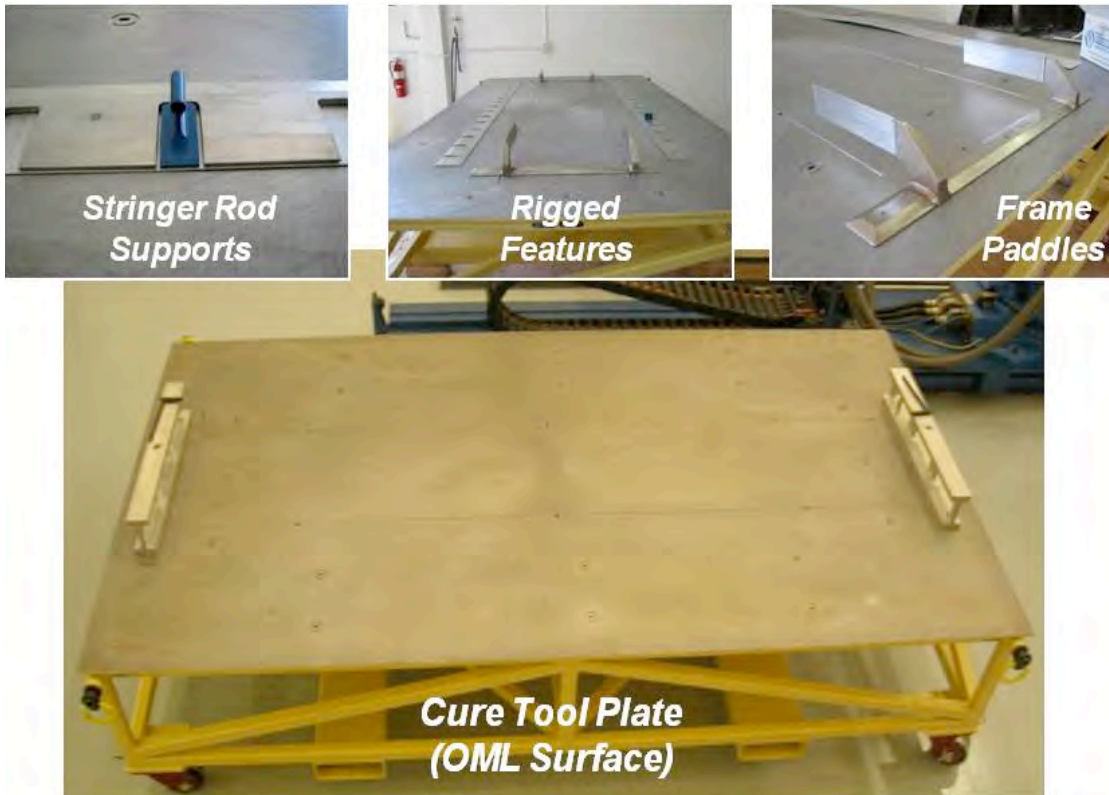


FIGURE 44. COMPLETED CURE TOOL

2.4 Panel Fabrication

The manufacturing approach for the PRSEUS pressure panel was based upon 20 years of experience in dry fiber preform construction and resin infusion processing at the Boeing Company. No new technology development took place during the fabrication of the panel. The carbon fiber warp/knit multi-axial fabrics and Vectran sewing thread used to build the preform was originally developed under the NASA AST Composite Wing program in the 1990's. The one-sided robotic stitching technology used to assemble the integrally stiffened dry fiber preform was invented in Germany in 1998 and further developed by Boeing over the last several years. The controlled atmospheric pressure resin infusion processes (CAPRI) used to infuse the preform was invented by Boeing in 1999. The pultruded carbon fiber rods used to stiffen the preform were developed by Lawrie Technologies for Boeing over the last two years. Recent developments by Boeing in soft tooling to improve vacuum bag installation and part quality were applied.

Fabrication of the preform and subsequent resin infusion processing took place in the Marvin B. Dow Stitched Composite Development Center at Boeing's Huntington Beach facility. The center contains over 5000-sq. ft. of clean room space for preform fabrication with robotic stitching and CNC ply cutting capability. Resin infusion processing took place in the adjacent shop area utilizing Advanced Processing Technology's (APT) servo rotary dispensing machine. This piece of equipment automatically degasses, meters, mixes and delivers the resin at temperature and pressure to the mold tool for infusion of the dry fiber preform. Curing of the part took place inside the development center's 32-ft. long walk-in oven.

The preform fabrication process began with the creation of flat patterns off of the engineering CAD models for the individual skin, frame and stiffener details. The flat patterns were nested to maximize material utilization and were cut out of 1.4-meter wide fabric using a CNC ply cutting table as shown in Figure 45. The individual pieces of fabric were then kitted and forwarded to the next subassembly for formation of the stiffener and frame preform components.

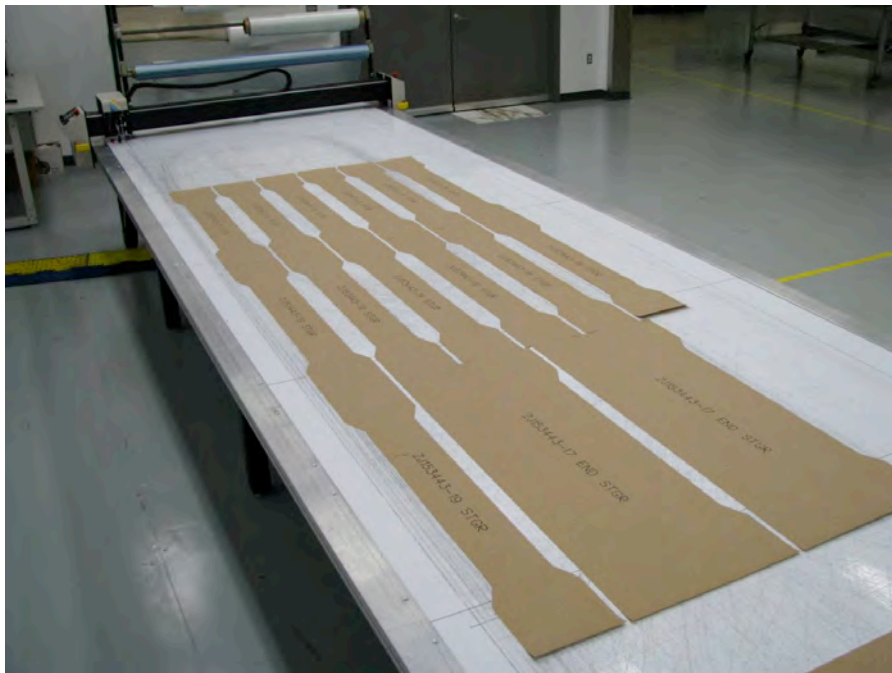


FIGURE 45. NESTED AND CUT FLAT PATTERNS FOR STRINGERS

Fabrication of the stringer preforms took place on a two-sided lock stitching sewing machine of a gantry type configuration. The stringer web ply stack was placed inside a rectangular stitching frame in the open (flat) condition. A small diameter steel cable (wire rope) was positioned along what was to be the top or bulb feature of the stiffener as shown in Figure 46. The fabric was then folded over to encapsulate the steel cable which was later used as a leader to pull a carbon fiber rod through the preform during panel assembly. The free edges of the web stack were clamped to the perimeter frame to prevent movement of the fabric during the sewing process. Two seams of stitching were inserted into the web of the collapsed stiffener. One seam was placed near the top of the stiffener web to establish the bulb feature. A second seam was placed near the base of the web at the tangent point of the web-to-flange radius shown in Figure 47.



FIGURE 46. STIFFENER PREFORM FABRICATION



FIGURE 47. STITCHED STIFFENER PREFORMS WITH LEADER WIRE INSTALLED

Fabrication of the frames started with the bonding of fiber glass laminated inserts into the CNC machine Rohacell foam core details. Net cut frame web ply stacks were then hand layed up over the core and secured in-place using a pneumatic staple gun as shown in Figure 48.



FIGURE 48. FRAME PREFORM ASSEMBLY SEQUENCE

Final assembly of the dry fiber preform for the integrally stiffened pressure panel was accomplished utilizing an assembly jig. The AJ replicated the inner mold line of the panel using a series of wood blocks positioned over a flat base structure. The frame preforms with rigid foam core were installed to the jig first followed by the installation of the stiffener preforms as shown in Figure 49.



FIGURE 49. FRAME AND STIFFENER INSTALLATION INTO PREFORM ASSEMBLY FIXTURE

Precured, pultruded carbon fiber epoxy rods were then pulled into the stiffeners using the “pre-installed” steel leader wires inside each stiffener perform as shown in Figure 50. Pulling the rod through the stiffener preform simultaneously formed the bulb feature of the stiffener and located the stiffener inside the keyhole feature of each frame web. The flanges of the frames and stiffeners were then folded down flat against the corresponding feature in the AJ.



FIGURE 50. PULLING OF RODS INTO STIFFENER PREFORM

Three dimensional woven dry carbon fiber fillets fabricated by Bally Ribbon Mills were utilized at the base of the stiffener web. The fillets were cut to length and secured to the stiffener using a hand tack stitch near each frame flange as shown in Figure 51. Next skin doublers and tear straps were positioned over the frame and stiffener flanges as shown in Figure 52. This was followed by the installation of the base skin stack as shown in Figure 53.

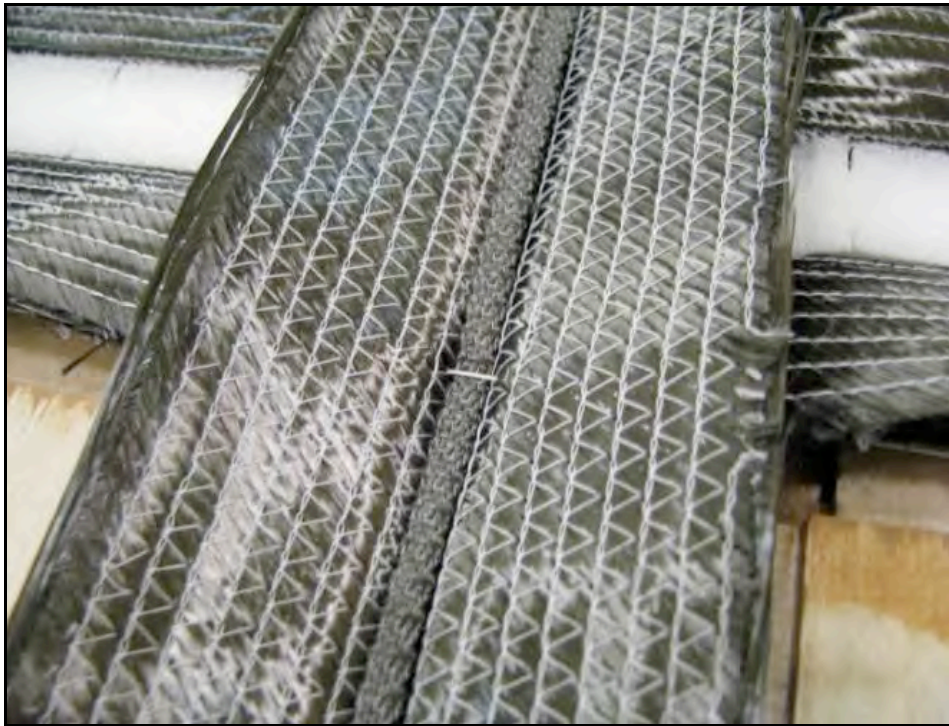


FIGURE 51. STIFFENER FILLET INSTALLATION

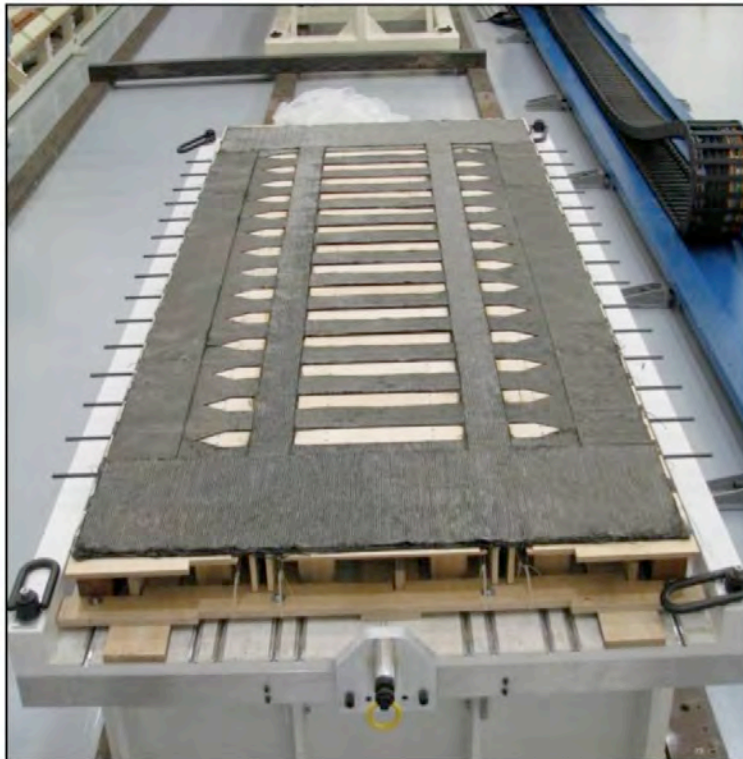


FIGURE 52. SKIN DOUBLER INSTALLATION COMPLETE



FIGURE 53. SKIN INSTALLATION COMPLETE

A six-axis robotic stitching system was used to insert seams of stitching to join the flanges of the frames and stiffeners to the skin shown in Figure 54. The one-sided sewing process utilizes a two needle sewing machine specially designed to produce a modified single thread chain stitch. Open channels in the preform AJ provide clearance for the sewing needles as they exit the bottom surface of fabric during seam installation. A 1200d Vectran sewing thread was used for final assembly stitching of the dry fiber preform. The stitched preform was then transferred to the mold tool using an over head crane seen in Figure 55. Banding straps were used to secure the preform to the AJ. The AJ with preform was then lifted and rotated 180 degrees and mated to the mold tool shown in Figure 56. The banding straps were then cut and the AJ was removed leaving the stitched preform deposited on the mold tool depicted in Figure 57.



FIGURE 54. ROBOTIC STITCHING OF DRY FIBER PREFORM ASSEMBLY



FIGURE 55. LIFTING OF AJ AND PREFORM USING OVERHEAD CRANE



FIGURE 56. AJ MATED TO MOLD TOOL DURING PREFORM TRANSFER



FIGURE 57. PREFORM DEPOSITED ON MOLD TOOL AFTER TRANSFER

Resin infusion processing of the stitched dry fiber preform was accomplished using the Boeing patented Controlled Atmospheric Pressure Resin Infusion process (CAPRI). A rigid steel mold tool was used to define the flat outer mold line surface of the panel. The panel's inner mold line surface was soft tooled using a nylon vacuum bag and rubber bagging aid details shown in Figure 58 and Figure 59. Stringer and frame positions were maintained using hard tooling pinned to the rigid outer mold line tool. The dry fiber preform was infused through-the-thickness from the outer mold line to the inner mold line. The Hexcel VRM34 resin was prepared and dispensed to the mold using Advanced Processing Technology's Servo Rotary Dispensing machine. This machine automatically degasses, meters, mixes and delivers the resin at a predefined temperature and pressure. Nylon tubing was used to transport the resin from the machine to grooves in the face of the mold tool. Flow media allocated over the mold tool distributed the resin across the surface of the preform. Active vacuum was applied to the mold near the outer perimeter of the part to remove all air molecules from the mold with the dry fiber preform inside prior to resin infusion processing. Resin infusion processing took place inside a walk-in oven at 140°F. Once infusion of the preform was complete the panel was then cured at 200°F for five hours. The nylon vacuum bag and inner mold line tooling details were next removed from the panel. The panel was then post cured at 350°F for two hours. Final part trim took place on a CNC machine to remove the 1.0-in. of excess material from the edges of the panel shown in Figure 60 and Figure 61.



FIGURE 58. SOFT TOOLING (BAGGING AIDS) INSTALLATION OVER STIFFENERS



FIGURE 59. VACUUM BAG INSTALLATION OVER DRY FIBER PREFORM



FIGURE 60. RESIN INFUSED NET MOLDED PANEL



FIGURE 61. "AS MOLDED" IML FEATURES OF PRSEUS PANEL

2.5 Pressure Restraint Fixture

The Pressure Vessel Restraint Fixture was designed and manufactured by ASC Process Systems in Sylmar, Ca. and is shown under production in Figure 62 and completed in Figure 63. This fixture weighs approximately 3800 lbs and its dimensions are I.D. 40 x L 115.5 x W 55.5 x H 49.25 inches. This fixture complies with Boeing ICD DWG ZJ153435 and Pressure Vessel Requirements Specification ZA153438 which detailed major interfaces, handling and access features, and requirements for installation of the PRSEUS panel specimen.



FIGURE 62. PRESSURE RESTRAINT FIXTURE DURING FABRICATION

This all-steel and welded assembly (Figure 13) is a semi-circular shell with end plates supported by a by 1-inch upper flange. Several welded stiffening plates on the sides, ends, and underneath the vessel help reduce local deflections. This fixture is designed to withstand a maximum internal pressure of 40 psi with a margin of safety greater than two. There are two elliptical openings in this fixture that allow for a technician to work from inside the tank. The man hole opening is 15.5 by 19.5 inches and the air vent hole opening is 12.5 by 16.5 inches. These openings allow for an average person access into the vessel after the panel has been installed as demonstrated in Figure 64.



FIGURE 63. PRESSURE RESTRAINT FIXTURE AS DELIVERED



FIGURE 64. FIXTURE MANHOLE OPENING

Other features on this restraint fixture include, a compressible rubber seal shown in Figure 65, a 1 by 3 inch wire harness feed thru-hole shown in Figure 66, lift hoist rings, forklift provisions, lockable steel casters, and drain provisions.

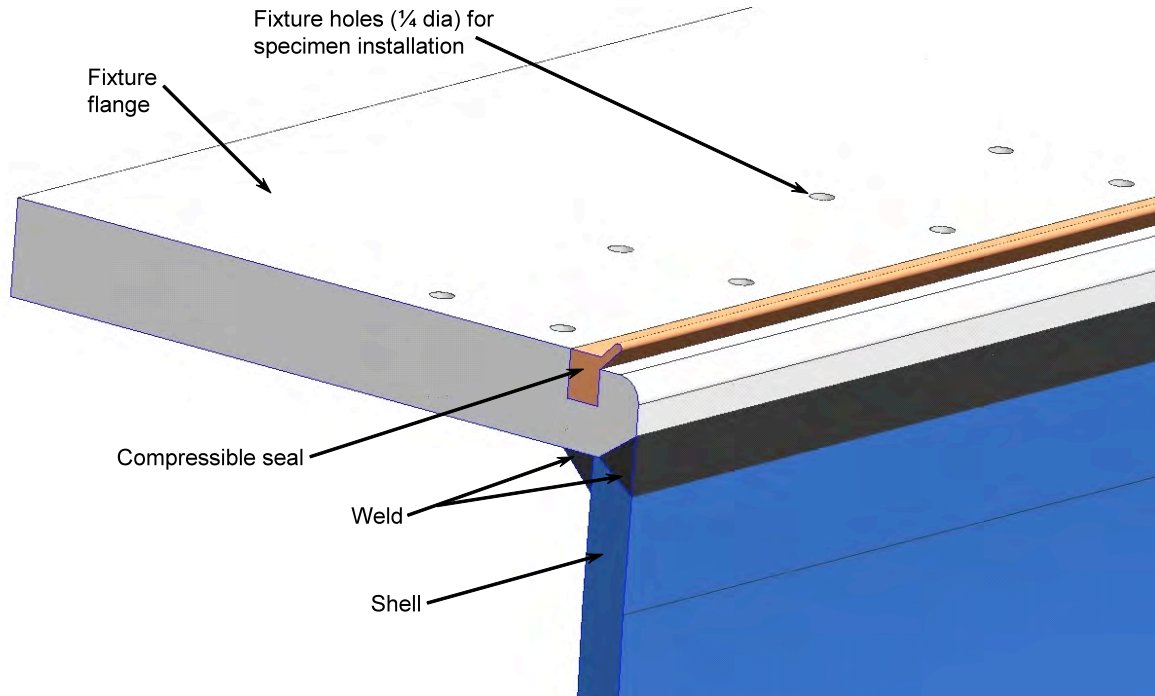


FIGURE 65. COMPRESSIBLE SEAL ON FIXTURE FLANGE

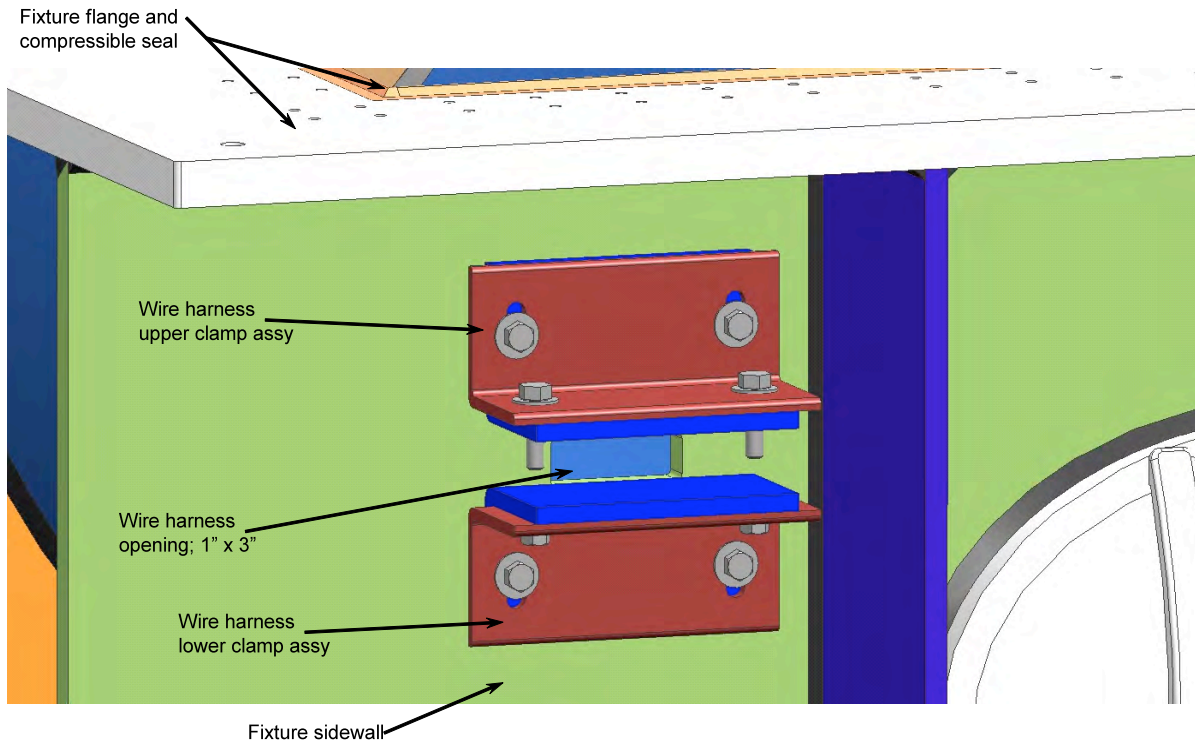


FIGURE 66. WIRE HARNESS PROVISIONS

A bench test of the wire harness configuration was conducted by ASC Process Systems by feeding 100-3 strain gage wires thru the foam and clamp angles shown in Figure 67. A soap and water mixture was sprayed and air pressure at 40 psi was applied to test for air leaks. No leaks were evident or present between the twisted wire bundles. Application of PR1422 or RTV sealant from inside the tank will be required to completely seal out between the wires.



FIGURE 67. WIRE HARNESS PROVISIONS BENCH TEST

The panel specimen is attached to the pressure vessel flange with 240 NAS fasteners. Two rows of $\frac{1}{4}$ dia bolts along each edge effectively constraining the panel edges to be fixed-ended in bending with help from the external stiffeners. Each frame end is attached by an internal clevis fitting using a bolted connection with four $\frac{3}{8}$ diameter NAS bolts as shown in Figure 68.

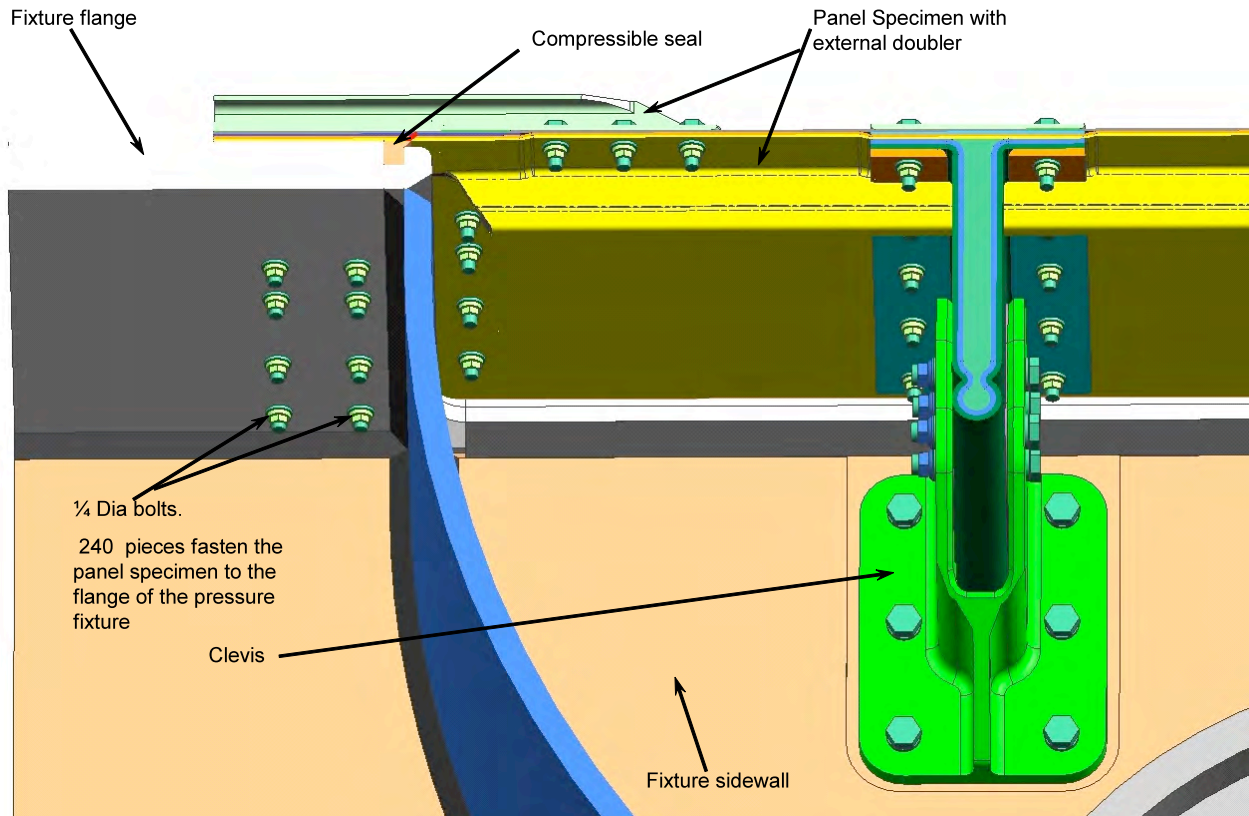


FIGURE 68. PANEL SPECIMEN ON PRESSURE RESTRAINT FIXTURE

The 240, 1/4 dia holes on the 1 inch thick flange are spaced adequately and to tight tolerances such that a drill template was not needed when drilling the panel specimen as shown in Figure 69 and Figure 70. This eliminates any drilling and hole location errors that would have occurred when transfer drilling many holes due to the excessive handling.



FIGURE 69. PANEL DRILLING USING 90-DEG DRILL



FIGURE 70. PANEL DRILLING USING STANDARD GUN DRILL

Placement of the pressure gage, safety relief valve, pressure transmitter and wire port, as identified in Figure 71, required avoiding interference with panel specimen installation and allowing accessibility in the shop working environment, during transportation and for conducting testing.

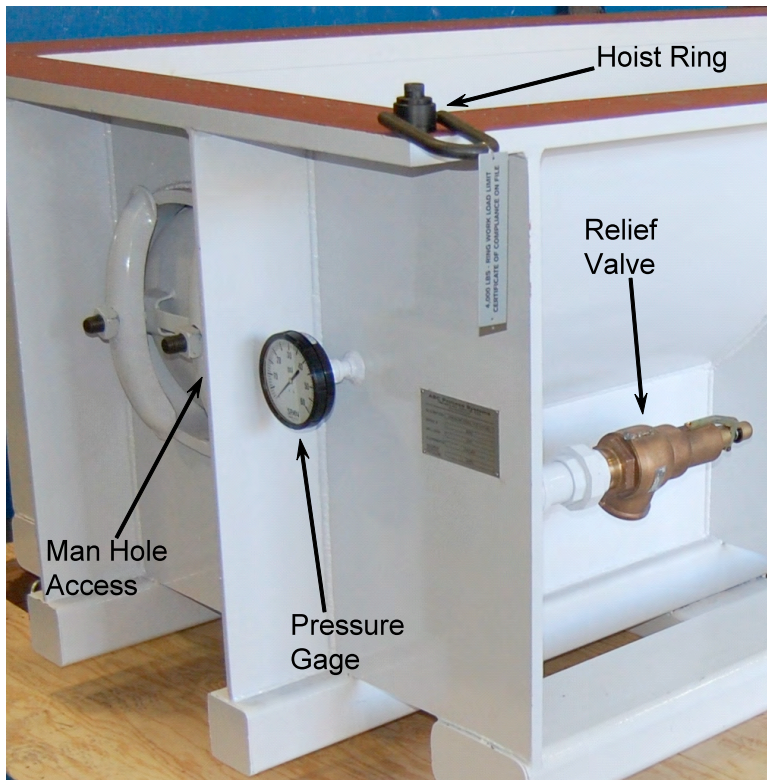


FIGURE 71. PRESSURE RESTRAINT FIXTURE

2.6 Specimen Preparation

The final pressure panel as-fabricated is shown in Figure 72. The panel was then machined to the test configuration to fit into the pressure vessel by an outside supplier as shown in Figure 73. The perimeter was trimmed to 48-in by 108-in. The frame ends were machined clean and square to the IML plane and the stringers were machined back from the panel edge.



FIGURE 72. AS-FABRICATED PRESSURE PANEL



FIGURE 73. TRIMMED PRESSURE PANEL

The stringers are cut back at the base 4.4-in from the panel edge and machined at a 30-degree angle from the vertical. The stringer webs are machined flush with the panel's IML surface to form the surface that will mate with the pressure vessel flange as shown in Figure 74. The composite panel IML and pressure vessel flange interface was then checked for fit and flushness when mated as shown in Figure 75.

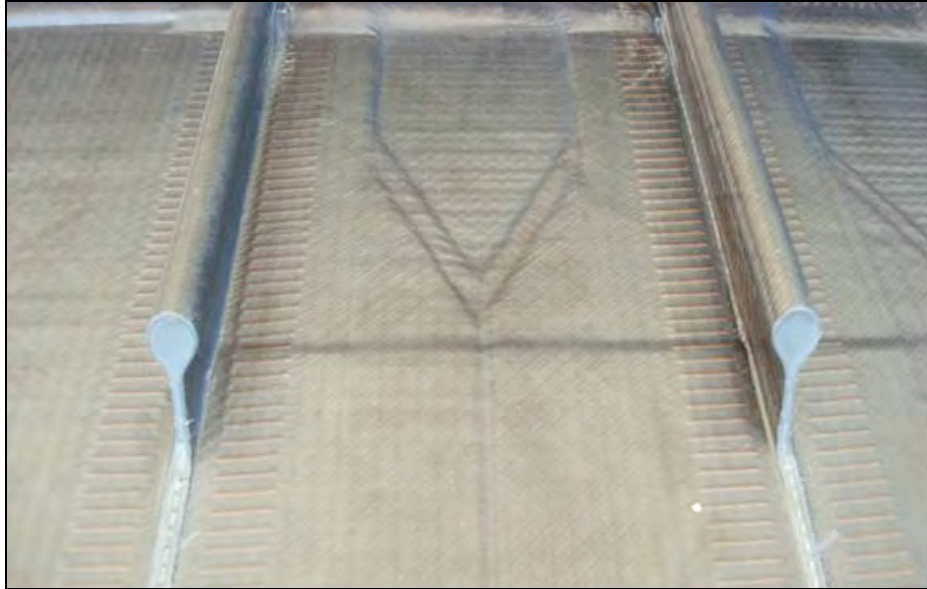


FIGURE 74. CLOSE-UP OF TRIMMED STRINGER



FIGURE 75. PANEL MATED TO THE PRESSURE VESSEL

After mating the panel with the pressure vessel, ten individual aluminum doublers were placed around the perimeter of the panel to form a strong interface for attachment to the pressure vessel. The doublers were precisely positioned on the composite panel and clamped securely in place as shown in Figure 76.

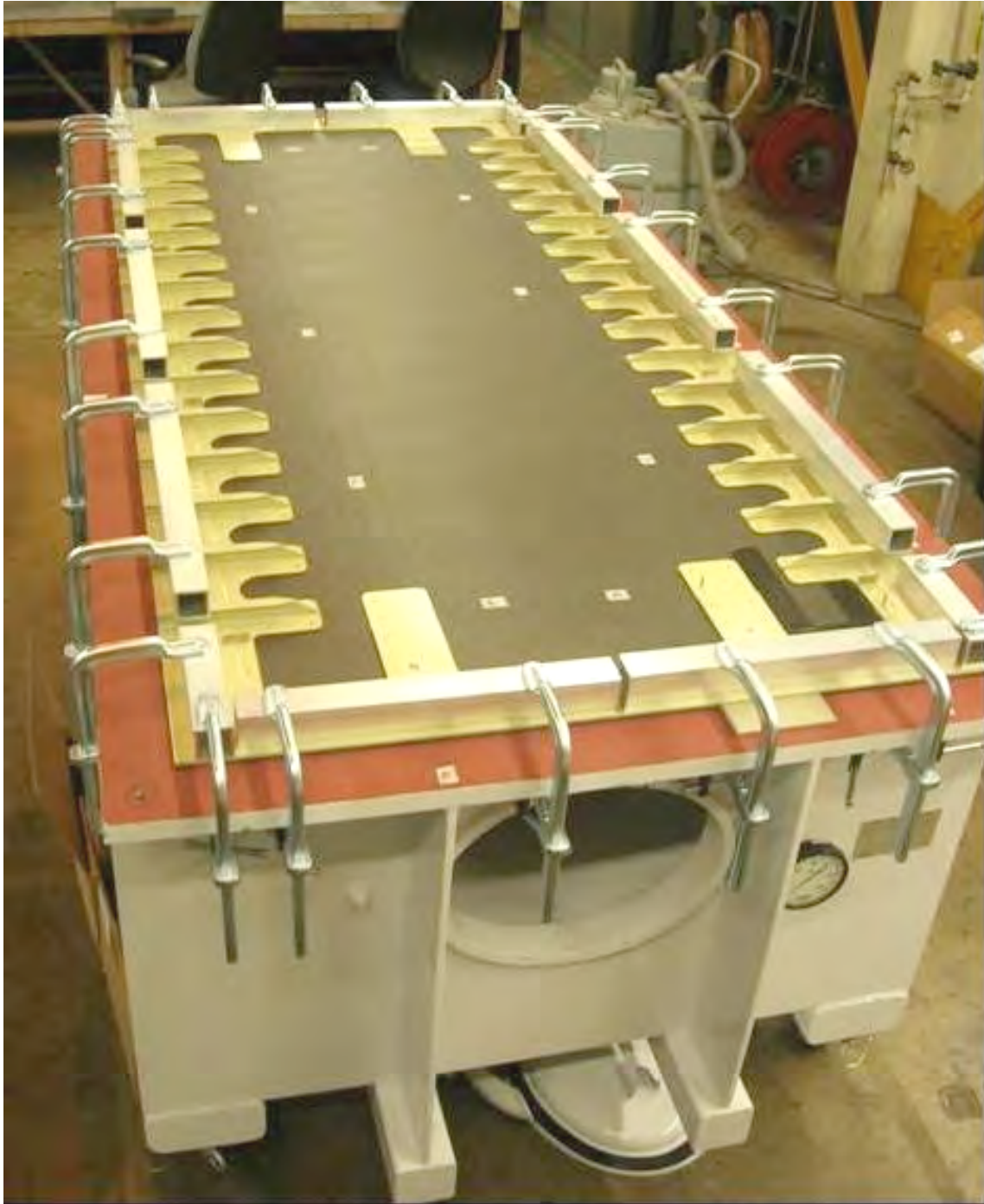


FIGURE 76. PANEL PRESSURE VESSEL WITH DOUBLERS IN PLACE

The aluminum doublers, with pre-drilled 0.156-in pilot holes, were used as a template to transfer those pilot holes to the composite panel. An egg cup and bushing were used to assure accurate, perpendicular holes through the material stack as shown in Figure 77.



FIGURE 77. PILOT HOLES IN DOUBLERS TRANSFERRED TO PANEL

After the pilot holes have been drilled through the composite panel, CLECO clamps are installed to keep the doubler and panel clamped together as shown in Figure 78. A close-up showing CLECO hole clamps in place and several doubler locating pins is shown in Figure 79. The panel was then masked and taped in preparation for grit blasting of bonding surfaces as shown in Figure 80. Figure 81 shows the bonding surfaces being grit blasted, which is necessary to promote adhesion and achieve the required bond strength between the doublers and the composite panel surface.



FIGURE 78. COMPLETION OF PILOT HOLES DRILLED THROUGH PANEL

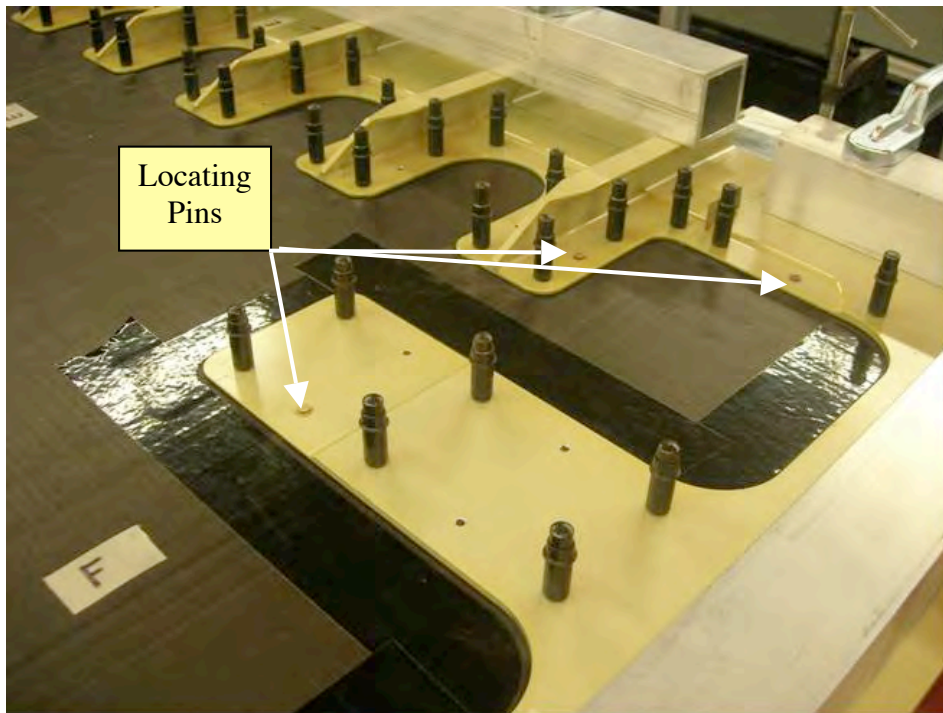


FIGURE 79. CLOSE-UP OF PILOT HOLES IN DOUBLERS



FIGURE 80. PANEL IS PREPARED FOR CLEANING



FIGURE 81. PANEL BEING GRIT-BLASTED

The adhesive used was Henkel EA9330.3 with 0.005-inch glass beads to maintain a minimum bond line thickness and is shown being applied in Figure 82 and Figure 83. The surface of the doubler was also coated with adhesive before the doubler is positioned on the panel.



FIGURE 82. ADHESIVE APPLIED TO PANEL



FIGURE 83. ADHESIVE APPLIED TO PANEL

After the doubler adhesive was cured, the panel was located for full-size hole drilling and fastener installation as shown in Figure 84. Using a drill guide and bushing to assure accurate, perpendicular holes through the material stack, the 292 pilot holes were drilled out to the full-size $\frac{1}{4}$ -inch diameter, readying the structure for fastener installation in Figure 85.

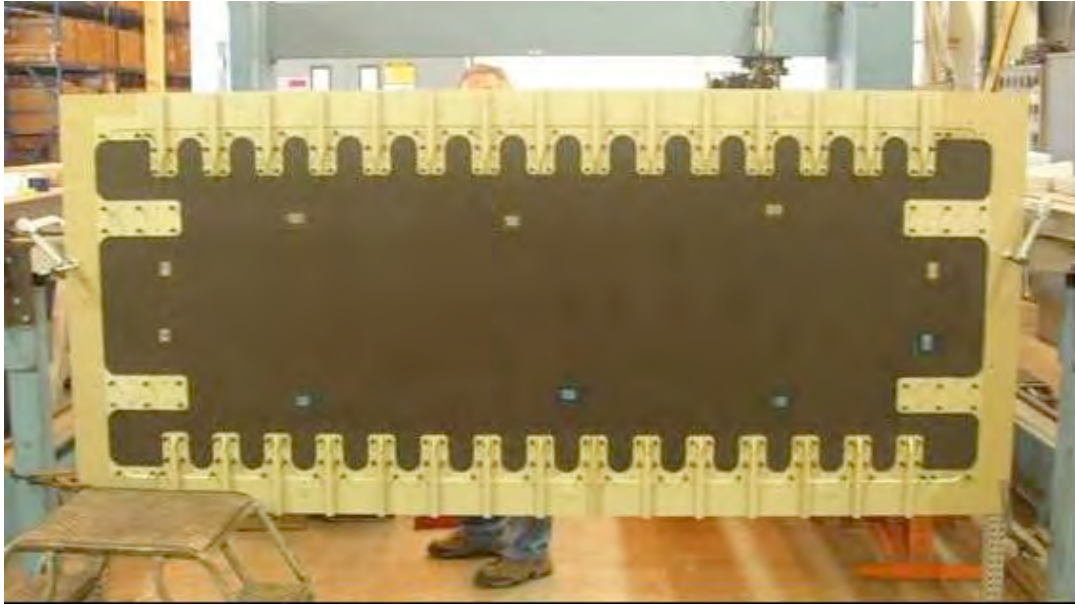


FIGURE 84. PANEL IS MOUNTED TO THE DRILLING FIXTURE



FIGURE 85. FULL-SIZED HOLES DRILLED

The NAS6403 fasteners were “wet” installed using a PRC-DeSoto PR1422 sealant to provide an air-tight installation and shown in Figure 86. Bolt heads were torqued and painted with a stripe to give a visual reference if fasteners were to loosen prior to pressure testing as shown in Figure 87.

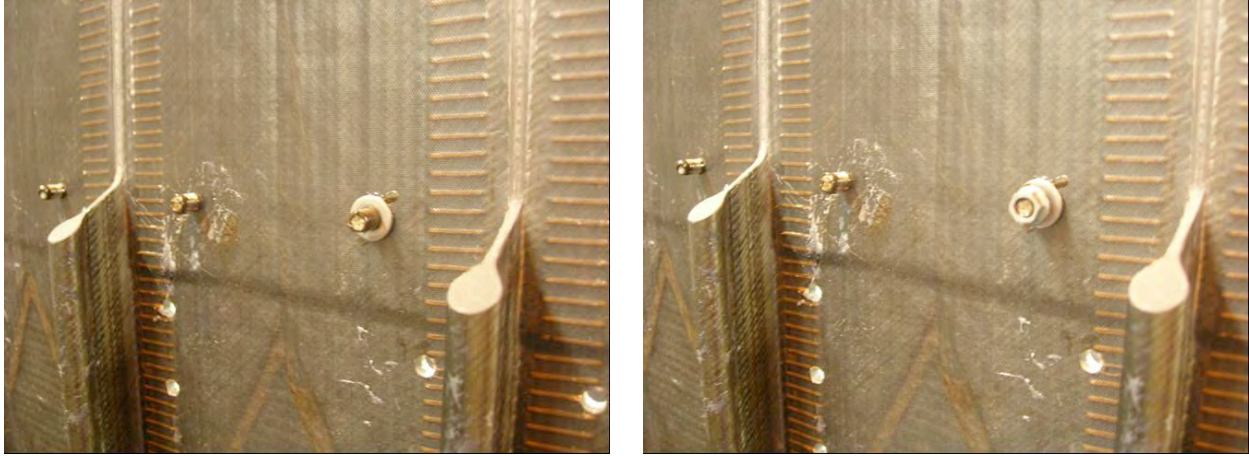


FIGURE 86. FASTENERS INSTALLED WITH SEALANT

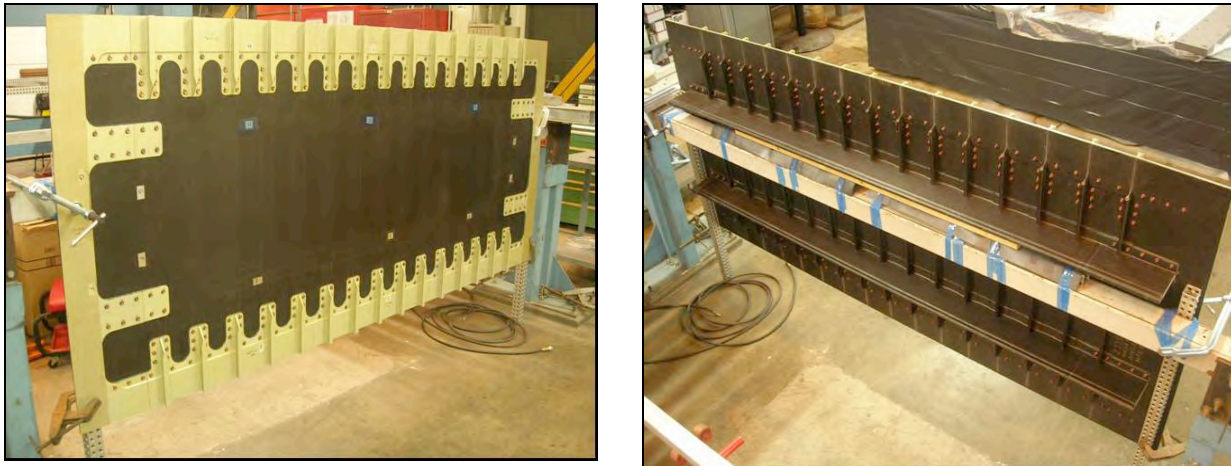


FIGURE 87. FASTENER INSTALLATION COMPLETE

2.7 Testing

The PRSEUS Pressure Panel was tested to isolate the secondary-bending effects experienced in the BWB pressure shell. This was the first time that a PRSEUS test panel was subjected to internal pressure loading. Because the 2P loading condition drives much of the BWB minimum skin gauge and stringer spacing design requirements for the shell region, this is a critical test in establishing the overall structural viability of the BWB airframe design approach.

The test specification document for this test, document number ZA153448, provides the test plan for a minimum-gauge fuselage panel that has been manufactured using resin infusion with stitched dry warp-knit fabric cured on an OML tool. The specimen, together with the pressure vessel assembly, was internally pressurized and tested at room-temperature in a dry condition at NASA Langley Research Center in the COLTS test facility.

The test specimen assembly drawing (ZJ153442/Appendix A) defines the test specimen in detail. The general configuration of the test specimen is shown for reference in Figure 88. The opening

in the fixture measures 100 x 40 inches and the outer dimensions of the test panel are 108 x 48 inches.



FIGURE 88. PRESSURE PANEL TEST SPECIMEN ASSEMBLY

The panel was tested using the sequence outlined in Table 3. The panel was first tested up to 2P without BVID to demonstrate the minimum capability of the panel. After that test, BVID was applied to the center stringer using 20 ft-lbs of impact energy. The intended impact location is shown in Figure 89. At the time that the damage was applied to the stringer, the impactor missed the intended stringer and instead hit the skin at the mid-bay and the edge of the stringer next to the center stringer as shown in Figure 91. As this impact energy was estimated to be close to the intended 20 ft-lb and the FEM results showed both stringers had similar strains, as shown in Figure 90, the test with damage was continued with the damage in the actual location without additionally impacting the original location.

TABLE 3. PRESSURE PANEL TEST LOAD SEQUENCE

Load Sequence	Load Set	Instructions	Comments
1	1P (9.2 psi)	Build pressure to 4 psi and stabilize. Then build pressure to 8 psi and stabilize, build up to test pressure of 9.2+0.1,-0.1 psi. Hold pressure at 9.2 psi for 1 minute, then depressurize	The panel is first pressurized to gather linear data. The data will be used to calibrate with analysis
2	2P (18.4 psi)	Build pressure to 9.2 psi and stabilize. Then build pressure to 16 psi and stabilize, build up to test pressure of 18.4+0.1,-0.1 psi. Hold pressure at 18.4 psi for 1 minute, then depressurize	Check 1P panel characteristics for linear behaviors. The panel will then be loaded up to 2P under pristine condition (no impact damage to the panel). The test will verify the loading capacity of minimum skin gauge design
3	2P+ (18.4 psi+)	Build pressure to 9.2 psi and stabilize. Then build pressure to 16 psi and stabilize, build up to 2P pressure of 18.4+0.1,-0.1 psi. Hold pressure at 18.4 psi for 1 minute. Then build pressure to 30 psi or till panel failure whichever reaches first. Hold for 1 minute, then depressurize if required	The panel will be impacted as defined in Section 2.2 before being pressurized. The panel will then be pressurized till final failure or 30 psi whichever reach first. This test will verify the ultimate capacities of the panel with BVID

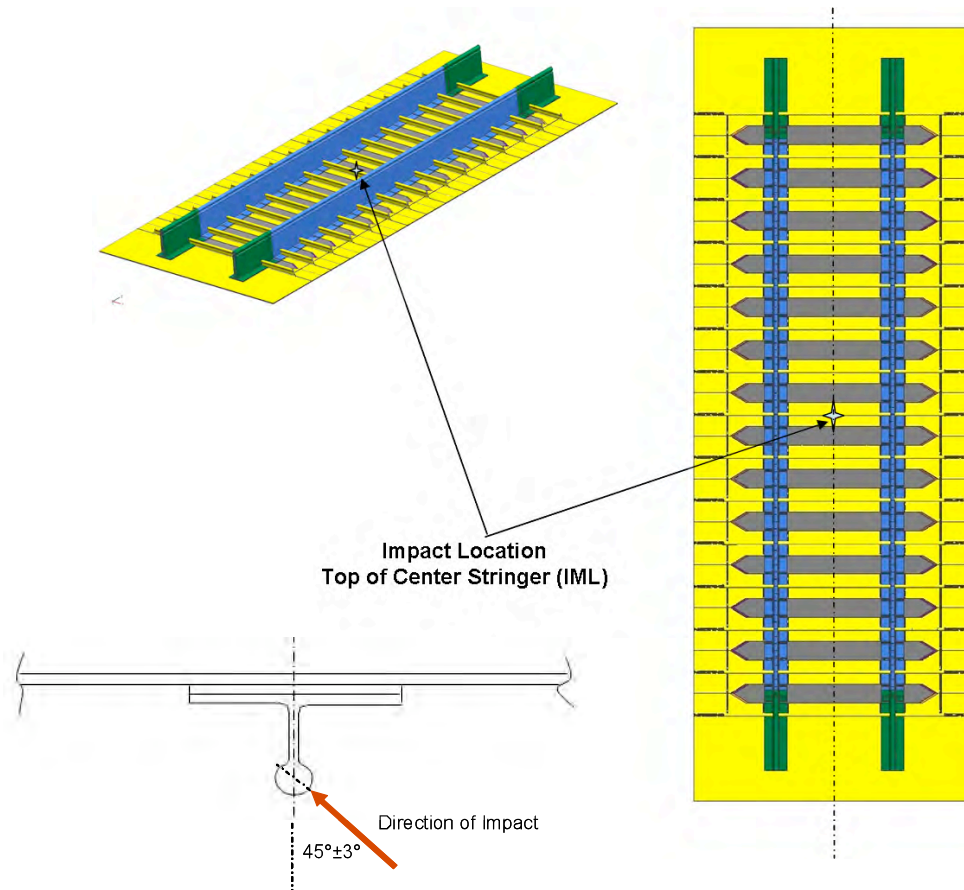


FIGURE 89. PRESSURE PANEL INTENDED IMPACT LOCATION (OML SIDE)

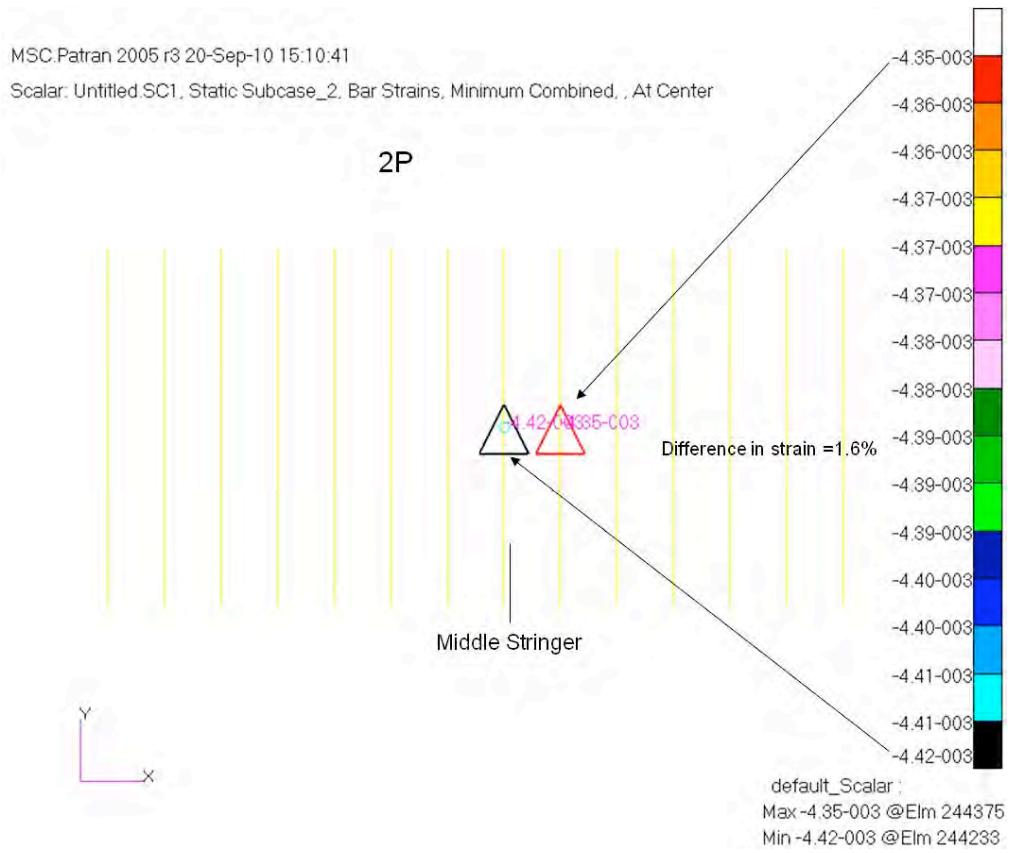


FIGURE 90. STRAIN AT MIDDLE STRINGER AND IMPACTED STRINGER SHOW SIMILAR RANGES

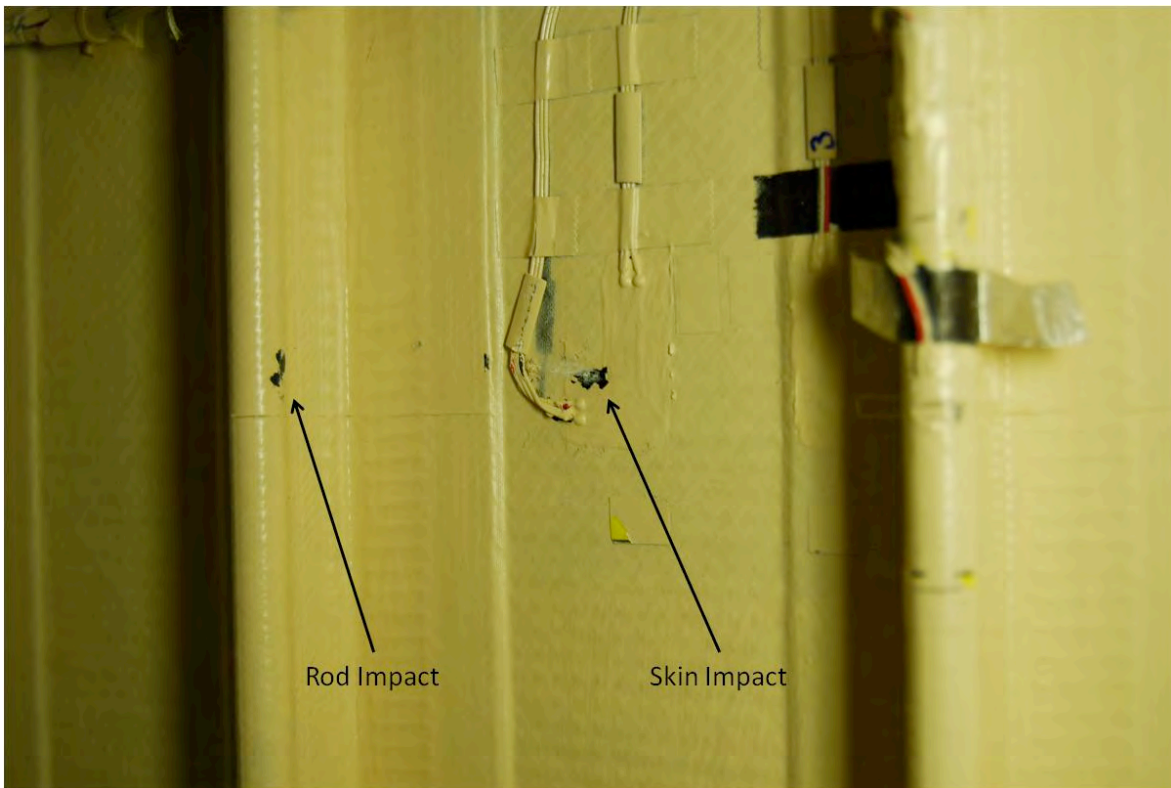


FIGURE 91. ACTUAL IMPACT LOCATIONS

In preparation for the test, the specimen interior surface was painted flat white, including skin, frame webs, stringer webs, and all flanges. The contrasting colors were used to aid in the crack propagation detection during the test. In addition, NASA LaRC applied splatter paint and set up and monitored Video Image Correlation in 3-Dimensions (VIC-3D) data acquisition to measure out of plane deflection and strain levels on the skin side of the panel for all load cycles. Pre- and post-test photos of the specimen and set-up were taken and a standard speed digital video with sound was taken of the OML side.

The testing of the pressure panel occurred over the course of two weeks first by testing an undamaged panel up to 2P and then by damaging and testing the same panel beyond 2P up to a predicted failure load at 3P.

Initially, the pressure panel was taken up to 18.4 psi (2P) without damage to confirm that the PRSEUS panel would not fail (Figure 92). The test was completed in a series of four steps. First, a pre-test was completed up to 0.5P to check the strain gauges. The panel was then pressurized to 1P, de-pressurized, and then pressurized to 2P. At 2P, the pressure panel held without any indication of failure thus meeting the objectives of the 2P pressure test (Figure 93). Next, the impacted panel was then tested to 2P again without any indication of failure. The pressure load was increased to 28.4 psi before failure occurred at the wrap stack around the rod on the center stringer. The failure was localized as shown in Figure 94. From the side view of the failed stringer in Figure 95, it can be seen that the wrap failed around the rod but the damage did not propagate past the stitching along the bottom of the stringer web demonstrating the capability of stitching to arrest damage. A comparison of the VIC and FEM analytical results showing the displacement values is picture in Figure 96.



FIGURE 92. PRESSURE PANEL IN COLTS FACILITY FOR TESTING

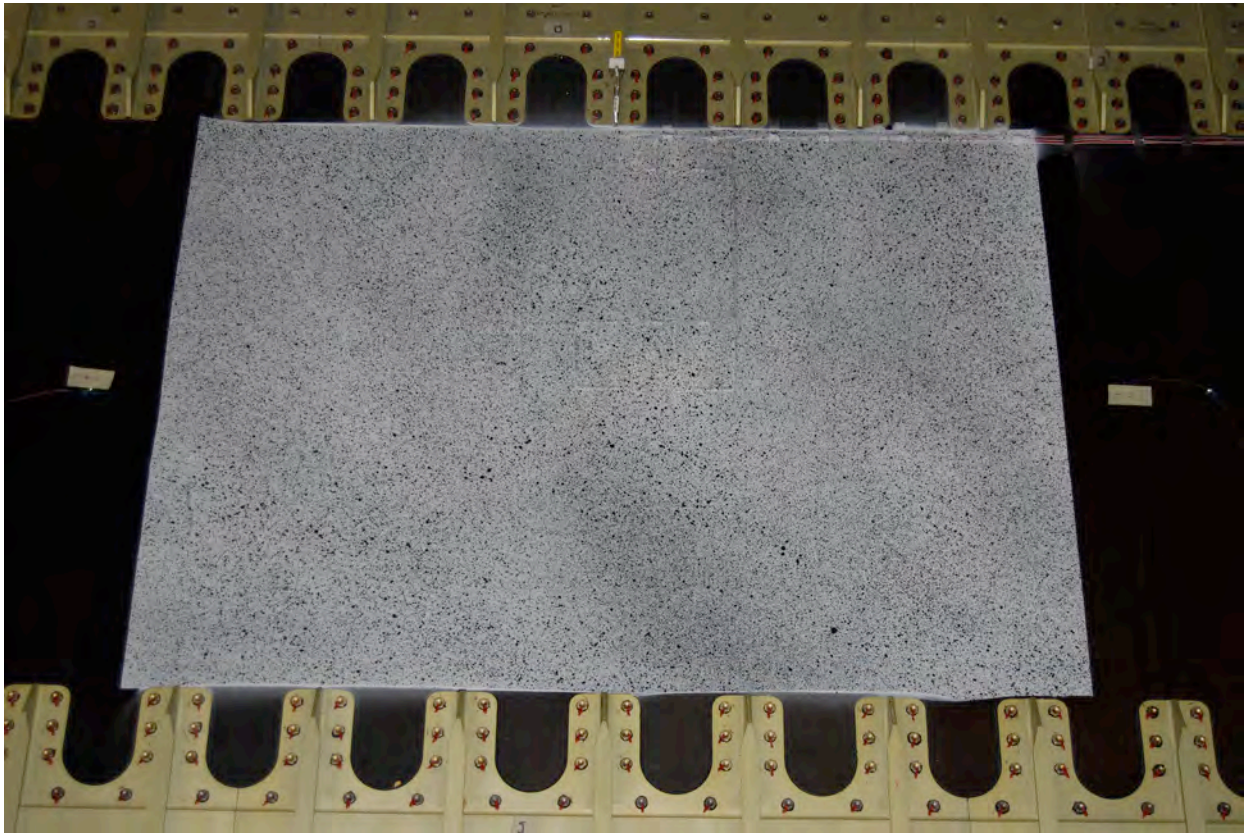


FIGURE 93. PRESSURE PANEL AFTER 2P TEST

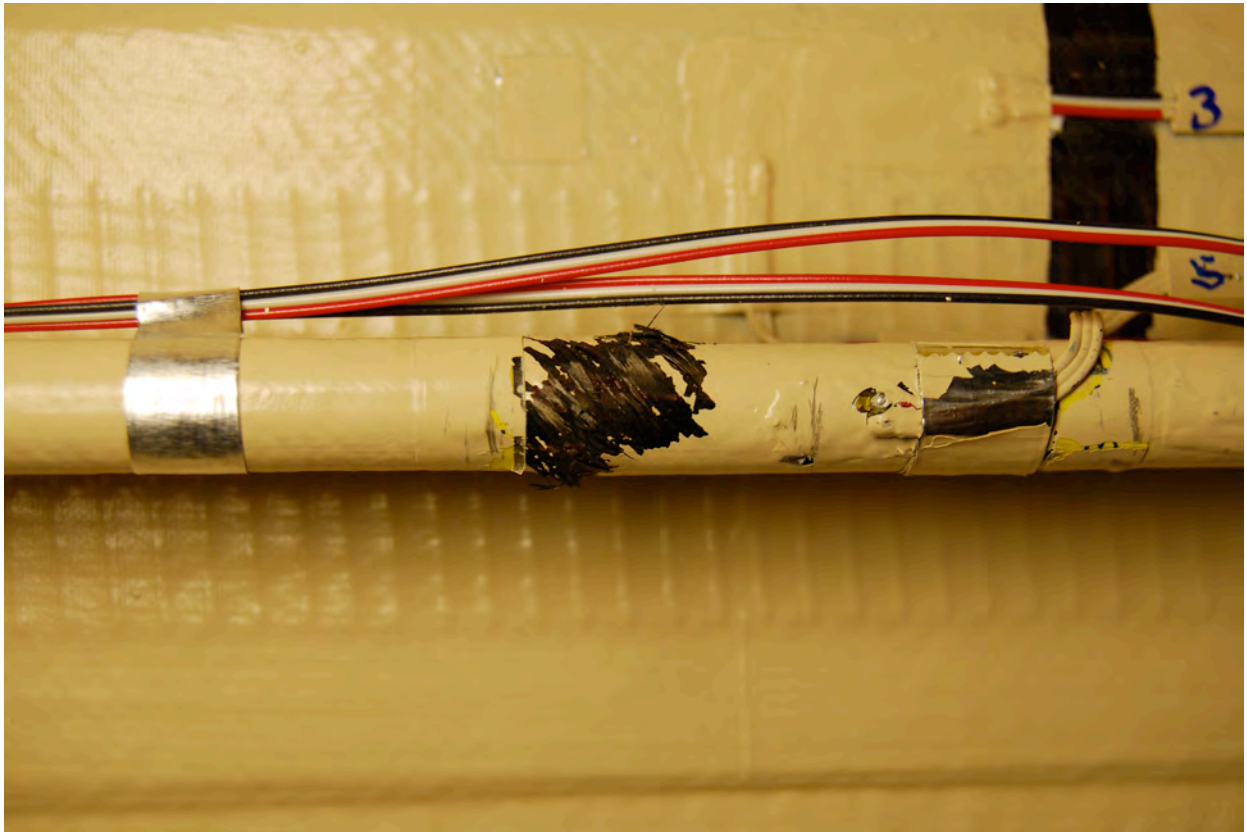


FIGURE 94. LOCALIZED FAILURE AT IMPACTED REGION AFTER 3P



FIGURE 95. DAMAGE ARRESTING BY STITCHING ON STRINGER WEB

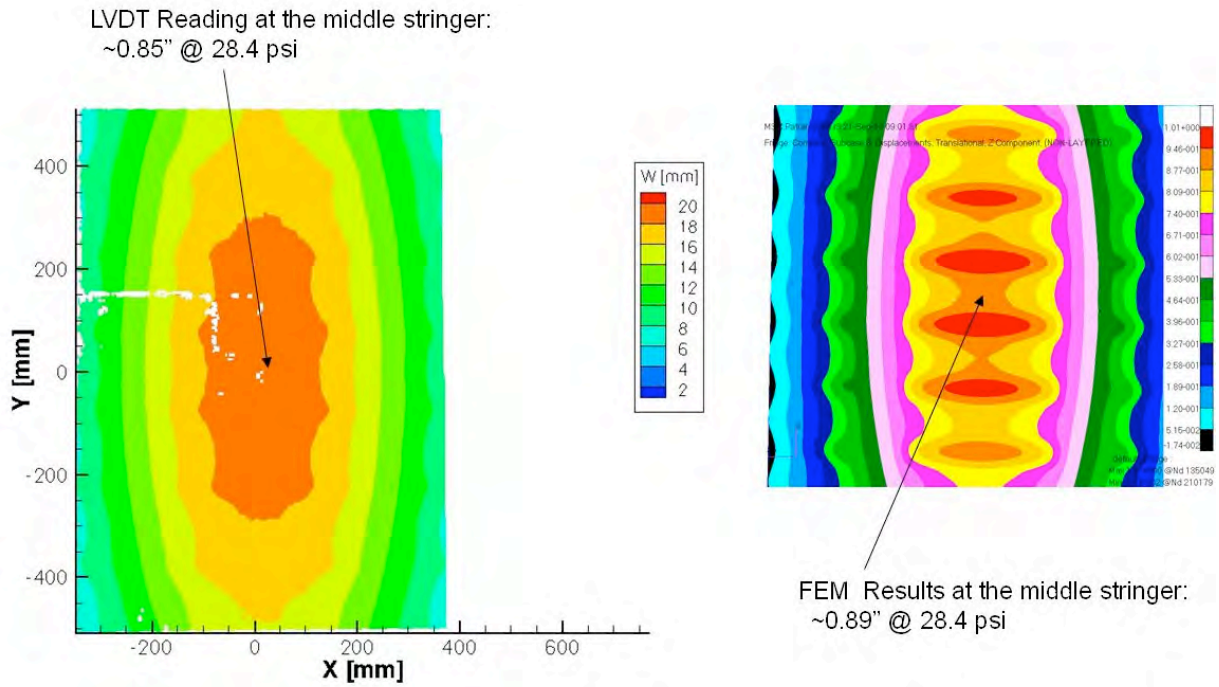


FIGURE 96. DISPLACEMENT COMPARISON BETWEEN FEM AND TEST VIC DATA

Since the majority of the panel remained intact after the failure, additional testing is being planned beyond the scope of the Phase II study.

3.0 CHORDWISE TENSION PANEL (WBS 3.5.2)

The objective of this subcomponent test was to demonstrate the distinctive damage-arrest design advantages of the PRSEUS concept and to validate the BWB minimum-gauge fuselage geometry developed during the Phase I trade studies. What made this test challenging, is that the primary fiber direction of the skin runs parallel to the frame direction rather than to the stringer (to accommodate the high spanwise loads found in the BWB). This makes crack turning more difficult because the favorable fiber-splitting phenomena that normally occurs in a 0-degree dominated skin lay-up is not present; now the stitched interfaces must work harder to initially stop damage growth and then later to maintain the turned-crack progression as it moves along the stringer flange.

3.1 Design

The basic design requirements for a transport aircraft are set by FAR Part 25, Airworthiness Standards: Transport Category Aircraft. These minimum design and compliance objectives, along with the manufacturer’s past experience, forms the basis on which new airplane design criterion are satisfied. Through a combination of analysis and testing, strength and deformation requirements are validated over a wide range of critical design conditions. How these unique design requirements are met is strongly influenced by the characteristics of the individual material systems chosen, and nowhere is the composites versus metals disparity greater than in how the design methodology has evolved to meet the multi-bay damage tolerance and residual strength requirements of FAR Part 25.571 (Damage – tolerance and fatigue evaluation of structure) summarized in Figure 97.

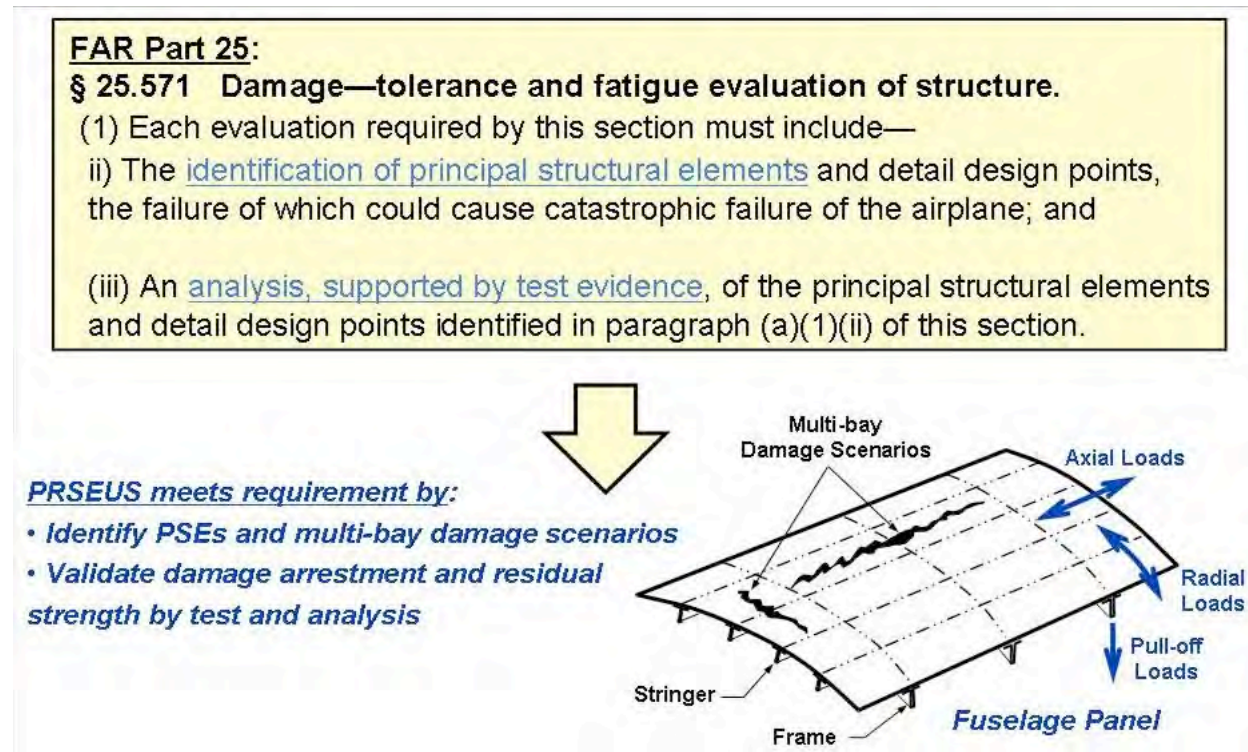


FIGURE 97. PART 25.571 DAMAGE TOLERANCE REQUIREMENTS

Here the layered arrangement and brittle fracture characteristics of a composite material system implies the need to utilize a safe-life design approach as described in Paragraph (c) of the FAR

part 25 [Fatigue (safe-life) evaluation], rather than the fail-safe methodology commonly used for ductile slow-growth metallic structures as outlined in Paragraph (b) [damage tolerance evaluation]. Arguably, this single difference constitutes the largest design penalty for a composite primary structure like the wing or fuselage. This is especially true for larger transport size aircraft because the weak resin interfaces of the composite material are not scalable; i.e. making thicker parts does not increase the interlaminar strength of the resin; which is required to react the higher out-of-plane loads inherent in the larger airplane. This is the fundamental problem facing the structural designer and cannot be overcome unless composite structures can be made with substantially higher interlaminar tension strengths (beyond what is possible using resin alone) to react the out-of-plane loadings and arrest damage propagation in a manner comparable to built-up metallic structures.

To become damage tolerant like metallic structures, whereby composite structures would meet the conventional crack-growth and damage-arrest methodologies described in Paragraph (b), requires additional z-direction reinforcement. This forms the basis for the PRSEUS design approach; it uses through-thickness stitching to increase the out-of-plane tension strength of the layered composite material system so that the damage tolerant requirements described in Paragraph (b) can be met. Additionally, it also enables an integral one-piece panel construction that is capable of reacting out-of-plane loads and local stress concentrations inherent in built-up panel assemblies.

The overarching goal of the PRSEUS design approach is to create an integral composite panel assembly that has an equivalent level-of-safety and crashworthiness to that of proven state-of-the-art aluminum structures that are multi-load path, redundant, damage arresting, and capable of redistributing internal loads to the undamaged regions of a damaged panel assembly. Such an ambitious agenda has been accomplished by stitching in all the critical transitions where stress concentrations normally occur between the skin, stringer, and frame elements (Figure 98). This permits the reaction of out-of-plane loadings, as well as a mechanism to arrest propagating cracks or delaminations within the layered material construction.

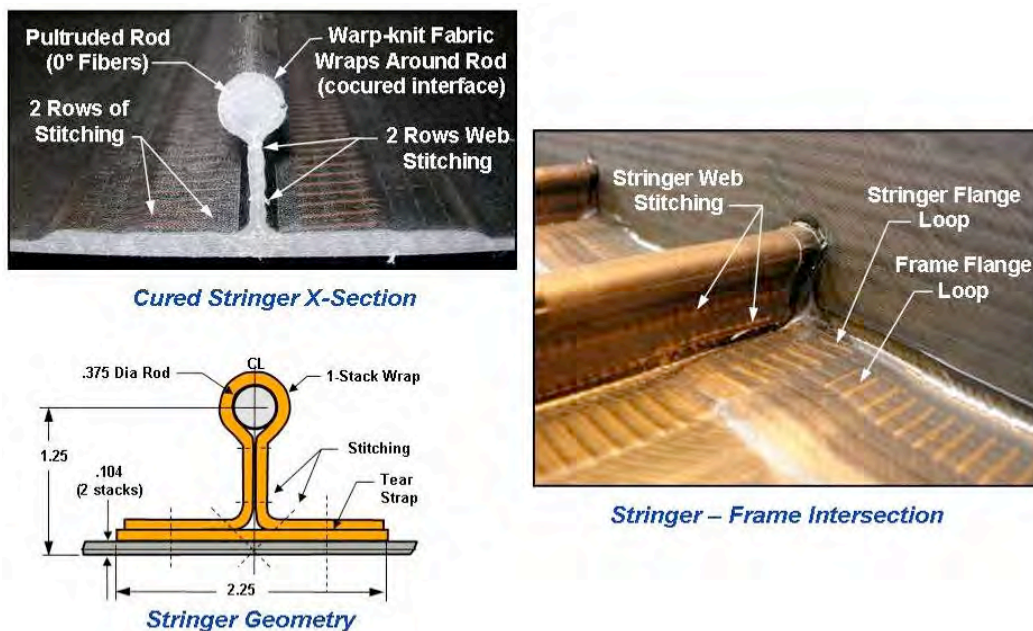


FIGURE 98. CRITICAL INTERFACES ARE STITCHED TO ARREST DAMAGE

By eliminating the primary deficiency of the layered composite material form, it now becomes possible to move beyond the safe-life, or no-growth, design philosophies commonly used for composite structures. This single change in design philosophy brings composite structures on an equal footing with standard metallic design practices, and is the single most important factor necessitating the use of through-thickness stitching, and yet it remains one of the least understood aspects for doing so.

The primary characteristic for meeting the multi-bay discrete source damage scenario, requires that a panel assembly have the capability to first arrest propagating cracks, and then as load levels are increased, it must also be capable of redistributing internal loads to the undamaged regions of the panel. Although this method of load redistribution is common for metallic skin-stringer designs, it has yet to be used for composite structures because damage propagation is difficult to stop in a laminated material system that relies on brittle resin interfaces. Whether cocured, or bonded, the resulting resin-dominated failure modes indicate that the laminate is not capable of reacting the out-of-plane or local bending loads prevalent in an advancing crack tip. As such, skin cracks typically skirt underneath the stringer members and continue into the adjacent skin bay unabated. This then overloads the stringer member resulting in a sequential-like failure mode. Strengthening this interface is the key to limiting damage growth and ultimately turning a crack to unload the crack tip. Stitching is the mechanism used to provide the necessary out-of-plane strength that permits the remaining undamaged skin and stiffener to work together (fail as a single unit, not sequentially) and maintain structural integrity under increasing load levels.

The fundamental aspects of this approach are outlined in Figure 99; here the orthogonally stiffened skin-stringer-frame structural panel is loaded in tension along the stringer direction. The central stringer member and a portion of the skin have been removed, and the panel loaded to 100% design limit load to satisfy the discrete source damage criterion.

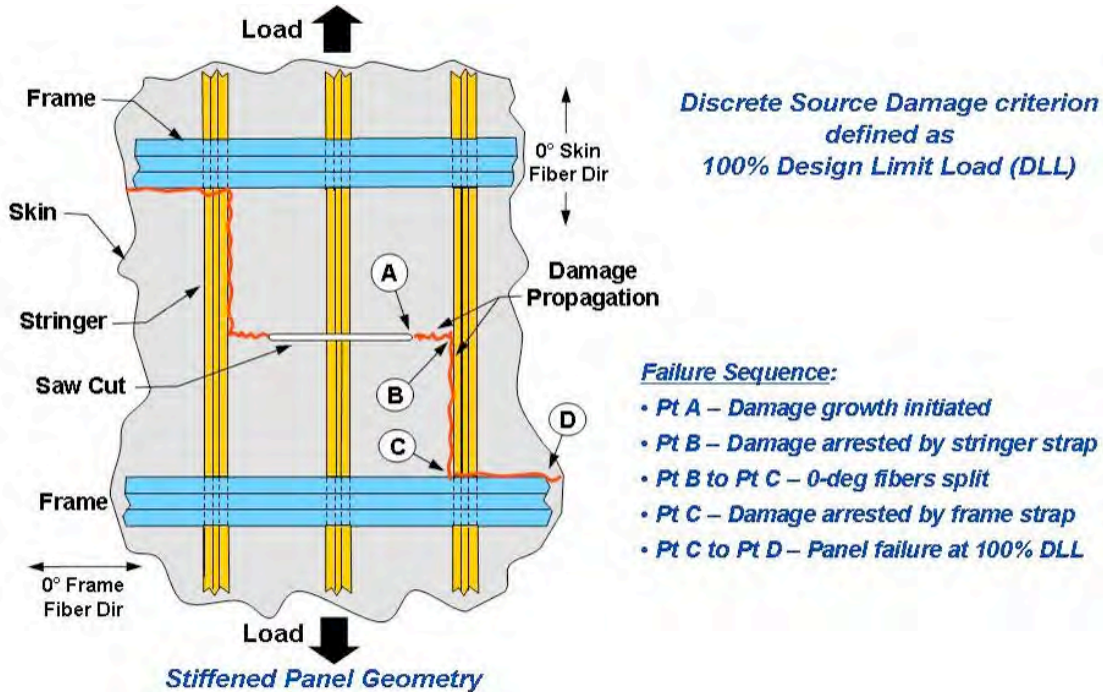


FIGURE 99. PANEL ASSEMBLY DAMAGE ARREST SEQUENCE FAILURE

Because the PRSEUS panel is stitched along all the critical interfaces, once the damage starts to propagate from Point A to Point B, it is arrested at Point B as the adjacent stringer, remaining skin, and tear strap act in unison to stop the progression. Then as the crack tip stress intensity exceeds the capability of the laminate, the crack turns 90-degrees and propagates from Point B to Point C; before finally encountering the intersection of the frame, remaining skin, and tear strap at Point C. Since the panel is symmetric, the failure pattern occurs in both directions (due to the resin weakness in the unstitched regions of the skin) and as such, this process unloads the entire two-bay region of the panel, while still maintaining the structural integrity of the adjacent stringers, remaining skin, and tear straps. Now the overall residual strength of the panel assembly can be determined as the damage propagates from Point C to Point D initiating the final fiber-dominated failure sequence of the panel assembly.

3.2 Analysis

The dog-bone shaped test specimen finite element model (Figure 100) was created with a 6-inch saw-cut to simulate the discrete damage site. A FEM-based analytical task was conducted to predict failure loads, modes, and determine the optimum strain gage placement for testing. A detailed test specification document that described the test set-up, instrumentation locations, and data recording requirements was prepared.

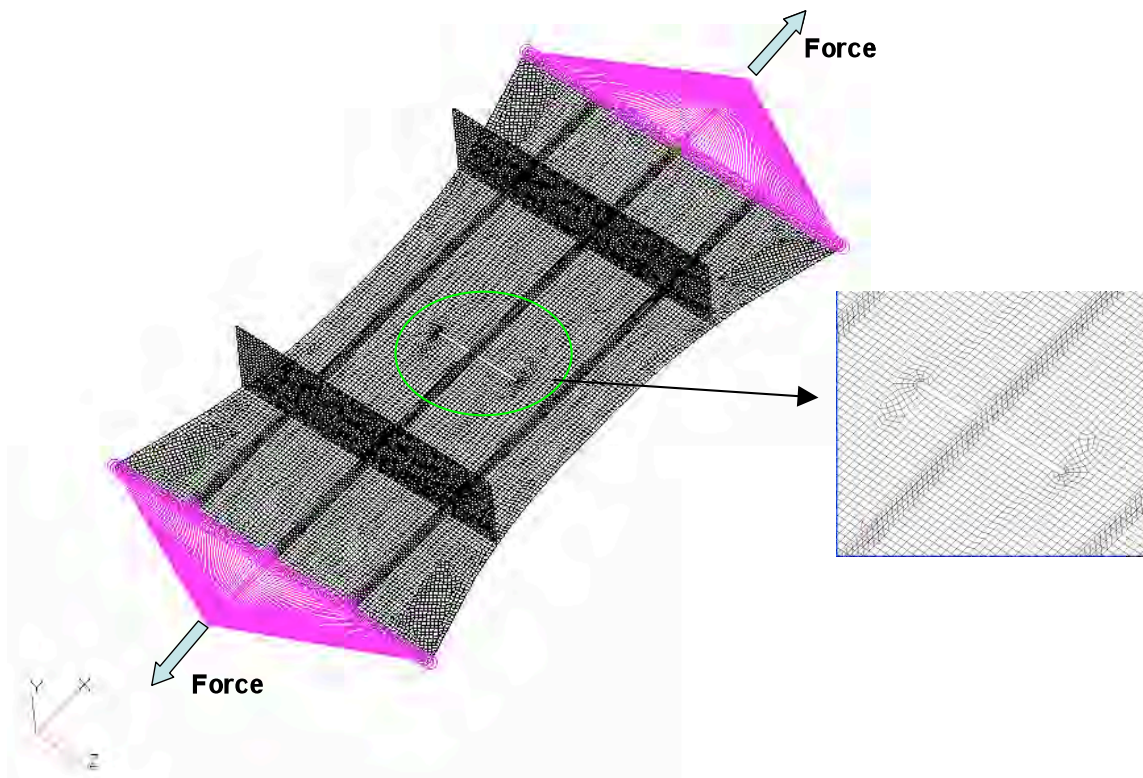


FIGURE 100. FINITE ELEMENT MODEL

A similar test specimen was constructed and tested under different CRAD contract (Reference 2) with the Air Force Research Laboratories (AFRL). The two test specimens have the same general geometries and materials layups. The difference mainly lies in skin fiber orientations and the skin thickness, shown in Figure 101. For the Phase II test panel, the skin 0-degree fiber orientation is along the frame direction, with minimum gauge skin thickness (one stack, 0.052-inches).

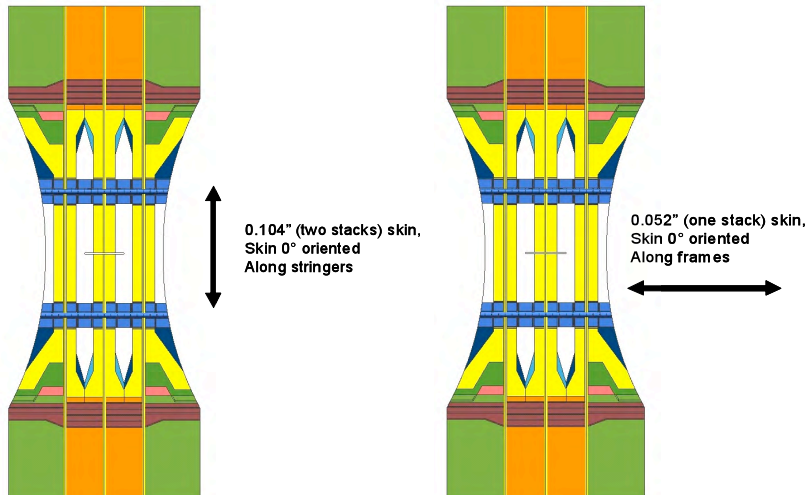


FIGURE 101. PHASE II PANEL (RIGHT) AND AFRL PANEL (LEFT) (REF. 2)

The new analysis leveraged the prior test results (Reference 2) to predict the ultimate failure for the panel. Two analysis approaches were used for this test specimen. The first approach used static models to predict structural failures at various damage states (initial damage, damage arrested at stringers, and ultimate panel failure). Maximum strain failure criteria were used under this approach. Based on the observed damage states and the corresponding measured strains from the AFRL test panel, the failure strain was applied to the new test panel in order to evaluate the corresponding (required) loads to propagate the damages and ultimately fail the panel. Under this approach, assumptions were made that the same failure pattern and crack growth paths would occur for the new panel, in particular, the crack would start to grow toward the stringers, be arrested, and then be turned. The final failure would occur after the cracks reached the frames and are arrested by the frame stitching. Table 4 summarizes the predicated loads at various damage states. Figure 104 through Figure 111 show the corresponding deflections, maximum principal strain for various elements (skin, stringer/rod).

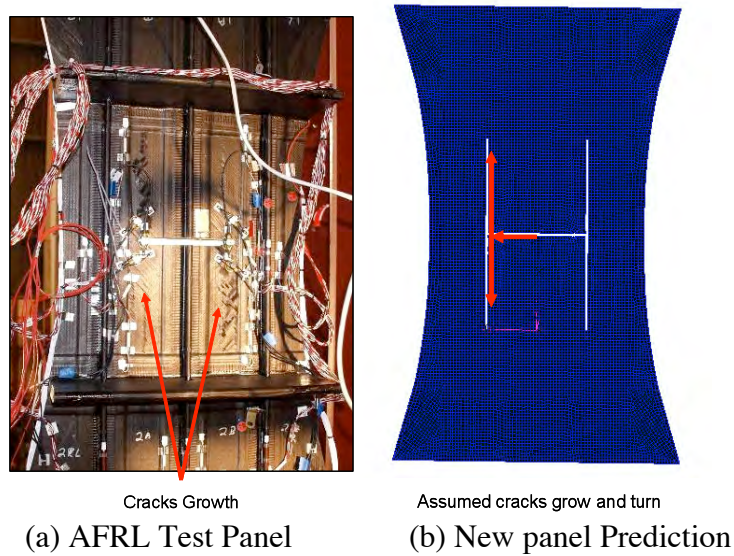
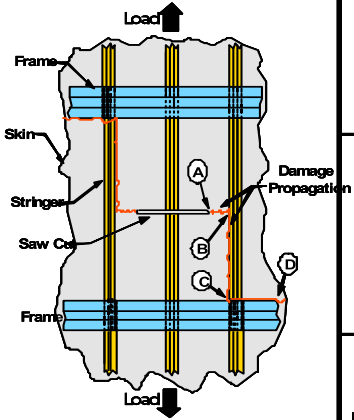
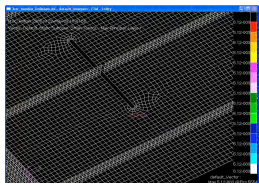
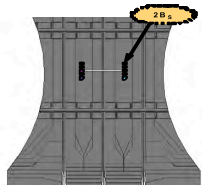
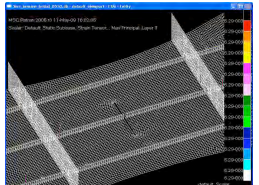
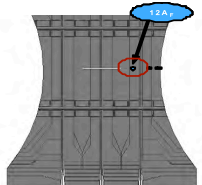
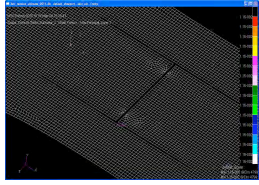
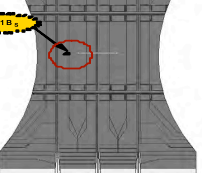


FIGURE 102. DAMAGE PROGRESSION COMPARISON

TABLE 4. TEST LOAD PREDICTIONS

	Damaged States	New Panel Load Prediction			Referenced AFRL Panel Test		
		Predicted Loads	Strain Values @ the Monitoring Point ($\times 10^{-6}$)	FEM Plots	Strain Gage Location	Measured Strain Values ($\times 10^{-6}$)	Strain Gage #
	Damage Growth Initiated at Point A	35 Kips	5120			5200	2Bs
	Fractured to Point B	89 Kips	6290			6300	12Af
	Ultimate Panel Failure at Point C	142 Kips	11500			11500	11Bs

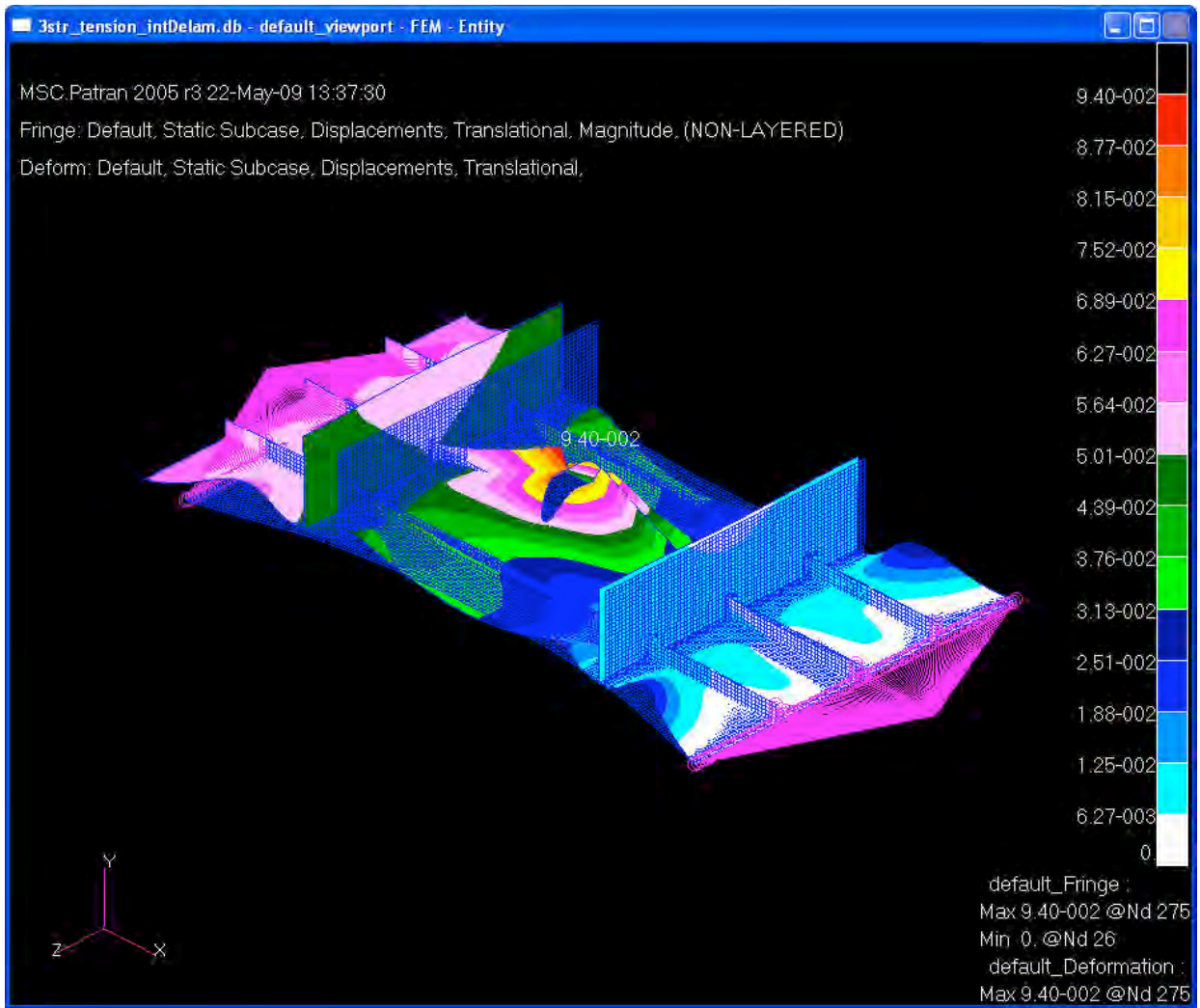


FIGURE 103. PANEL RESPONSE - DAMAGE INITIATION – DISPLACEMENT (IN)

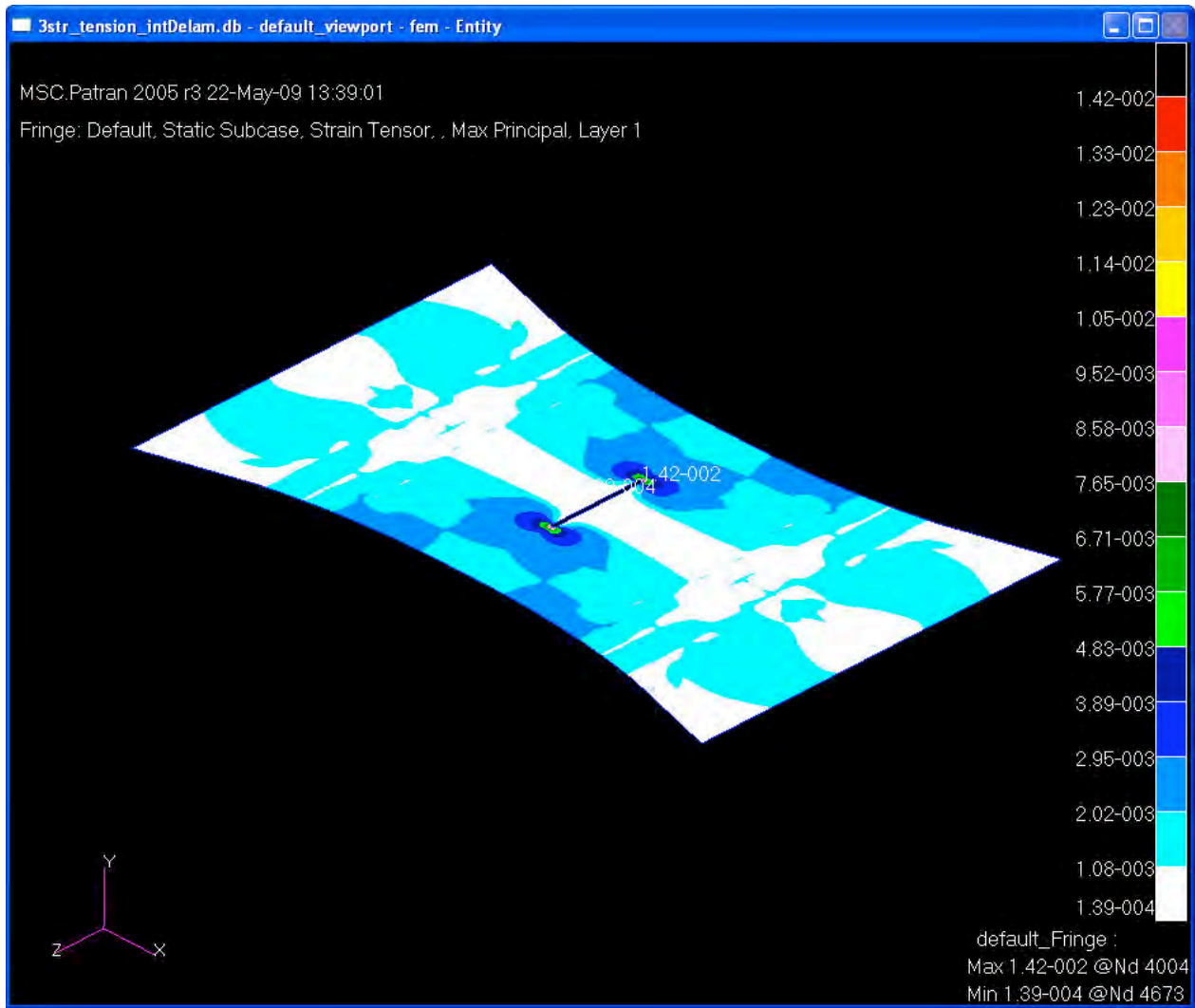


FIGURE 104. PANEL RESPONSE - DAMAGE INITIATION – PRINCIPAL STRAIN FOR SKIN

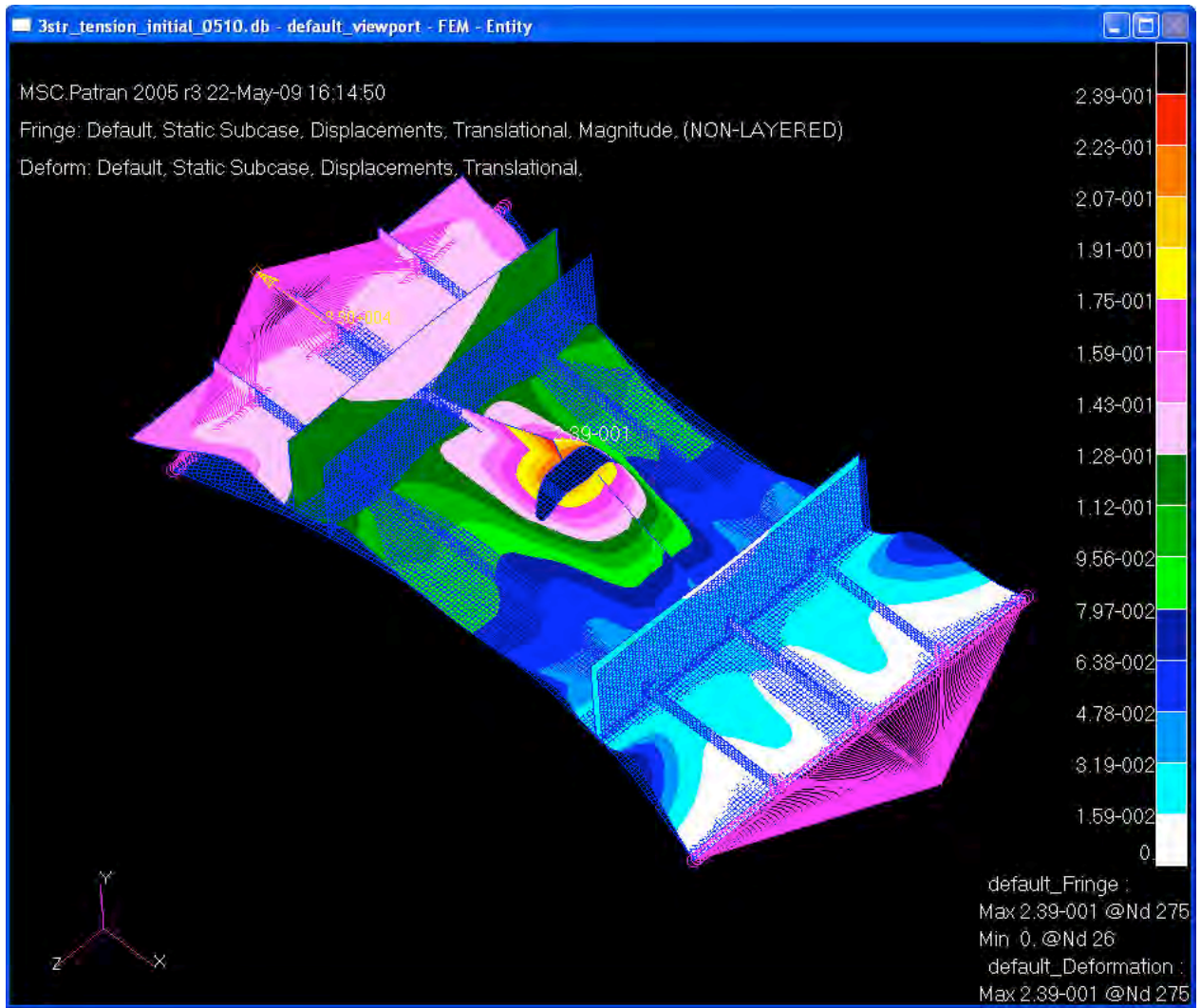


FIGURE 105. PANEL RESPONSE - CRACK GROWTH TO POINT B – DISPLACEMENT (IN)

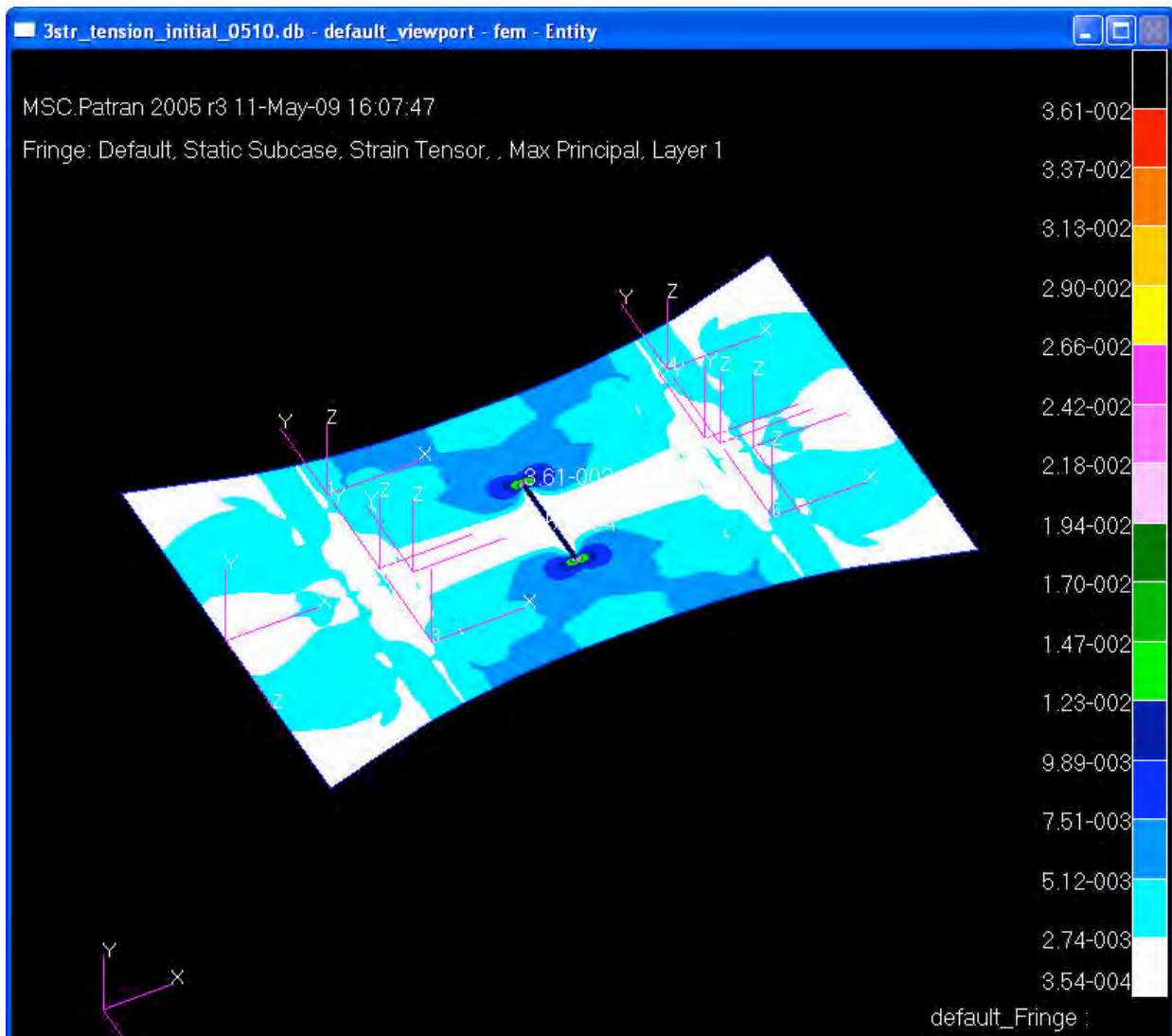


FIGURE 106. PANEL RESPONSE - CRACK GROWTH TO POINT B – PRINCIPAL STRAIN FOR SKIN

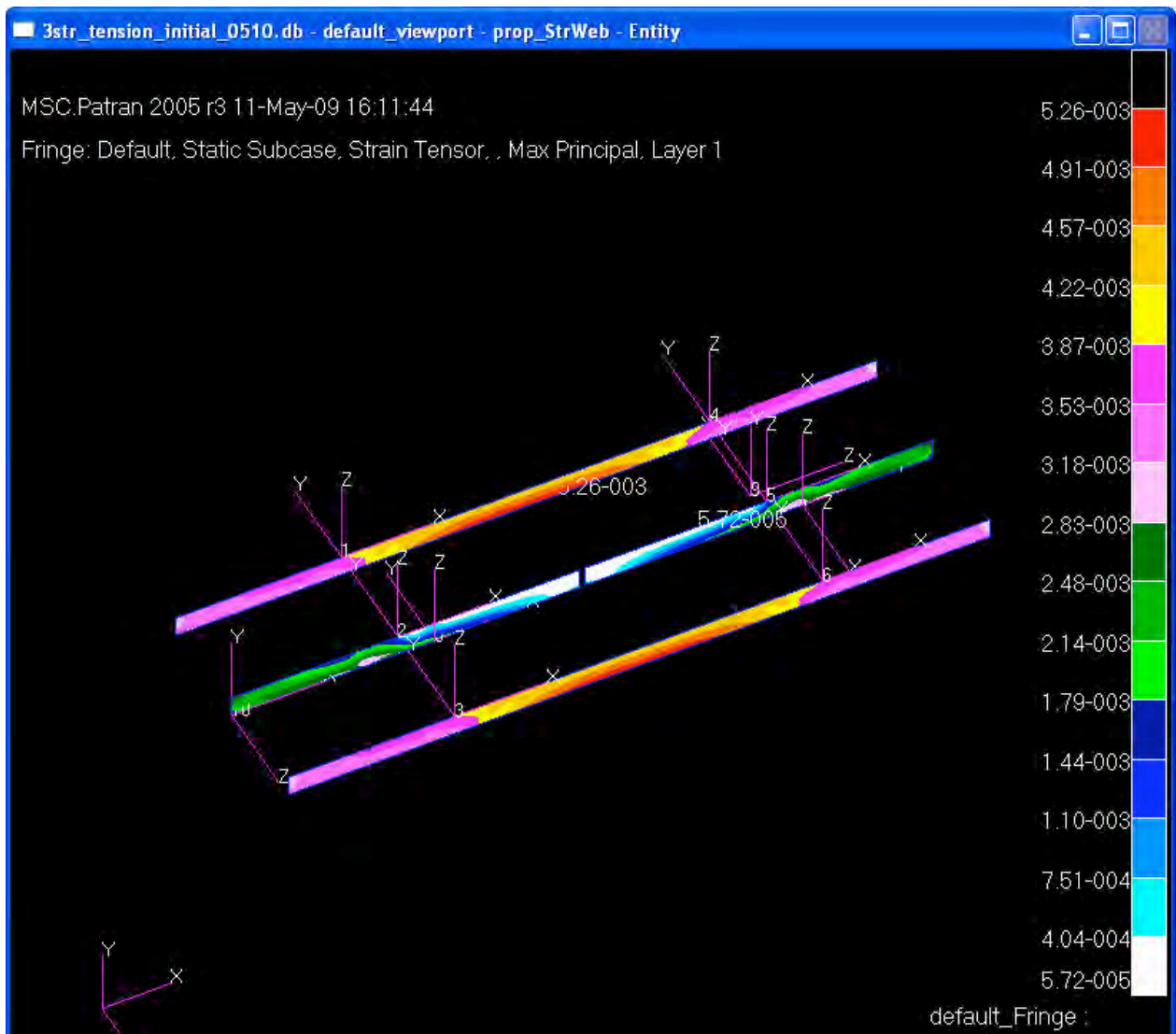


FIGURE 107. PANEL RESPONSE - FRACTURED TO POINT B – PRINCIPAL STRAIN FOR STRINGERS

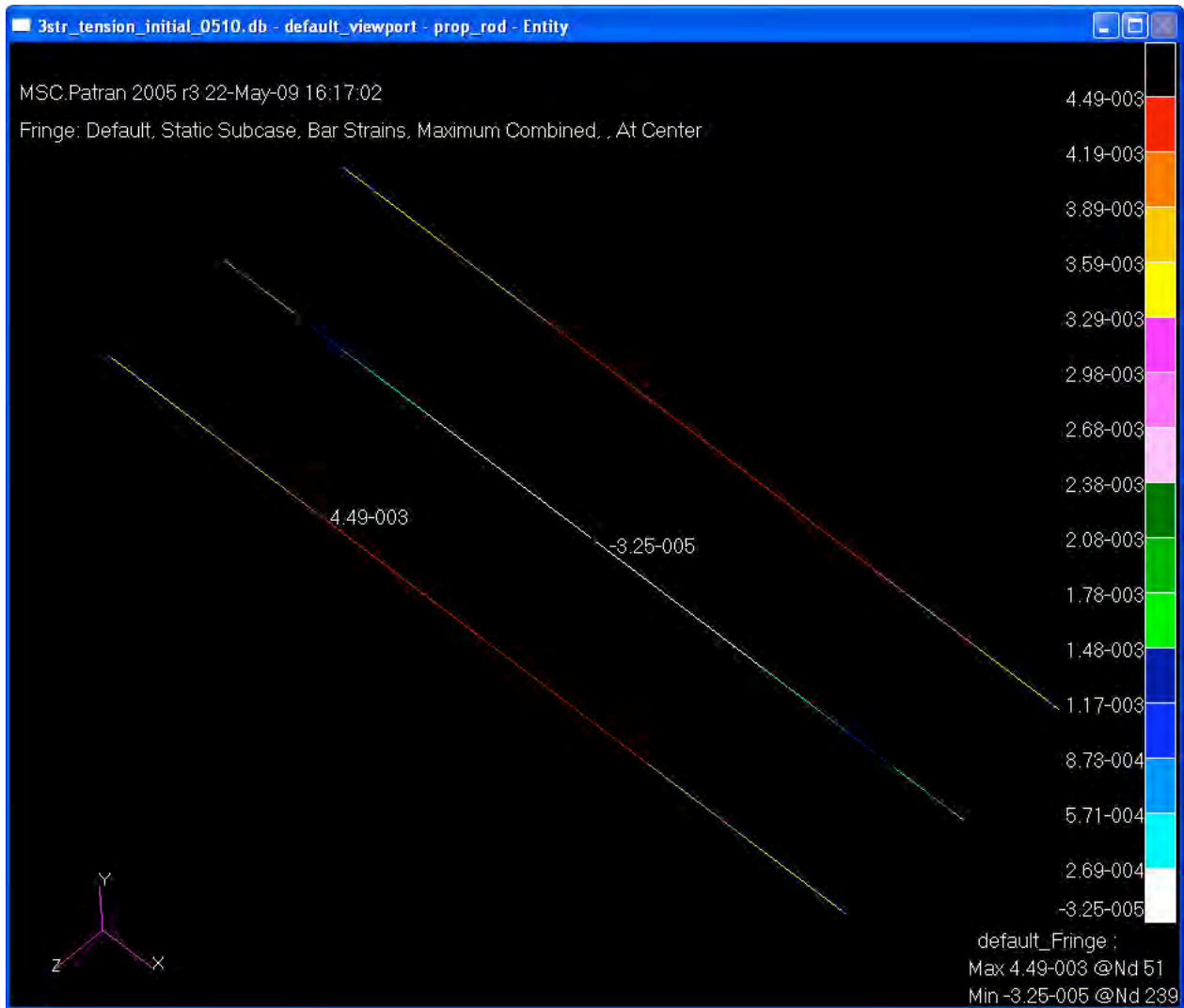


FIGURE 108. PANEL RESPONSE - FRACTURED TO POINT B – PRINCIPAL STRAIN FOR RODS

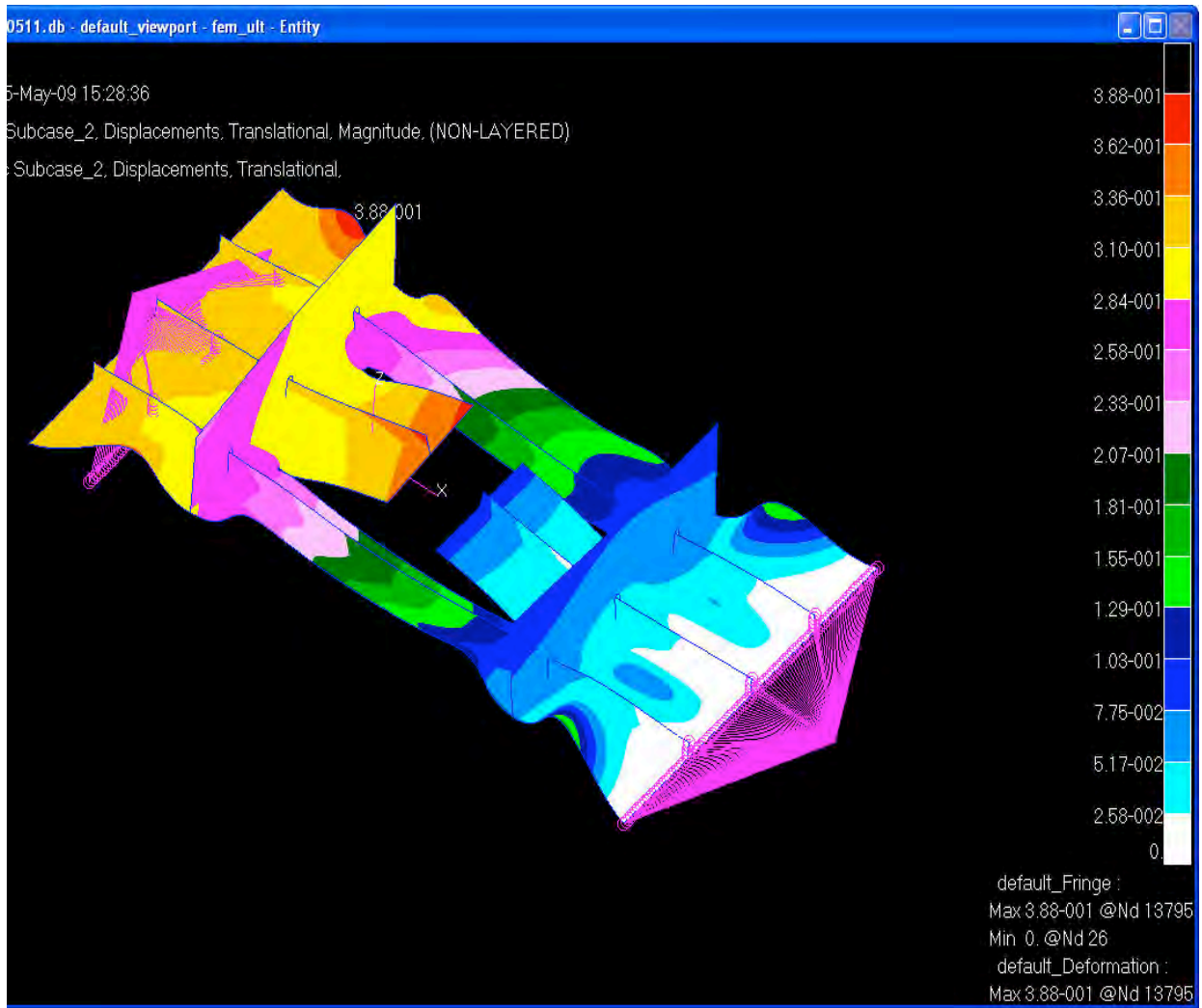


FIGURE 109. PANEL RESPONSE - ULTIMATE PANEL FAILURE – DISPLACEMENT (IN)

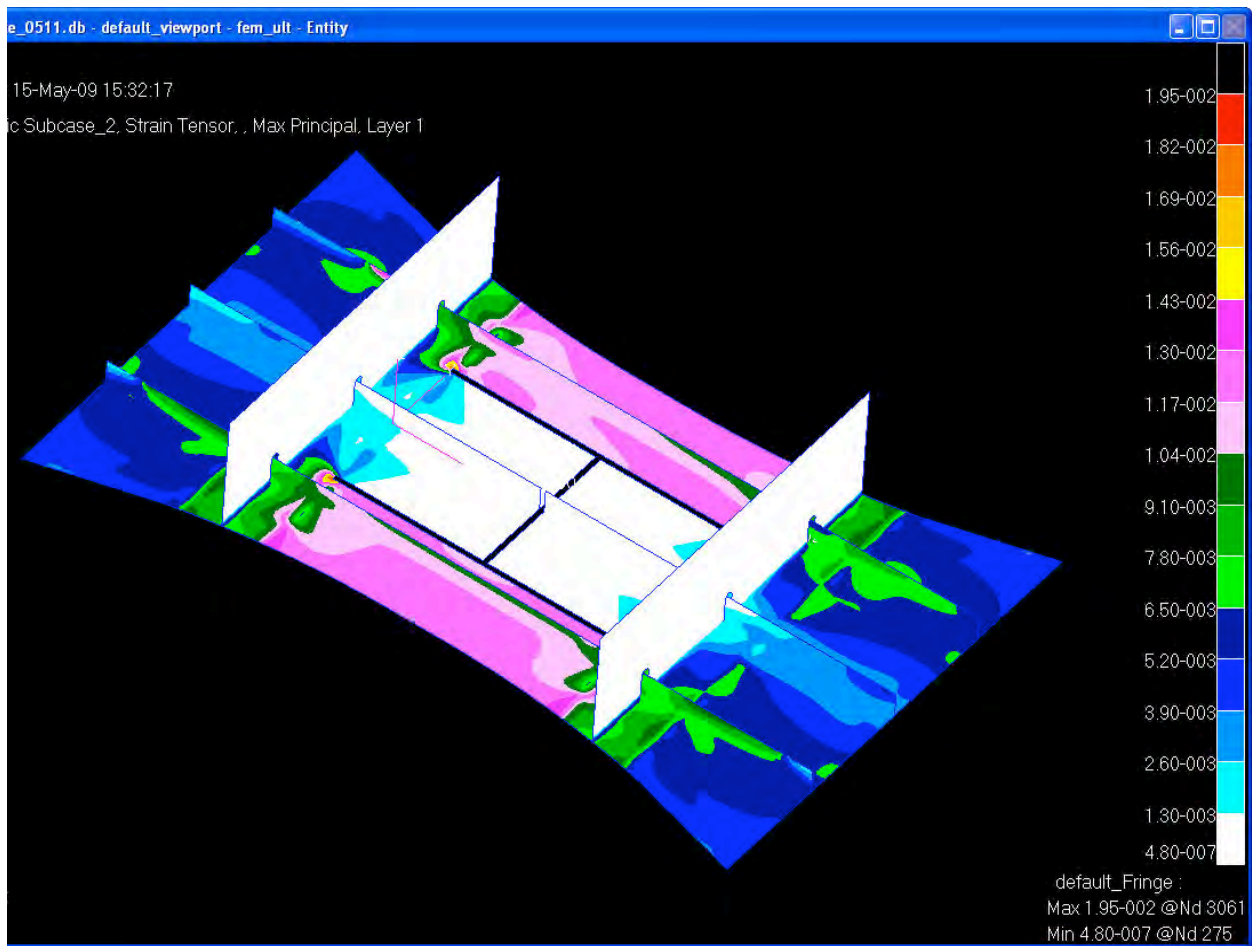


FIGURE 110. PANEL RESPONSE - ULTIMATE PANEL FAILURE – PRINCIPAL STRAIN FOR SKIN

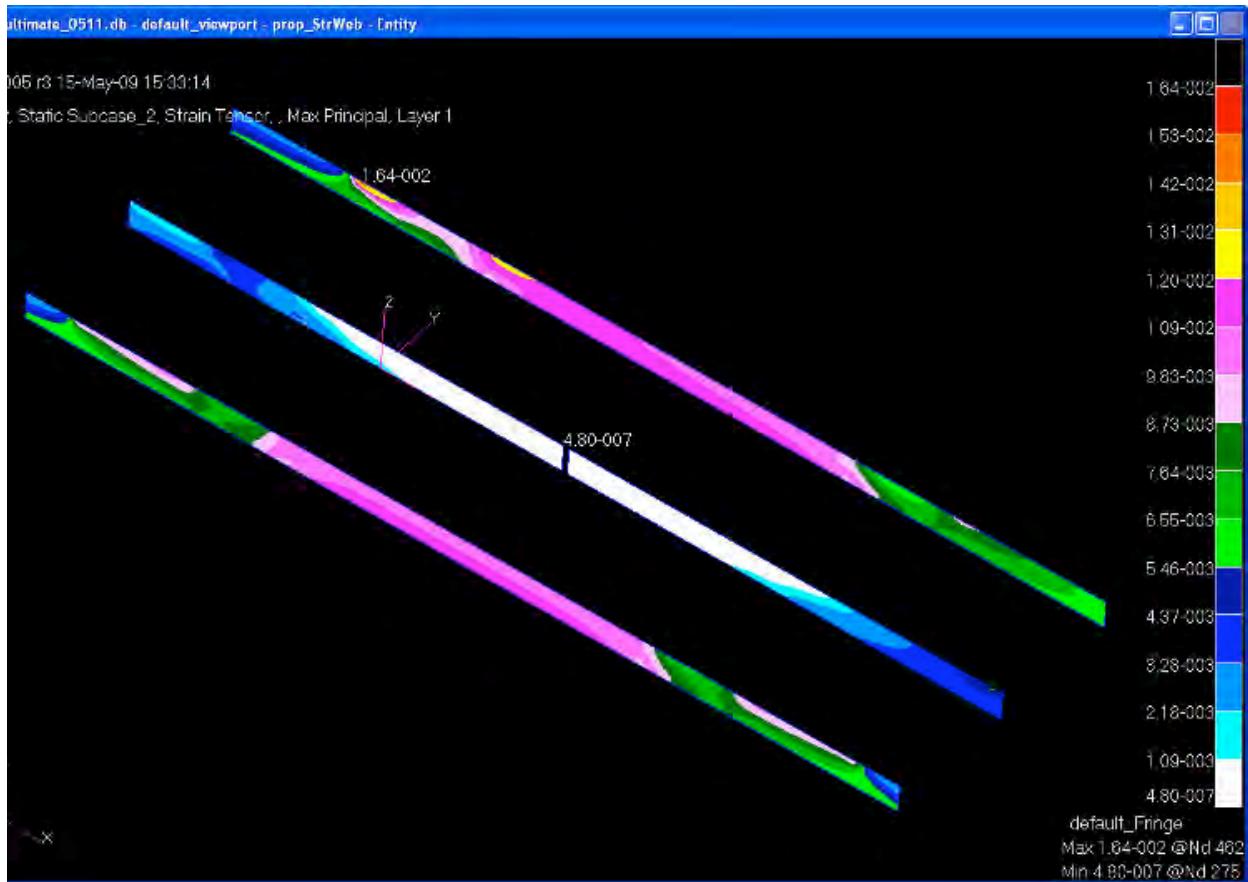


FIGURE 111. PANEL RESPONSE - ULTIMATE PANEL FAILURE – PRINCIPAL STRAIN FOR STRINGERS

To further investigate the failure mechanisms and attempt to analytically predict crack propagation for the test panel, a nonlinear FEM analysis was conducted based on MSC NASTRAN MARC Progressive Failure Analysis (PFA) techniques. The finite element models were refined to model the structural elements ply-by-ply. Referencing prior AFRL test results, the max stress failure criteria were applied in this analysis. Not knowing the exact impact of stitching on structural element properties, assumptions were made to artificially increase structural element allowables in its transverse direction in the region of the stitching. Further studies would be required to better understand the micro-mechanics of these 3-D reinforced elements. Figure 112 shows the load-deflection curve from the analysis. Figure 114 through Figure 117 highlight the failure index based on the Tsai-Wu failure criterion for the middle ply (layer 4) of skin at various damaged states. The PFA predicts that the final panel failure would occur at approximately 142 kips.

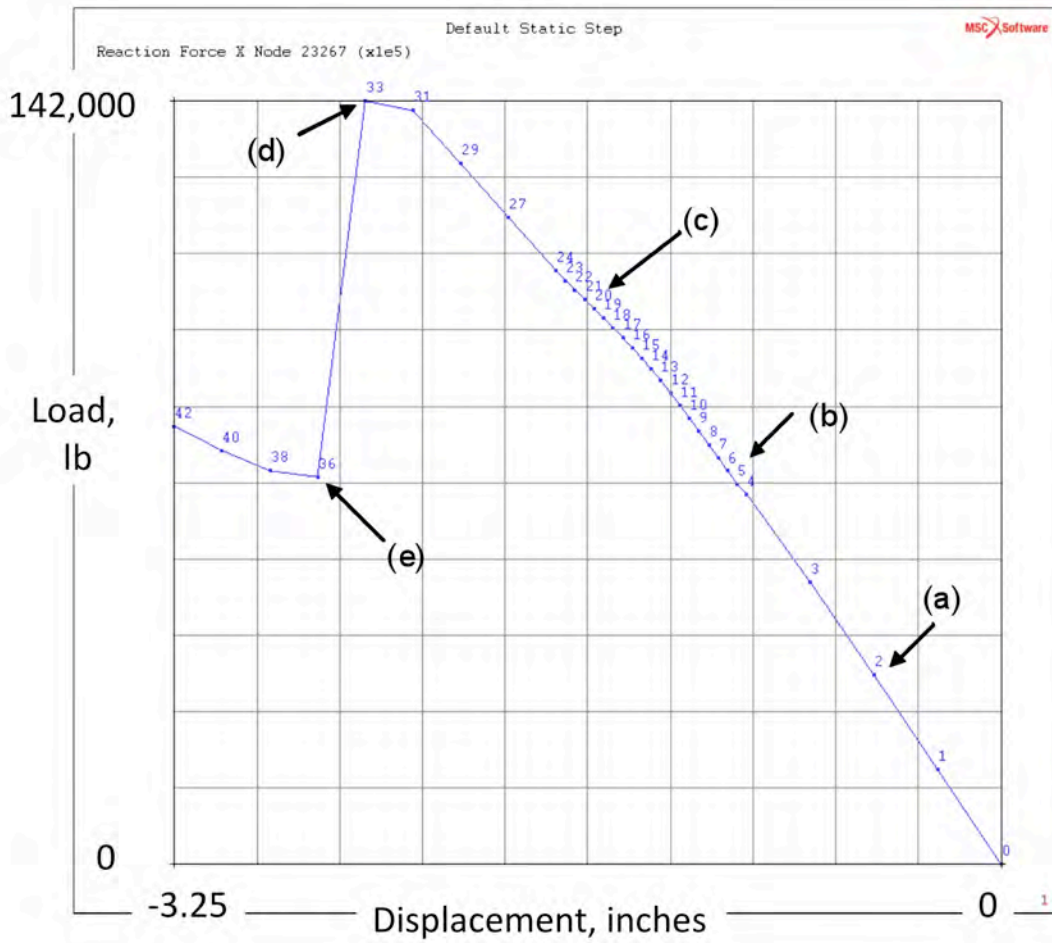
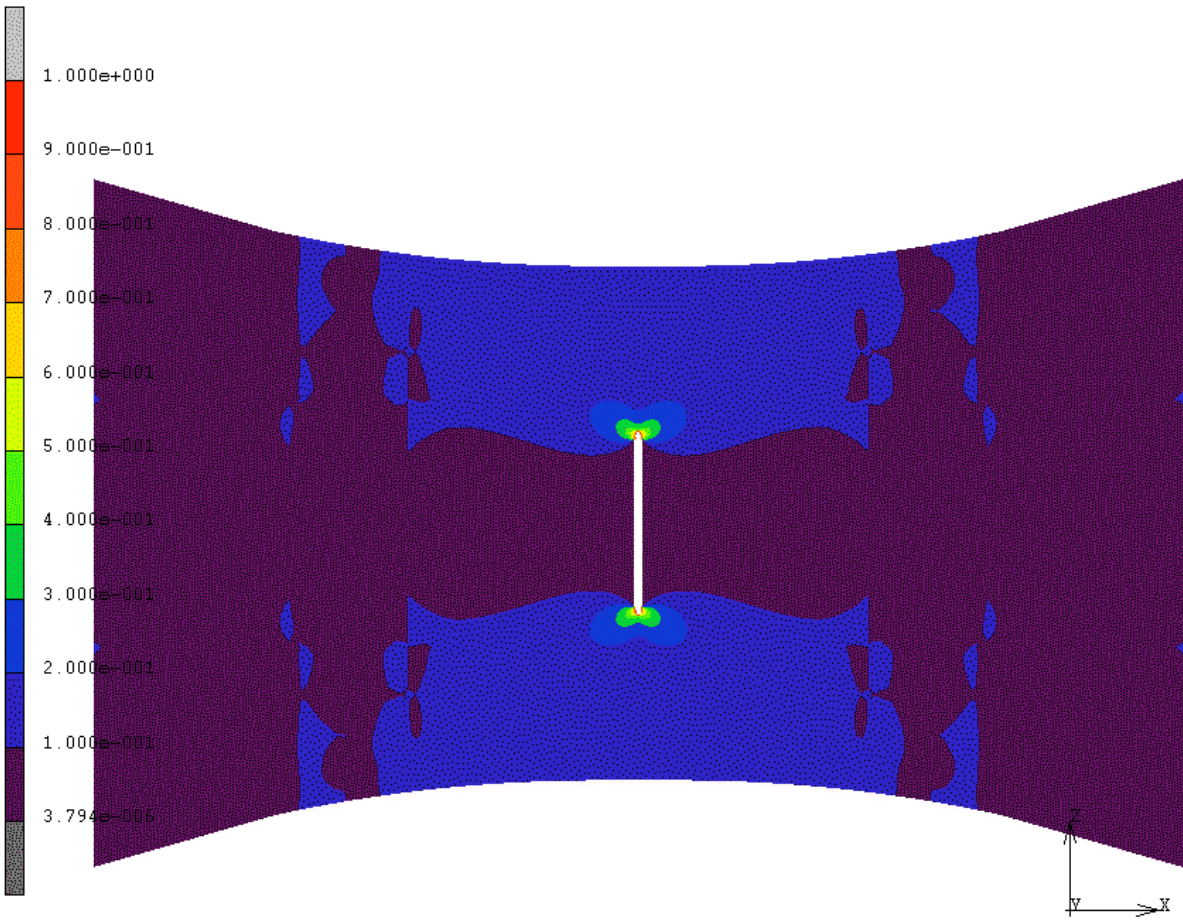


FIGURE 112. LOAD -DEFLECTION CURVE

Inc: 2
Time: 2.000e-001

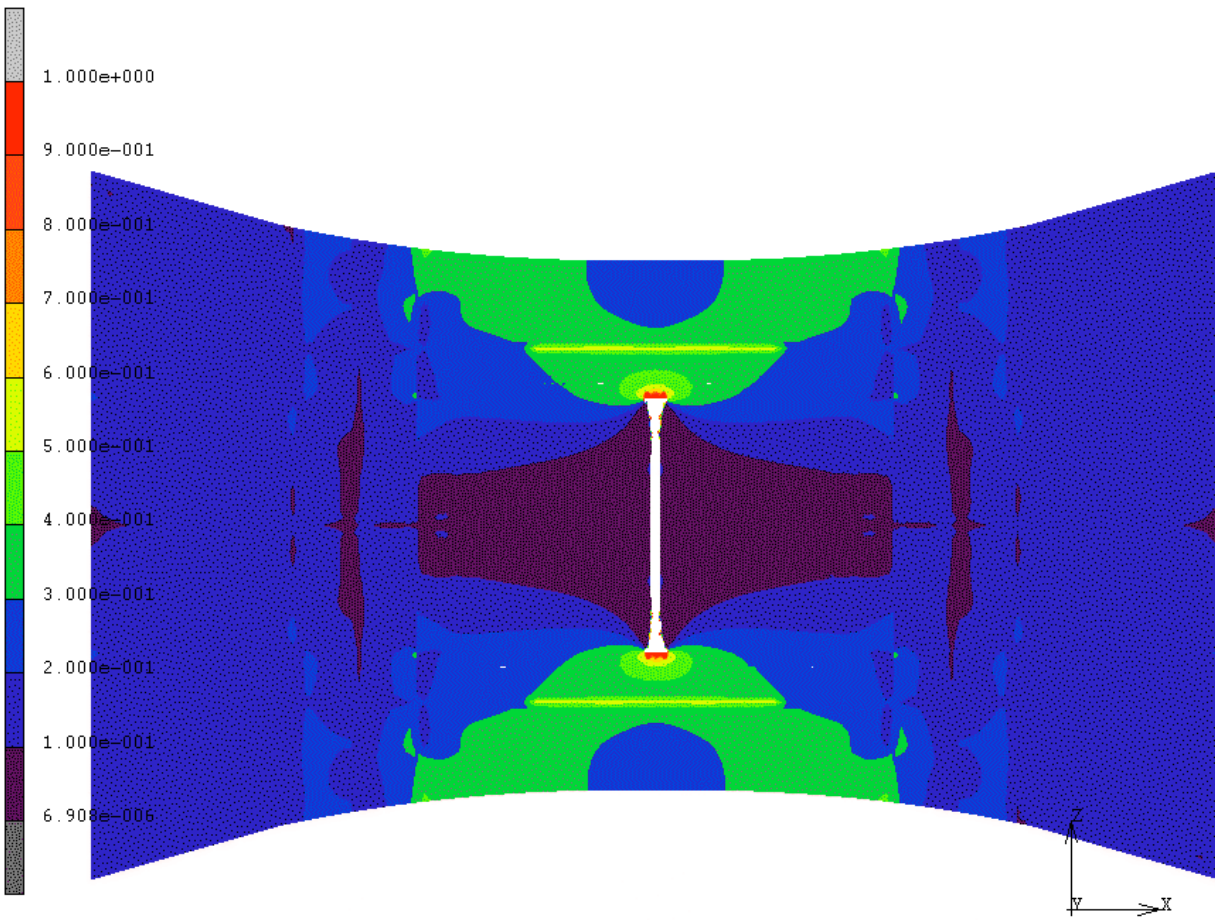


Default Static Step
1st Failure Index Layer 4

2

FIGURE 113. FAILURE INDEX FOR SKIN MID-PLY – CRACK GROWTH INITIATED

Inc: 5
Time: 4.150e-001



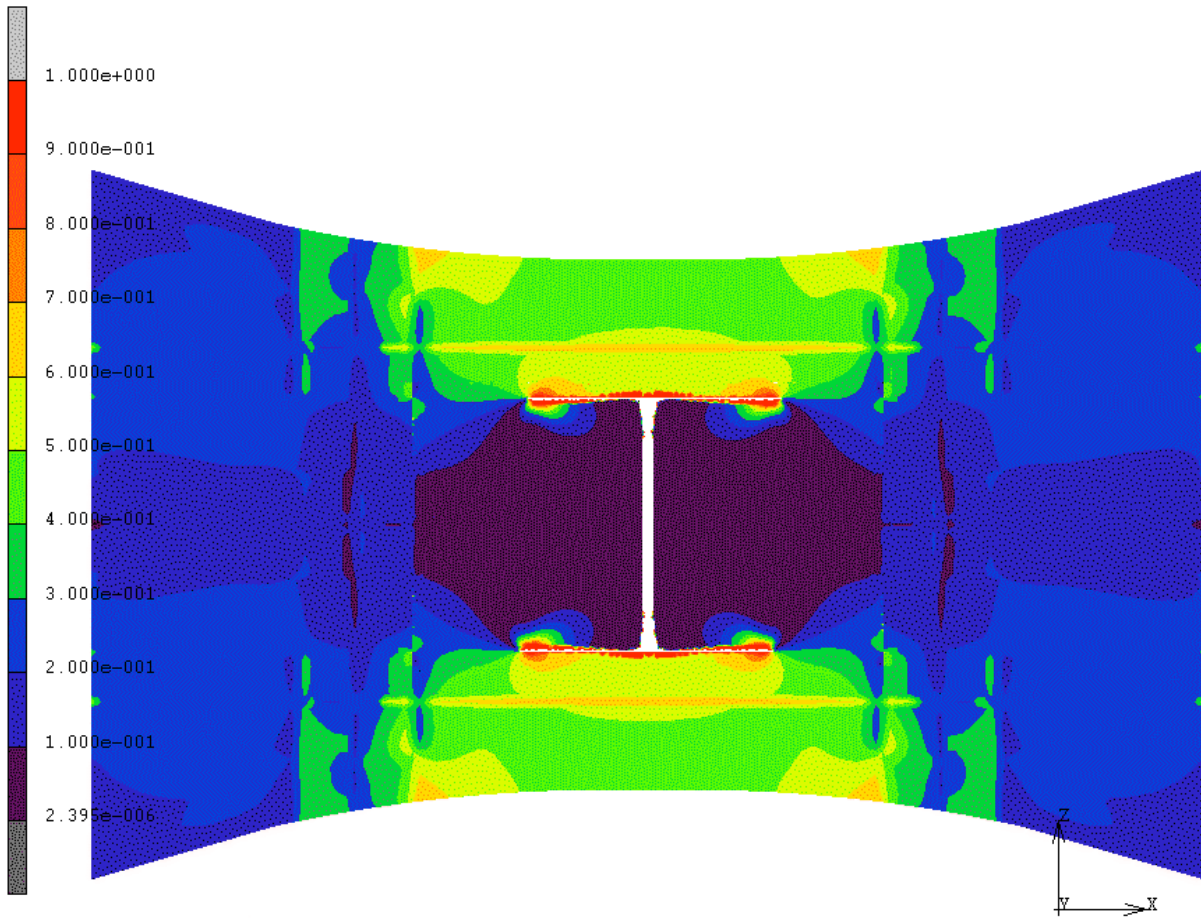
Default Static Step

1st Failure Index Layer 4

2

FIGURE 114. FAILURE INDEX FOR SKIN MID-PLY – CRACK REACHED STRINGER FLANGES

Inc: 20
Time: 6.400e-001



Default Static Step

1st Failure Index Layer 4

2

FIGURE 115. FAILURE INDEX FOR SKIN MID-PLY – CRACK ARRESTED AND TURNED

Inc: 33
Time: 1.000e+000

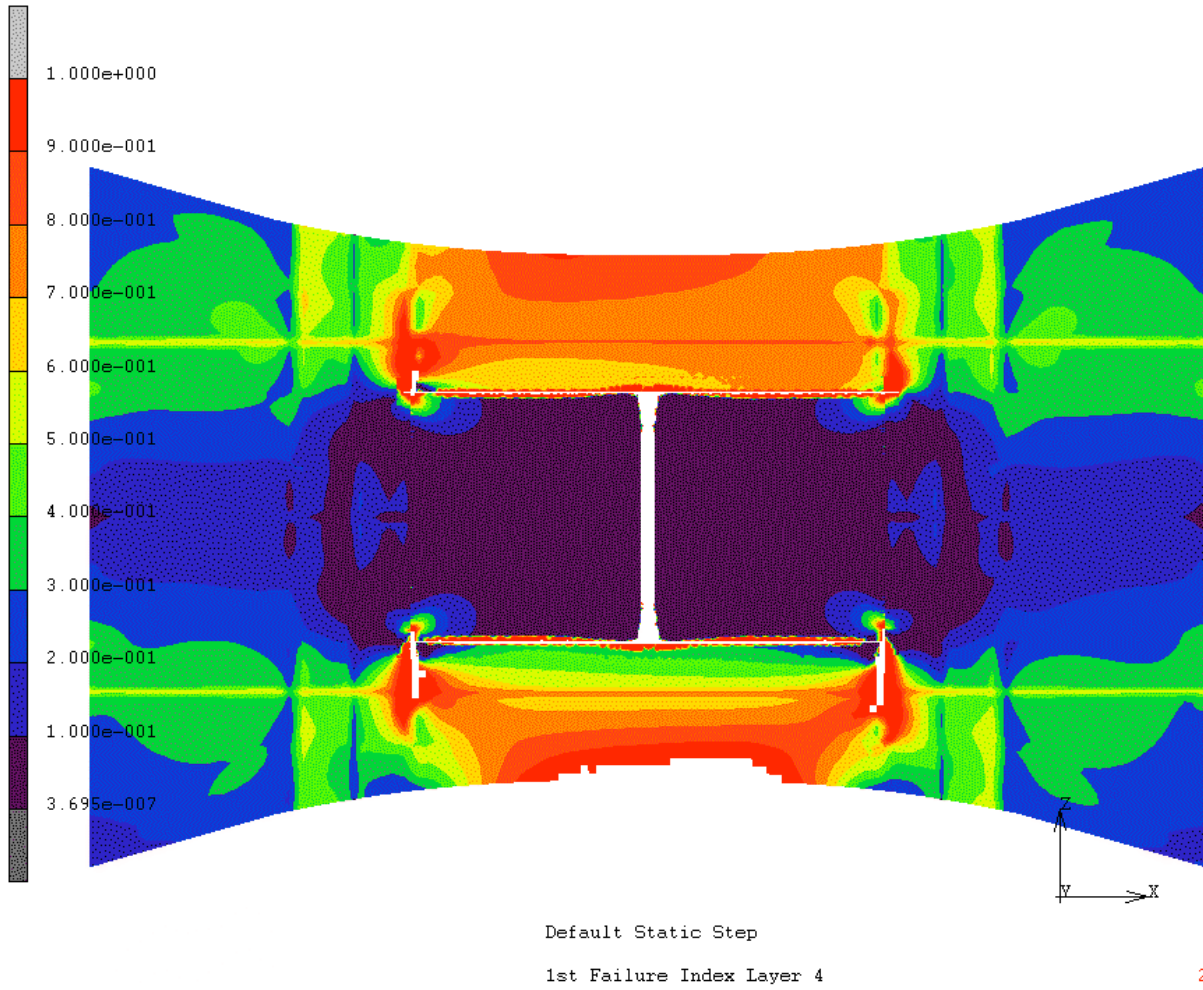


FIGURE 116. FAILURE INDEX FOR SKIN MID-PLY – CRACK ARRESTED AT FRAMES, REACHED ULT LOAD

Inc: 36
Time: 1.075e+000

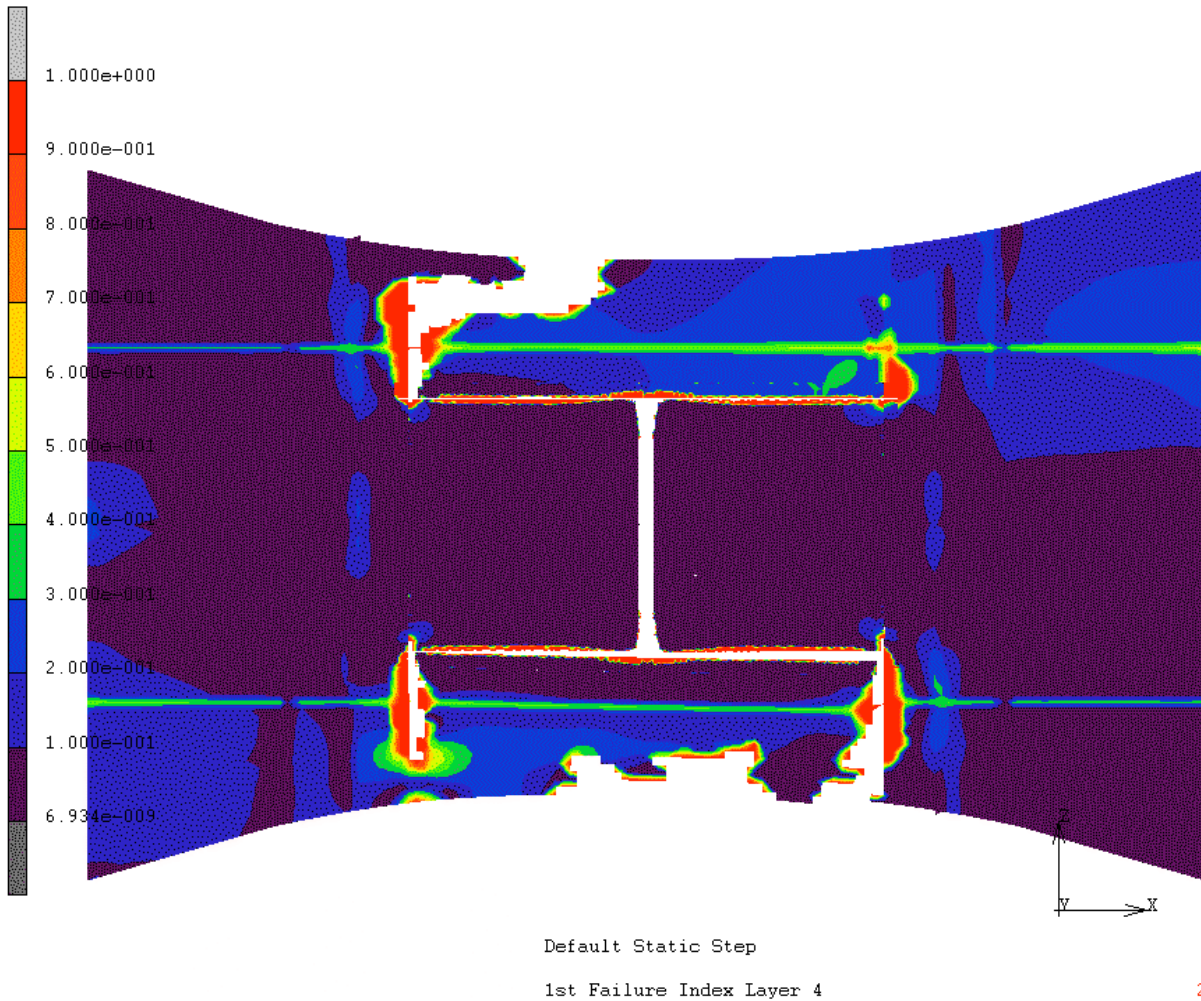


FIGURE 117. FAILURE INDEX FOR SKIN MID-PLY – PANEL RUPTURED

To effectively capture the behavior of the test panel, including crack initiation, crack growth patterns and paths, etc., a total of fifty-nine strain gages were allocated for the test specimen. The FEM results are used for optimal placements of these strain gages. Test specifications are generated and can be referenced per Boeing internal Test Specification Document ZA153441. Figure 118 through Figure 119 show the general layout of the strain gages.

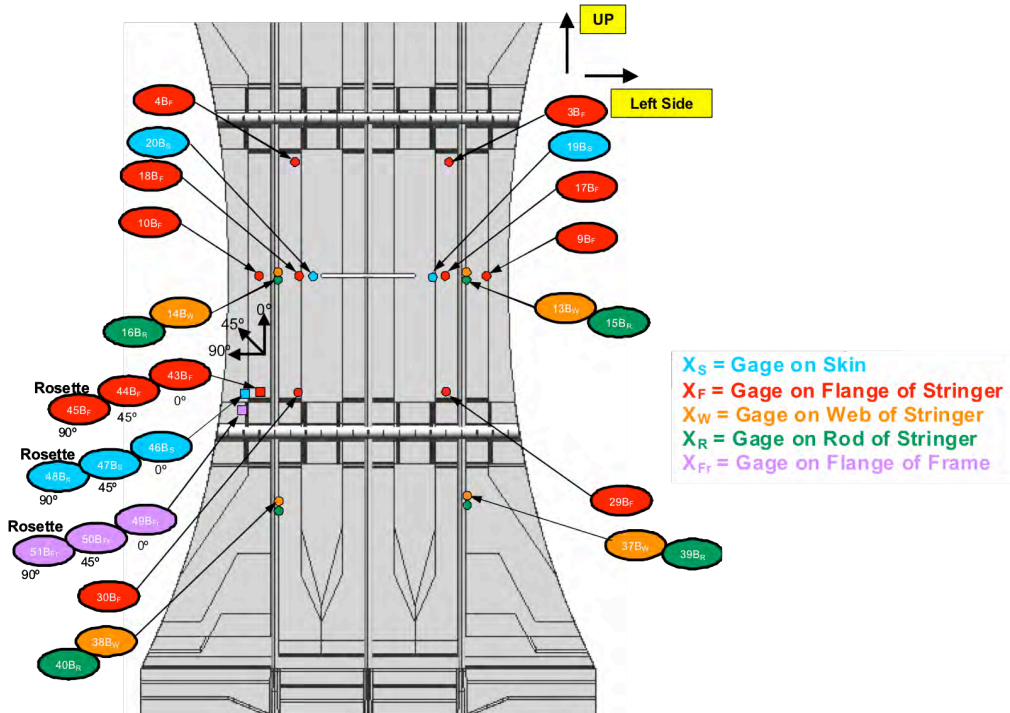


FIGURE 118. IML STRAIN GAGES

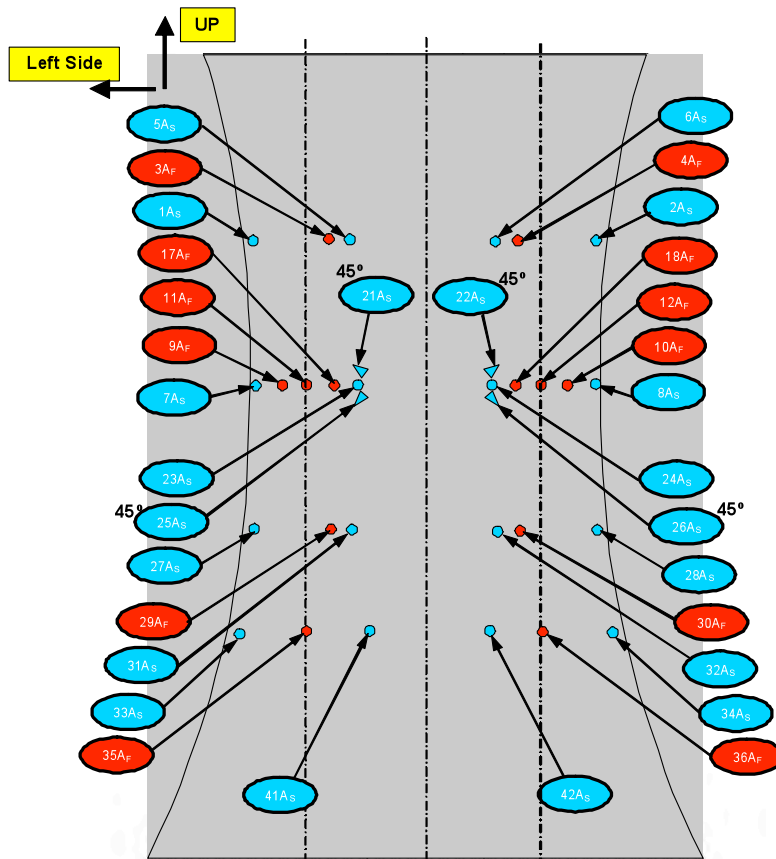


FIGURE 119. OML STRAIN GAGES

3.3 Panel Fabrication

The test specimen panel blank was fabricated using nominal PRSEUS stitching and resin infusion parameters. The only differences from previously fabricated panels were the use of a single stack skin (0.052-inch thick) and a change in its principal axis direction (parallel to the frame). Both the stitching frame and cure tooling (Figure 120) were existing tools that were fabricated under previous contracts. This allowed the panel fabrication work to start at the outset of the Phase II effort.



FIGURE 120. EXISTING STITCHING AND CURE TOOLS USED

Although the existing tool set was designed for a 7-stringer by 4-frame panel, the flexibility of the PRSEUS fabrication approach permitted the removal of stringer and frame elements without affecting the tooling. The final specimen blank (Figure 121) is a 5-stringer by 2-frame panel configuration with additional IML stacks added at each end to increase the bearing area for the end grip fasteners. In the final dog-bone shaped specimen, the edge stringers were trimmed away to create the proper 3-stringer net-section at the center of the panel.

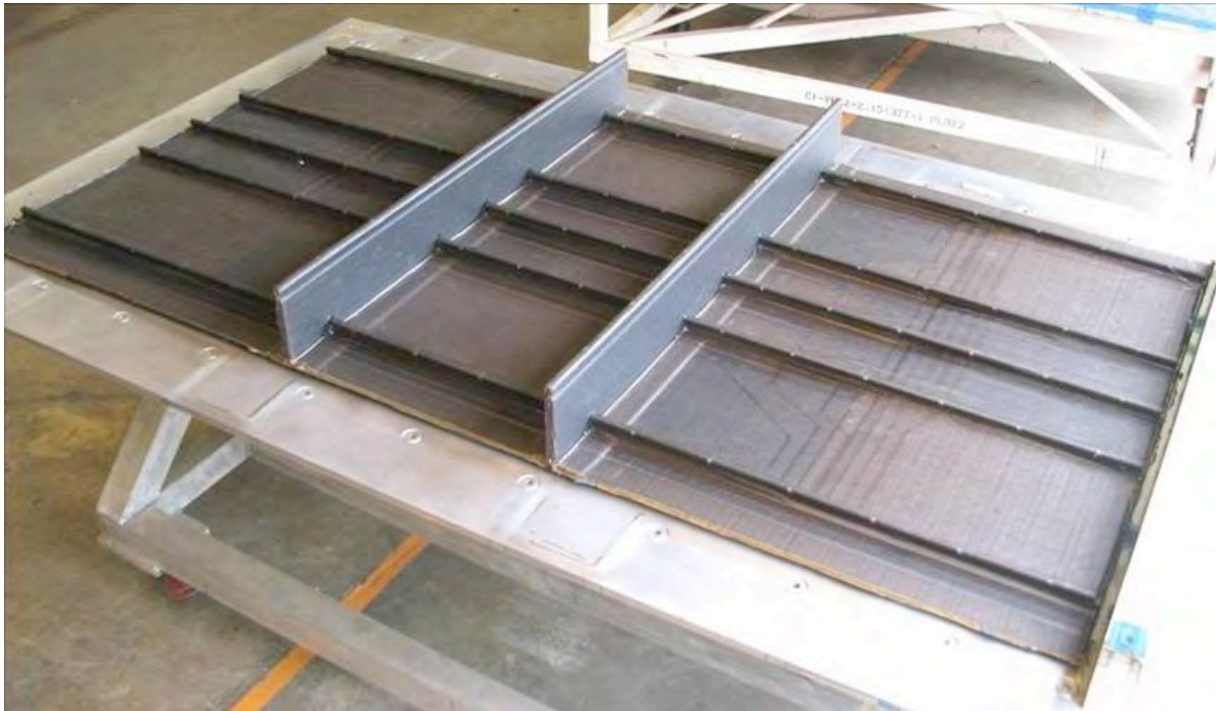


FIGURE 121. INFUSED SPECIMEN BLANK PRIOR TO EDGE TRIM

3.4 Specimen Preparation

Oddly enough, preparing the panel blank into the final test specimen configuration was more involved than the actual fabrication steps used to build the original panel blank. The end grip hardware that was added to the panel consisted of three main elements (Figure 122): 1) end plates, 2) stringer doublers, and 3) skin doubler trays. Each of the details is needed to help transition the loads out of the composite test specimen and into the large diameter pinned connections at the ends.



FIGURE 122. END GRIP HARDWARE DETAIL PARTS

The existing end plates are test hardware and were not fabricated under this contract. The consumable items, such as the stringer and skin doubler details, were machined and prepared by an outside vendor and then delivered to Boeing.

The details were assembled onto the ends of the panel (Figure 123) using an elevated-temperature bonding operation. Each of the primary steps in the end hardware assembly operation is shown in Figure 124. First the stringer doublers are fitted and bonded into place, then the skin doublers are bonded, and finally, the end plates are drilled and fasteners installed.

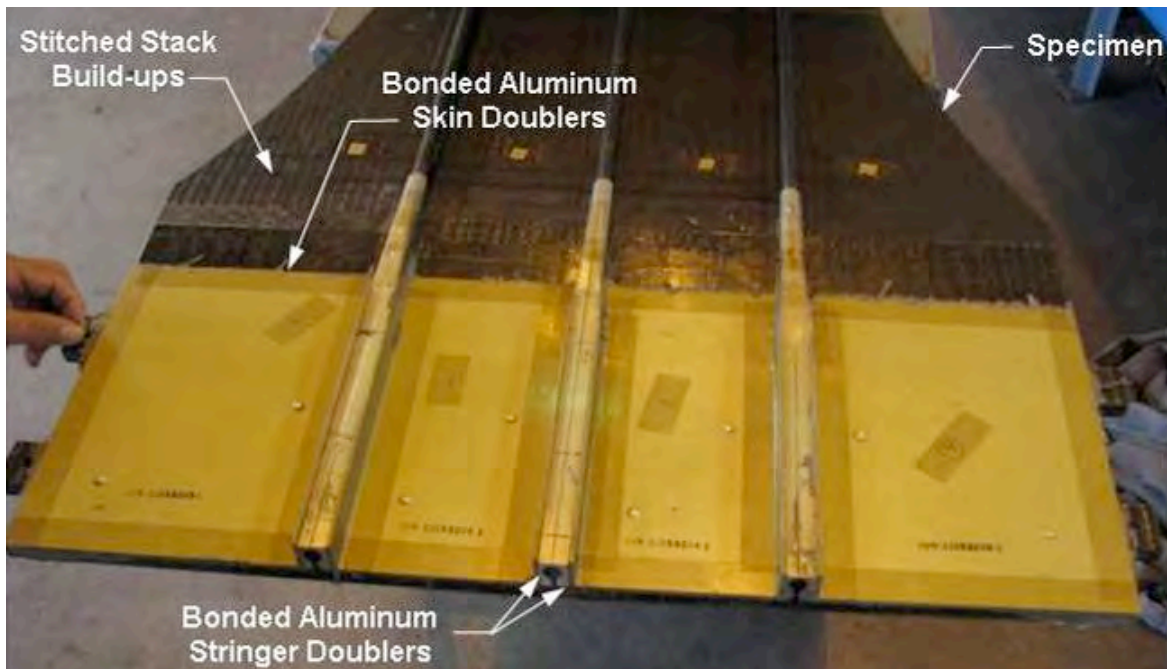


FIGURE 123. BONDED ALUMINUM STRINGER AND SKIN DOUBLERS



FIGURE 124. STEPS TO END GRIP PREPARATION

Strain gages were added to the specimen (Figure 125) per the instructions of Test Specification Document ZA153441.

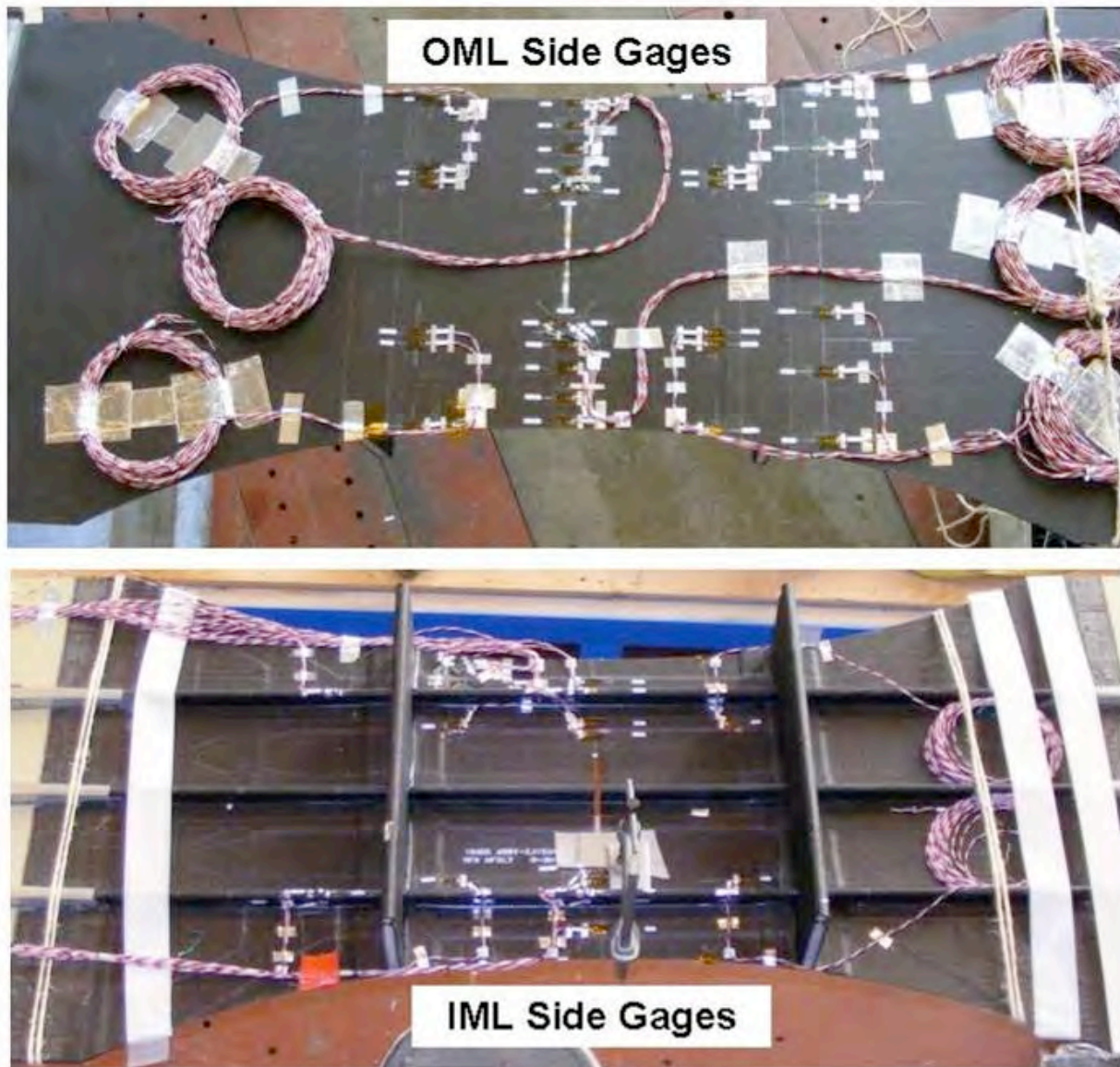


FIGURE 125. SPECIMEN STRAIN GAGE PLACEMENT

The completed specimen was then delivered to the test frame and installed. (Figure 126)



FIGURE 126. SPECIMEN DELIVERY TO BOEING HUNTINGTON BEACH TEST LAB

3.5 Testing

The specimen was installed into the load frame and mated to a calibrated load cell capable of providing sufficient force to fail the specimen in tension as shown in Figure 127. The final gage and instrumentation connections were made to the recording equipment for specimen checkout. The neutral axis of the specimen was aligned with the centerline of the load frame and checked per the test specification document (ZA153441).

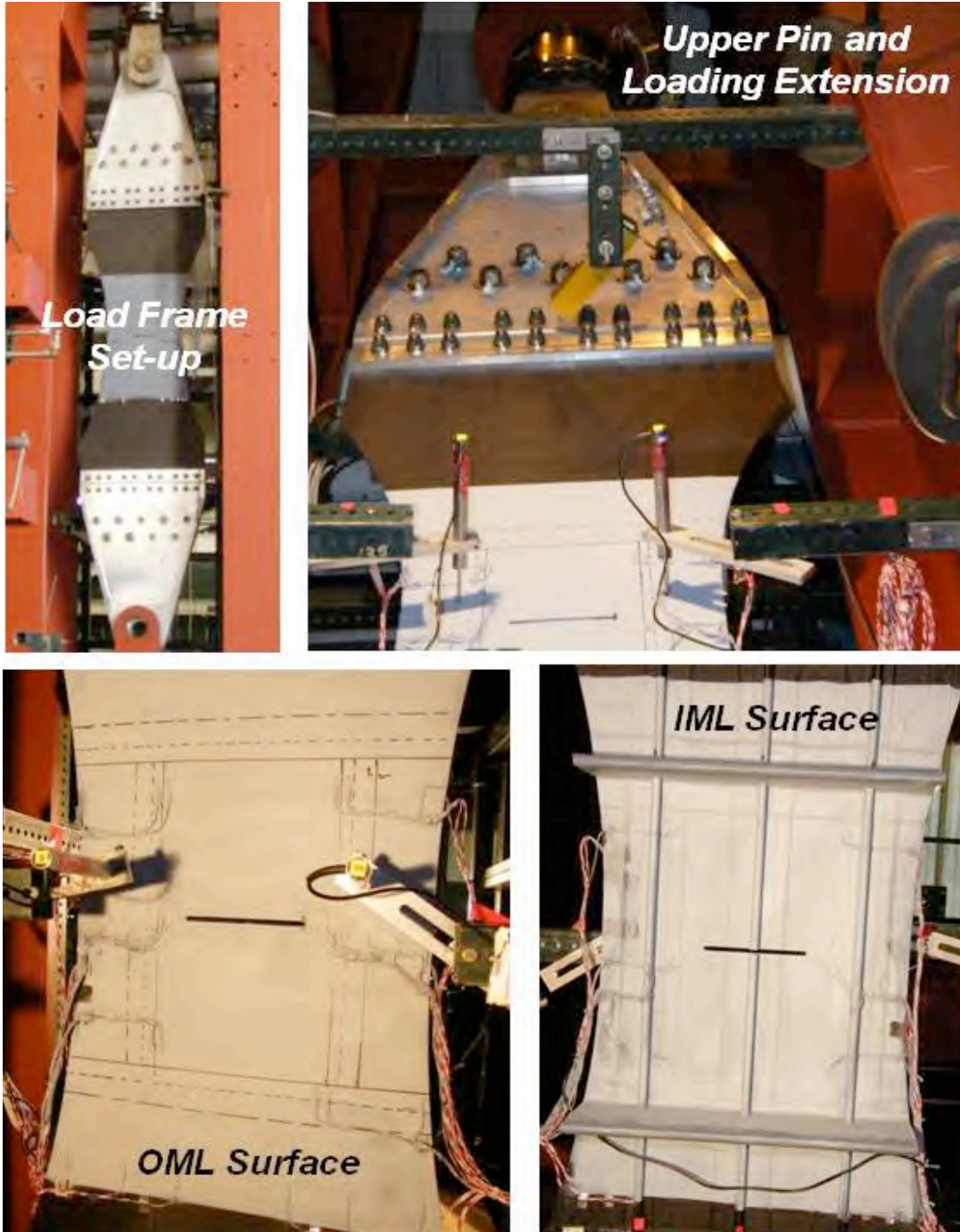


FIGURE 127. GENERAL TEST ARRANGEMENT

The actuator displacement and deflection transducers were used to accurately measure axial and out-of-plane displacements as the specimen was loaded (Figure 128). Six sets of measurements were made:

- 1) Skin displacement between the two center frames at Stringer 1
- 2) Skin displacement between the two center frames at Stringer 2;
- 3) Skin displacement between the two center frames at Stringer 3
- 4) Overall pin-to-pin displacement of the specimen
- 5) Skin out of plane displacement at Stringer 1
- 6) Skin out of plane displacement at Stringer 3

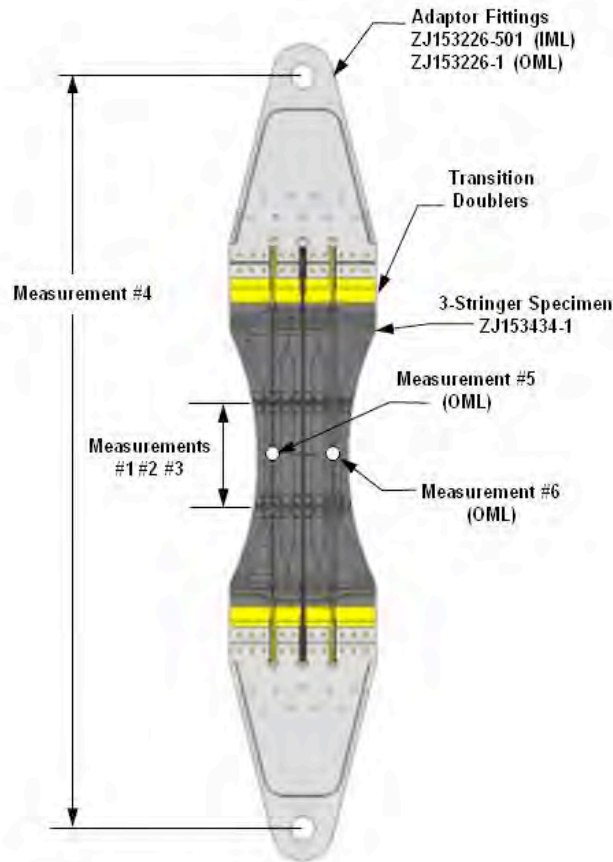


FIGURE 128. SPECIMEN ARRANGEMENT AND DISPLACEMENT GAGE PLACEMENT

Approximately fifty axial strain gage type FSE-00-25S-35-S3ET (or equivalent) and three rosettes were installed per drawing ZJ153434. All axial strain gages were positioned parallel to the specimen length except for strain gages 21As, 22As, 25As & 26As which were positioned along 45° axes. The three rosettes are positioned at 0°, 45° & 90°. Figure 129 shows the approximate strain gage locations and label identification markings. Strain gages were positioned on the external (smooth “A” side) and the internal (stringer “B” side) surfaces. Some local surface preparation may be required to create a flat area for the internal strain gages. Each strain gage was connected using #26 gage wire (or equivalent) with a plug (wire termination will be determined by system needs). All strain gages were painted with M-Coat D and labeled with ID markings on each strain gage (location photos are included in Appendix B)

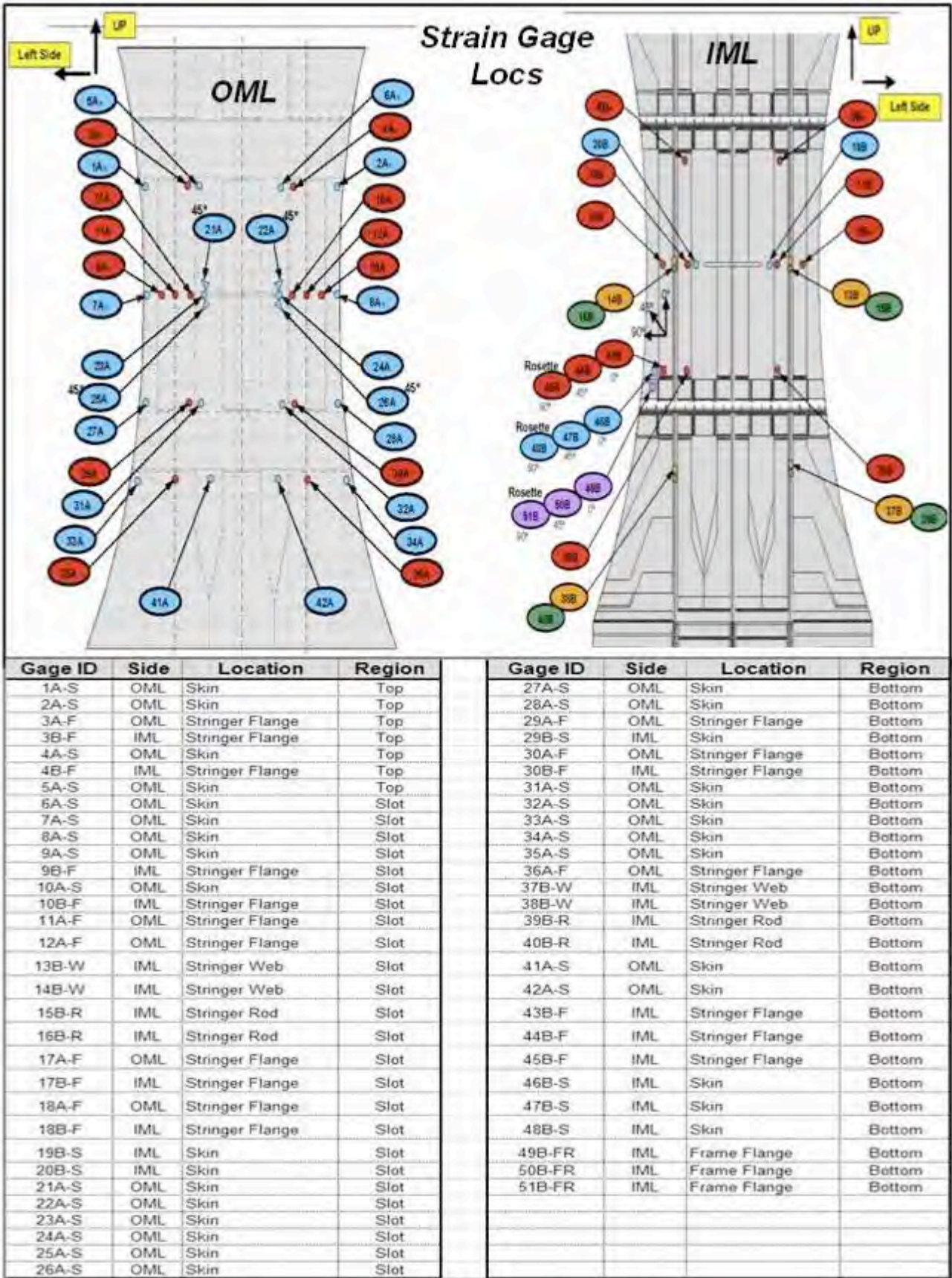


FIGURE 129. STRAIN GAGE IDENTIFICATION AND LOCATIONS

In addition to the strain, displacement, and load readings, still photographs and video data were also recorded. Video screens for the front and back-side video cameras are shown in Figure 130.



FIGURE 130. VIDEO PANELS USING DURING TESTING

Per the test specification, the specimen was statically loaded to failure with only brief pauses allowed to photograph local failure events leading up to the final catastrophic failure of the specimen. The loading was progressively increased and held during the following events:

Load (Kips)	Observation/Event Descriptions
46	Initial growth from slot edge
64	Damage arrested at stringer flange (both sides)
90	Vertical propagation along stringer flange
122	Propagation along both stringer flanges
136	Delaminations at edges of dog-bone shape
138	Skin fails, stringer separates, load drops
(load drop)	
125	Remaining stringer separates from skin
142	Edge failures in upper region of dog-bone shape
146	Stringer rod fails leading to final specimen failure

FIGURE 131. KEY FAILURE EVENTS DURING LOAD

Over the course reaching the final specimen failure, two load drops occurred: first, as the skin failed and the stringer separated at 138 Kips, and then again at 125 Kips as the remaining stringer separated during the ramp back up to final failure at 146 kips. The load-vs-displacement plots for

the test are shown below in Figure 132. The longitudinal displacements (Gages 1-3) match reasonably well, but there were some discrepancies on the out-of-plane measurements (Gages 5 and 6). The large, and nonlinear response at the outset, coming from Gage 5 was never resolved.

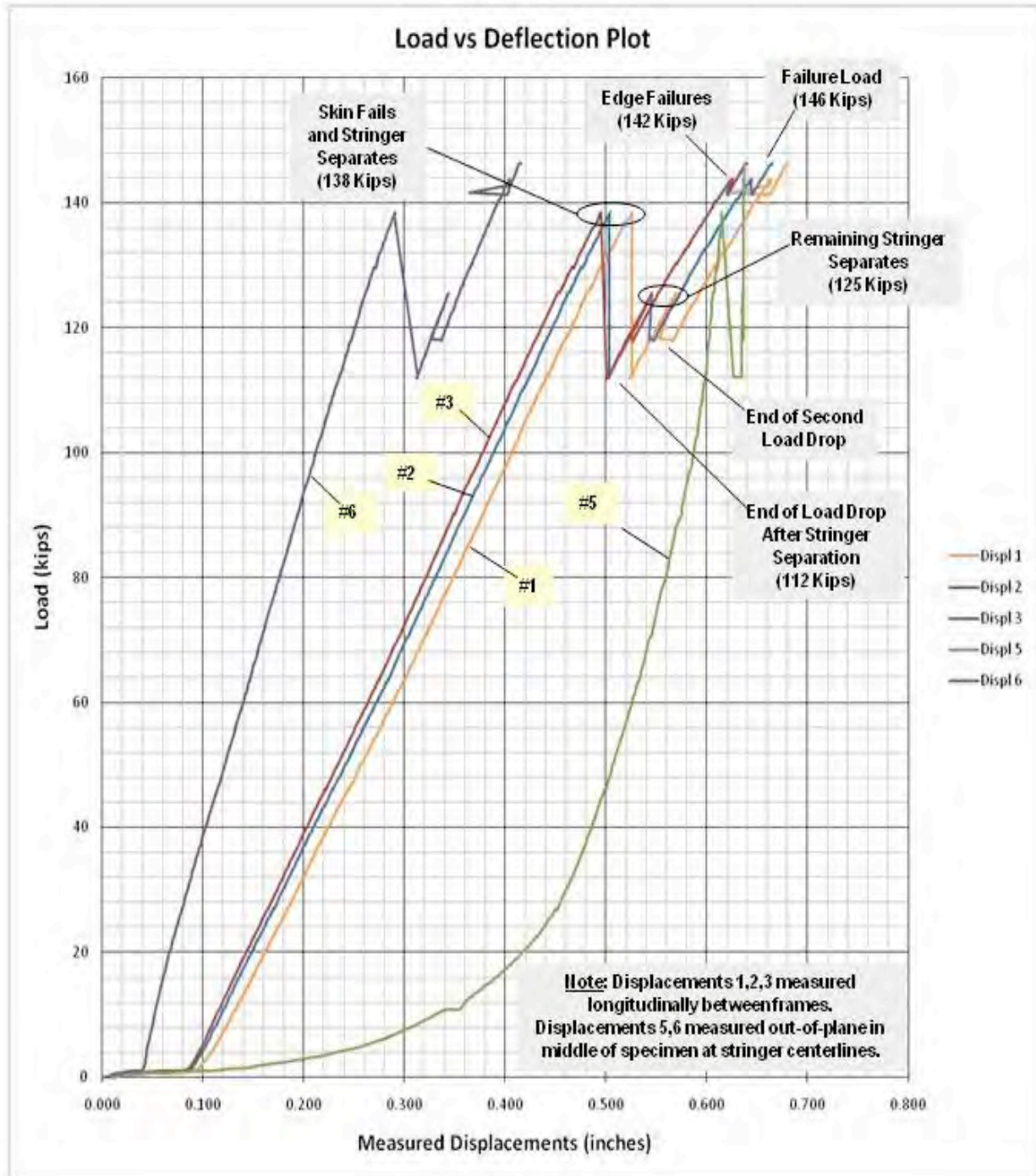


FIGURE 132. LOAD VERSUS DISPLACEMENT MEASUREMENTS

Strain gage readings were recorded and the plots are included in Appendix B. A progressive series of photographs of the key damage events were taken on the white-painted IML and OML surfaces of the test section (Figures 133 and 134).

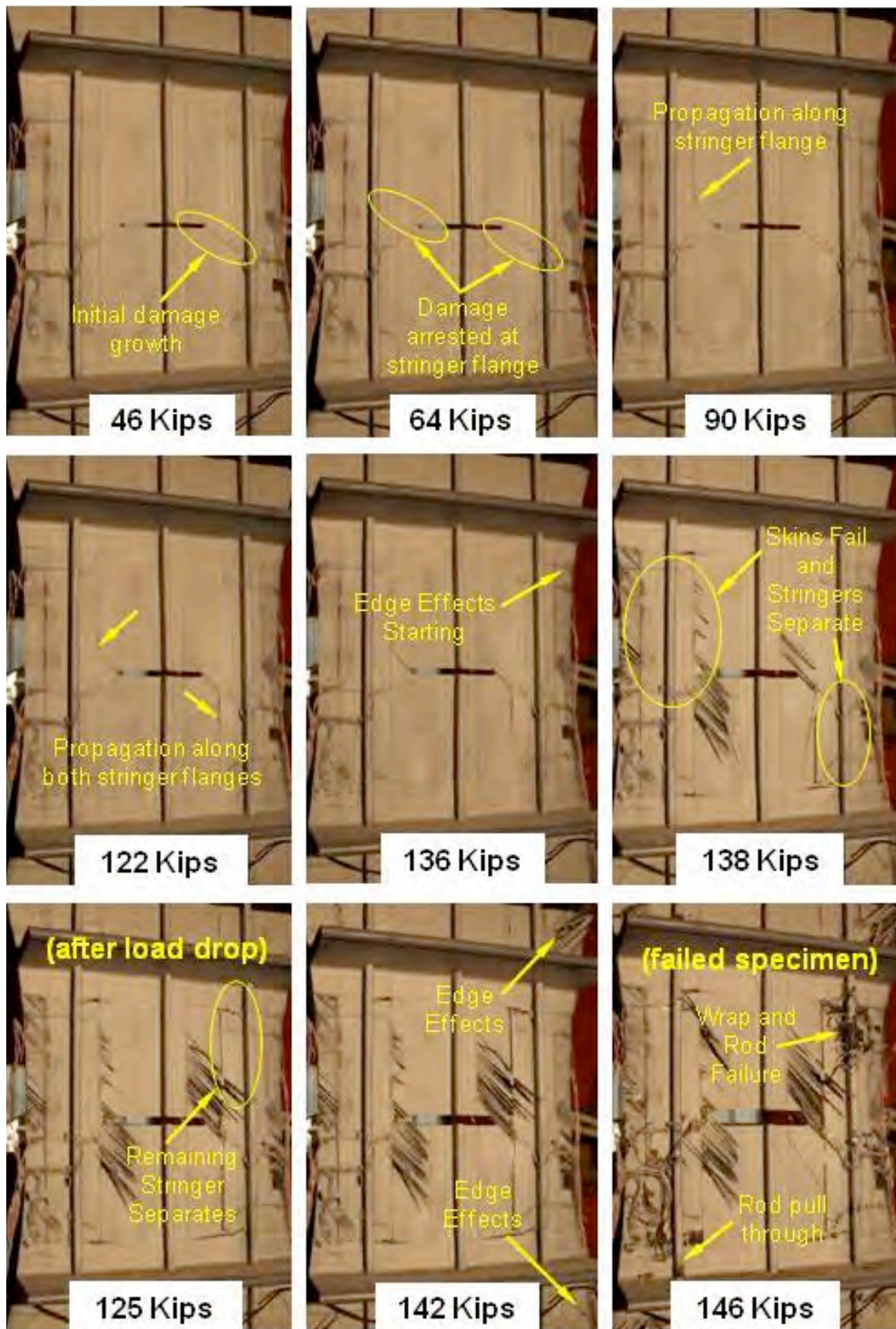


FIGURE 133. DAMAGE PROGRESSION ON IML SURFACE

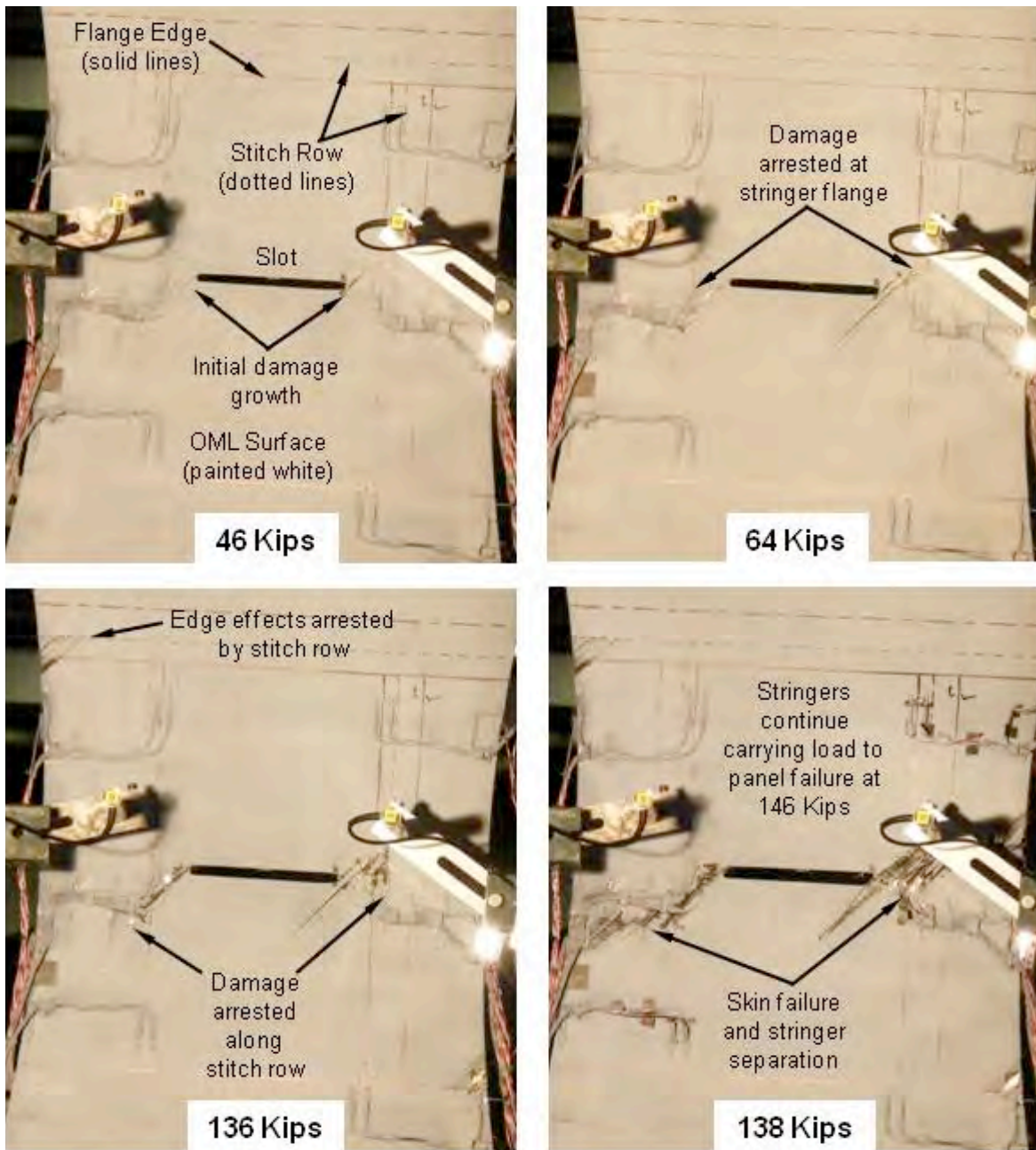


FIGURE 134. DAMAGE PROGRESSION ON OML SURFACE

The damage growth and arrestment capability of the stitch rows is evident in photographs, particularly in the OML photographs (Figure 134). As the damage grew from the slot to the stringer stitching (dotted lines), it was stopped in the horizontal direction and then grew vertically up the stringer a small distance during the loading from 64-to-138 Kips before the skin finally failed and the stringer separated. After the load drop to 112 Kips, the loading was ramped back up to final failure at 146 Kips. The post-failure surfaces of the specimen are shown in Figures 135 and 136, with close-up pictures of the key failures in Figure 137.

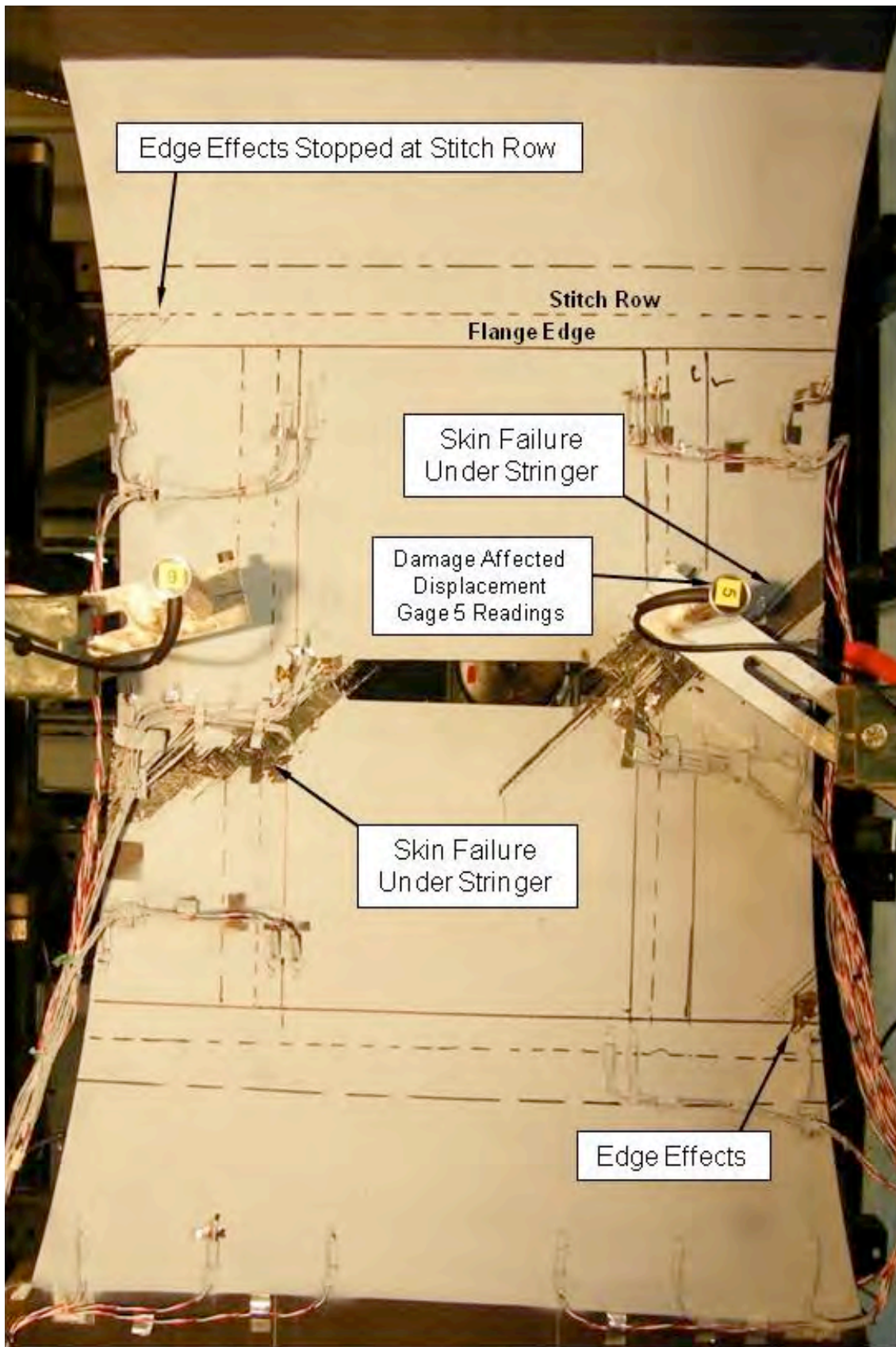


FIGURE 135. POST-FAILURE OML SURFACE

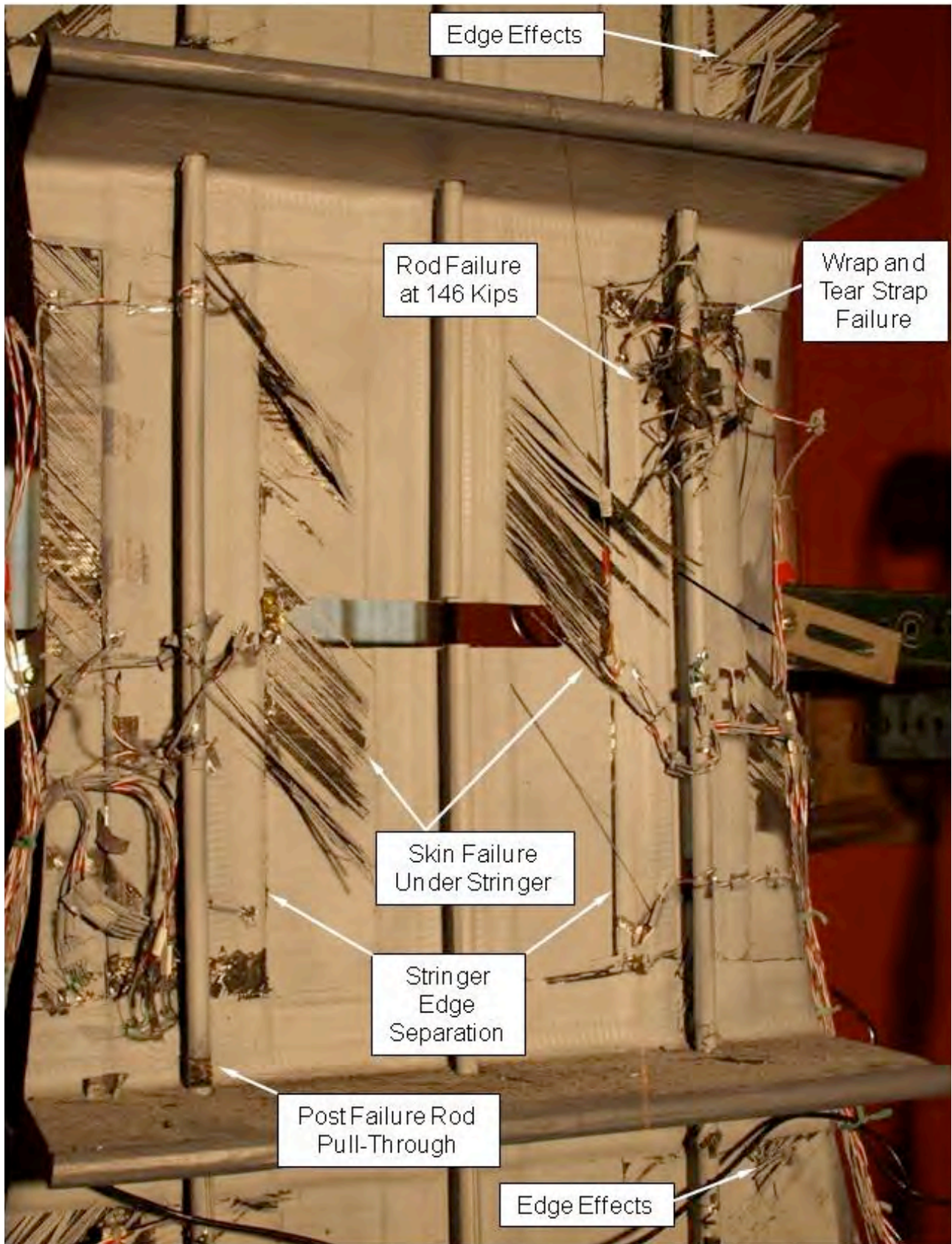


FIGURE 136. POST-FAILURE IML SURFACE

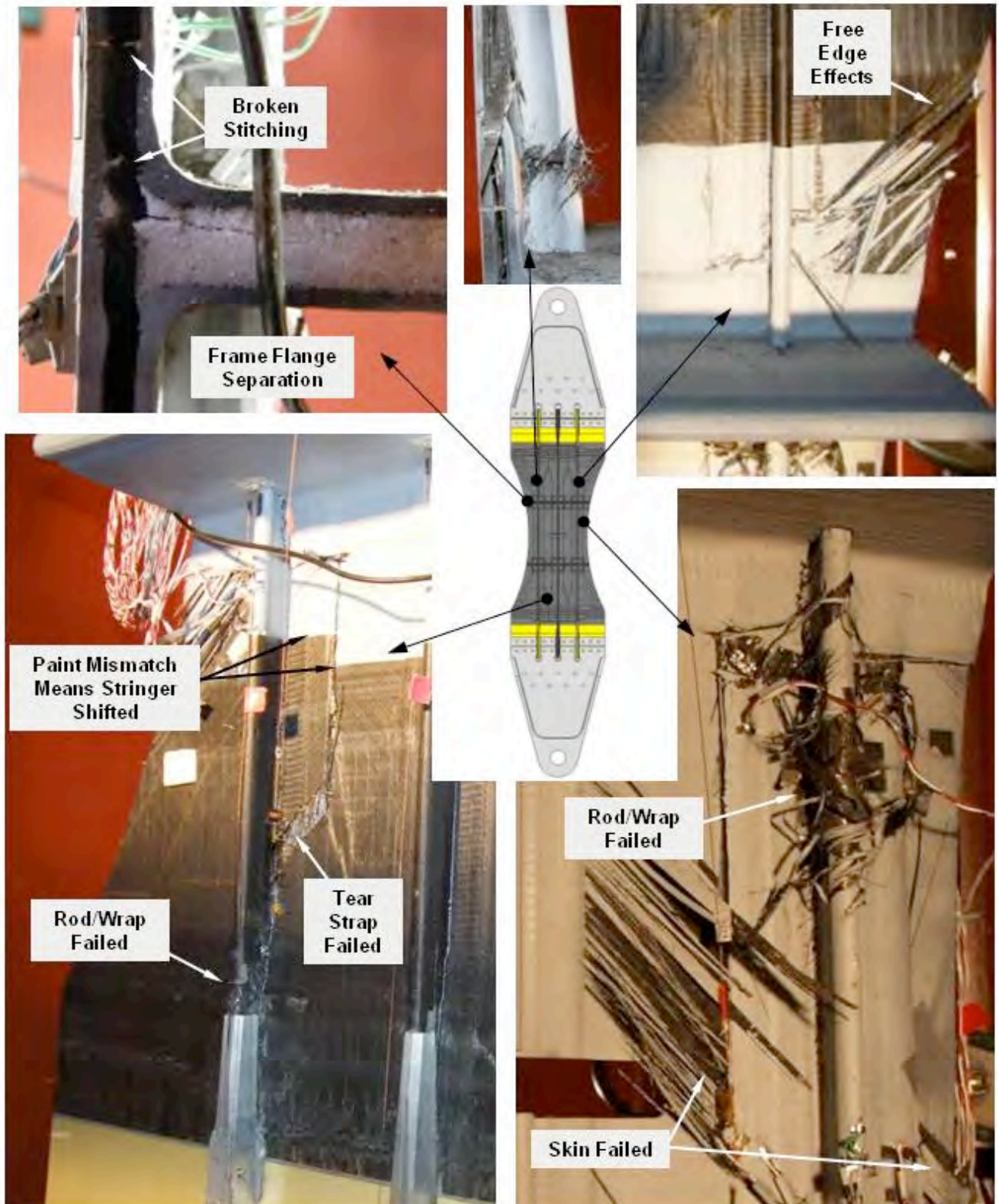


FIGURE 137. SPECIMEN POST-FAILURE PHOTOGRAPHS

Other than the odd reading from Displacement Gage #5, all of the other test proceedings went as planned; with all of the key events of the damage progression sequence being observed and recorded. The primary failures of the skin, stringers, and rod elements all corresponded to

measured load drops captured by the instrumentation. Comparison of the magnitudes for the pre-test damage-arrest at stringer and final failure events were also very well predicted (Figure 138 and 139).

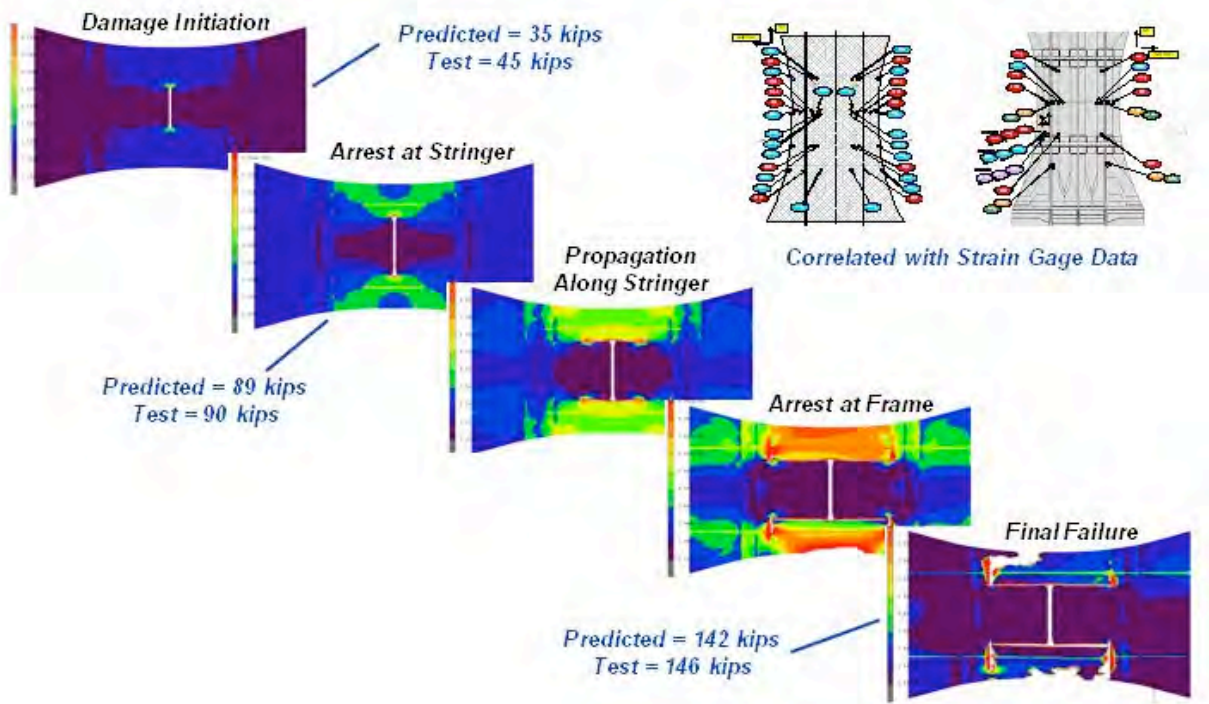


FIGURE 138. PRE-TEST PROGRESSIVE FAILURE ANALYSIS

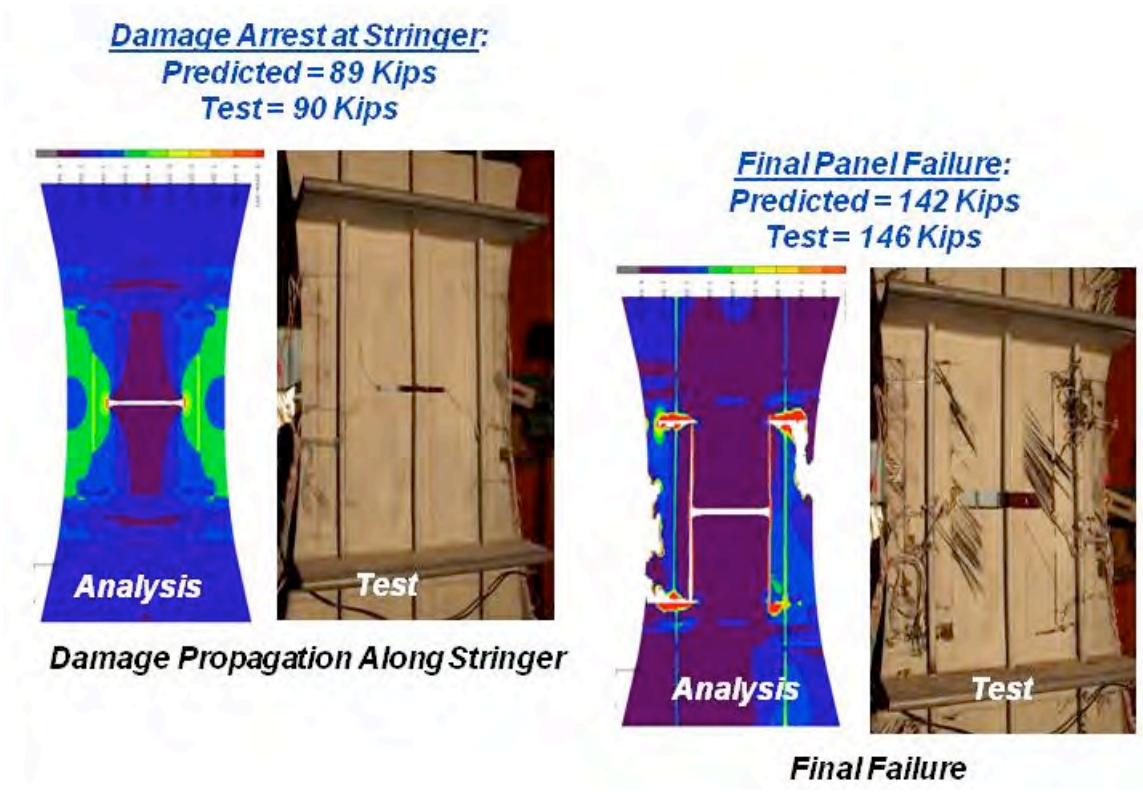


FIGURE 139. COMPARISON TO PRE-TEST PROGRESSIVE FAILURE ANALYSIS

4.0 SPANWISE COMPRESSION PANEL (WBS 3.5.3)

The primary purpose of this subcomponent test was to assess the buckling stability of the PRSEUS integral frame feature. Because the frame and skin stacks are infused as a singular element, without shear clips or fasteners, the ensuing panel geometry is a highly effective component under compressive loading. This test simulated the spanwise compression loads that are imparted on the upper portion of the pressure shell by the positive 2.5-g maneuver wing bending loads. The 2-frame compression specimen geometry shown in Figure 140 will be used for this test.

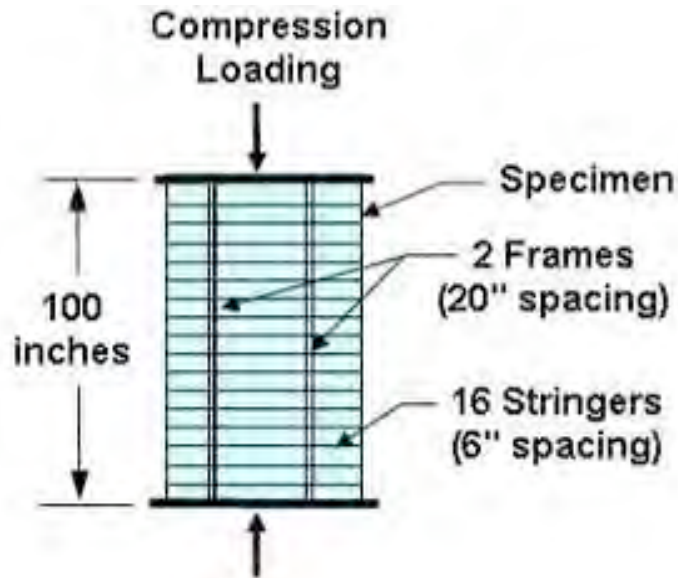


FIGURE 140. SPANWISE COMPRESSION PANEL SPECIMEN CONCEPT

4.1 Design

Two detail design drawings were created, one for the specimen blank (cured PRSEUS panel prior to edge trim) and another for the final test specimen configuration with the potted end plates and side restraints installed (Appendix C).

Extra features were added to the basic 2-frame, 15-stringer, 30-inch by 90-inch panel to smoothly transition the platen end loads into the nominal test section of the panel. Additional skin stacks and stitching are added at the ends to compensate for local stress concentrations around the potted end plates. The extra doubler stacks were added to the end of the stringer bays and around the frame caps extending all the way down to the third stringer. An external OML stack was also added extending down to the first end stringer. The added stack materials at the ends can be seen in Figure 141.

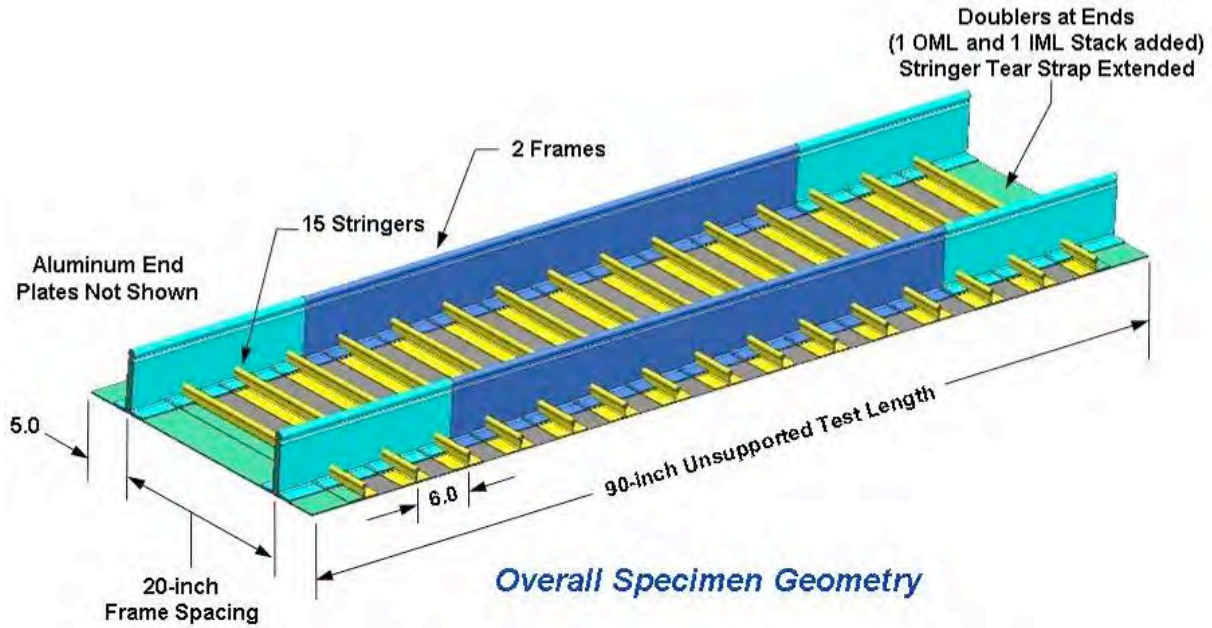


FIGURE 141. COMPRESSION PANEL SPECIMEN

The panel specimen was fitted with machined aluminum potted endplates and placed in the testing fixture shown in Figure 142. Side edge restraints were used to stabilize the free edges of the skin while cap screws prevented the thin gauge skins along the edge from buckling as the panel specimen is compression loaded. Since the cap screws do not penetrate the panel, the screws just touch the skin on the IML side of the specimen, load is not transferred into restraint members.

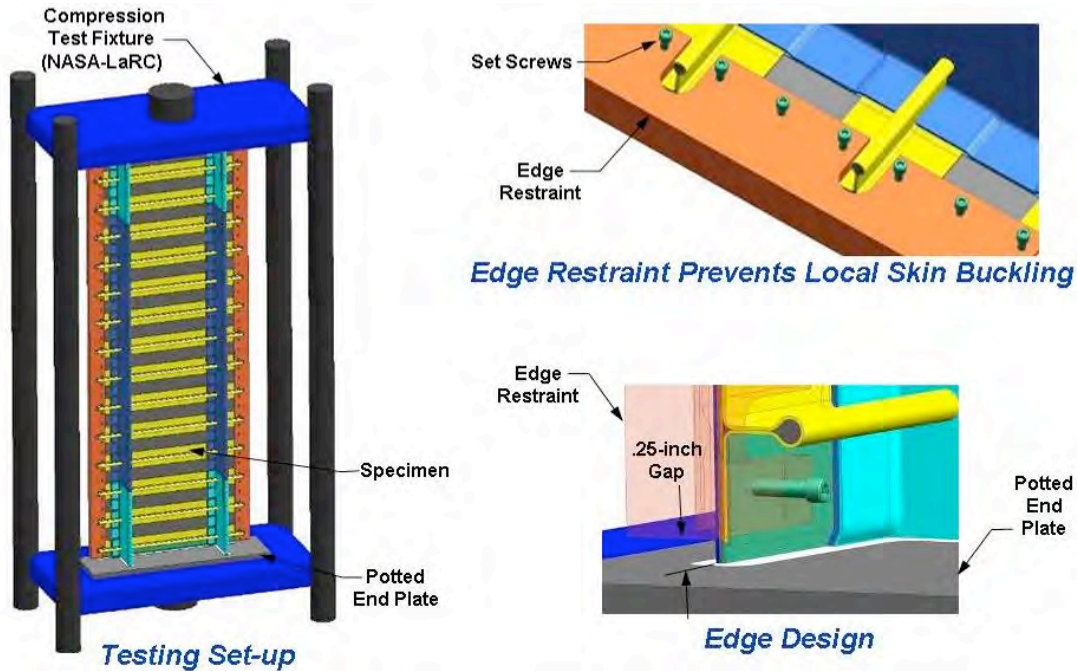


FIGURE 142. GENERAL FEATURES OF SPECIMEN DESIGN

4.2 Analysis

A FEM-based analytical task was performed to predict failure loads, modes, and determine the optimum strain gage placement for testing. A linear approach was used to check the onset of skin buckling and to assess initial strength margins. Nonlinear runs were then used to determine overall panel buckling modes and to assess local strength failures in critical regions. The resulting failure loads were compared to one another to determine whether the panel was strength or stability critical.

The analysis results were used to assess the buckling stability of the PRSEUS frame by simulating the spanwise compression loads caused by the pull-up wing-bending maneuver (2.5-g). The analysis and test results demonstrate stability capability beyond design limit loads, the strength capability beyond expected compression loads, and validation of the analytical predictions and methods.

The methodology used to generate the specimen loads is shown in Figure 143. For the ultimate load case, the expected running load under compression would be 5,000-lbs/in. With the baseline PRSEUS frame spacing of 16 inches in the aft region where the spanwise load are the highest, this comes out to approximately 80,000-lbs per frame, or about 160,000-lbs for the 2-frame geometry used in the specimen design.

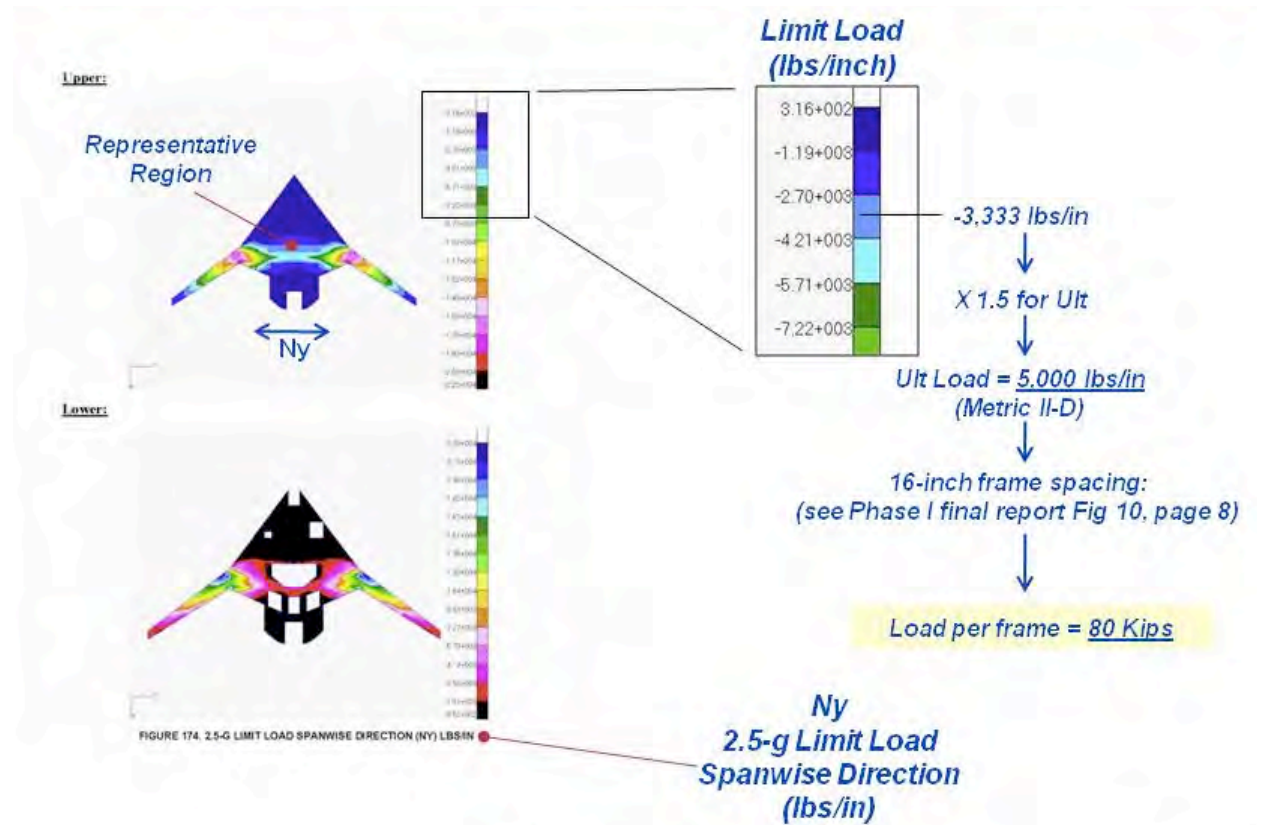


FIGURE 143. DESIGN ULTIMATE RUNNING LOAD CALCULATION

The FEM was a simple model made from shell elements to represent the skin, rod elements to represent the pultruded rods, and solid elements for the foam core (Figure 144). The panel has one short edge fixed with an enforced displacement to simulate the compression load applied on the other edge (RBE2 elements). In this model, the center region of the specimen is a finer mesh

to better view the strains in the test region. The panel model was 30-inches by 90-inches in the section being tested between the potted ends plates. The aluminum beam restraints along the long edge of the panel are modeled using beam elements that are attached to the edge of the panel using RBE2 elements only restricting the out-of-plane motion of the panel.

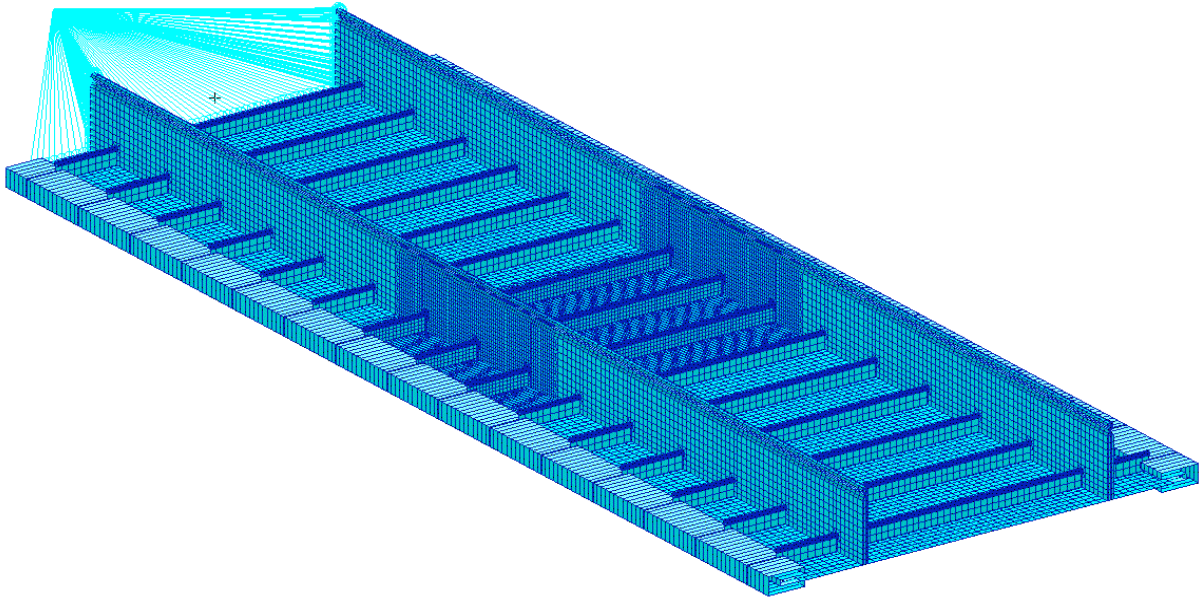


FIGURE 144. COMPRESSION PANEL FINITE ELEMENT MODEL

Initial results from the nonlinear analysis show that local buckling of the skin occurs at 59,000 lbs (Figure 145). At 59,000 lbs, skin buckling occurs at approximately 30% of ultimate load as required by the BWB design requirements.

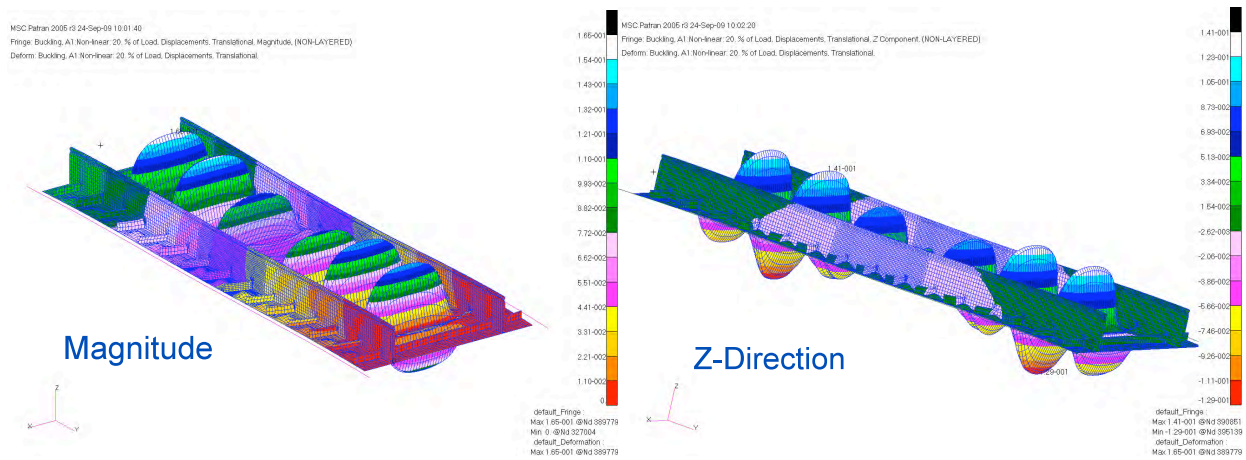


FIGURE 145. SKIN BUCKLING OF THE COMPRESSION PANEL AT 59,000 LBS

A plot of the displacements as the compression load increases also shows when this linear buckling of the skin occurs in Figure 146. Beyond 59,000 lbs, there is no additional buckling or sharp load changes until 200,000 lbs. At this point, the frames continue to carry load until approximately 207,000 lbs where global buckling of the frames occur.

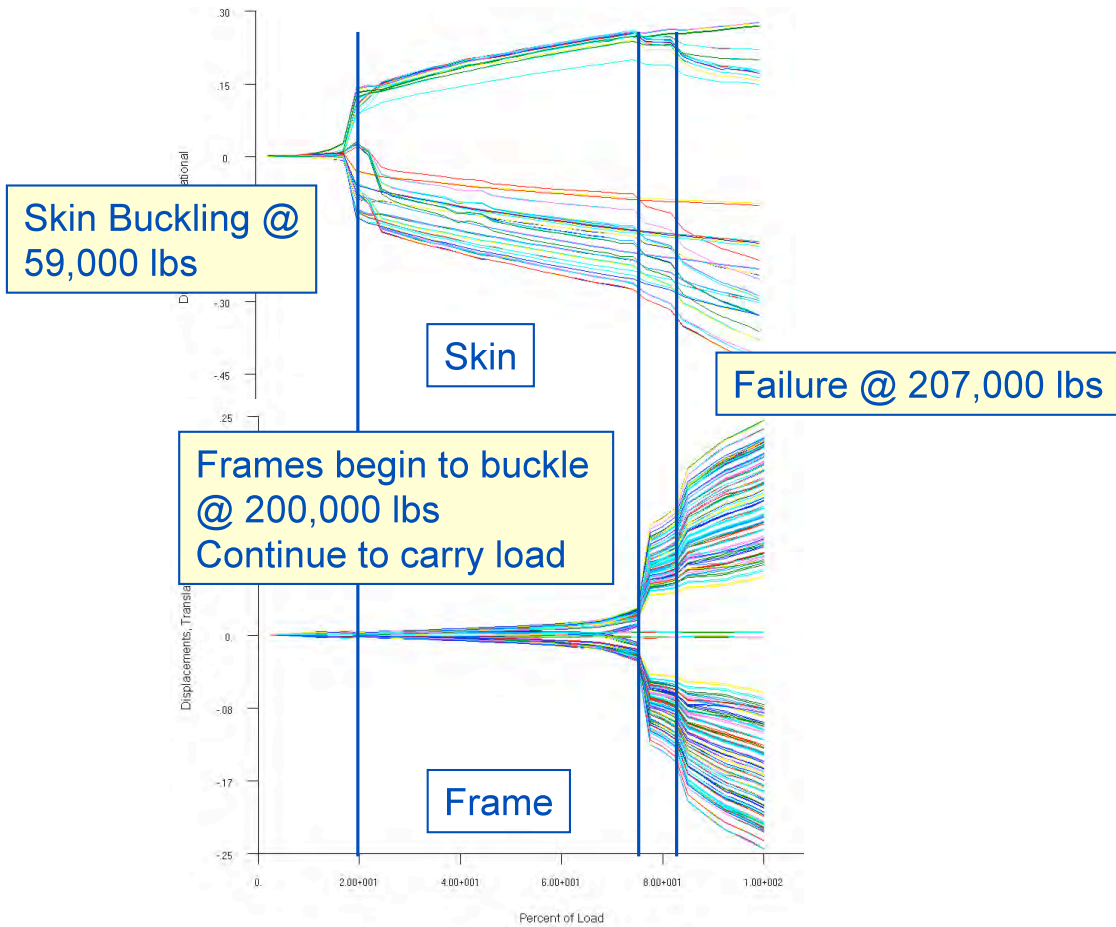


FIGURE 146. SKIN AND FRAME DISPLACEMENTS PLOTS AS A FUNCTION OF LOAD

Displacement plots of the frame at 207,000 lbs depict buckling of the frame section as shown in Figure 147. These results show that the compression panel is stable above 200,000 lbs, which meets the 5,000-lb/in requirement.

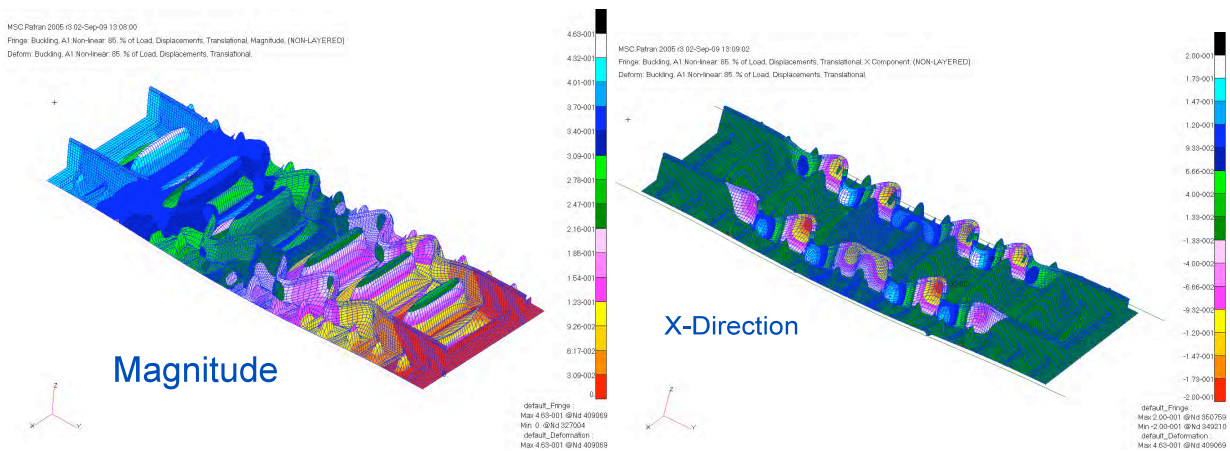


FIGURE 147. GLOBAL BUCKLING OF THE COMPRESSION PANEL AT 207,000 LBS

At this load, the strain in the panel is investigated to determine whether or not the strains indicate the panel fails in strength or if the panel buckled prior to reaching the test design value. The test

design value was set at 0.0065-in/in of strain based on the results of the single-frame compression test completed in Phase I of this contract and shown in Figure 148.

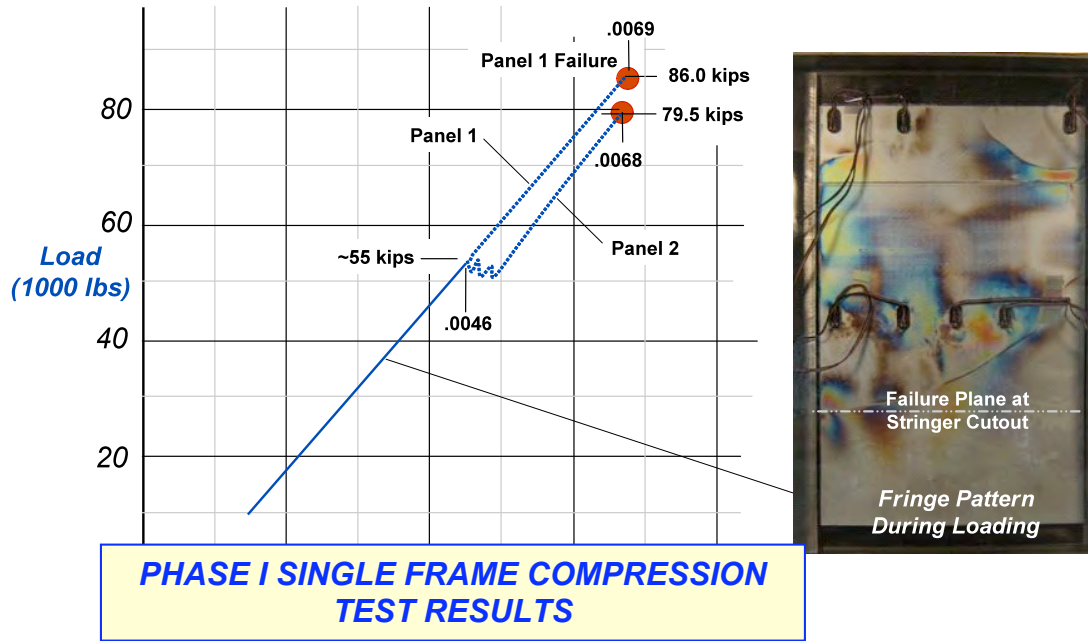


FIGURE 148. PHASE I COMPRESSION SPECIMEN FAILURE STRAINS USED FOR PHASE II

Strain results from the nonlinear analysis in both the x- & y-strain are plotted in Figure 149 using global coordinates. The y-direction strain (in the direction of the frame) is the most critical and shown closer up in Figure 150. The peak strain in this figure occurs just above the stringer keyhole cutout in the frame web. This is the location where the single-frame compression panel failed in Phase I and the predicted location of failure in this compression test as well. Other high strain locations exist at the panel edges, where the aluminum edge restraint is connected and local skin buckling occurs, and the frame caps, where bending of the frame due to buckling occurs, and are expected locations for peak strains. The strain design value of 0.0065-in/in is shown in the figure.

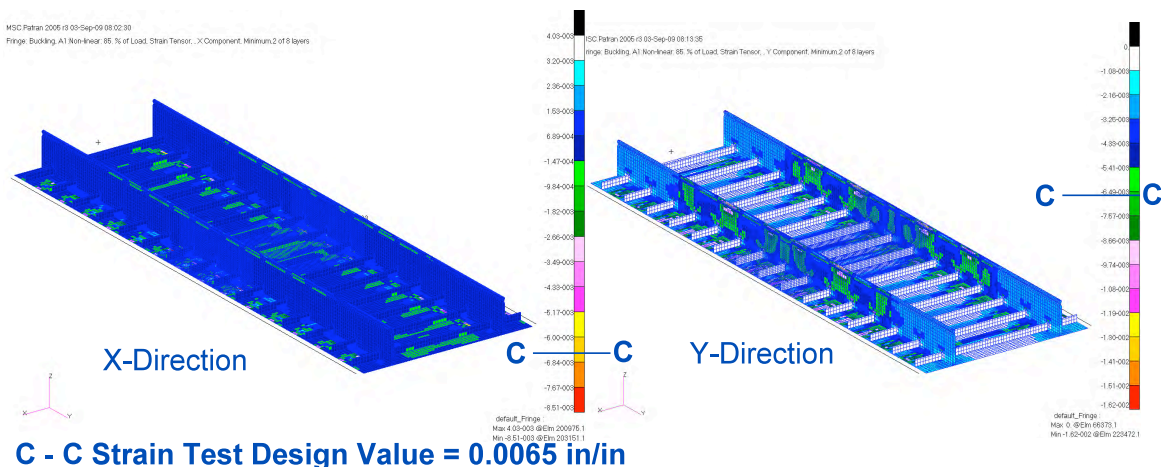


FIGURE 149. STRAIN RESULTS IN THE X- AND Y-DIRECTION FOR THE GLOBAL PANEL

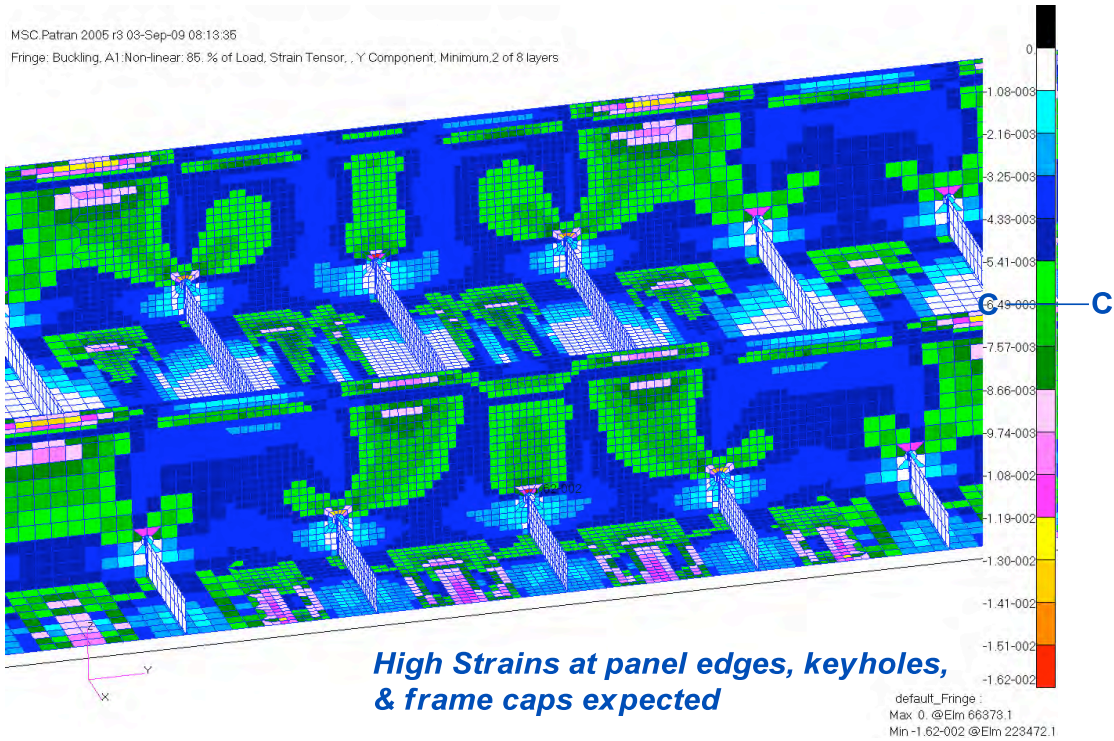


FIGURE 150. Y-DIRECTION STRAINS SHOWN AT CRITICAL LOCATIONS

The FEM minimum principal strain results also correlate with the y-direction results in showing the critical locations and peak strains in Figure 151.

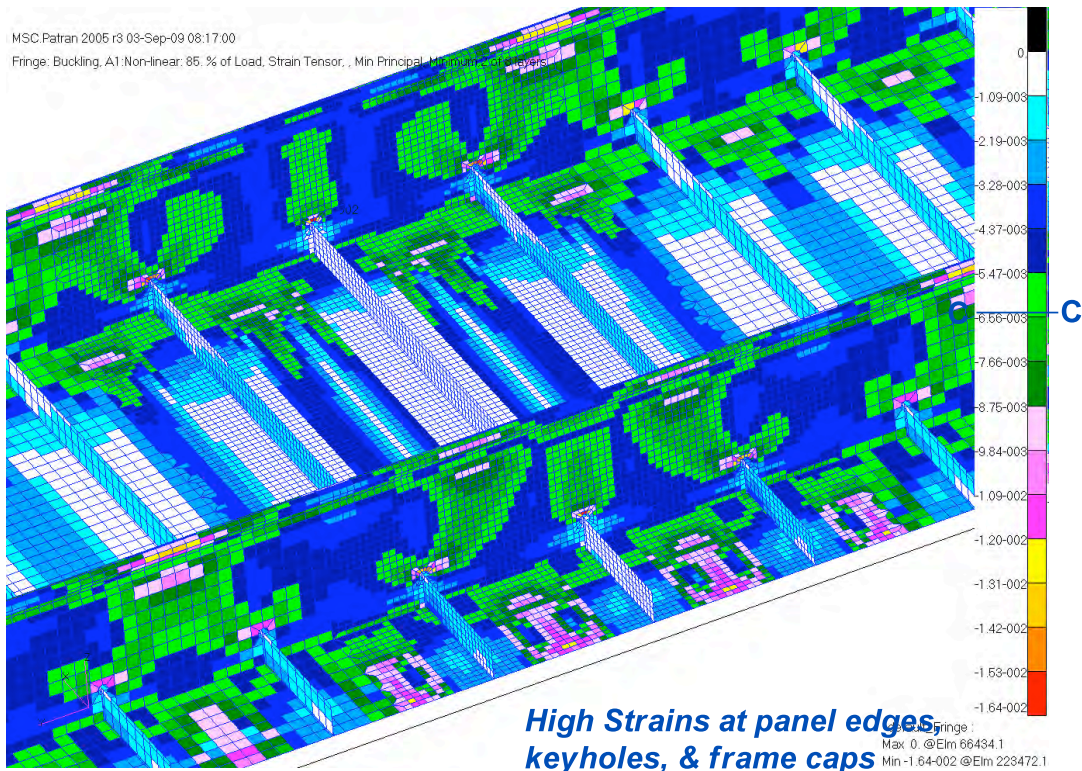


FIGURE 151. MINIMUM PRINCIPAL STRAINS SHOWN AT CRITICAL LOCATIONS

A section of the frame panel just above the keyhole where failure of the panel is expected to initiate is inspected to determine the strain load at buckling in the y-direction strain and in minimum principal strain in Figure 152.

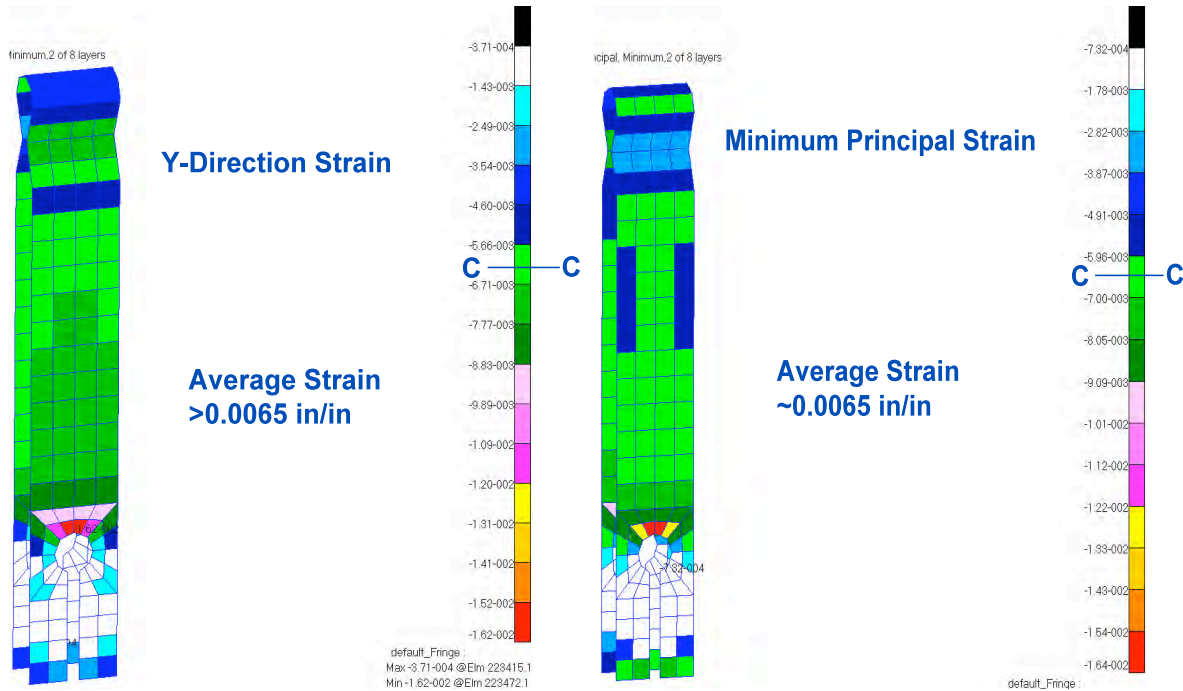


FIGURE 152. Y-DIR AND MIN PRINCIPAL STRAINS ON FRAME AT CRITICAL LOCATIONS

These results show strain values at or near the test design value for strain of 0.0065 in/in. Based on these results, the prediction was made that the compression panel will fail under both buckling and strength at approximately 207,000 lbs. This result would meet the requirement of carrying 5,000 lbs/in for even the 20-inch frame spacing and demonstrate the stability capability beyond design limit loads and the strength capability beyond expected compression loads meeting the objectives of the demonstration.

A detailed test specification document was also prepared that described the test set-up, instrumentation locations, and data recording requirements. The FEM results have been used for optimal placements of the strain gages shown in Figure 153 through Figure 155. To effectively capture the behavior of the frame specimen under compression, 80 strain gages were applied to the panel per the Test Specification Document ZA153382.

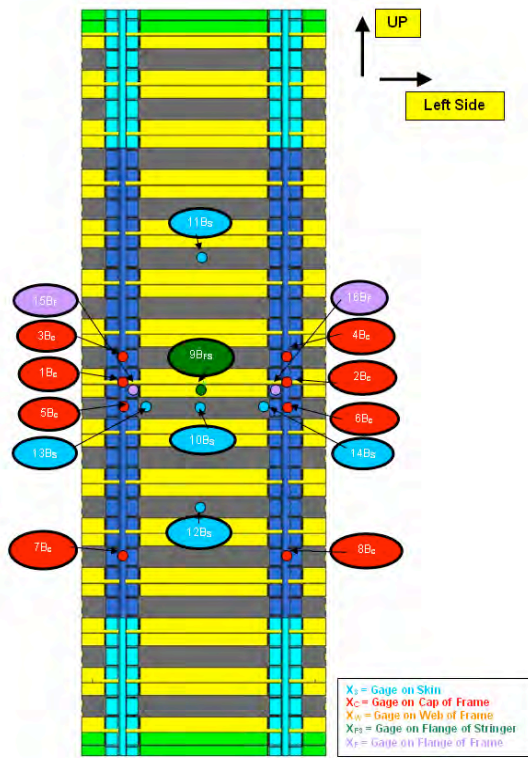


FIGURE 153. COMPRESSION TEST STRAIN GAGE PLACEMENT – IML STRAIN GAGE LOCATIONS

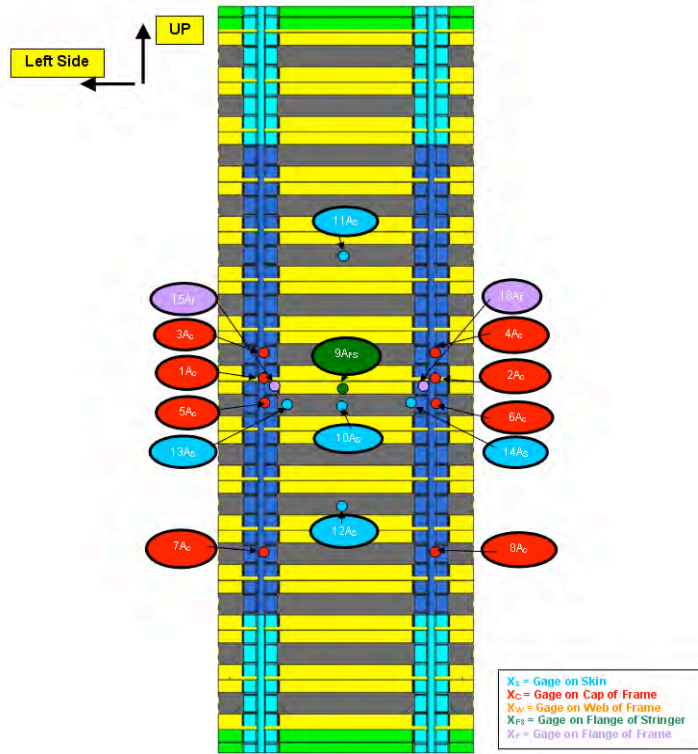


FIGURE 154. COMPRESSION TEST STRAIN GAGE PLACEMENT – OML STRAIN GAGE LOCATIONS

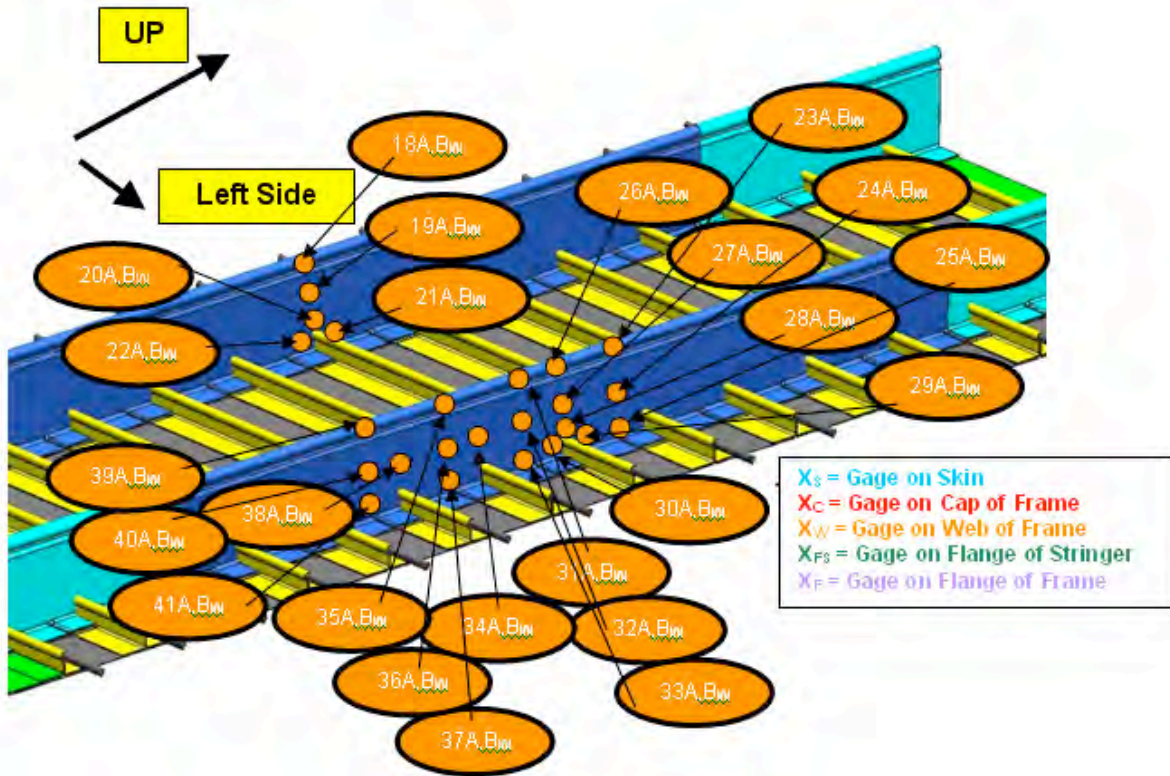


FIGURE 155. COMPRESSION TEST STRAIN GAGE PLACEMENT – FRAME STRAIN GAGE LOCATIONS

4.3 Panel Fabrication

The manufacturing approach for the PRSEUS spanwise compression panel was identical to that used for the internal pressure panel. The only difference being a slight reduction in overall width and length for the compression panel. For a detailed explanation on how the panel was fabricated see Section 2.4 of this report. The resin infused spanwise compression panel prior to final part trim can be seen in Figure 156.



FIGURE 156. SPANWISE COMPRESSION PANEL AFTER RESIN INFUSION PROCESSING

4.4 Specimen Preparation

Upon completion of final post-cure operation, the PRSEUS spanwise compression panel was prepared for structural testing. The panel was placed on a CNC machine to remove the 1.0-in. of excess trim from all edges. Machined aluminum end frames were then cleaned, etched and primed for bonding to the panel. The panel was placed onto a granite surface table for potting of the end inside the aluminum frame. Modular tooling was erected around the panel to maintain its perpendicularity to the table surface and position inside the aluminum frame (Figure 157 and Figure 158). Hysol EA9394 paste adhesive was used for the potting process. Once the adhesive had cured the panel was rotated 180° and the other end was potted. The ends of the panel were then CNC machined to meet parallel and perpendicularity requirements for the compression test (Figure 159).



FIGURE 157. POTTING OF ENDS OF COMPRESSION PANEL



FIGURE 158. POTTED END OF COMPRESSION PANEL



FIGURE 159. MACHINING OF POTTED END PLATES

4.5 Testing

The objective of the compression test was to confirm the advantages of the integral frame design approach to carry BWB spanwise loads. The purpose of this test was to validate the compressive load-carrying capability of a PRSEUS crown panel (in the frame direction) by simulating panel conditions encountered during the 2.5-g pull-up airplane maneuver.

The test specification document for this test, identified as document number ZA153382, provided the test plan for a minimum-gauge fuselage panel under compression loads. The specimen was tested at room-temperature in a dry condition under compressive axial loads at NASA Langley Research Center.

The test specimen assembly drawing (ZJ153436) defines the test specimen in detail. The general configuration of the test specimen is shown for reference in Figure 160. The specimen was a 90-inch by 30-inch composite panel and was delivered with ends potted and restraints ready to be installed in the test set-up by NASA LaRC.



FIGURE 160. COMPRESSION PANEL TEST SET-UP

In preparation for the test, the specimen interior surface was painted flat white, including skin, frame webs, stringer webs, and all flanges. The contrasting colors were used to aid in the crack propagation detection during the test. In addition, NASA LaRC applied splatter paint and set up and monitored Video Image Correlation in 3-Dimnsnsions (VIC-3D) data acquisition to measure out of plane deflection and strain levels on the skin side of the panel for all load cycles. Pre- and post-test photos of the specimen and set-up were taken and a standard speed digital video with sound was taken of the OML side.

Electronic displacement indicators were used to monitor panel deflection during the test. The actuator displacement transducer measured displacement when the specimen was under load. Four measurements were also monitored on the frame for in-plane displacement and two measurements were taken on the skin for out-of-plane displacement.

As this was the first compression test of a panel as long as the distance between the ribs, the panel was tested in pristine condition to provide the baseline stability vs. strength comparison. Future test panels are expected to be damaged and compared with this baseline test. For this test, the panel was loaded statically to failure with loading held at limit load and ultimate load for a minimum of 3 seconds each. The panel is shown in the test fixture prior to the test in Figure 161.

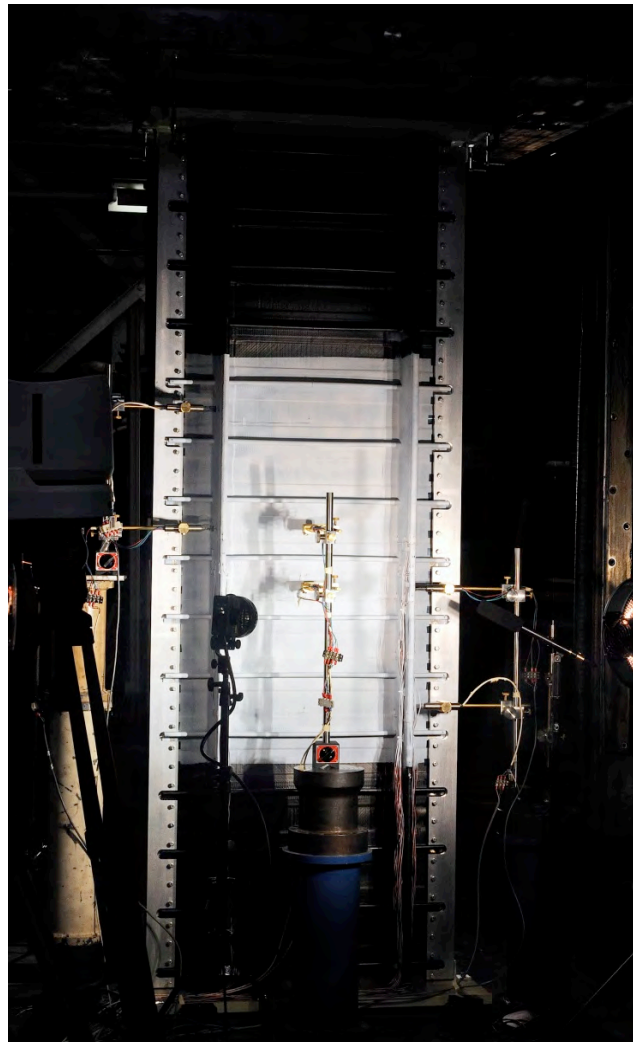


FIGURE 161. COMPRESSION PANEL IN TEST FIXTURE

Prior to loading, the VIC data was checked to identify initial conditions and out of plane imperfections in the panel as shown in Figure 162. In this plot, the red lines in the figure indicate strain gage wires and not the panel surface. This data shows that the magnitude is small at approximately 0.02 inches at the center of the panel.

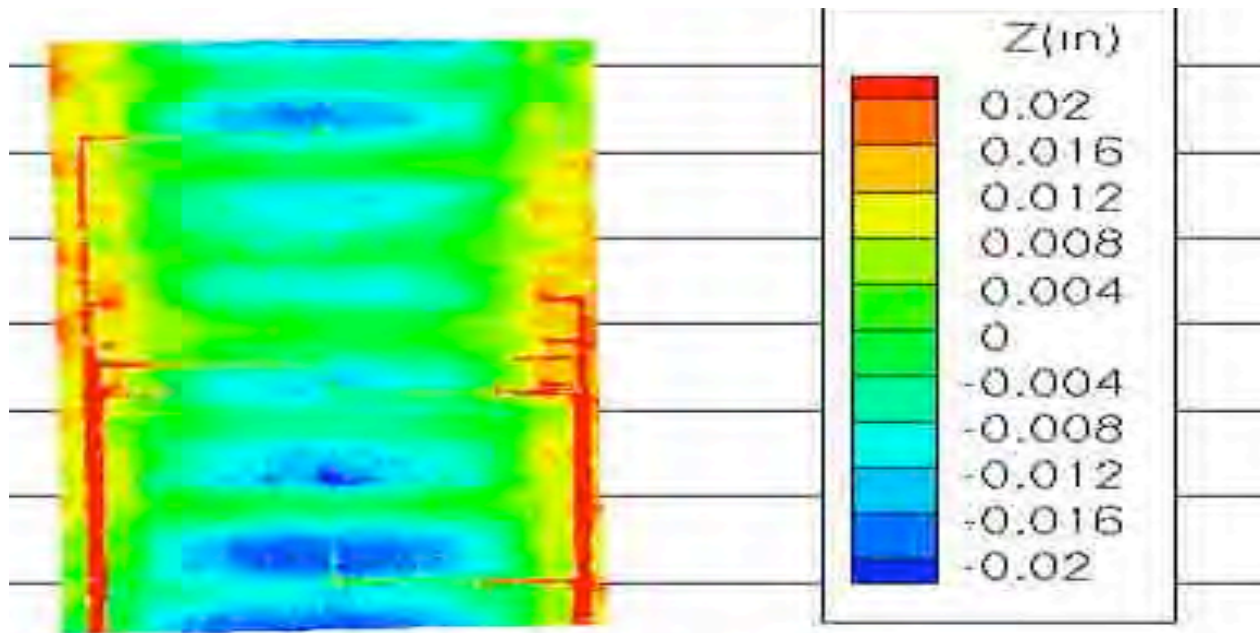


FIGURE 162. INITIAL OUT-OF-PLANE DISPLACEMENT SHOWING PANEL IMPERFECTIONS

The load was incrementally increased to failure. The VIC data and out-of-plane displacements from the LVDTs were captured as the load increased (Figure 163). The data shows that the panel underwent nonlinear deformation almost immediately during loading and the skin buckling shape began to form at approximately 23,000 lbs. The first sounds indicative of local failures occurred at 90,000 lbs. At this point in the test, separation could be seen between the frame flange and the skin where the buckling occurred and skin deflected away from the flanges. The panel continued to carry load as separation continued at each bay. The loading increased to 147,000 lbs when the panel failed across the width as shown in Figure 164 and Figure 165. Failure of the panel occurred across the third bay above the center stringer, which was the last fully painted bay.

Analysis predictions indicated that failure would occur at the center of the panel and therefore highspeed video was aimed at the center stringer and the two surrounding it. As failure occurred farther out from those stringers, the initiation of the failure was only captured on regular speed camera from the OML. Additional analysis and investigations are necessary to identify the failure mechanism without high speed video at the location. Through the entire test, only the skin showed buckling and the frames remained stable through the loading and failed in strength. Test results and strain plots also indicate that the panel did not demonstrate global buckling behavior and material strength was the failure mechanism. The test demonstrated that the PRSEUS configuration could withstand stability loading beyond strength capability.

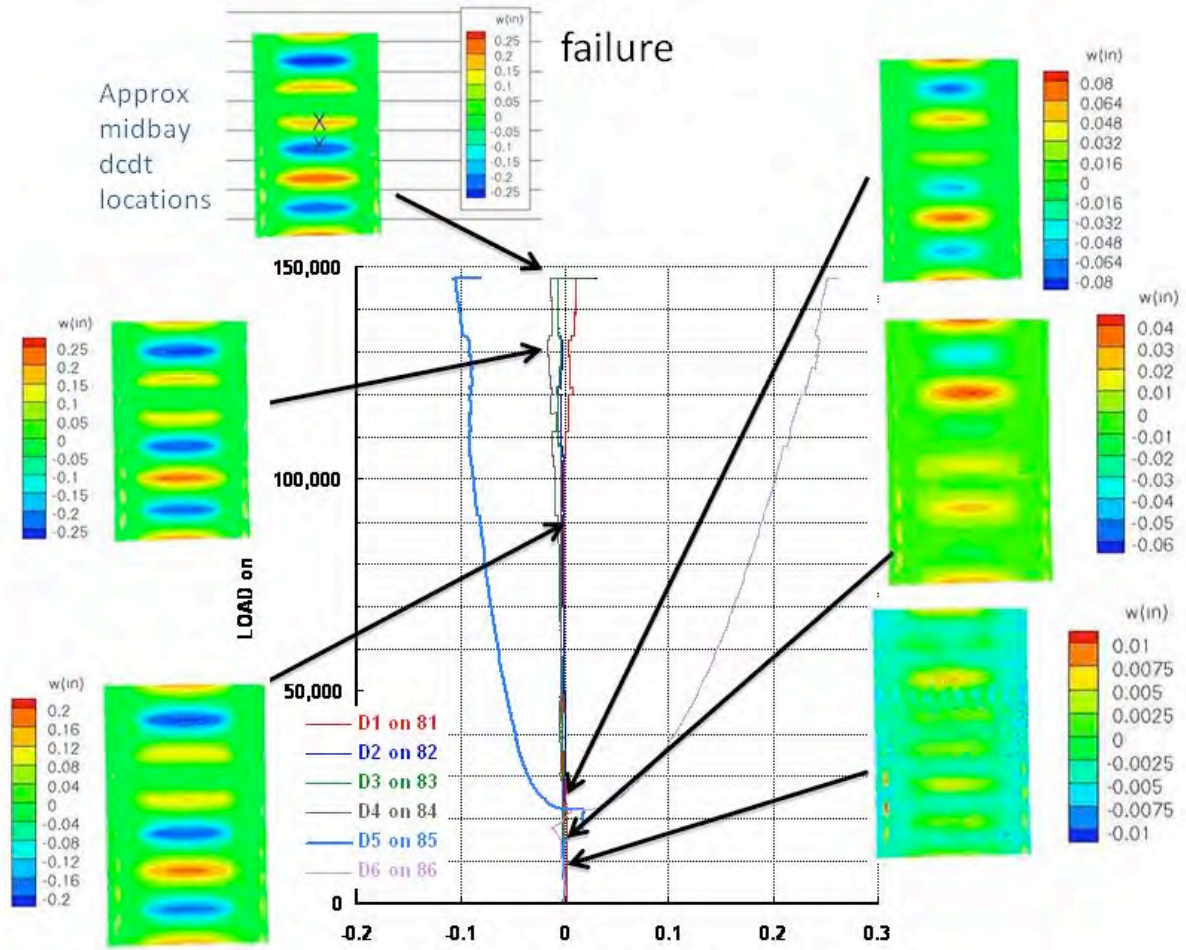


FIGURE 163. OUT-OF-PLANE LVDT MEASUREMENTS AND VIC PLOTS AS LOAD INCREASES



FIGURE 164. FAILURE ACROSS WIDTH OF PANEL

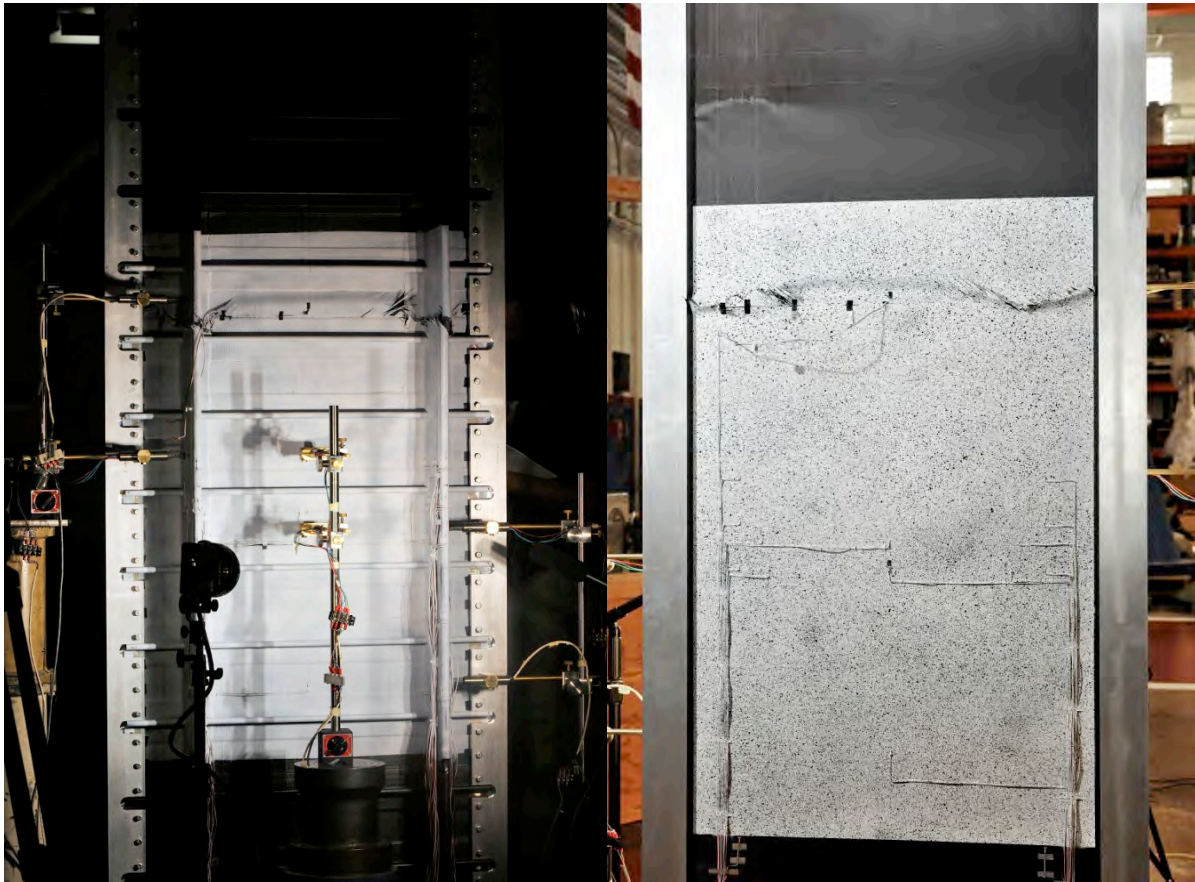


FIGURE 165. IML (LEFT) AND OML (RIGHT) VIEWS OF THE PANEL FAILURE

As shown in Figure 166, failure did not appear to initiate at the top of the stringer keyhole on the frame web as originally anticipated. Pictures indicate that failure initiated in the corner of the stringer and frame web intersection on the right frame when looking at the IML. As the failure propagated across the frame web, as shown in Figure 167, it next failed across the bay starting where the separation of the skin and flange occurred. The failure propagated across the open bay to the left frame where it failed similarly to the right as shown in Figure 168 and Figure 169. Video of the OML section shows that after the failure occurred across this bay, a delamination failure could be seen in the bay above it as shown in Figure 170 and Figure 171.



FIGURE 166. RIGHT IML VIEW OF FRAME WITH INITIAL FAILURE



FIGURE 167. RIGHT IML VIEW OF FRAME AND SKIN FAILURE



FIGURE 168. LEFT IML VIEW OF FRAME AND SKIN FAILURE



FIGURE 169. LEFT IML VIEW OF FRAME FAILURE

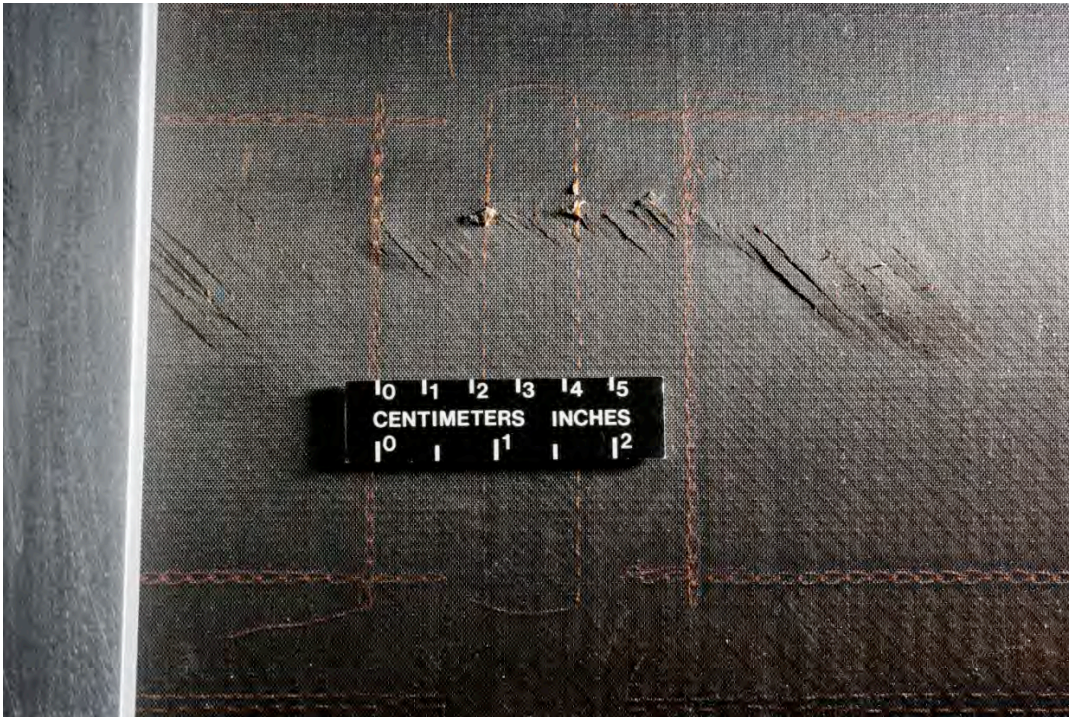


FIGURE 170. UPPER DELAMINATION AFTER INITIAL FAILURE

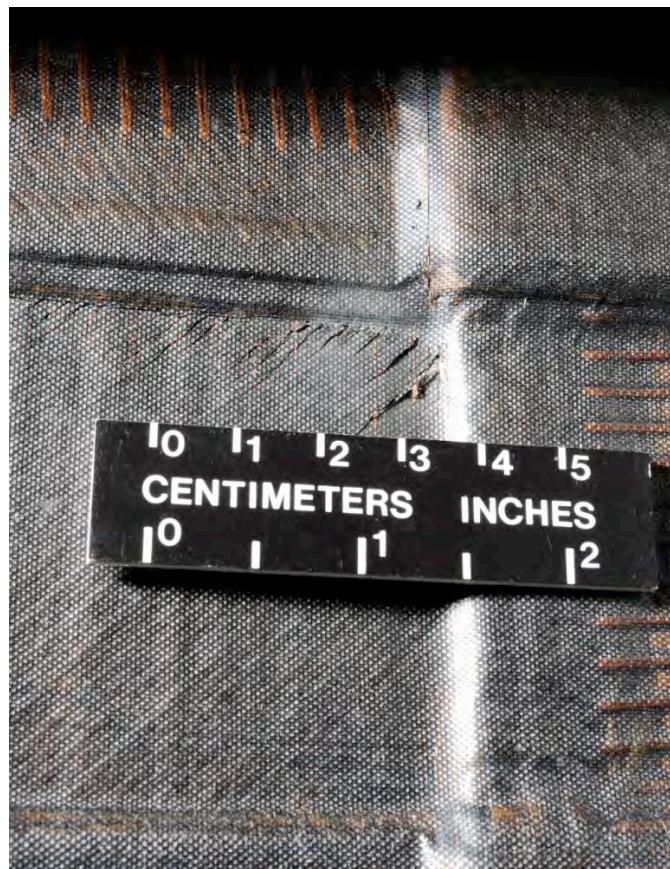


FIGURE 171. CLOSE-UP OF UPPER DELAMINATION AFTER INITIAL FAILURE

At the failure load of 147,000 lbs, the VIC data shows the maximum out of plane deflection through the bay where the failure occurred as shown in Figure 172. At this point, VIC data showing strain also indicates peak values at the edges where the restraints contact the panel as shown in Figure 173. Shear strain results plotted immediately prior to failure were also low except for peaks at the edges as shown in Figure 174. These results indicate that additional exploration of the edge effects due to the steel restraints would be required.

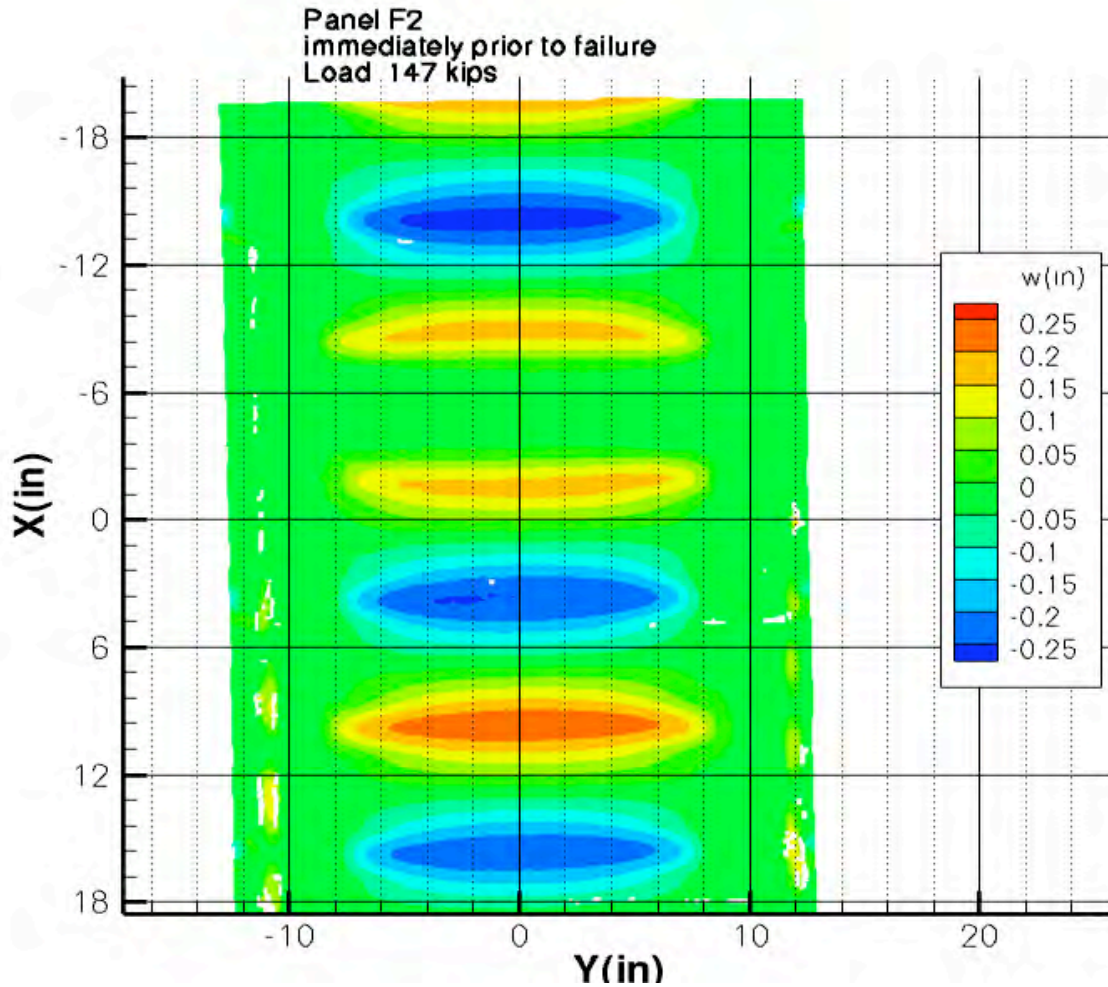


FIGURE 172. OUT-OF-PLANE DEFLECTION AT FAILURE WITH MAXIMUM AT FAILURE LOCATION

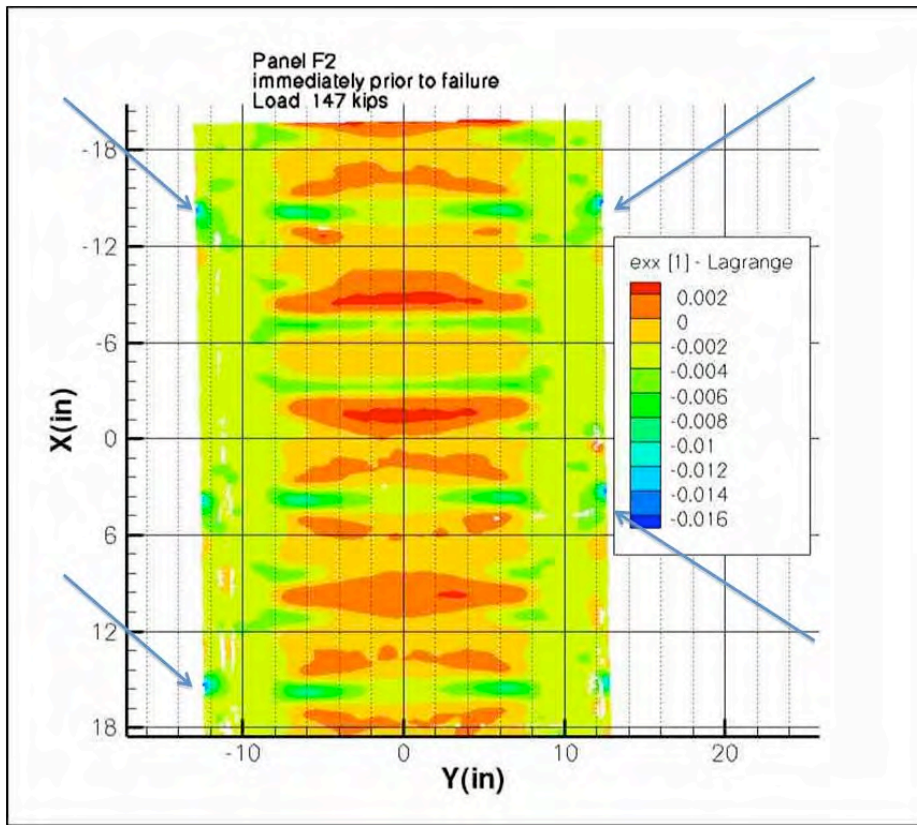


FIGURE 173. STRAIN DATA FROM THE VIC RESULTS

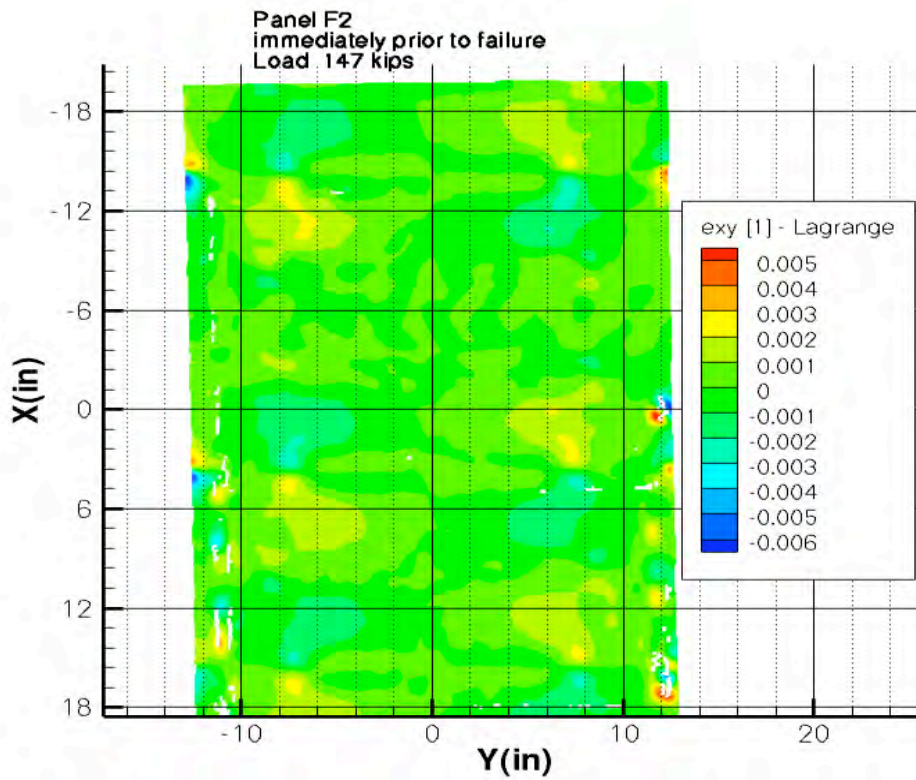


FIGURE 174. SHEAR STRAIN RESULTS FROM VIC DATA

5.0 PANEL SIZING ENHANCEMENTS

During the Phase I trade studies several opportunities were identified to improve the interoperability of the HyperSizer analysis code and the PRSEUS structural concept. Such modifications were necessary due to the unique structural features of the rod-stiffened design and its ability to operate well into the post-buckled design regime. The goal of such change was twofold: 1) more accurately reflect the actual structural response, and 2) simplify the user interface to permit novice users to conduct trade studies using the PRSEUS structural concept.

5.1 Code Change Guidelines

Based on the Phase I trade study results, a set of software changes and analytical enhancements were written up for HyperSizer analysis code. The following changes were defined to guide the HyperSizer code modifications for the PRSEUS module development that were completed by Collier Research Corporation:

Stiffness formulation - Compute the fully defined 6x6 stiffness matrix for the panel which includes the skin, stiffener web and axial rod, and the thickened laminate pad ups underneath the stiffener (stringer stack and stringer tear strap) and frame (frame cap stack). Include the foam core web frame in the panel stiffness formulation.

Failure analyses – Apply all standard HyperSizer failure analyses for all of the PRSEUS panel objects such as stiffener and skin. This includes local buckling, cross section crippling, and material strength and panel buckling.

Local pressure effects - Develop analytical and energy solutions for the pressure loading on the skin supported by the rod stiffener and panel frame for rectangular shapes for both simple and fixed boundary conditions.

Panel pressure effects - Develop analytical and energy solutions for the pressure loading on panel as supported between the bulkhead substructure for rectangular shapes for both simple and fixed boundary conditions.

Post-buckling - Develop post buckling analysis capability of the skin. Compute post buckling strength for uniaxial loadings and for biaxial loadings. Quantify load redistribution into the unbuckled skin and panel stiffener after post buckling. Also quantify the resulting effective width and panel overall effective stiffness. Compute all updated failure mode margins-of-safety such as panel buckling, cross section crippling, and material strength.

Rod local failures – Evaluate options for including the rod stiffener in panel crippling calculations.

Update material allowables - Provide options for analysts to choose from for predicting composite strength, including ply based and laminate based failure predictions. New options for laminate strength will be provided for CAI, TAI, SAI, BVID. The user will be able to enter strain cutoff values such as 0.004 or any other value based on the percent of plies in each angle direction. Crippling analysis and post buckling strength is highly dependent on the composite strength failure criteria and associated strain allowables. The analyst should be able to choose the crippling strength composite theory.

Optimization capabilities - Sizing variables should include skin laminate layup and thickness, stiffener web layup and thickness, rod diameter, stiffener height and spacing, and frame web height, frame spacing, and frame laminate layup and thickness, etc.

PRSEUS input screen module into the HyperSizer - An image of the PRSEUS concept should be included on the variables tab for sizing optimization and on the failure tab for indication of the panel-specific object margins-of-safety.

5.2 PRSEUS Interface Development

The PRSEUS panel concept was implemented into an unreleased Beta Version of the HyperSizer Software (this version was called HyperSizer 5.9.0). All HyperSizer database infrastructure, thermo-elastic formulation and failure analysis methods were developed and initially verified against independent FEA. All of the failure modes were fully included in HyperSizer.

A brand new panel Family grouping was created in HyperSizer. The purpose of this new family was to implement the PRSEUS panel concept. However, the name has been kept generic and more in-line with other panel concepts (such as "Uniaxial Stiffened Panel Family"). While the focus of this effort was on implementation of PRSEUS with composite materials and rod stiffeners, this family could also be used to implement a general composite or metallic panel where instead of a pultruded rod, the stiffener could simply be a "bulb" of material at the end of the stiffener web.

The snapshot of the PRSEUS panel shown in the HyperSizer Sizing form interface is shown in Figure 175. Note that in some of the HyperSizer snapshots shown in this report, the PRSEUS images that were inserted into the software were placeholder figures only. Higher quality images will be incorporated into the code after the panel concept has become fully functional.

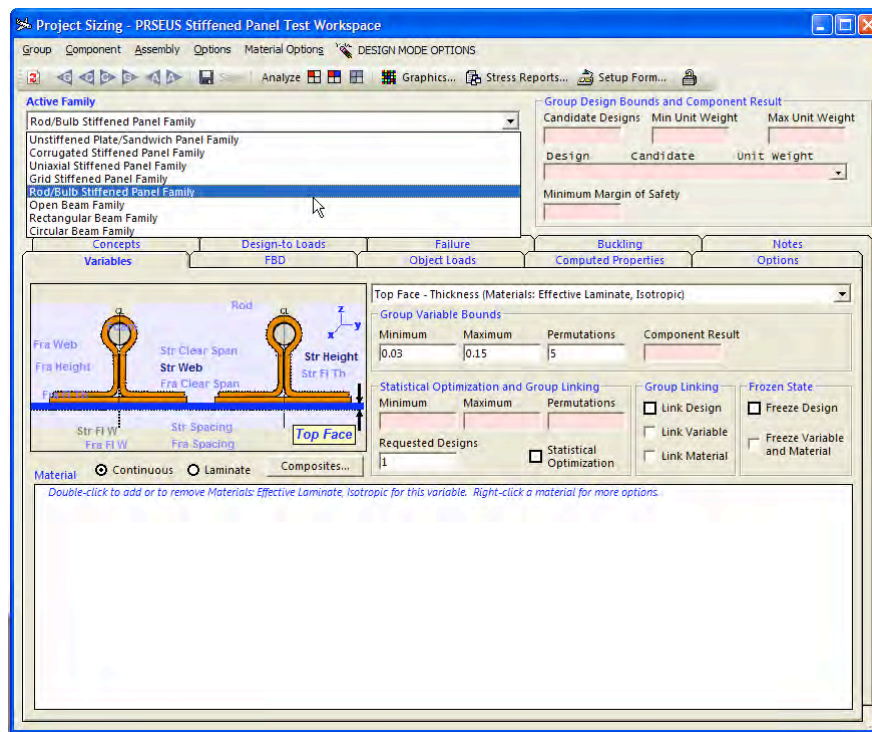


FIGURE 175. PRSEUS INTERFACE SCREEN WITHIN HYPERSIZER

5.3 Sizing Code Improvements

Although some geometry-based changes were necessary to the thermoelastic formulation of the entire panel 3D cross section into a 2D planar equivalent representation, the majority of the work was directed at tailoring specific failure equations for the PRSEUS concept. Two important failure types of failure were identified as missing: 1) local post buckling of the facesheet, and 2) flexural-torsional buckling of the panel stiffener. The latter of these was especially important in order to predict stability of the stiffening rod. Methods for both of these failure methods have been developed and verified against FEA as part of the PRSEUS panel development. The following failure modes are also relevant for PRSEUS (Table 5).

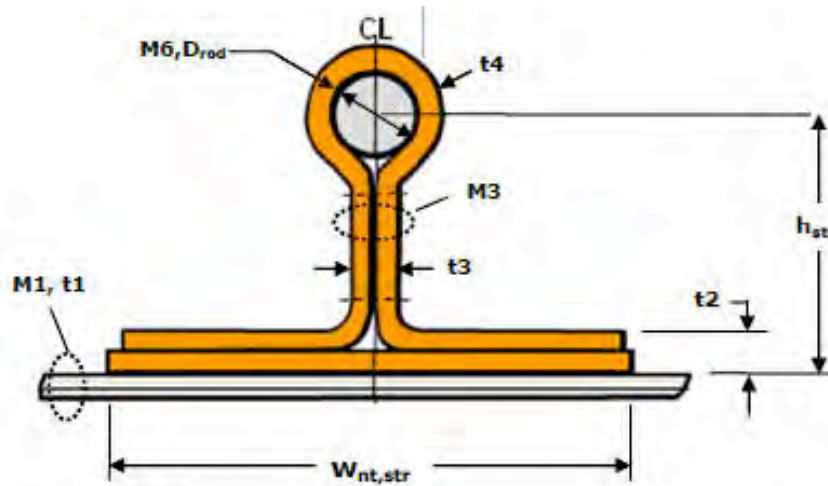
TABLE 5. RELEVANT FAILURE MODES FOR PRSEUS

Mode	Component(s)	Description/Method
Panel Buckling	Panel	<ul style="list-style-type: none"> Based on panel-level smeared ABD Stiffness Matrix and panel Transverse Shear Flexibility (TSF)
Crippling	Panel	<ul style="list-style-type: none"> Based on loads on overall panel (N, M, Q) Predicts overall panel collapse after local buckling of a portion of the panel concentrated in the remaining stable cross-section exceeds material ultimate strength
Johnson-Euler Buckling-Crippling Interaction	Panel	<ul style="list-style-type: none"> This method combines the effects of panel buckling and crippling to predict ultimate failure load of the panel
Composite Strength	Web, Facesheets	<ul style="list-style-type: none"> Based on loads (N, M, Q) on panel Many standard failure criteria (max stress/strain, Tsai-Hill, Hoffman, etc.)
Local Buckling	Web, Facesheets	<ul style="list-style-type: none"> Objects modeled as rectangular plates with simple support on all edges Many times this failure mode is not considered to be catastrophic
Local Post Buckling	Facesheets	<ul style="list-style-type: none"> Re-distributes load from buckled (ineffective) portion of panel to a calculated "effective" width. PRSEUS panel shown (both in analysis and test) to carry substantial post-buckling loads Predicts failure in post buckling due to crippling, material strength, panel buckling
Flexural-Torsional Buckling	Panel, Stiffeners	<ul style="list-style-type: none"> Failure of the panel due to "tipping" of the stiffener under compressive load. Calculates stability of stiffener by modeling the interface between stiffener and facesheet as a combination of linear and rotational spring constants Closed-form physics based method originally developed for metallic fastened panels extended to composite bonded panels including PRSEUS configuration

5.4 User Documentation

The HyperSizer User's manual was compiled to facilitate use of this new PRSEUS design capability within HyperSizer. Appendix D documents a complete step-by-step process for PRSEUS panel optimization through an example. Figure 175 in Section 5.2 shows a typical

sizing form for the PRSEUS design. Like other structural concepts, standard ‘Tabs’ have been adopted for the PRSEUS design as well. These include ‘Variables’, ‘Concepts’, ‘FBD’, ‘Design-to Loads’, ‘Failure’, ‘Object Loads’, ‘Buckling’, etc. A unique accomplishment under this contract was sizing integration of PRSEUS frames with the panel. It allows users to size PRSEUS panel in a more cohesive approach. This capability was made available only to the PRSEUS concept within HyperSizer. Figure 176 shows sizing variables for the stringer and Figure 177 & Figure 178 show sizing variables for the frame and the panel, respectively. Users need to notice that certain assumptions were made in the current version of this development; (1) It was always assumed that the rod overwrap is half the thickness of the stringer web, (2) if users want to size stringer flange (t_2) independently from stringer web (t_3), or frame flange (t_7) independently from frame web (t_5), it is always recommended to use hyperlaminates for the composite layup and material definitions. Otherwise, if effective laminate is selected (Figure 175), the program assumes that the web has same material as flanges for stringers (M3) as well as for frames (M5). Figure 179 & Figure 180 show how a typical hyperlaminates is defined for a stringer and a frame, respectively.



Geometric Variables

Sizing Variable	Symbol
Top Face - Thickness	t_1
Stringer Web - Thickness	t_3
Stringer Height	h_{str}
Stringer Spacing	S_{str}
Stringer Flange Width	$w_{nt, str}$
Stringer Flange Thickness	t_2
Stiffening Rod - Diameter	D_{rod}
Stringer Clear Span*	$F_{w, str}$

* Dependent Variable

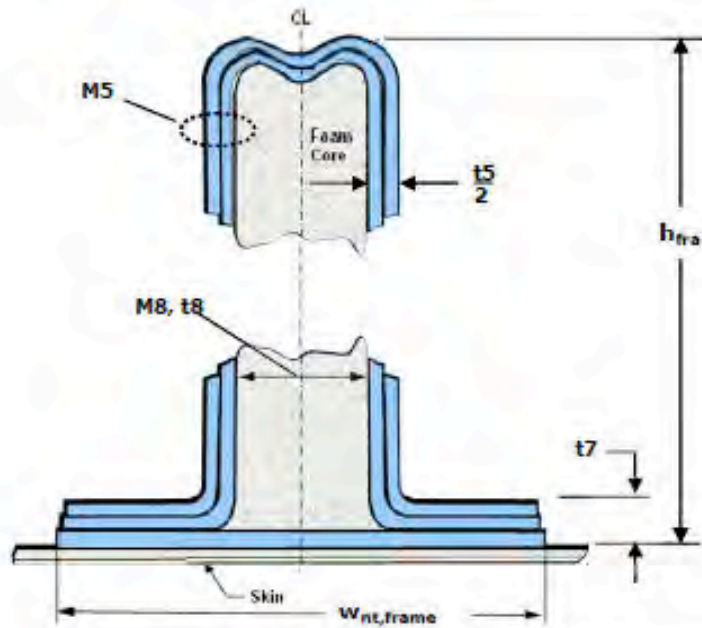
Notes:

- If M3 is a HyperLaminate, the layup and thickness of the stringer flange (t_2) is a function of the thickness and layup of the stringer web variable (t_3).
- If M3 is an Effective Laminate, then the stringer flange thickness (t_2) is an independently sized variable with the same material as M3.
- The Rod overwrap is always assumed to be 1/2 the thickness of the stringer web.

Material Variables

Sizing Variable	Symbol	Material Type
Top Face - Material	M_1	Metal, Layup, Effective or Discrete Laminate
Stringer Web - Material	M_3	Metal, Layup, Effective or Discrete Laminate (HyperLaminate)
Stiffening Rod - Material	M_6	Metal, Effective Laminate

FIGURE 176. SIZING VARIABLES FOR STRINGER



Geometric Variables

Sizing Variable	Symbol
Frame Web - Thickness	t_s
Frame Height	h_{fra}
Frame Spacing	S_{fra}
Frame Flange Width	$w_{nt,frame}$
Frame Flange Thickness	t_7
Frame Foam - Thickness	t_g
Stiffening Rod - Diameter	D_{rod}
Frame Clear Span*	$F_{w,tra}$

* Dependent Variable

Material Variables

Sizing Variable	Symbol	Material Type
Frame Web - Material	M_5	Metal, Layup, Effective or Discrete Laminate (HyperLaminate)
Frame Foam - Material	M_g	Foam

Notes:

- Layup and thickness of the frame web (t_s) includes material on both sides of the foam core, each wall has thickness = $t_s/2$.
- If M5 is a HyperLaminate, the layup and thickness of the frame flange (t_7) is a function of the thickness and layup of the frame web variable (t_s).
- If M5 is an Effective Laminate, then the flange thickness (t_7) is an independently sized variable with the same material as M5.

FIGURE 177. SIZING VARIABLES FOR THE FRAME

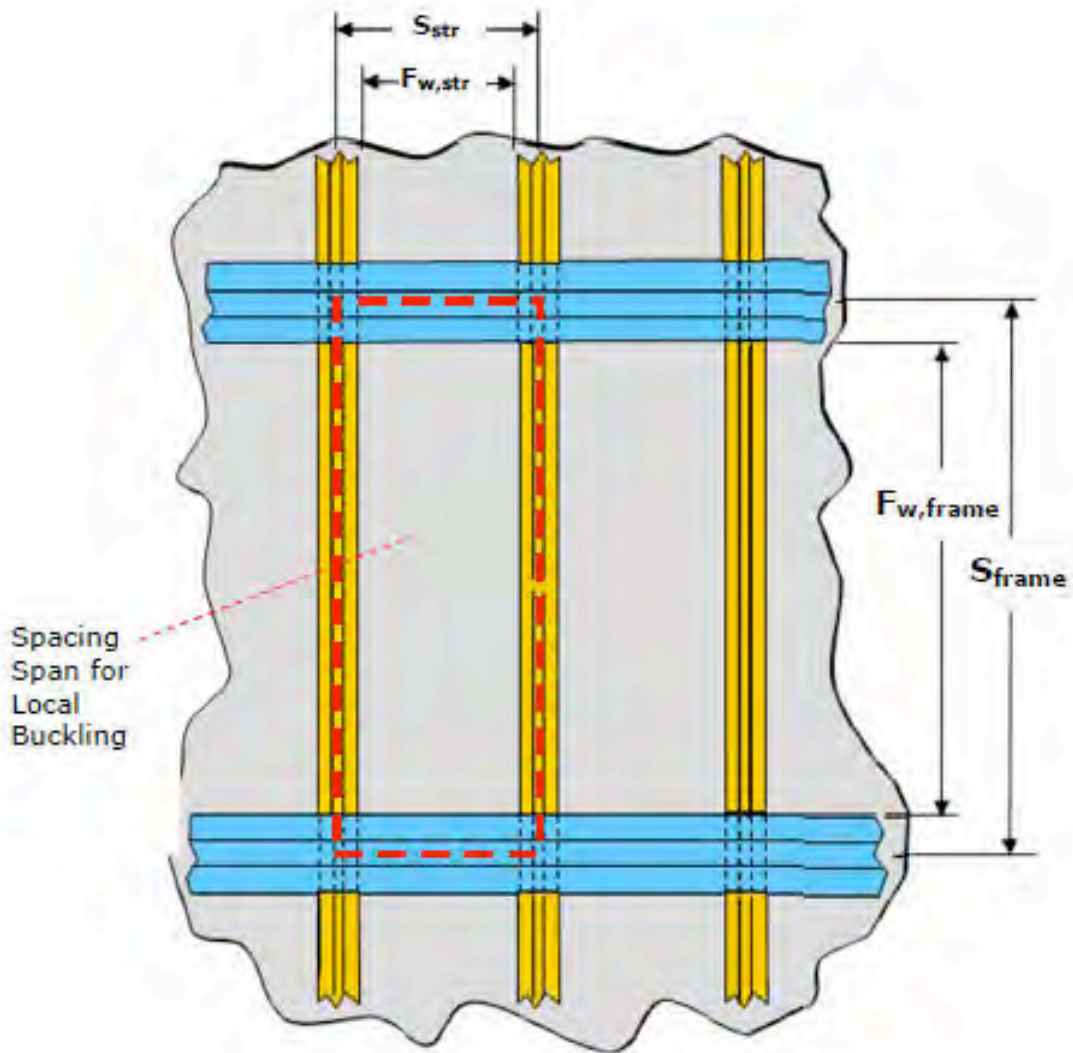
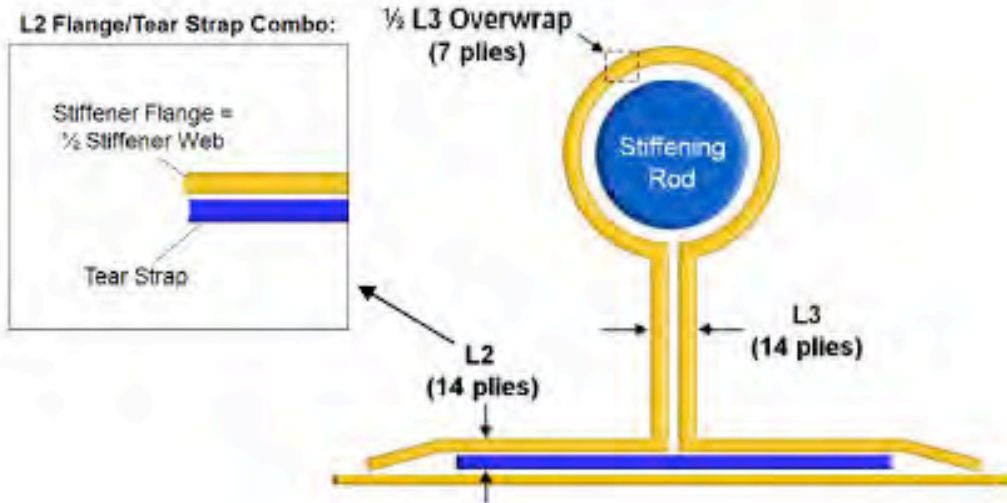


FIGURE 178. SIZING VARIABLES FOR THE PANEL

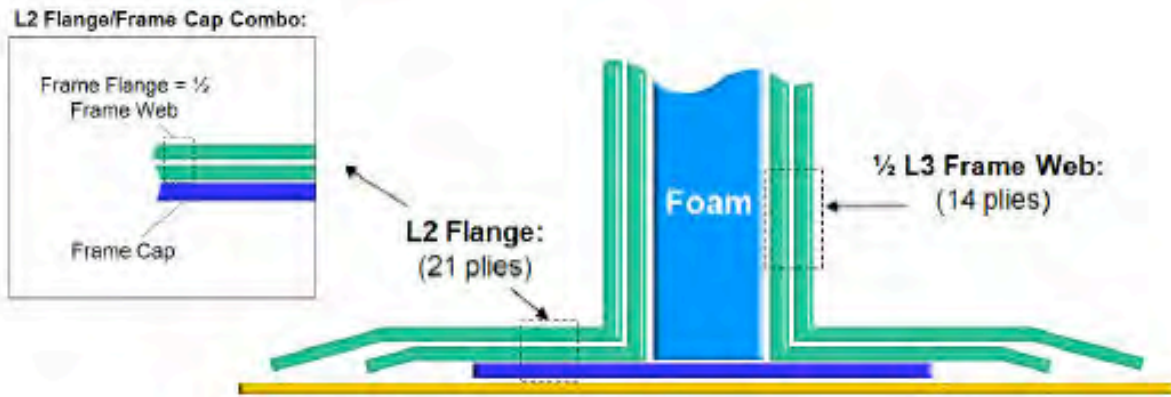


Ply Sequence Top to Bottom

1	Ply	Angle	L2	L3	L4	Thickness	Density
14	1	+45°	■	■	□	0.0056	0.057
13		-45°	■	■	□	0.0056	0.057
12		0°	■	■	□	0.0117	0.057
11		+90°	■	■	□	0.0062	0.057
10		0°	■	■	□	0.0117	0.057
9		-45°	■	■	□	0.0056	0.057
8		+45°	■	■	□	0.0056	0.057
7		+45°	■	■	□	0.0056	0.057
6		-45°	■	■	□	0.0056	0.057
5		0°	■	■	□	0.0117	0.057
4		+90°	■	■	□	0.0062	0.057
3		0°	■	■	□	0.0117	0.057
2		-45°	■	■	□	0.0056	0.057
1	B	+45°	■	■	□	0.0056	0.057

Stringer Flange (L2) Frame Flange (L3)
 Total Plies: 14 Total Plies: 14

FIGURE 179. EXAMPLE OF HYPERLAMINATES FOR STRINGER FLANGE DEFINITIONS



Ply Sequence Top to Bottom							
i	Ply	Angle	L2	L3	L4	Thickness	Density
Stack 1 (7 Plies) Active for L2 and L3	28	+45°	■	■	□	0.0056	0.057
	27	-45°	■	■	□	0.0056	0.057
	26	0°	■	■	□	0.0117	0.057
	25	+90°	■	■	□	0.0062	0.057
	24	0°	■	■	□	0.0117	0.057
	23	-45°	■	■	□	0.0056	0.057
	22	+45°	■	■	□	0.0056	0.057
Stack 2 (7 Plies) Active for L2 and L3	21	+45°	■	■	□	0.0056	0.057
	20	-45°	■	■	□	0.0056	0.057
	19	0°	■	■	□	0.0117	0.057
	18	+90°	■	■	□	0.0062	0.057
	17	0°	■	■	□	0.0117	0.057
	16	-45°	■	■	□	0.0056	0.057
	15	+45°	■	■	□	0.0056	0.057
Stack 3 (7 Plies) Active for L2 and L3	14	+45°	■	■	□	0.0056	0.057
	13	-45°	■	■	□	0.0056	0.057
	12	0°	■	■	□	0.0117	0.057
	11	+90°	■	■	□	0.0062	0.057
	10	0°	■	■	□	0.0117	0.057
	9	-45°	■	■	□	0.0056	0.057
	8	+45°	■	■	□	0.0056	0.057
Stack 4 (7 Plies) Active for L3 Only	7	+45°	□	■	□	0.0056	0.057
	6	-45°	□	■	□	0.0056	0.057
	5	0°	□	■	□	0.0117	0.057
	4	+90°	□	■	□	0.0062	0.057
	3	0°	□	■	□	0.0117	0.057
	2	-45°	□	■	□	0.0056	0.057
	1	+45°	□	■	□	0.0056	0.057

Frame Flange (L2)
Total Plies: 21
Frame Flange (L3)
Total Plies: 28

FIGURE 180. EXAMPLE OF HYPERLAMINATES FOR FRAME FLANGE DEFINITIONS

In HyperSizer, panel analyses were divided into discrete ‘Analysis Objects’.

Table 5 lists relevant failure modes for PRSEUS. Table 6 shows how those failure modes are applicable to individual analysis objects. Users can reference Appendix D for the definitions of each ‘Object’.

TABLE 6. ANALYSIS OBJECTS FOR PRSEUS DESIGN

Object	Applicable Failure Modes
Open Span	Material Strength (Max Strain, stress, Tsai-Hill, etc)
Bonded Combo - Stringer	Material Strength
Bonded Combo - Frame	Material Strength
Stringer Web	Material Strength Local Buckling (Long., Shear, Interaction) - Simple-Simple-Simple-Simple Boundary Condition
Frame Web	Material Strength Foam Sandwich Wrinkling Local Buckling (Long., Shear, Interaction) - Simple-Clamped-Simple-Free Boundary Condition
Stiffening Rod	Flexural Torsional Buckling Max Stress/Strain
Frame Core	Sandwich Wrinkling
Spacing Span	Local Buckling (Biaxial, Shear, Interaction) - Simple-Simple-Simple-Simple Boundary Condition
Frame Span	Panel Buckling Between Frames - Flat Panel Unsymmetric - S-S-S-S BC - Curved Panel Rayleigh Ritz - Any BC - Full Cylinder NASA SP-8007 - with and without transverse shear flexibility
Panel Span	Panel Buckling of Full Panel Span - Flat Panel - Curved Panel Rayleigh Ritz - Any BC - Full Cylinder NASA SP-8007

For local buckling analysis, by defaults, the spacing span has simple boundary conditions on all edges. Using this assumption, HyperSizer may produce slightly conservative buckling results because the stringer & frame can provide some fixity at the edges. This effect increases as the stringer becomes stiffer. For this reason, a backdoor flag for the Percent Fixity was provided which may be used to ‘tune’ the spacing span buckling results. Enter a value between 0 and 1 (0=simple, 1=fully fixed) to alter the local buckling results for this analysis (Figure 181).

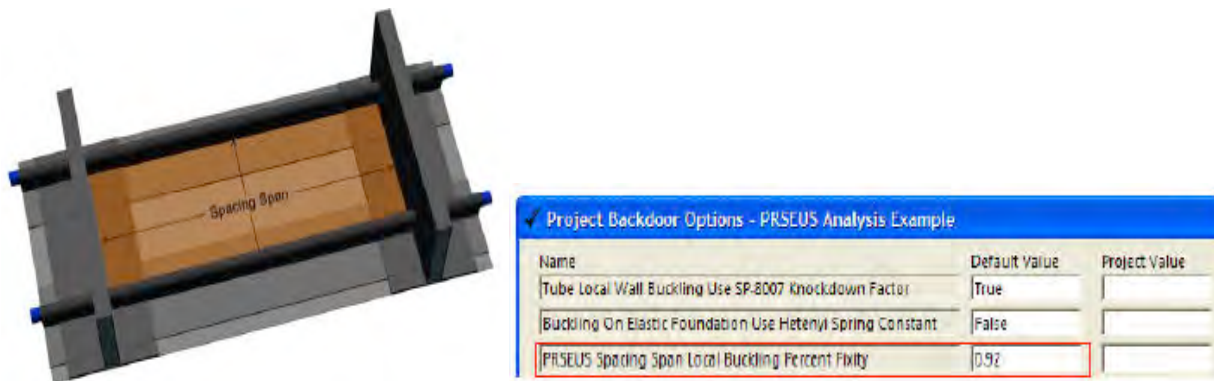


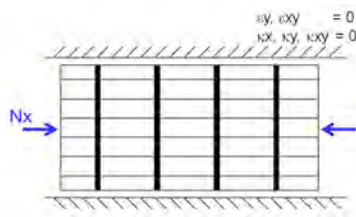
FIGURE 181. SPACING SPAN BUCKLING

5.5 Validation/Checkout

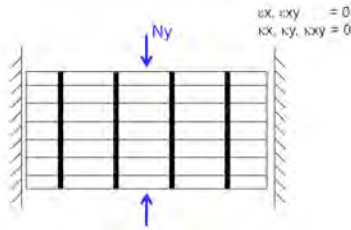
To verify the accuracy of the new PRSEUS module within HyperSizer, numerical validations were conducted. These include validation of HyperSizer’s thermoelastic formulation to demonstrate that (1) the homogenization of the panel into a panel level ABD response was accurate, (2) the localization of panel level loads to object level loads was accurate, and (3) verification of structural response matches between FEA and HyperSizer results. The same PRSEUS configuration as defined in Section 5.4 (seven-stringer panel) is used for this study.

Global Panel ABD Matrix Response - The ABD matrix verification is performed by constructing a discrete FEM model of a PRSEUS panel and applying four separate loads to obtain load-strain and moment-curvature response to back-out panel level ABD matrices.

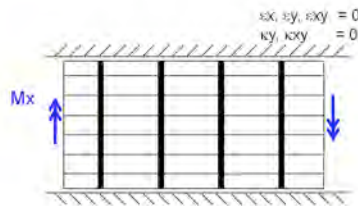
Case 1: Applied N_x



Case 2: Applied N_y



Case 3: Applied M_x



Case 4: Applied M_y

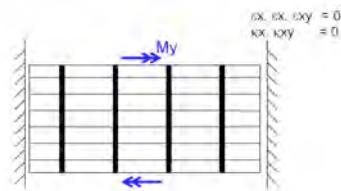


FIGURE 182. GLOBAL ABD MATRIX ASSESSMENT

Panel Level Load-Strain Comparisons - The panel strain response to the 4 load cases are listed below in Table 7 for HyperSizer and FEA:

TABLE 7. LOAD-STRAIN COMPARISONS

LC 1 - Applied Nx			
	FEA	HyperSizer	Difference
Nx (lb/in)	2,381	2,381	0.0%
Ny (lb/in)	261	252	3.4%
ex ($\mu\text{in/in}$)	1,561	1,591	-1.9%
LC 2 - Applied Ny			
	FEA	HyperSizer	Difference
Nx (lb/in)	142	137	3.4%
Ny (lb/in)	1,250	1,250	0.0%
ey ($\mu\text{in/in}$)	850	879	-3.4%
LC 3 - Applied Mx			
	FEA	HyperSizer	Difference
Mx (lb-in/in)	1,000	1,000	0.0%
kx ($\times 10^6 \text{in}^{-1}$)	1,176	1,175	0.2%
LC 4 - Applied My			
	FEA	HyperSizer	Difference
My (lb-in/in)	1,000	1,000	0.0%
ky ($\times 10^6 \text{in}^{-1}$)	144	142	1.3%

ABD Calculations - The force and moment resultants from the four load cases are compared to the strains and curvatures to derive panel level ABD terms:

TABLE 8. STIFFNESS COMPARISON

	LC #	Formula	FEA	HyperSizer	Difference
A 11	1	Nx/ex	1,525,408	1,496,577	1.9%
A 12	1	Ny/ex	167,155	158,401	5.2%
A 22	2	Ny/ey	1,471,330	1,422,520	3.3%
A 21	2	Nx/ey	167,155	158,401	5.2%
B					
B 11	1	Mx/ex	753,385	746,099	1.0%
B 22	2	My/ey	1,797,302	1,789,474	0.4%
D					
D 11	3	Mx/kx	849,881	851,322	-0.2%
D 22	4	My/ky	6,953,642	7,044,432	-1.3%

Object Load Comparison - The HyperSizer computed object loads are compared to the FEA computed element loads. The FEA loads are extracted from the center of the panel to eliminate any boundary condition effects so that a more accurate evaluation of HyperSizer's load calculation is achieved as shown in Figure 183.

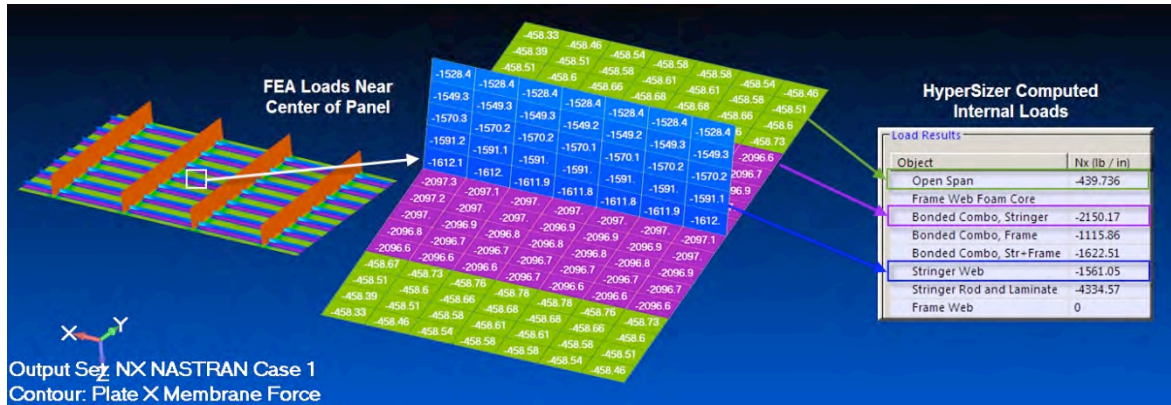


FIGURE 183. OBJECT LOADS

A summary of the internal load comparison between FEA and HyperSizer is shown Table 9. These object forces are used for performing local buckling, crippling, and material strength analysis.

TABLE 9. OBJECT LOAD COMPARISONS

Object Nx Loads	FEA	HyperSizer
Open Span (lb/in)	-458	-440
BondedCombo, Stringer	-2097	-2150
Bonded Combo, Frame	-939	-1115
Stringer Web	-1570	-1561
Stiffening Rod (lb)	-4267	-4334

Verify HyperSizer Local Buckling Results - The detailed NASTRAN and Abaqus FEMs were created by HyperSizer's FEM Gen capabilities.

Figure 184 shows the buckling solution from FEA and Table 10 lists the eigenvalue comparison.

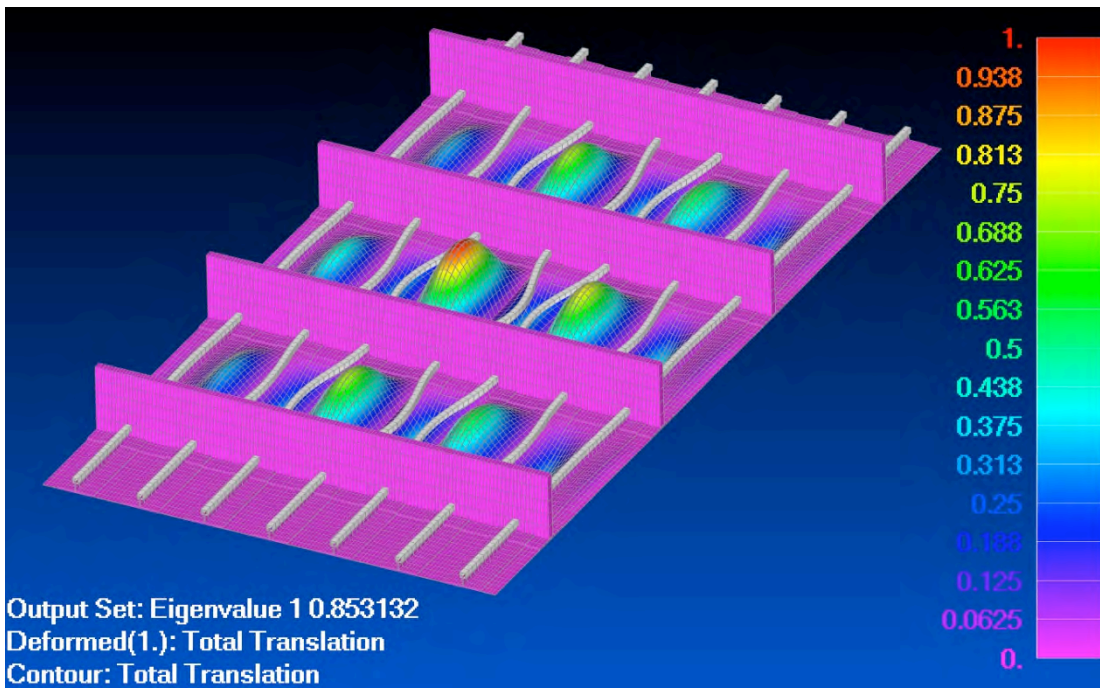


FIGURE 184. FEA BUCKLING EIGENVALUE SOLUTION (1ST MODE SHAPE)

TABLE 10. EIGENVALUE COMPARISON

	Eigenvalue	Buckling Mode
HyperSizer	0.79	Open Span
FEA	0.85	Open Span

HyperSizer's local buckling eigenvalue was slightly more conservative because the assumed boundary conditions for the open span were simply supported. In reality the stiffener supplies the skin with some rotational fixity which effectively increases the panel's critical buckling load.

Post Buckling Behavior - One of the significant accomplishments under the current contract was the addition of local post buckling capabilities within HyperSizer for the PRSEUS concept. In reality, when local buckling in the spacing span occurs, a portion of the buckled spacing span becomes non-effective and will carry no additional load. HyperSizer can calculate this reduction in effective area with its local post-buckling capability.

In order to verify any postbuckling result, linear static and eigenvalue FEA was no longer sufficient. The user must rely on a geometric nonlinear finite element analysis in order to verify any post-buckled results. Abaqus finite element models were generated to serve this purpose.

The first results of the post-buckling result are Load vs. Strain (Figure 185). In nonlinear postbuckling analysis, it is difficult to ascertain what constitutes a "buckling" event. In the results shown here, two events were used to determine when buckling occurs. First, negative eigenvalue buckling refers to the solver reporting negative eigenvalues while decomposing the stiffness matrix for inversion. The first negative eigenvalue shown in the following figure

indicate the onset of local buckling. A secondary event that indicates the presence of local buckling was a change in the panel stiffness matrix. These are shown below and indicate secondary buckling events such as a mode change, or the final panel collapse.

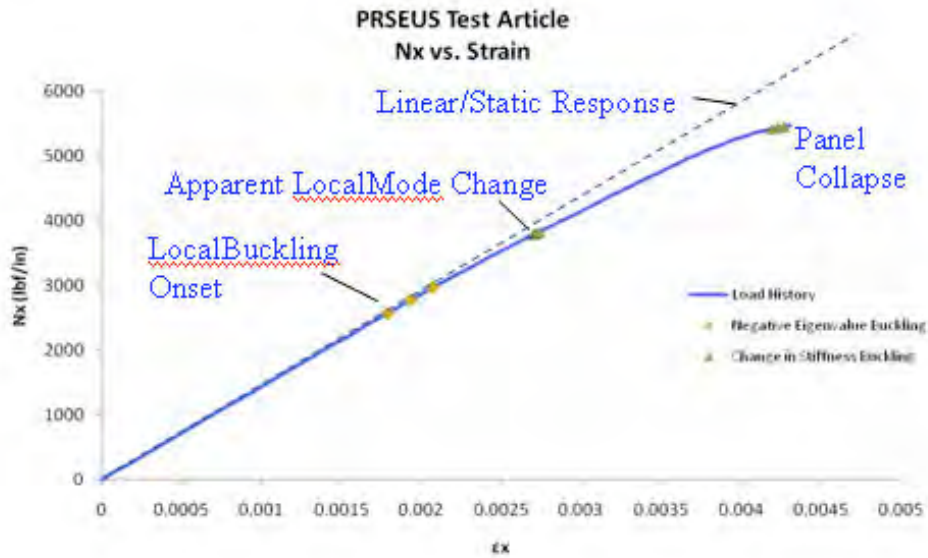


FIGURE 185. LOAD VS. STRAIN

Figure 186 shows the initial local buckling mode shape at a load of 108 kips. The local buckled shapes can be seen in the second and fourth bays and are beginning to develop in the third. These mode shapes match the linear eigenvalue results. The contours represent the magnitude of out-of-plane deflection.

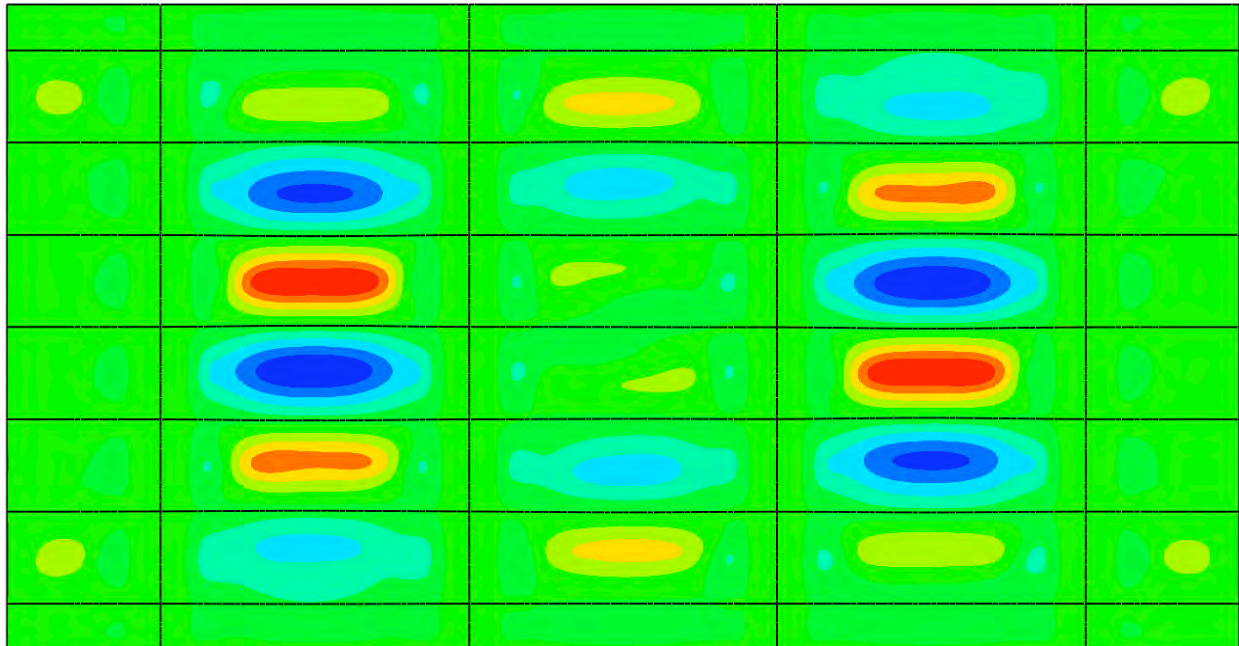


FIGURE 186. INITIAL BUCKLING MODE

Figure 187 shows snapshots for this FE analysis at a point just before final collapse. This result is at 227 kips. Notice that there was substantial deformation of the straight stiffener path as the stiffeners start to substantially tip.

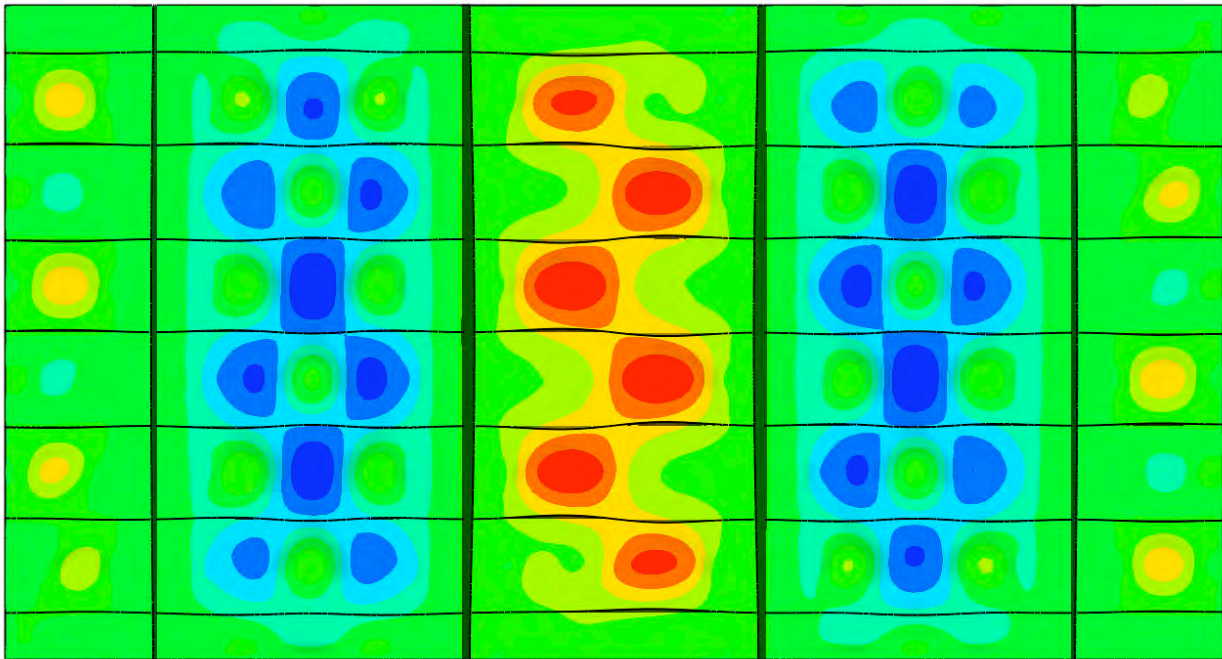


FIGURE 187. MODE BEFORE FINAL COLLAPSE (TOP VIEW)

Also of note is the deformed shape of the panel shown from the side (Figure 188). As the stiffeners tip over the load that they are carrying is beginning to offload from the very stiff rod into the facesheet. As this happens the effective bending stiffness of the panel was rapidly diminishing and the panel is beginning to take on a flexural (i.e. panel) buckling mode shape.

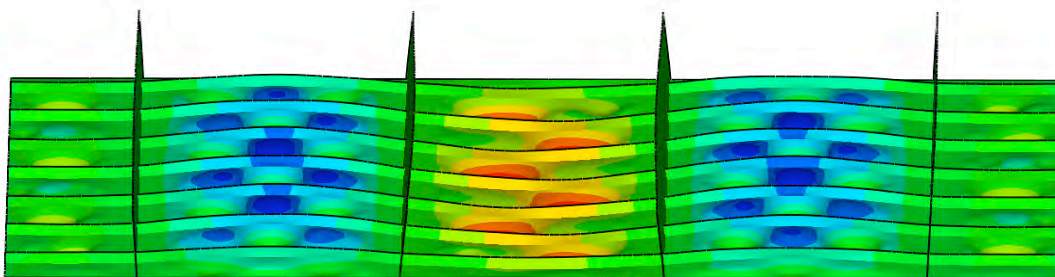


FIGURE 188. MODE BEFORE FINAL COLLAPSE (SIDE VIEW)

In summary, the non linear FEA showed a torsional buckling mode of the stiffeners which leads very quickly to panel collapse by overall panel buckling. The load level of collapse is 229 kips which compared very favorably to HyperSizer's predicted collapse of 222 kips.

6.0 VEHICLE SIZING UPDATES

In Phase I, PRSEUS panels were approximately represented in HyperSizer. The vehicle was then sized based on these approximations. With availability of this new PRSEUS sizing capability from HyperSizer, the vehicle sizing has been updated. The same Phase I Study BWB configuration and the associated baseline FEM have been used for this new study (Ref. 1).

6.1 Update BWB FEM

Unlike previous studies, the new PRSEUS concept within HyperSizer allows full-design integration (Ref. section 5.1, skin panel, stringer and frame). Optimized designs were exported as 2D elements (PSHELLS) with smeared equivalent properties. Therefore, the FE model needed to be revised to reflect this fact. Like the studies in Phase I, current optimal resizing was limited to pressurized cabin regions. Only the top and bottom panels were modeled with the PRSEUS design and optimized. The rest of the structures of the vehicles were kept in earlier configurations. Figure 189 and Figure 190 show the initial and updated FEMs where the beam frame elements in the initial model are smeared into the plate elements in the updated model in the top and bottom skin panels.

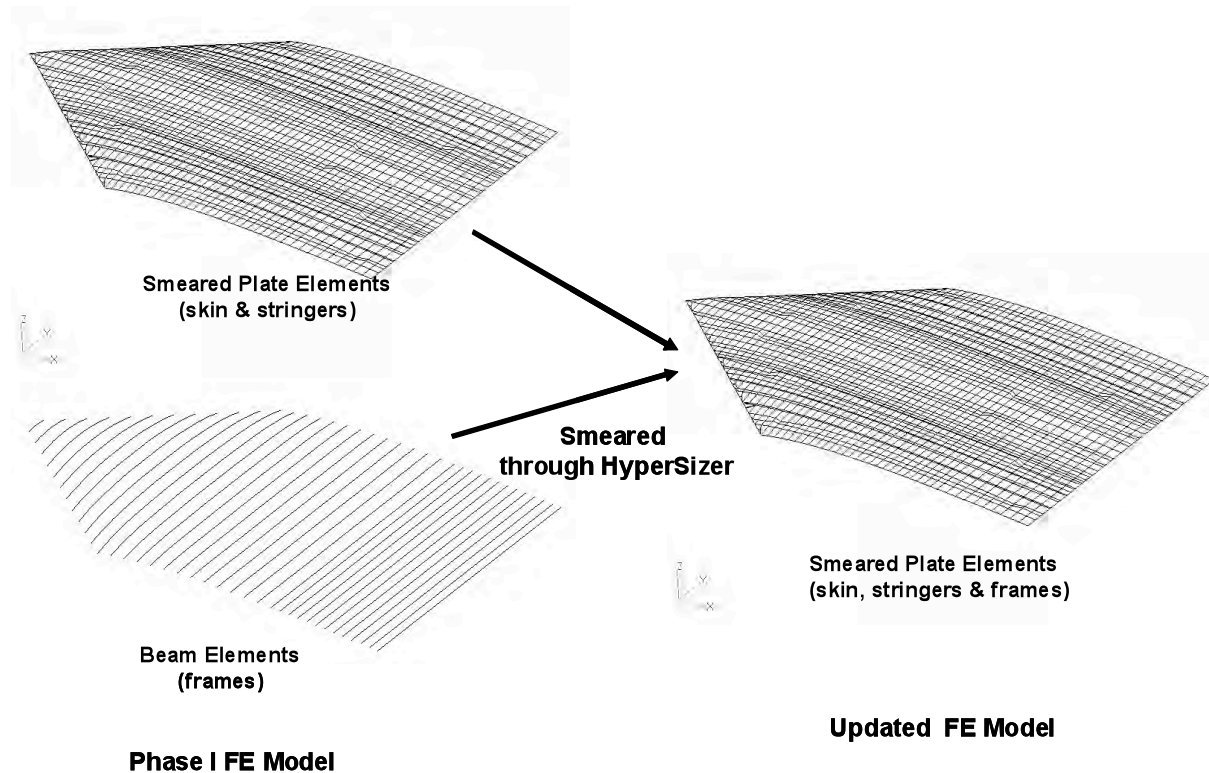


FIGURE 189. UPPER SKIN PANELS FEM

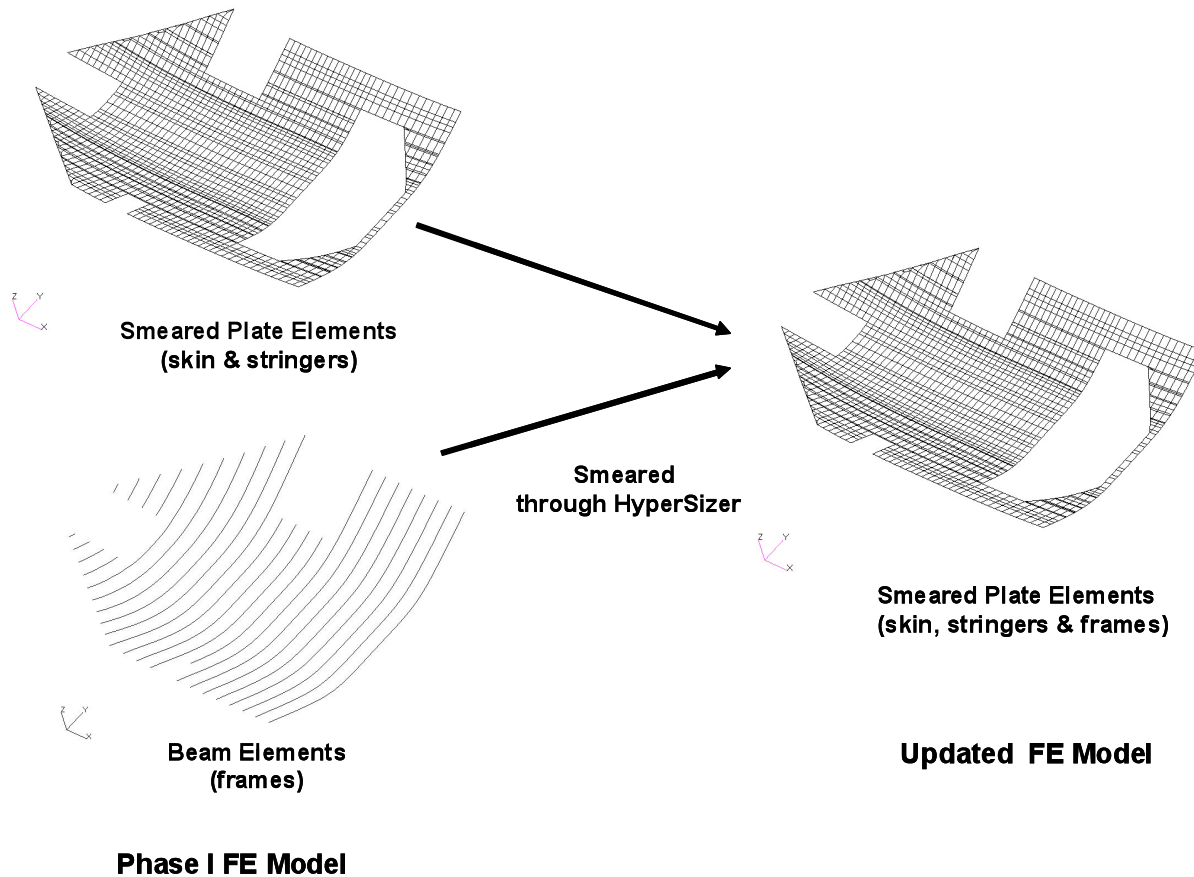


FIGURE 190. LOWER SKIN PANELS FEM

6.2 Incorporate New HyperSizer

As described in Section 5.4, the new HyperSizer is capable of defining PRSEUS configuration with accuracy. The new unique failure criterion was also specifically developed for the PRSEUS design (Section 5.3, Table 5). To define the PRSEUS panels for the BWB vehicle, the same design regions (panels or property groups) as those in Phase I were used. There were total of 21 design regions (panels) for the pressurized upper skin and 30 for the lower skin. The frame spacing was kept constant (16 inches for fuselage section 1 and 24 inches for Sections 2-5) in this study.

Table 11 lists the design limits for stringer panel and frames. The standard 6" frame was used. The design variables were skin thickness and stringer height. All designs used stacks of preassembled AS4 standard modulus (33 million) carbon fibers (DMS 2436 Type, 1 Class 72, Grade A). Each stack has 7 plies in a +45, -45, 0, 90, 0, -45, +45 pattern knitted together. The percentage of fiber by area weight was (44/44/12) using a (0/45/90) nomenclature. The zero direction of skin laminate was parallel with the frame direction. Figure 191 shows a typical setup template within HyperSizer used to connect the FEM with the PRSEUS panels. Figure 192 shows a typical sizing form for the PRSEUS concept. Hyperlaminates were used to define both stringers and frames.

TABLE 11. DESIGN LIMITS

Stringer Panel

Stringer Height	1.25"-1.75"
Stringer Spacing	6"
Skin Thickness	> 1 stack (0.052")
Strap Width	2.06"
Strap Thickness	0.052" (1 stack)
Web Thickness	0.104"
Rod Diameter	0.375"

Frame

Frame Height	6"
Strap Width	3.4"
Strap Thickness	0.052"
Web Foam Thickness	0.5"
Web Face Sheet Thickness	>0.104"

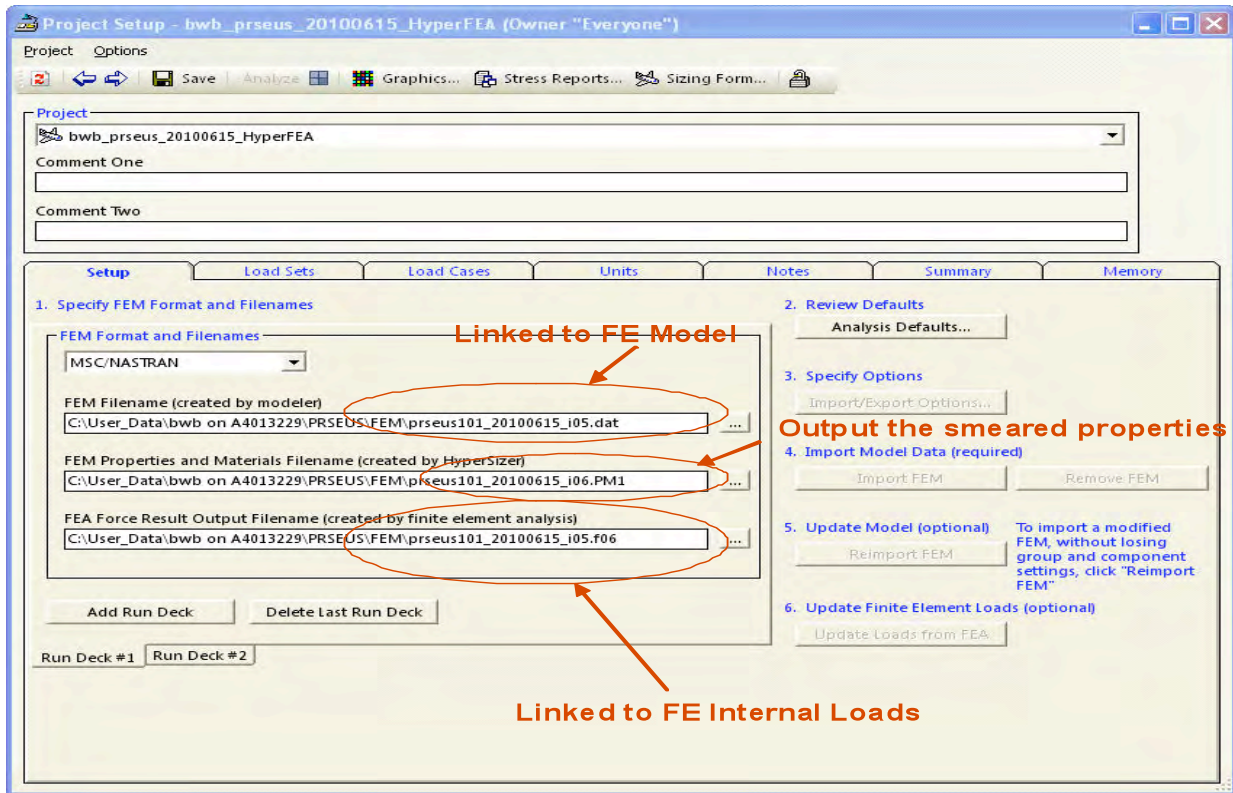


FIGURE 191. FEM SETUP TEMPLATE

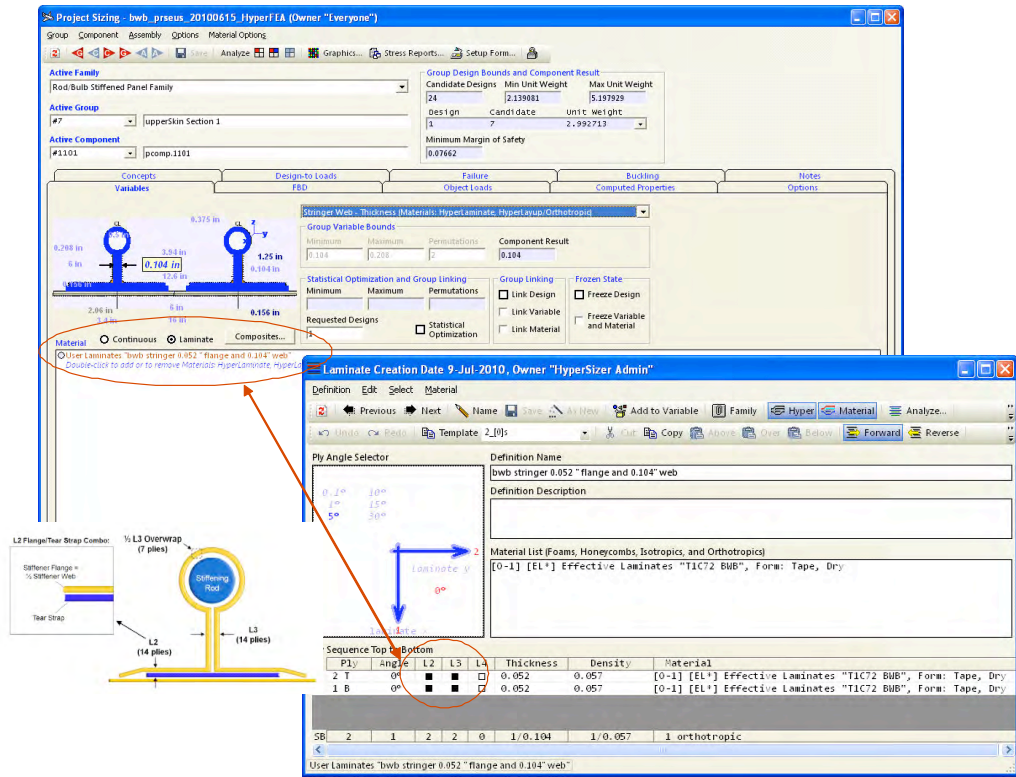


FIGURE 192. SIZING FORM FOR PRSEUS

6.3 FEM-based Structural Sizing

The vehicle-level BWB-5-200G finite element model was originally used for the PRSEUS structural concept study in the pressurized region in Phase I. This updated model included deletion of frame elements for the upper and lower skin panel in the pressurized cabin due to the fact of that the frames are integral part of PRSEUS configuration within HyperSizer. The final FEM model (Figure 193) featured the vehicle’s fuselage skins, frames, ribs, spars and floors, wing skins, spars and ribs, vertical stabilizer, movable control surfaces and high-lift devices, and bulkheads. But the sizing optimization was limited to crown and keel panels in the pressurized region.

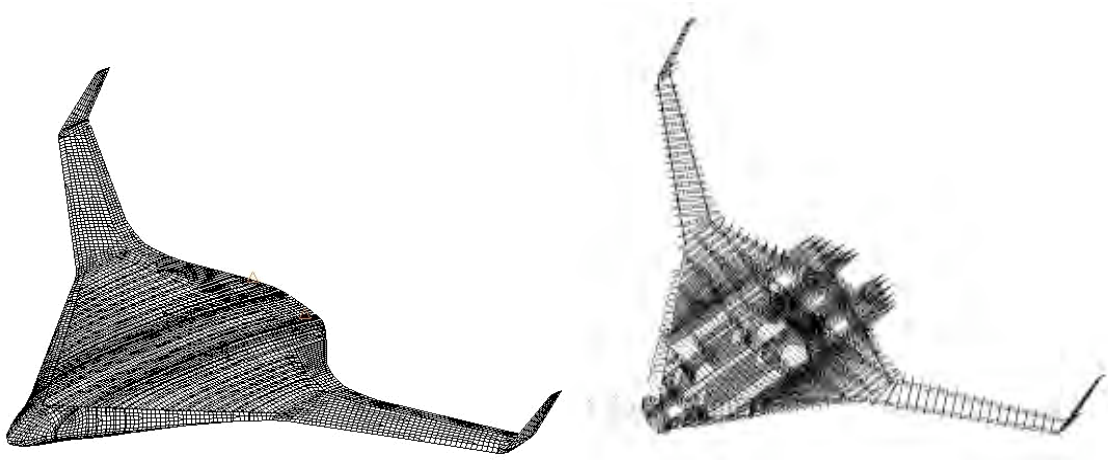


FIGURE 193. BWB FINITE ELEMENT MODEL

Three- and four-node bending plate elements were used for skin, spar, and rib webs. Bending bar elements were used to represent frames, and floor beams. Axial rod elements were used to represent spar and rib caps. Stringers and frames in PRESUS panels were not discretely modeled but instead, were smeared as equivalent properties for the stiffened panel simulations (PSHELL/MAT2 in NASTRAN), which were then locally sized in HyperSizer as true skin-stringer-frame geometries.

Principal concentrated masses, including landing gear, engines, and major systems, were included to account for internal and external subsystems. The weight of furnishings and payload was applied to passenger and cargo floors/beams as distributed non-structural masses.

Structural Sizing - To conduct vehicle-level optimization efficiently, a two-stage global-local optimization approach was used (Figure 194). The FEM-based global sizing step constrains the overall vehicle-level stiffness and internal load distributions in order to satisfy vehicle-level, or airplane, design requirements. While a local panel-level analysis code checks whether local panel-level design parameters, such as panel stability or panel strength, are violated using the overall global stiffness requirements calculated from the vehicle-level analyses.

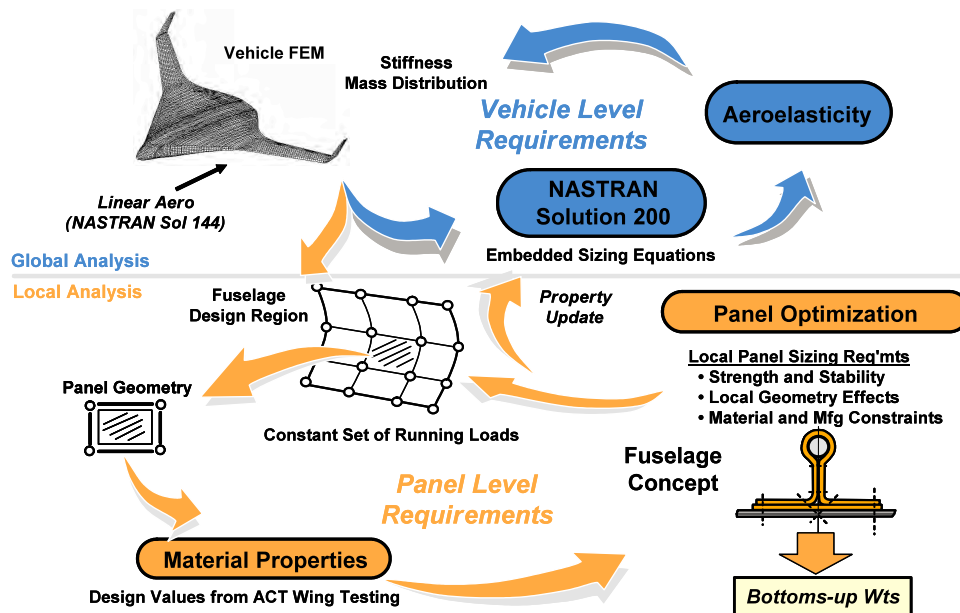


FIGURE 194. GLOBAL-LOCAL OPTIMIZATION APPROACH

Starting with the vehicle finite element model, loads, boundary conditions, and design constraints/requirements, a global optimization was performed using the optimization capabilities of MSC/NASTRAN (Sol 200) and local panel optimization was completed using the HyperSizer. Over a series of iterations, the NASTRAN internal loads were imported back and forth into HyperSizer until convergence of mass and stiffness was achieved. The HyperSizer code performed the local structural optimization using pre-defined material/structural properties and geometric design constraints to assess panel suitability for strength and stability constraints.

The resulting panel cross-sections were then idealized and exported back to the NASTRAN model as equivalent plate elements to simulate a PRSEUS fuselage panel response at the airplane level. Each time, the resized elements were used to create an updated NASTRAN design model for maneuver-load sizing (Figure 195). Once the models converged, the final sized weights were multiplied by non-optimum factors to generate a final “as-fabricated” weights distribution

needed to balance the model. This final step was conducted outside the automated FEM optimization process.

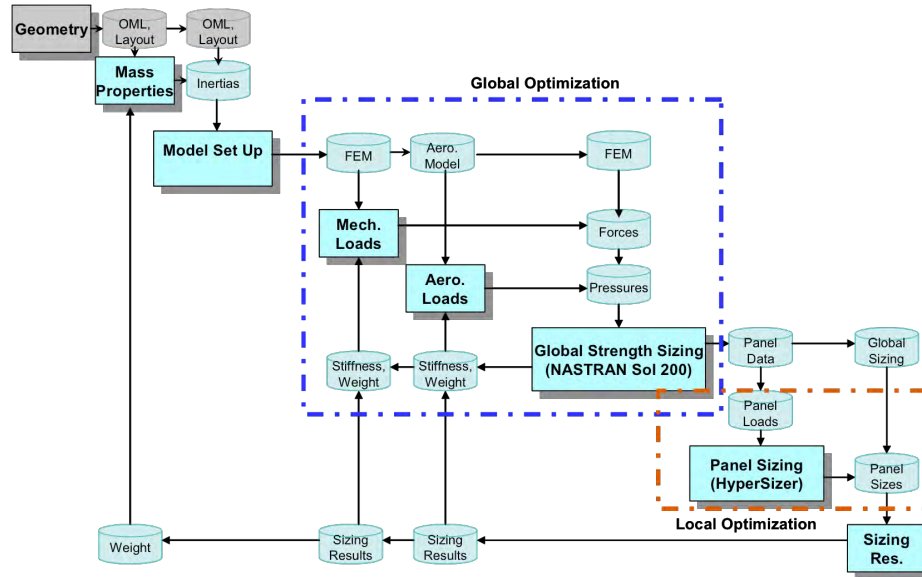


FIGURE 195. GLOBAL-LOCAL PROCESS FLOW

The vehicle-level structural sizing was based on a MTOGW of 408,700 lbs at the forward C.G. limit. The objective function being optimized was the overall vehicle weight. NASTRAN Sol 200 optimized the primary structure weight using global strength as the design criteria. As stated earlier, the optimization was limited to the pressurized fuselage cabin regions (Section 1, 2, 3, 4, 5). The bulkhead regions within the pressure cabin were held constant because their overall weights and load paths would not vary significantly as the skin panel and frame selections were changed. The remaining portions of the airframe, such as inboard & outboard wings and all substructures were also held constant in the sizing studies by maintaining the structural gauges established from the original baseline (sandwich shell fuselage) FEM used in the prior trade study.

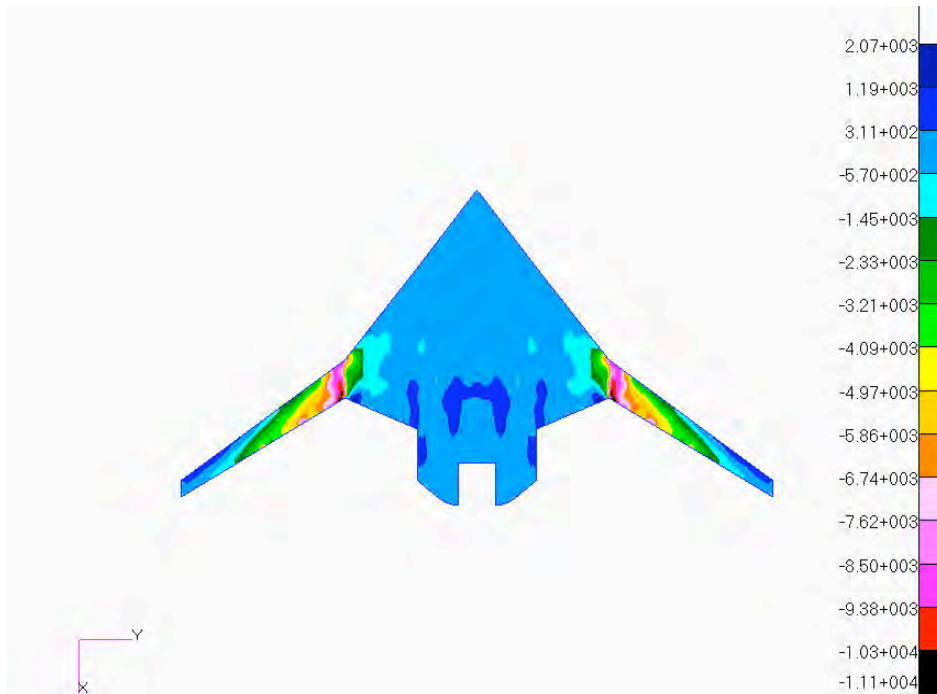
Internal Loads – The fourteen external load cases that were determined to be the most critical for sizing were applied to the updated finite element model in the structural optimization. A representative collection of critical running load plots is shown in the following figures (maneuver cases shown without internal pressure):

- 1) 2.5-g Limit Load Streamwise Direction (Nx) – Figure 196
- 2) 2.5-g Limit Load Spanwise Direction (Ny) – Figure 197
- 3) -1.0-g Limit Load Streamwise Direction (Nx) – Figure 198
- 4) -1.0-g Limit Load Spanwise Direction (Ny) – Figure 199
- 5) 1.33P Limit Load Streamwise Direction (Nx) – Figure 200
- 6) 1.33P Limit Load Spanwise Direction (Ny) – Figure 201
- 7) 2.0-g Taxi Bump Limit Load for Lower Cover – Figure 202

As expected, the plots show the critical maneuver loads (2.5 and -1.0-g) are dominant in the shell region adjacent to the wing, but less so moving forward. Whereas the forward portion of the

fuselage shell is dominated by the 2P pressure loading ($2P = 1.33P \times 1.5$). This observation was consistent throughout the sizing process.

Upper:



Lower:

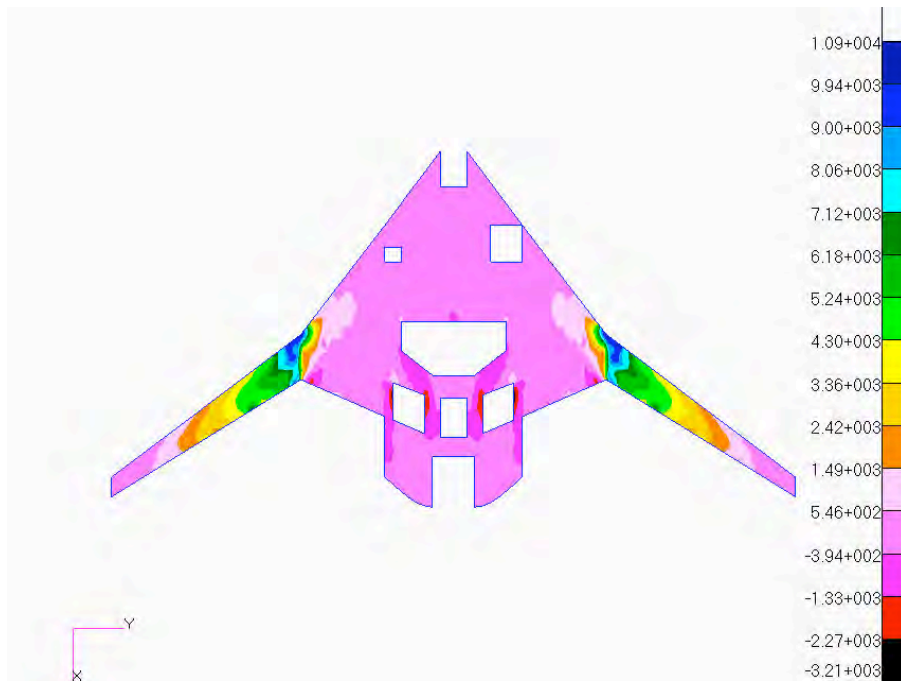
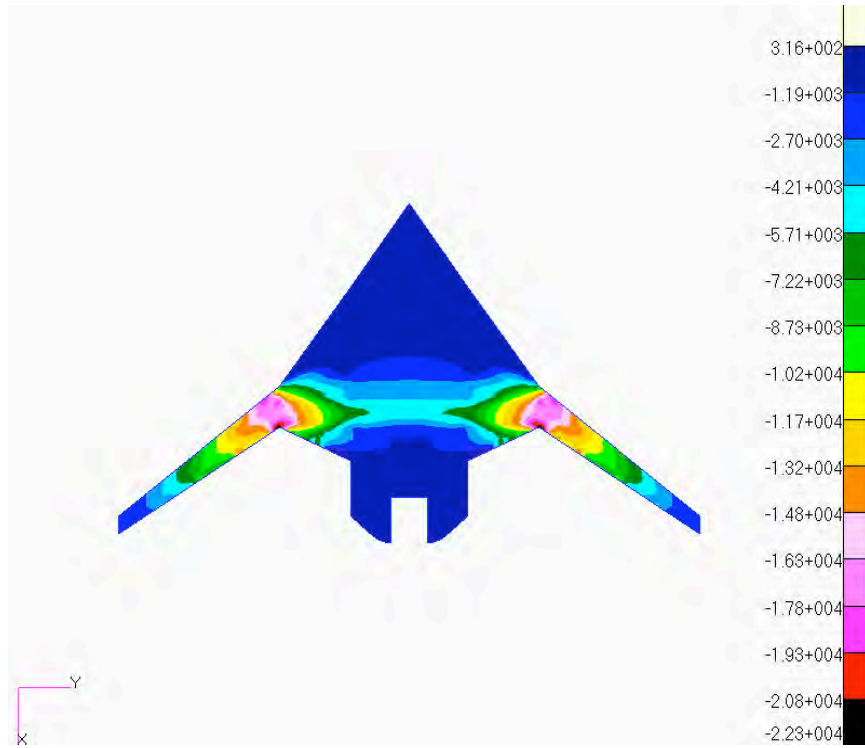


FIGURE 196. 2.5-G LIMIT LOAD STREAMWISE DIRECTION (NX) LBS/IN

Upper:



Lower:

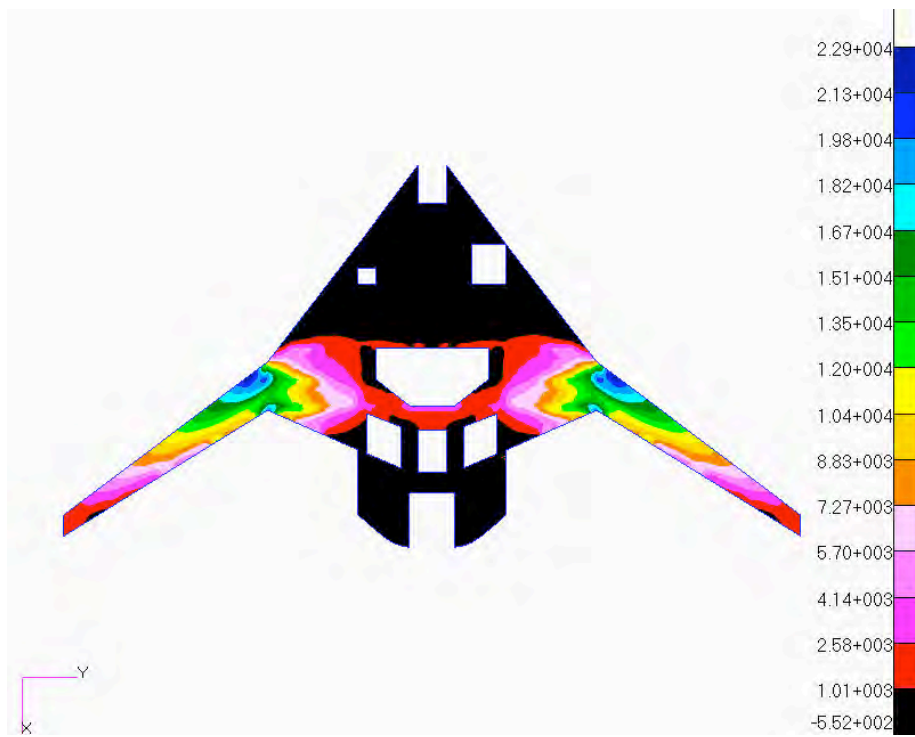
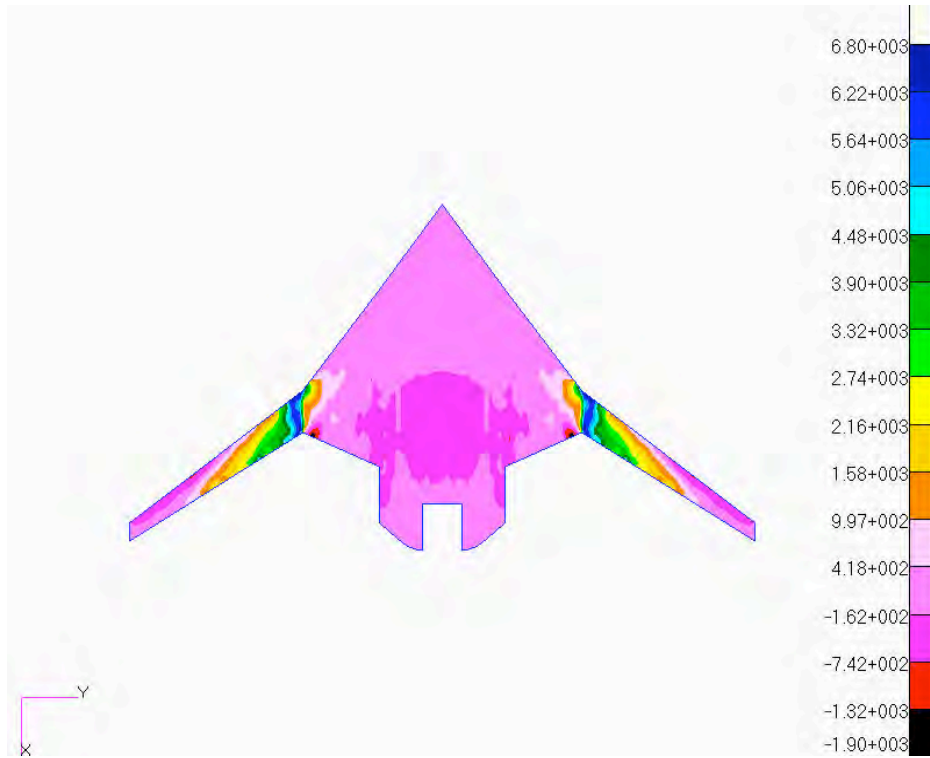


FIGURE 197. 2.5-G LIMIT LOAD SPANWISE DIRECTION (NY) LBS/IN

Upper:



Lower:

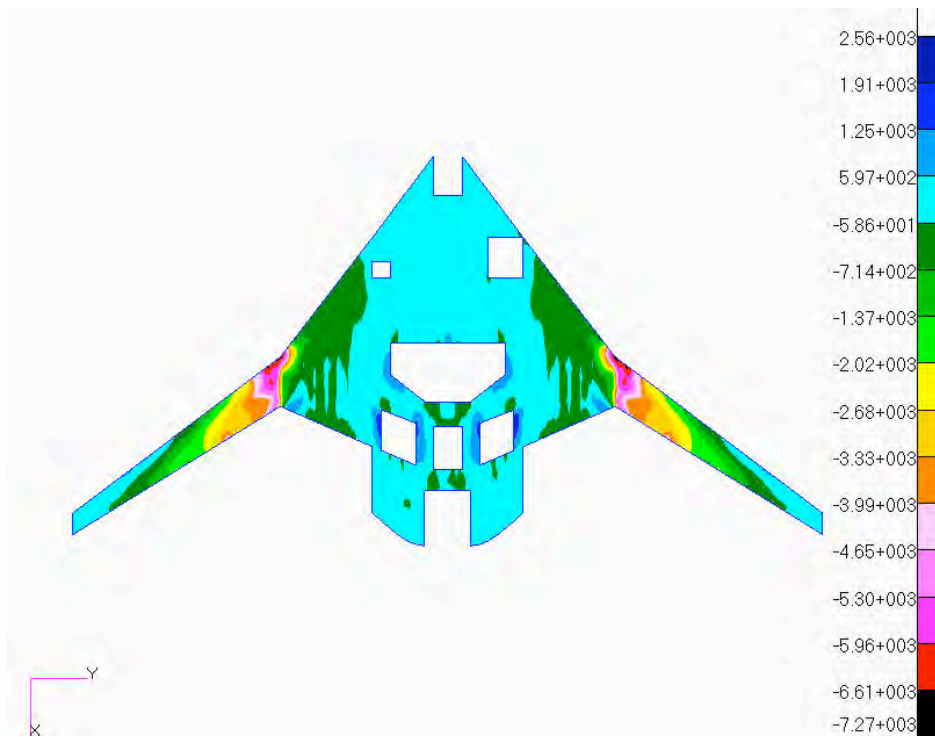
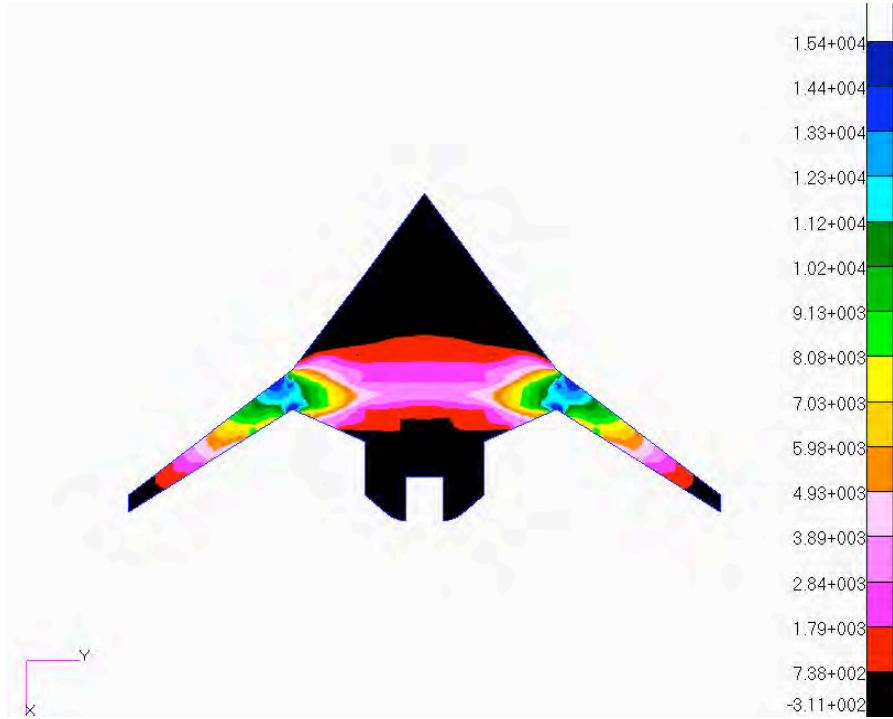


FIGURE 198. -1.0-G LIMIT LOAD STREAMWISE DIRECTION (NX) LBS/IN

Upper:



Lower:

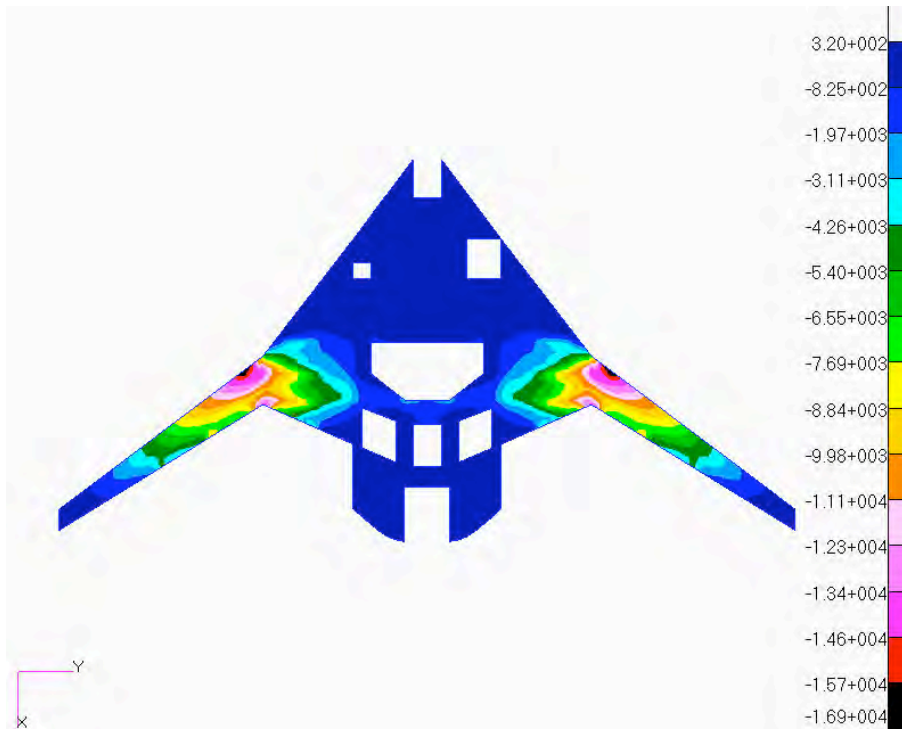
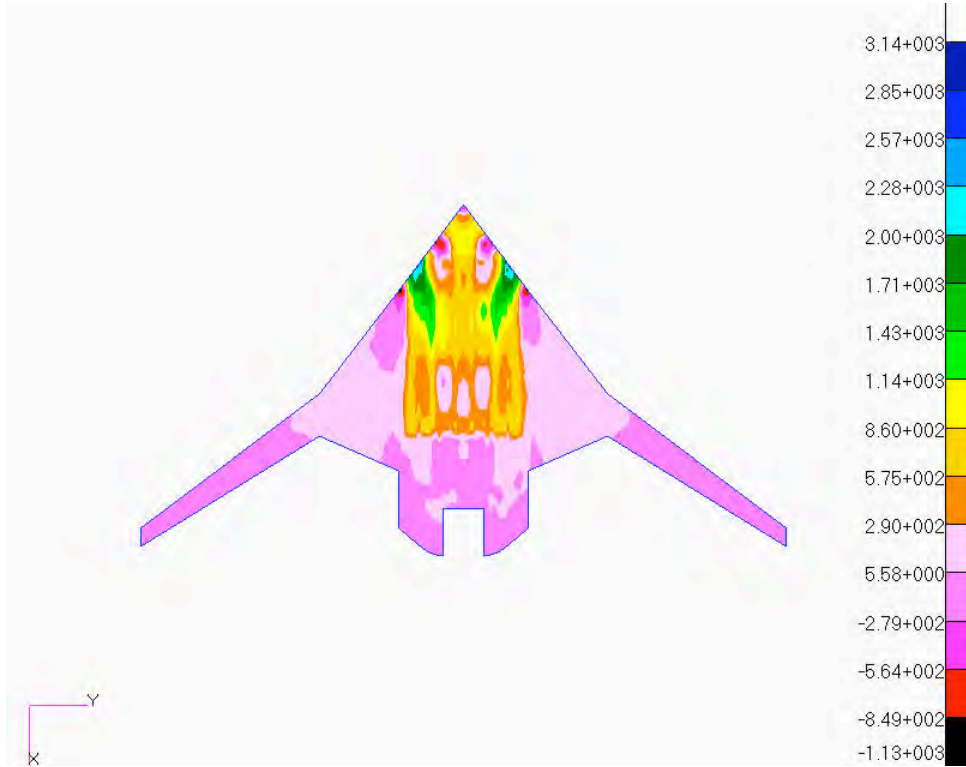


FIGURE 199. -1.0-G LIMIT LOAD SPANWISE DIRECTION (NY) LBS/IN

Upper:



Lower:

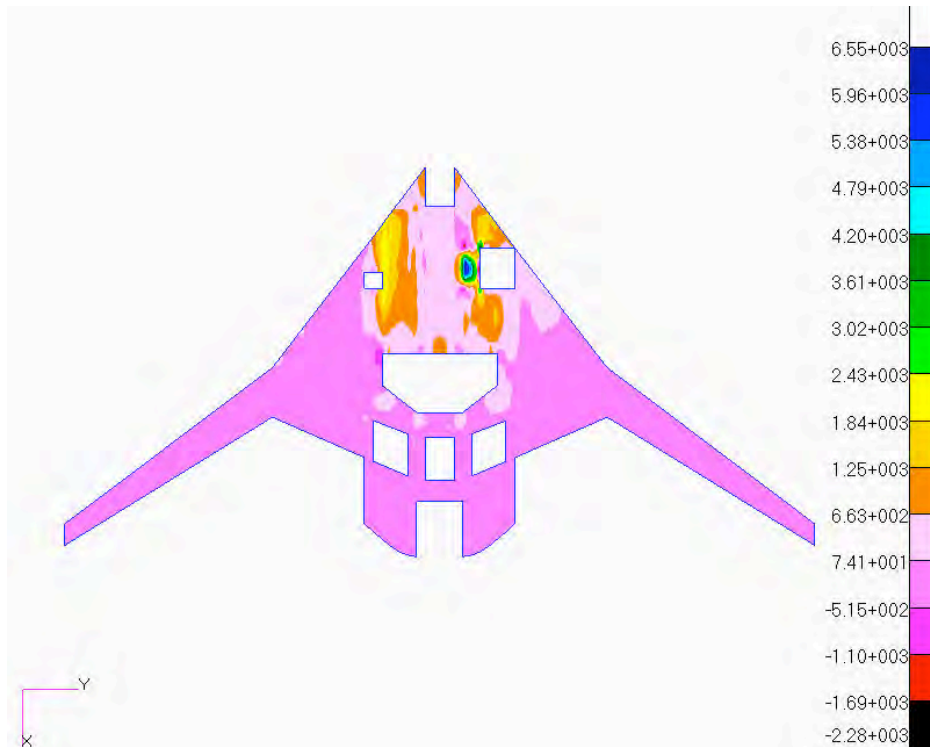
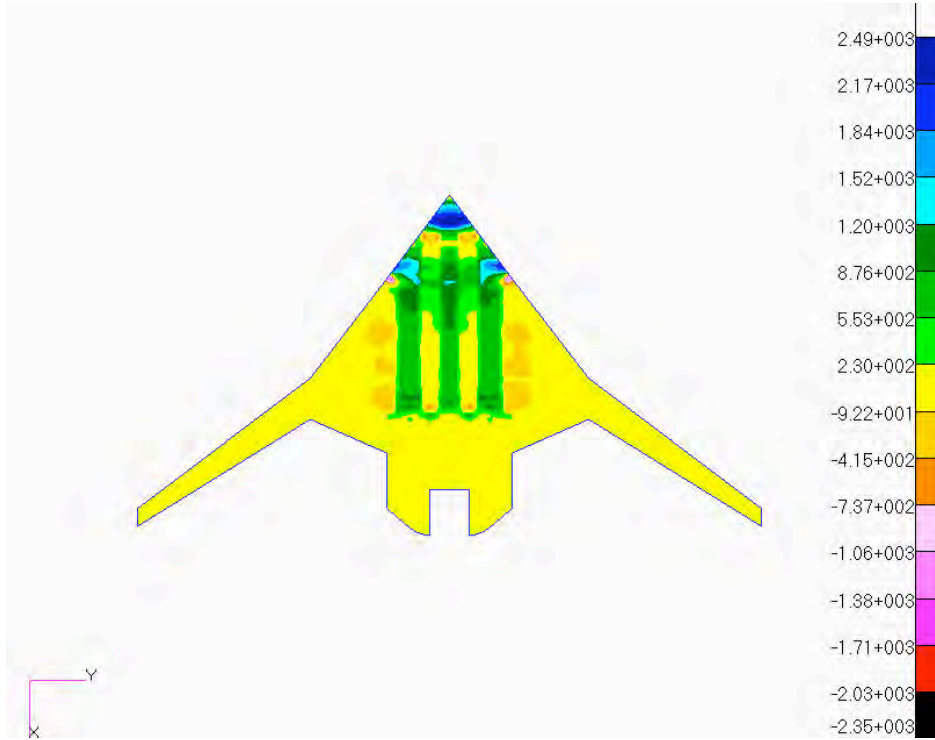


FIGURE 200. 1.33P LIMIT LOAD STREAMWISE DIRECTION (NX) LBS/IN

Upper:



Lower:

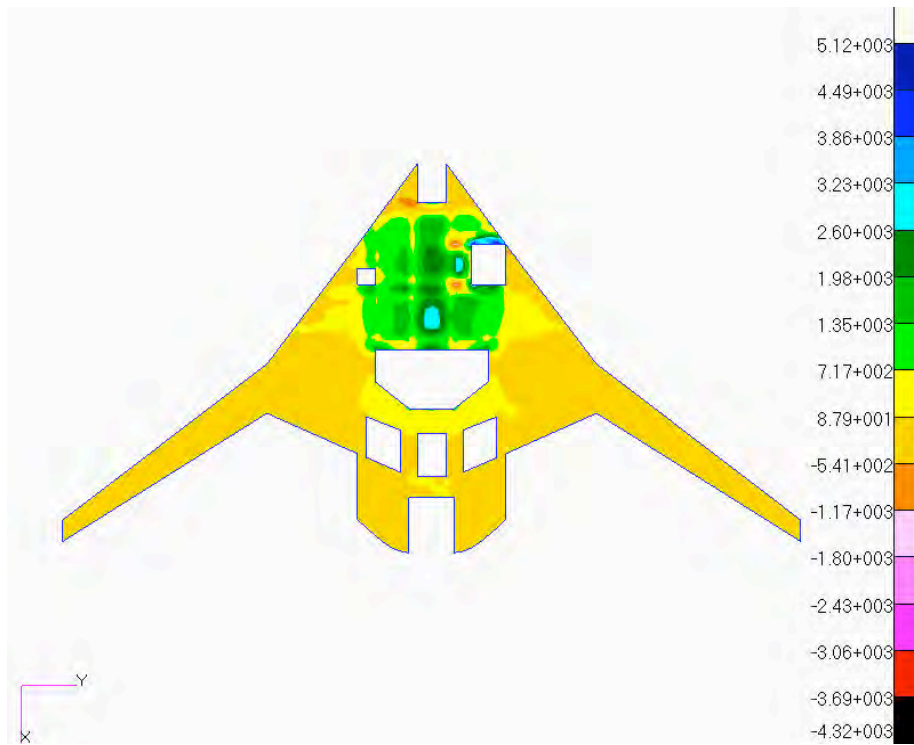
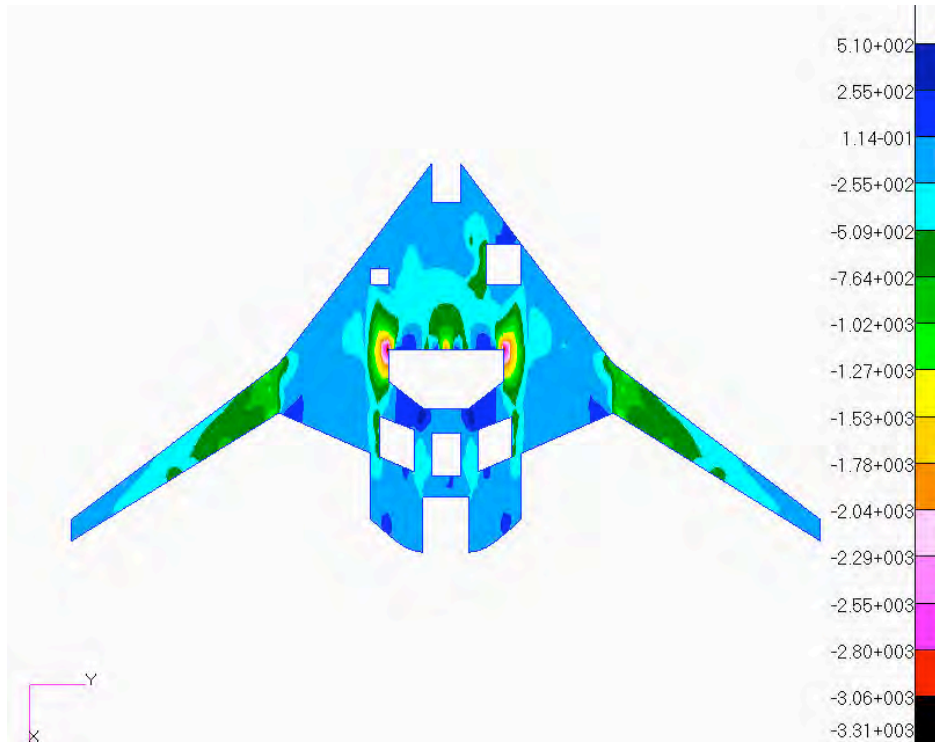


FIGURE 201. 1.33P LIMIT LOAD SPANWISE DIRECTION (NY) LBS/IN

Nx:



Ny:

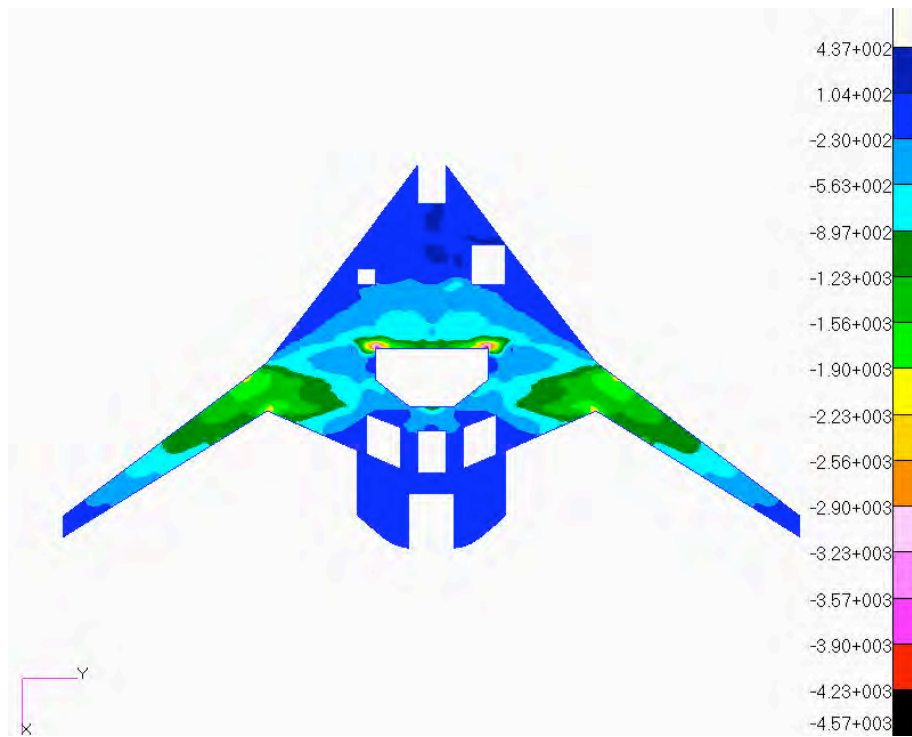
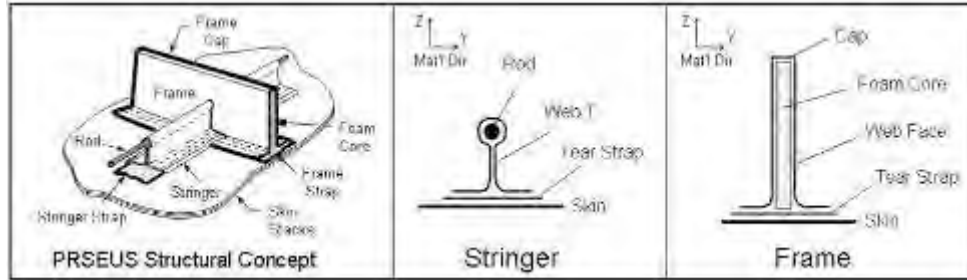


FIGURE 202. 2.0-G TAXI BUMP FOR LOWER COVER LBS/IN

Sizing Results - The final sizing results for the fuselage PRSEUS panels are summarized in the following figures (Figure 203 and Figure 204). The critical load conditions are 2.5-g and 2P for the upper skins, and the -1.0-g, 2.0-g Taxi Bump and 2P conditions for the lower skins. In Phase I, PRSEUS panel had to be approximated using I-stiffened panel inside of HyperSizer. The PRSEUS frames had to be modeled and optimized separately from panels themselves. Because of lacking of integration between frames and panels, in Phase I, panel dimensions had to be limited to a single frame bay for buckling analysis. This approximation may work fine for local buckling, but could well miss the global buckling modes for PRSEUS panels. With this new PRSEUS module of HyperSizer, users are able to model PRSEUS configurations in accuracy as designs. Most importantly, it enables fully integrated frame-panel optimization for PRSEUS concept.

From the sized new results (Figures 202 – 203), it is noticed that in comparison with Phase I, for some panels, critical failure modes have become global buckling instead of material strengths as identified in Phase I. These mode switches are all contributed to the new capability of frame-panel integration and it enables to capture multi-bay panel failure behaviors. Fortunately, there are no significant changes for the final sizes between Phase I and Phase II results. It indicates that approximate method used in Phase I was conservative and reasonable.

SIZING SUMMARY FOR UPPER COVER SKINS:



Design Region ID#	FEM Prop ID#	Skin Thickness (inches)	# Stacks	Stringer H (inches)	Str Strap W (inches)	Str Strap T (inches)	Str Web T (inches)	Rod Dia (inches)	Frame H (inches)	Fra Strap W (inches)	Fra Strap T (inches)	Fra Web T (inches)	Critical Load	Critical Design Mode
I	1101	0.156	3	1.25	2.06	0.052	0.104	3/8"	6	3.4	0.052	0.104	2.5G	Buckling
II	1102	0.156	3	1.25	2.06	0.052	0.104	3/8"	6	3.4	0.052	0.104	2.5G	Buckling
III	1103	0.208	4	1.25	2.06	0.052	0.104	3/8"	6	3.4	0.052	0.104	2.5G	Strength
IV	1104	0.208	4	1.25	2.06	0.052	0.104	3/8"	6	3.4	0.052	0.104	2.5G	Strength
V	1201	0.156	3	1.25	2.06	0.052	0.104	3/8"	6	3.4	0.052	0.104	2P	Strength
VI	1202	0.156	3	1.25	2.06	0.052	0.104	3/8"	6	3.4	0.052	0.104	2P	Strength
VII	1301	0.104	2	1.25	2.06	0.052	0.104	3/8"	6	3.4	0.052	0.104	2P	Strength
VIII	1302	0.104	2	1.25	2.06	0.052	0.104	3/8"	6	3.4	0.052	0.104	2P	Strength
IX	1303	0.104	2	1.25	2.06	0.052	0.104	3/8"	6	3.4	0.052	0.104	2P	Strength
X	1304	0.104	2	1.25	2.06	0.052	0.104	3/8"	6	3.4	0.052	0.104	2P	Strength
XI	1305	0.104	2	1.25	2.06	0.052	0.104	3/8"	6	3.4	0.052	0.104	2P	Strength
XII	1306	0.104	2	1.25	2.06	0.052	0.104	3/8"	6	3.4	0.052	0.104	2P	Strength
XIII	1391	0.156	3	1.25	2.06	0.052	0.104	3/8"	6	3.4	0.052	0.104	2P	Strength
XIV	1392	0.156	3	1.25	2.06	0.052	0.104	3/8"	6	3.4	0.052	0.104	2P	Strength
XV	1501	0.104	2	1.25	2.06	0.052	0.104	3/8"	6	3.4	0.052	0.104	2P	Strength
XVI	12010	0.156	3	1.25	2.06	0.052	0.104	3/8"	6	3.4	0.052	0.104	2P	Strength
XVII	13010	0.104	2	1.25	2.06	0.052	0.104	3/8"	6	3.4	0.052	0.104	2P	Strength
XVIII	13020	0.104	2	1.25	2.06	0.052	0.104	3/8"	6	3.4	0.052	0.104	2P	Strength
XIX	13040	0.156	3	1.25	2.06	0.052	0.104	3/8"	6	3.4	0.052	0.104	2P	Strength
XX	13050	0.156	3	1.25	2.06	0.052	0.104	3/8"	6	3.4	0.052	0.104	2P	Strength
XXI	15010	0.104	2	1.25	2.06	0.052	0.104	3/8"	6	3.4	0.052	0.104	2P	Strength

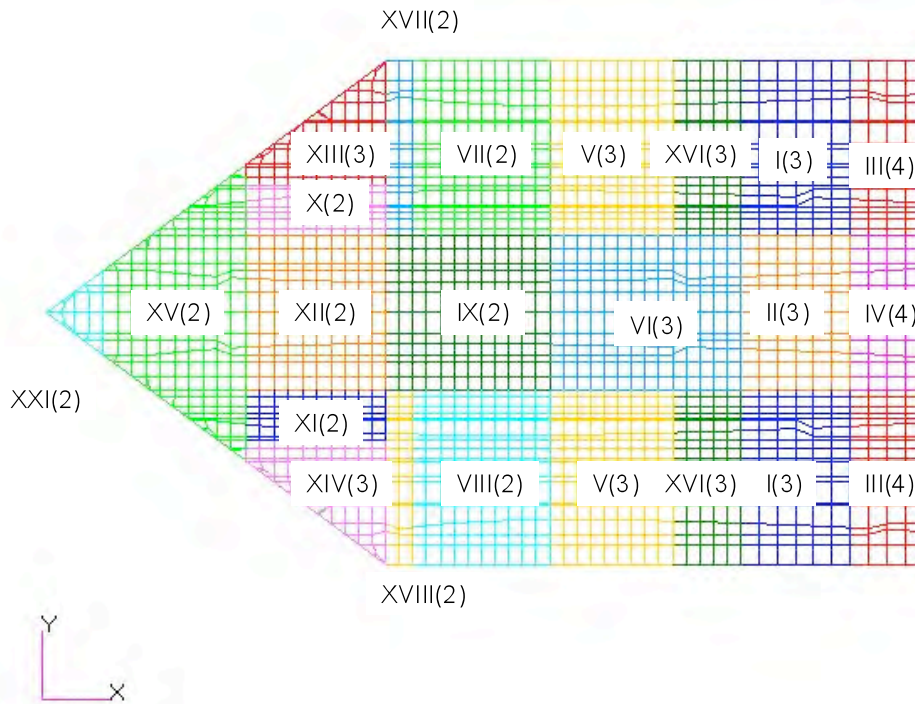
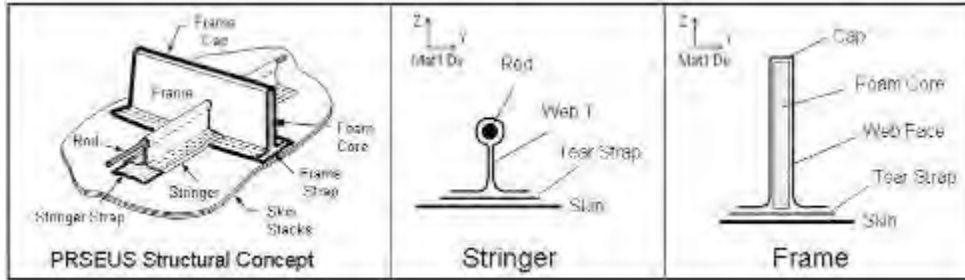


FIGURE 203. UPPER SKIN DESIGN REGIONS AND NUMBER OF SKIN STACKS

SIZING SUMMARY FOR LOWER COVER SKINS:



Design Region ID#	FEM Prop ID#	Skin Thickness (inches)	# Stacks	Stringer H (inches)	Str Strap W (inches)	Str Strap T (inches)	Str Web T (inches)	Rod Dia (inches)	Frame H (inches)	Fra Strap W (inches)	Fra Strap T (inches)	Fra Web T (inches)	Critical Load	Critical Design Mode
I	2002	0.156	3	1.25	2.06	0.052	0.104	3/8"	6	3.4	0.052	0.104	-1.0G	Buckling
II	2101	0.104	2	1.25	2.06	0.052	0.208	3/8"	6	3.4	0.052	0.104	2G Taxi	Buckling
III	2102	0.104	2	1.25	2.06	0.052	0.208	3/8"	6	3.4	0.052	0.104	2G Taxi	Buckling
IV	2103	0.156	3	1.25	2.06	0.052	0.104	3/8"	6	3.4	0.052	0.104	-1.0G	Buckling
V	2104	0.104	2	1.25	2.06	0.052	0.208	3/8"	6	3.4	0.052	0.104	-1.0G	Buckling
VI	2105	0.104	2	1.25	2.06	0.052	0.208	3/8"	6	3.4	0.052	0.104	-1.0G	Buckling
VII	2106	0.156	3	1.25	2.06	0.052	0.104	3/8"	6	3.4	0.052	0.104	-1.0G	Buckling
VIII	2201	0.104	2	1.25	2.06	0.052	0.104	3/8"	6	3.4	0.052	0.208	2G Taxi	Buckling
IX	2202	0.156	3	1.25	2.06	0.052	0.104	3/8"	6	3.4	0.052	0.208	2P	Strength
X	2203	0.156	3	1.25	2.06	0.052	0.208	3/8"	6	3.4	0.052	0.208	2P	Strength
XI	2204	0.104	2	1.25	2.06	0.052	0.208	3/8"	6	3.4	0.052	0.104	2P	Buckling
XII	2205	0.104	2	1.25	2.06	0.052	0.104	3/8"	6	3.4	0.052	0.156	2P	Strength
XIII	2206	0.104	2	1.25	2.06	0.052	0.208	3/8"	6	3.4	0.052	0.104	2G Taxi	Buckling
XIV	2207	0.208	4	1.25	2.06	0.052	0.104	3/8"	6	3.4	0.052	0.104	2G Taxi	Buckling
XV	2208	0.156	3	1.25	2.06	0.052	0.104	3/8"	6	3.4	0.052	0.104	2P	Strength
XVI	2209	0.208	4	1.25	2.06	0.052	0.104	3/8"	6	3.4	0.052	0.104	2G Taxi	Buckling
XVII	2301	0.104	2	1.25	2.06	0.052	0.104	3/8"	6	3.4	0.052	0.104	2P	Strength
XVIII	2302	0.052	1	1.25	2.06	0.052	0.104	3/8"	6	3.4	0.052	0.104	2P	Strength
XIX	2303	0.104	2	1.25	2.06	0.052	0.104	3/8"	6	3.4	0.052	0.104	2P	Strength
XX	2304	0.156	3	1.25	2.06	0.052	0.208	3/8"	6	3.4	0.052	0.208	2P	Strength
XXI	2305	0.052	1	1.25	2.06	0.052	0.104	3/8"	6	3.4	0.052	0.208	2P	Strength
XXII	2306	0.104	2	1.25	2.06	0.052	0.104	3/8"	6	3.4	0.052	0.156	2P	Strength
XXIII	2501	0.104	2	1.25	2.06	0.052	0.104	3/8"	6	3.4	0.052	0.104	2G Taxi	Buckling
XXIV	2502	0.104	2	1.25	2.06	0.052	0.104	3/8"	6	3.4	0.052	0.104	2G Taxi	Buckling
XXV	21010	0.104	2	1.25	2.06	0.052	0.208	3/8"	6	3.4	0.052	0.104	2G Taxi	Buckling
XXVI	21020	0.104	2	1.25	2.06	0.052	0.208	3/8"	6	3.4	0.052	0.104	2G Taxi	Buckling
XXVII	22040	0.104	2	1.25	2.06	0.052	0.104	3/8"	6	3.4	0.052	0.104	2P	Strength
XXVIII	22060	0.104	2	1.25	2.06	0.052	0.104	3/8"	6	3.4	0.052	0.104	2P	Strength
XXIX	23010	0.104	2	1.25	2.06	0.052	0.104	3/8"	6	3.4	0.052	0.208	2P	Strength
XXX	23020	0.052	1	1.25	2.06	0.052	0.104	3/8"	6	3.4	0.052	0.104	2P	Strength

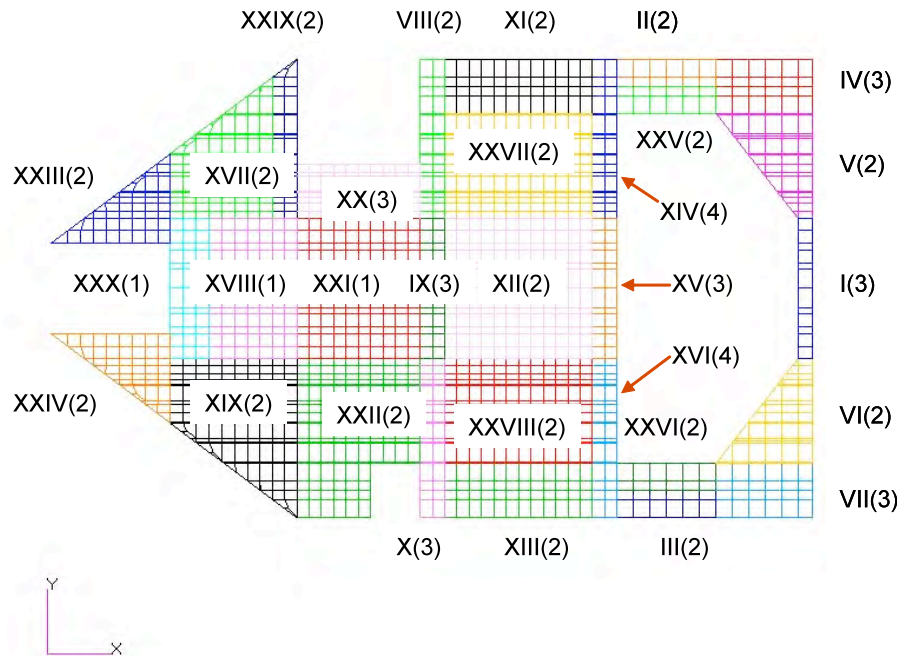


FIGURE 204. LOWER SKIN DESIGN REGIONS AND NUMBER OF SKIN STACKS

6.4 Updated Weights Statement

The overall aircraft weights summary for the baseline BWB-5-200G configuration was further refined into a detailed breakdown for the pressurized portion of the center body (Figure 205). The bottoms-up calculation methodology utilized the FEM-based sizing results which combined with a series of non-optimum factors to arrive at the final as-fabricated weight values for the airframe.

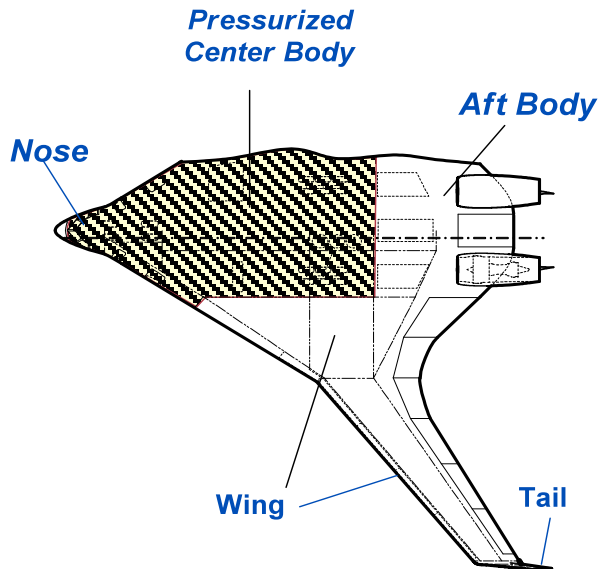


FIGURE 205. BWB PRESSURIZED REGION

The non-optimum weight factors were based on data generated from two prior studies: 1) a Boeing in-house composite structures design study (Reference: HSR Report MDC 98K0303, Weight/Size Estimate Algorithms for Global Optimization of High Speed Civil Transport Aircraft, 1998) and, 2) the NASA TCAT Phase I Study (4). The data from these two studies was used to establish the relative weight penalty that would be assessed to account for factors not considered in the structural analyses.

Weight penalties for the non-optimum increments were added to the idealized structural weight values calculated by the FEM sizing task. A 20% non-optimum factor was assessed for the PRSEUS skin-stringer concept. The 20% value is equivalent to the beaded-hat skin-stringer concept that was analyzed in the TCAT study as two skin-stringer concepts would have similar non-optimum characteristics. No further effort was completed under this study to further develop or refine a specific set of non-optimum factors for the PRSEUS concept.

The detailed panel-level weights for the center body are shown for Phase I and II in Table 11. Non-optimum values were also added to the pressurized shell, frame and bulkhead structural results to generate the final as-fabricated weight components. The results represent a side-by-side vehicle-level weight comparison between those two studies. It is noticed that there are no significant changes in weight. Consistent results have been shown between Phase I and Phase II as demonstrated through final structural sizing. It is noted that the upper and lower skin panels on the right column include frame weights.

TABLE 12. PRESSURIZED CENTER BODY WEIGHT

Weight Item Description	Sized in Phase I	Sized in Phase II*
FEM Sized Pressured Body Structure Weight		
Upper Skin Panel	3903	5431
Lower Skin Panel	2938	3715
Frames	2438	0
Y-Braces and Posts	2143	2143
Internal Cabin Ribs	5330	5330
SOB Rib	1071	1071
Floor Panel and Beams - Upper Cabin, Lower Cargo and Bulk Cargo	5281	5281
Internal Spars and Bulkheads	4041	4041
Pressurized Leading Edge Structure	4384	4384
Lower Body Pressure Bulkheads and Frames	904	904
Sub Total Pressurized Body Structure Weight	32433	32300
Non-Optimum Weight Allowance		
Skin Panel - Doublers, Cutouts, Splices and Attach	1368	1368
Frame - Doublers, Cutouts, Splices and Attach	244	244
Ribs and Floor - Doublers, Cutouts, Splices and Attach	2051	2051
Lighting Protection	280	280
Veil-Ply	233	233
Paint, Primer, Sealant	651	651
Sub Total Non-Optimum Weight	4828	4828
Total Pressurized Body Structure Weight - Lbs	37261	37128

* Upper Skin & Lower Skin Panels WT Include Frames'

6.5 Test Loads

Test loads for the three specimen tests completed in this phase were broken out and developed prior to the completion of the vehicle sizing updates as design, analysis, and fabrication occurred. These final test loads were compared to the results of the vehicle sizing trades at the end of the study, but after the tension panel test was completed. Test loads were based on sizing results from the vehicle sizing trades in Phase I and pre-determined critical load conditions for the BWB (Reference 1).

Pressure Panel - Test loads for the pressure panel were determined by the cabin pressure load case. As pressurization of the shell drives the sizing of the skin where other loads are low in the non-circular BWB fuselage sections, the cabin over-pressurization load case is found to be a design driver. This internal pressure load case consists of pressure equal to twice the maximum allowable cabin pressure differential and does not include other external loads. The pressure differential of 18.4 psi is used for the 2P pressurization load case. A plot of the test region defined by the 2P case applicable to the pressure panel, near the front end of vehicle, is shown in Figure 206 under limit load.

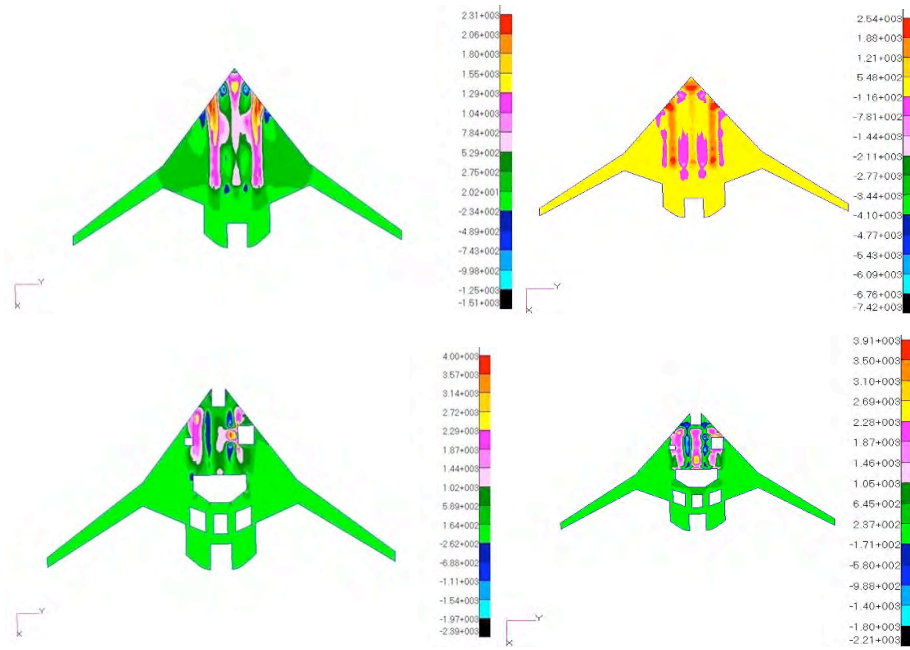


FIGURE 206. 1.33P LIMIT LOAD NX (LEFT) AND NY (RIGHT)

Chordwise Tension Panel - In Phase I, it was identified that the -1.0g maneuver condition was the most critical tension case for the skin structure. The typical running load seen in the skin structure of the BWB in this load case is shown in Figure 207. The peak Nx ultimate running load in this case is approximately 1,000 lbs/inch.

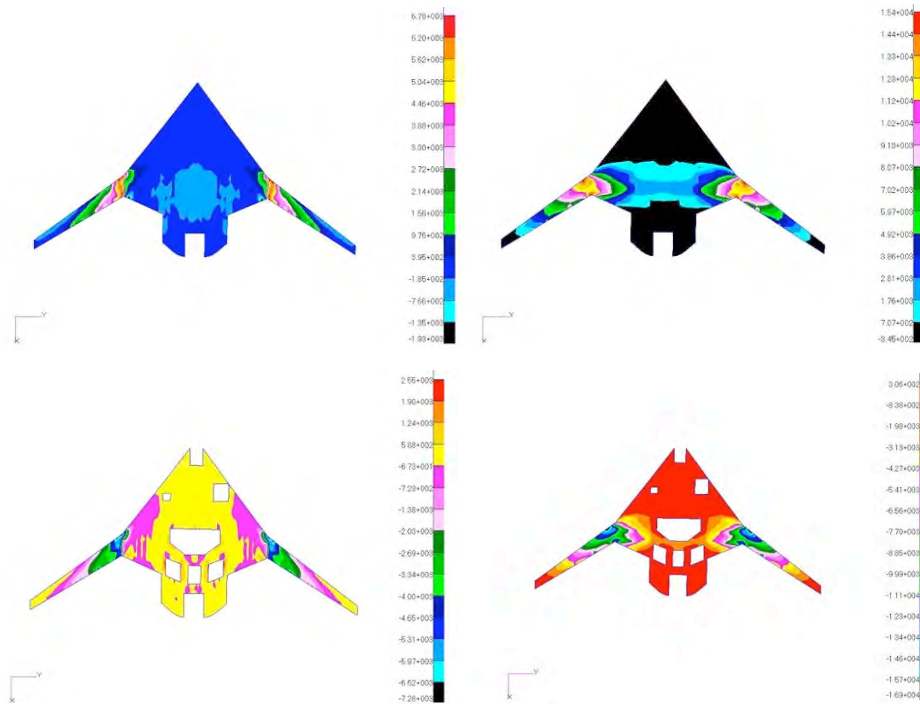


FIGURE 207. -1.0-G LIMIT LOAD NX (LEFT) AND NY (RIGHT)

Testing of the chordwise tension panel in this task demonstrated that the PRSEUS configuration panel can withstand beyond the 1,000 lbs/inch required to meet the loading requirements of the BWB.

Spanwise Compression Panel - The most significant load case identified in Phase I is the 2.5g maneuver condition. The Phase I vehicle sizing assessments showed a significant compression load across the upper panel of the fuselage section under this critical load case as shown in Figure 208. The fuselage section sees a maximum of -1,900 lbs/inch in the skin and an additional -1,433 lbs/inch in the frame sections. At ultimate load, this creates a critical running load of -5,000 lbs/inch in the spanwise direction, or 80,000 lbs per frame for the 16-inch spacing in this region. As the BWB non-circular fuselage can be stability critical in the spanwise direction due to long lengths of unsupported panel between rib structures, this load case was identified as a critical condition and minimum design requirement in the frame-direction.

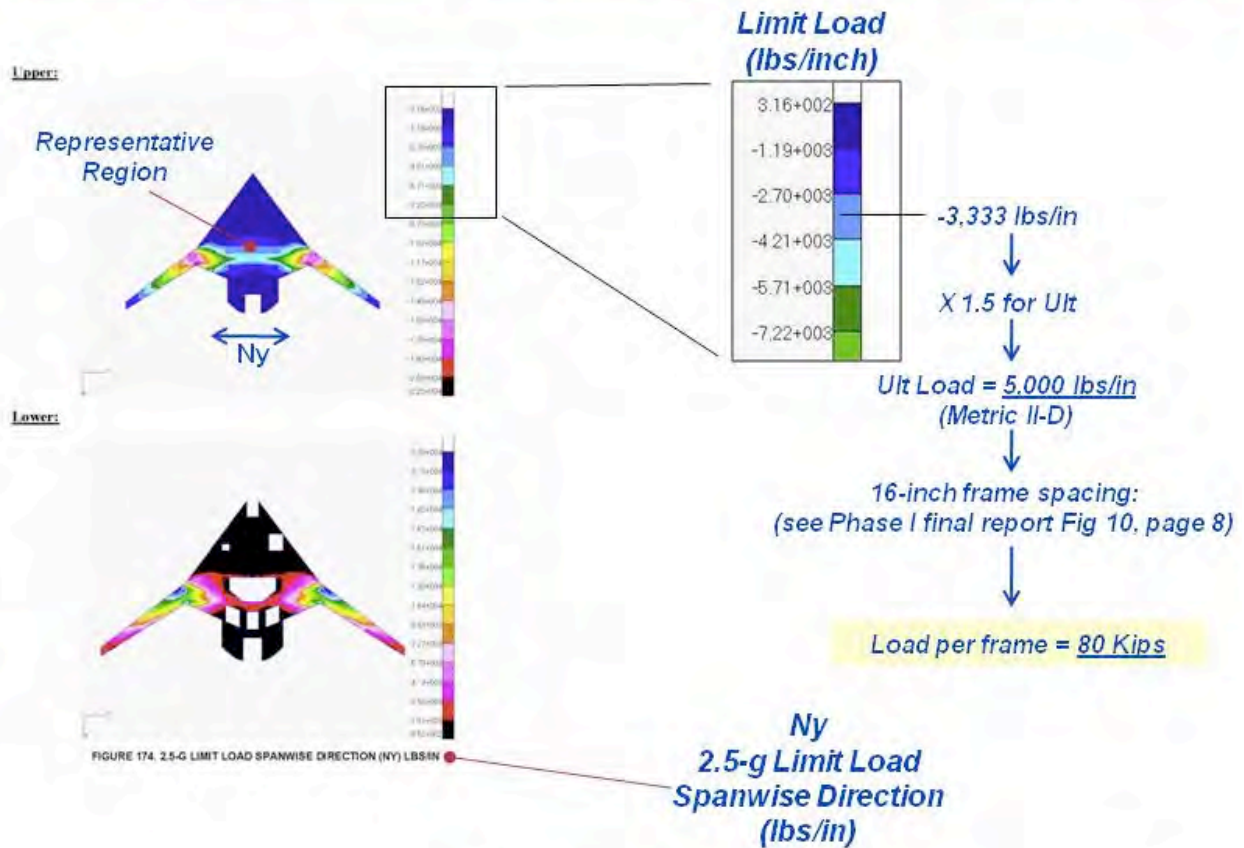


FIGURE 208. 2.5-G MANEUVER LOAD CASE

7.0 PHASE II - METRICS AND CONCLUSIONS

The Phase II metrics were derived directly from the vehicle-level trades that were completed during the Phase I portion of the study. This approach was taken to ensure that the weight targets, specimen geometries, and load levels selected for the Phase II subcomponent test program would be relevant and ultimately capable of closing the HWB baseline airframe configuration (BWB-5-200G).

7.1 Metrics

At the beginning of Phase II, the following four metric criteria were selected to measure the success of the subcomponent testing:

- 1) Metric II-A: Pressure panel test exceeds 2P loading requirement (18.4 psi).
- 2) Metric II-B: Damage arrestment demonstrated for 2-bay crack tension panel where final failure load exceeds the crack initiation load by a factor of 1.5.
- 3) Metric II-C: Failure load for fatigue cycled single-stringer compression specimens is within 5% of statically tested specimens from Phase I.
- 4) Metric II-D: Panel general buckling load parallel to frames exceeds -5,000 lbs/in.

The knowledge gained during Phase I was used as the basis for developing increasing levels of specimen complexity to isolate and validate the three primary loading directions found on the BWB/HWB pressure cabin (N_x , N_y , N_z). In each case, the magnitude of the metric was intended to correspond with a specific load case and location on the airframe, which in turn could be used to validate the analytical results and assumptions generated during the trade studies. The relationship between the Phase II metrics established at the outset of the program and the final test results are shown in Figure 209.

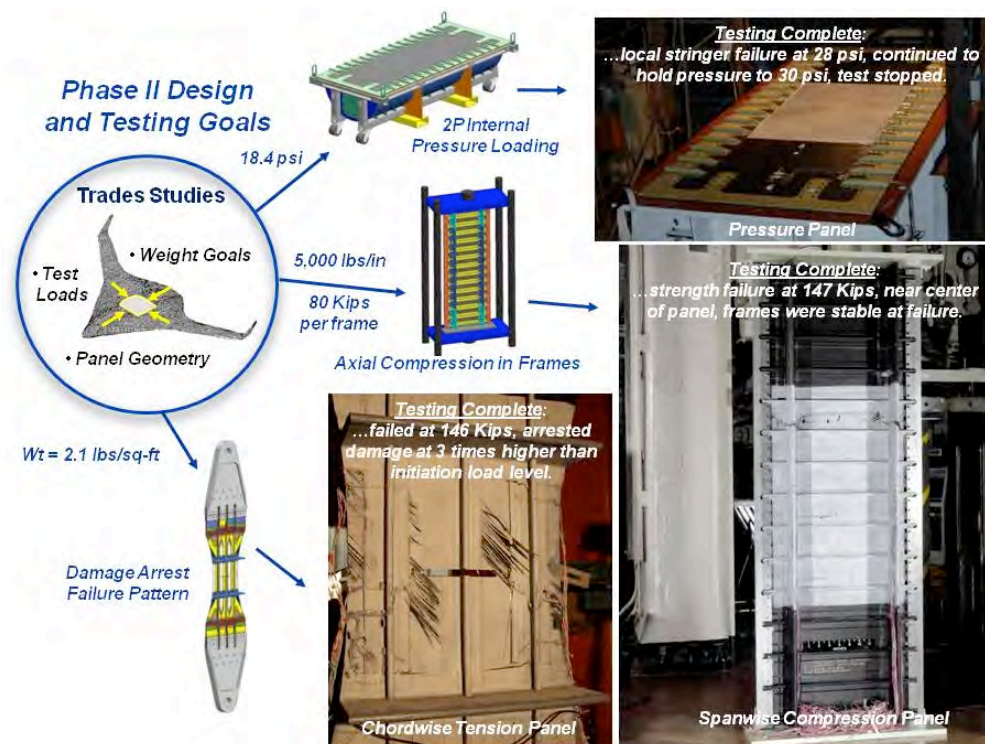


FIGURE 209. METRIC VALUES ESTABLISHED FOR PHASE II TESTING

A summary of all six NRA Phase I and Phase II metrics is provided in Table 13.

TABLE 13. SUMMARY OF NRA PHASE I AND II METRICS

<i>Metric</i>	<i>Metric Descriptions</i>	<i>Goal</i>	<i>Measured</i>
I-A	<i>PRSEUS 10% lighter than sandwich</i>	<i>-10%</i>	<i>-10.4% (analysis)</i>
I-B	<i>Buckling load exceeds strength design failure load</i>	<i>> 0%</i>	<i>+75% (tested)</i>
II-A	<i>Minimum gauge panel meets 2P load case</i>	<i>18.4 psi</i>	<i>28.4 psi (tested)</i>
II-B	<i>Stitching arrests damage to permit 1.5 times higher loading</i>	<i>>150%</i>	<i>>300% (tested)</i>
II-C	<i>Fatigue cycled specimens are within 5% of static test results</i>	<i>< 5%</i>	<i>within 5% (tested)</i>
II-D	<i>Buckling load for min gauge panels = 80,000 lbs/frame</i>	<i>160 Kips</i>	<i>147 Kips (tested)</i>

All of the test results exceeded the metric goals, except for the 2-frame spanwise compression panel (Metric II-D), which was about 7% below the stated target value of 80 Kips per frame (equivalent to 5,000 lbs per inch with 16-inch frame spacing, see Section 4.2 for calculation method). Although at first glance, this particular test result was below the target value, it is more an artifact of how the metric was initially determined at the outset of the program - prior to having the vehicle-level airframe sizing work described in Section 6 completed. Now that the Phase II sizing results are complete, a more precise assessment can be made between the running load that was achieved during the test (roughly 74 Kips for each frame) and the minimum gauge panel weight (2.1 lbs per sq-ft) that was tested.

In the fuselage crown region where the spanwise (N_y) compressive running loads are the highest (5,000 lbs/inch, see running load plots, Section 6.3), the corresponding panel gauges sized in the trade studies are comprised of 4-stack skins (.208-inch thick skins) with 16-inch frame spacing. The corresponding unit weight for these panels is 3.4 lbs/sq-ft, making them about 60% heavier than the minimum gauge panel design that was tested where the unit panel weight = 2.1 lbs/sq-ft. Considering this large weight difference (1.3 lbs/sq-ft) between what-was-sized versus what-was-tested, missing the II-D metric value by only 7% actually should be viewed positively, as only a small amount of additional material (much less than 60%) would be needed to achieve a 7% higher load level. This can be attributed to the PRSEUS integral frame design which remained stable, without any indications of column instability throughout the entire load regime of testing prior to the ultimate failure of the specimen. In terms of how this result will affect the airframe sizing for the as-sized panel weights, the net result is that the as-sized panels could be made even lighter than the 4-stack skins that were analytically derived. This would lead to a lower airframe weight than what was reported for the crown panel region of the cabin where the spanwise 2.5-g maneuver loads are the highest.

Favorable results were also generated in each of the other subcomponent tests as the metric values were handily exceeded by the testing. These positive results indicate that as each component of loading (N_x , N_y , N_z) are brought together into the more complex testing that will be required to replicate the HWB combined-loads environment, ample margin still exists within the PRSEUS structural concept to accommodate the interaction that is expected between the in-plane and out-of-plane loading. The complexity of this interaction forms the basis of the development activities going forward beyond the Phase II program. Although increasing levels of loading complexity will be used in the ensuing test program, the basic metric values established during Phase II will continue to form the basis for quantitatively measuring the

success of testing for the HWB pressure cabin design. The relationship between the Phase II metrics and future testing and development activities is shown in Figure 210.

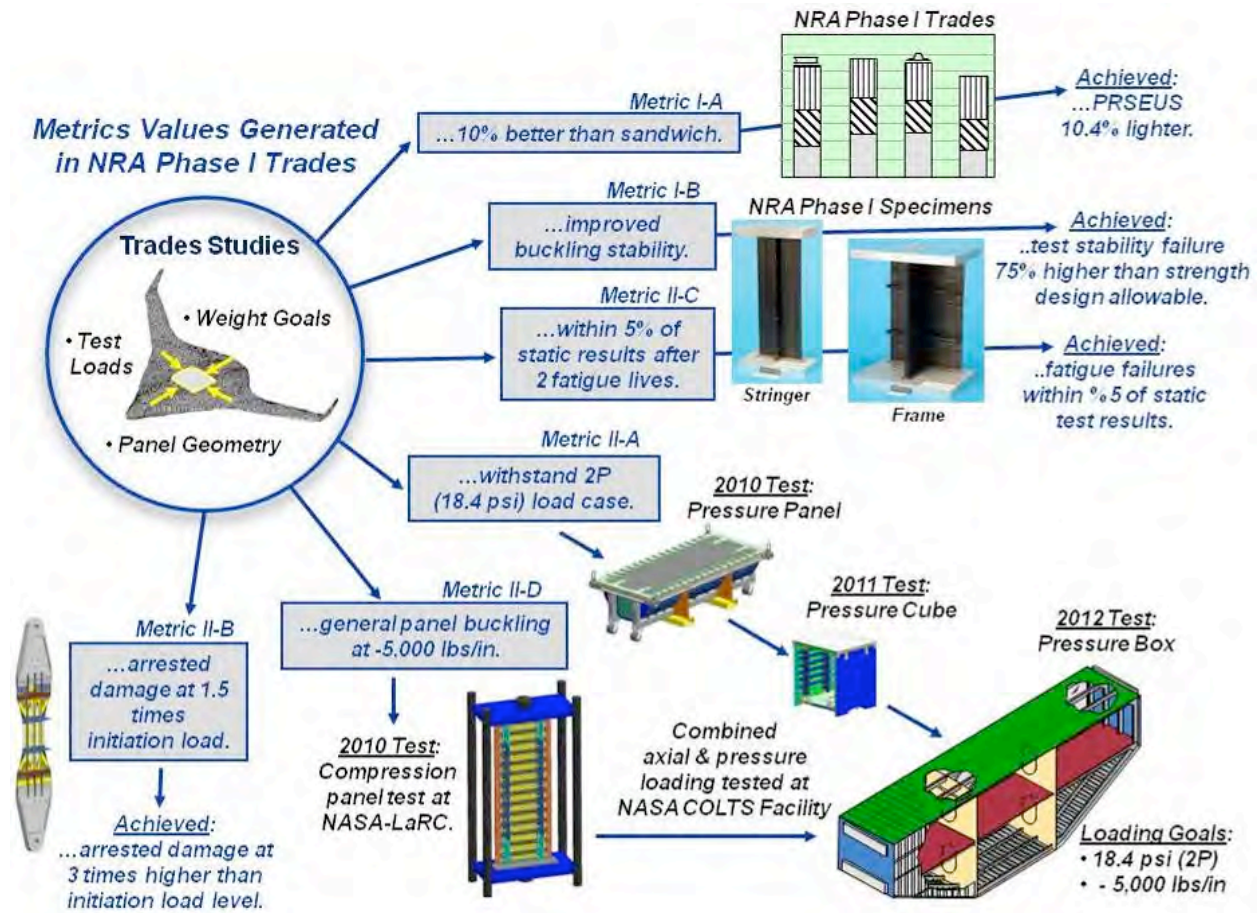


FIGURE 210. METRIC TARGET RELATIONSHIP TO FUTURE DEVELOPMENT ACTIVITIES

7.2 Conclusion

This Phase II development effort was planned as an intermediate step in the evolution of the HWB pressure cabin. For the first time ever, large subcomponent-level testing was undertaken with a structural concept that was capable of meeting both the producibility and performance challenges of the non-circular HWB airframe. Throughout the course of this effort, the fundamental enabling aspects of the HWB pressure cabin design were analytically characterized by FEM-based trade studies and then validated by testing in a representative loading condition - which was used to substantiate the trade study results with actual test data. Beyond exceeding the metric values described in the preceding section, these tests laid the foundation for the evolution of BWB pressure cabin design and ultimately validate that it will be possible to design large flat-sided composite structures that can be internally pressurized, yet remain light enough to retain the superior operating performance enabled by the HWB airfoil shape.

REFERENCES

¹ NASA Phase I Final Report, “Damage Arresting Composites for Shaped Vehicles”, Velicki, A., NASA/CR-2009-215932, Contract NNL07AA48C Project No. 4200208122, September 2008.

² AIR VEHICLE TECHNOLOGY INTEGRATION PROGRAM (AVTIP), Delivery Order 0059: Multi-role Bomber Structural Analysis, AFRL-VA-WP-TR-2006-3067, Krishna Hoffman, MAY 2006, Final Report for 14 December 2004 – 08 May 2006, AFRL-VA-WP-TR-2006-3067.

³ Velicki, A. and Thrash, P.J., “Advanced Structural Concept Development Using Stitched Composites”, 49th AIAA/ASME/ASCE/SHS/ASC Structures, Structural Dynamics, and Materials Conference, 7-10 April 2008, Schaumburg, IL, AIAA Paper 2008-2329.

⁴ Velicki, A. and Hansen, D., “Novel Blended Wing Body Structural Concepts Phase I Final Report, “Final Report for NNL04AA36C CLIN 0001, 13 July 2004.

APPENDIX A – PRESSURE BOX TEST PANEL

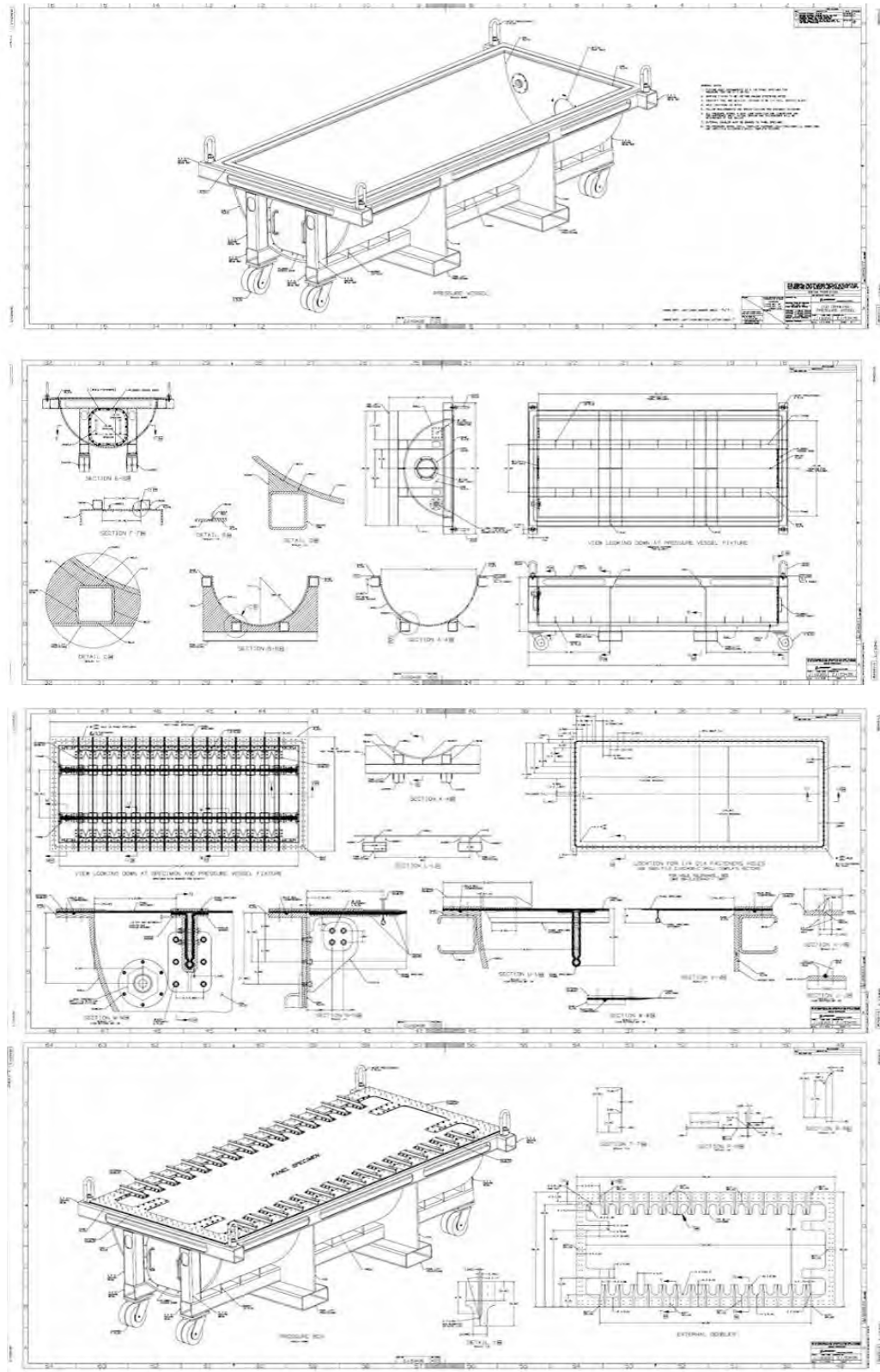


FIGURE 211. PRESSURE TEST FIXTURE ICD PROVIDED TO VENDOR

APPENDIX B – CHORDWISE TENSION PANEL

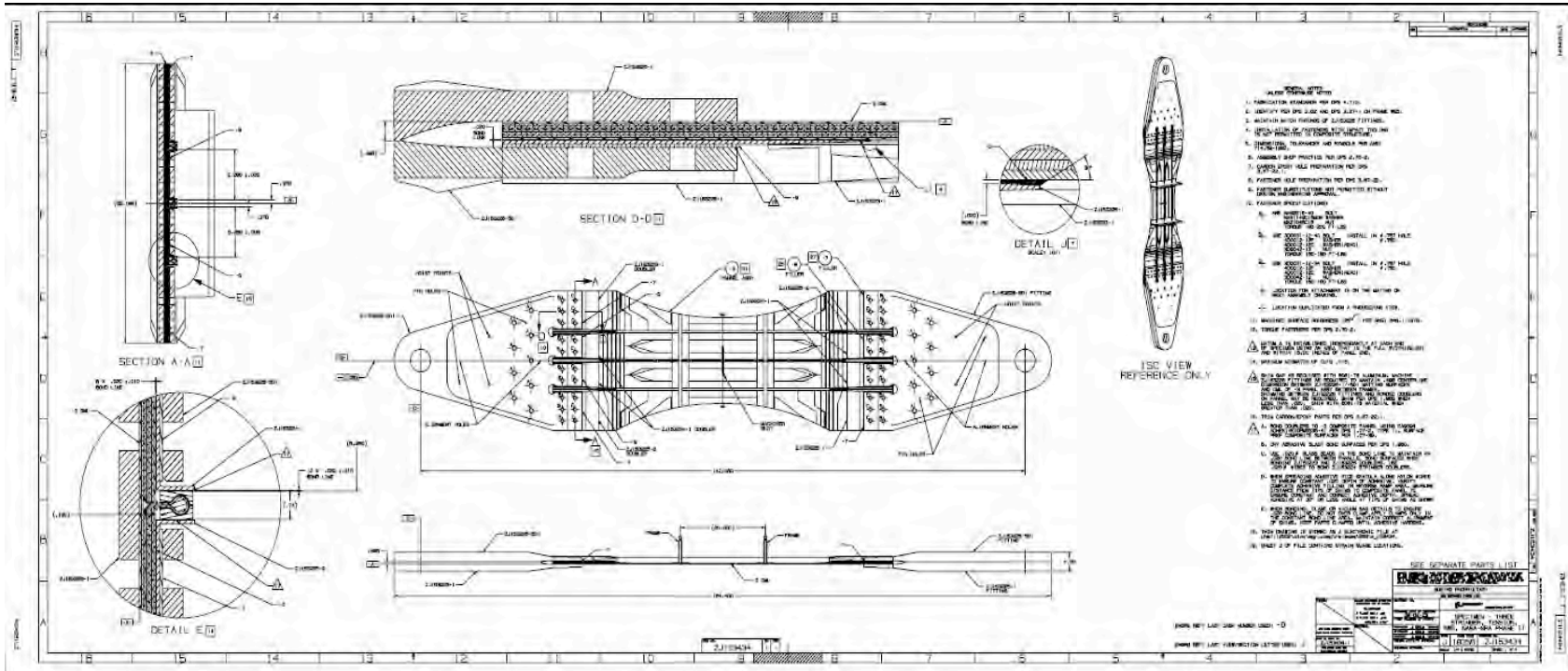


FIGURE 212. CHORDWISE TENSION PANEL DRAWING

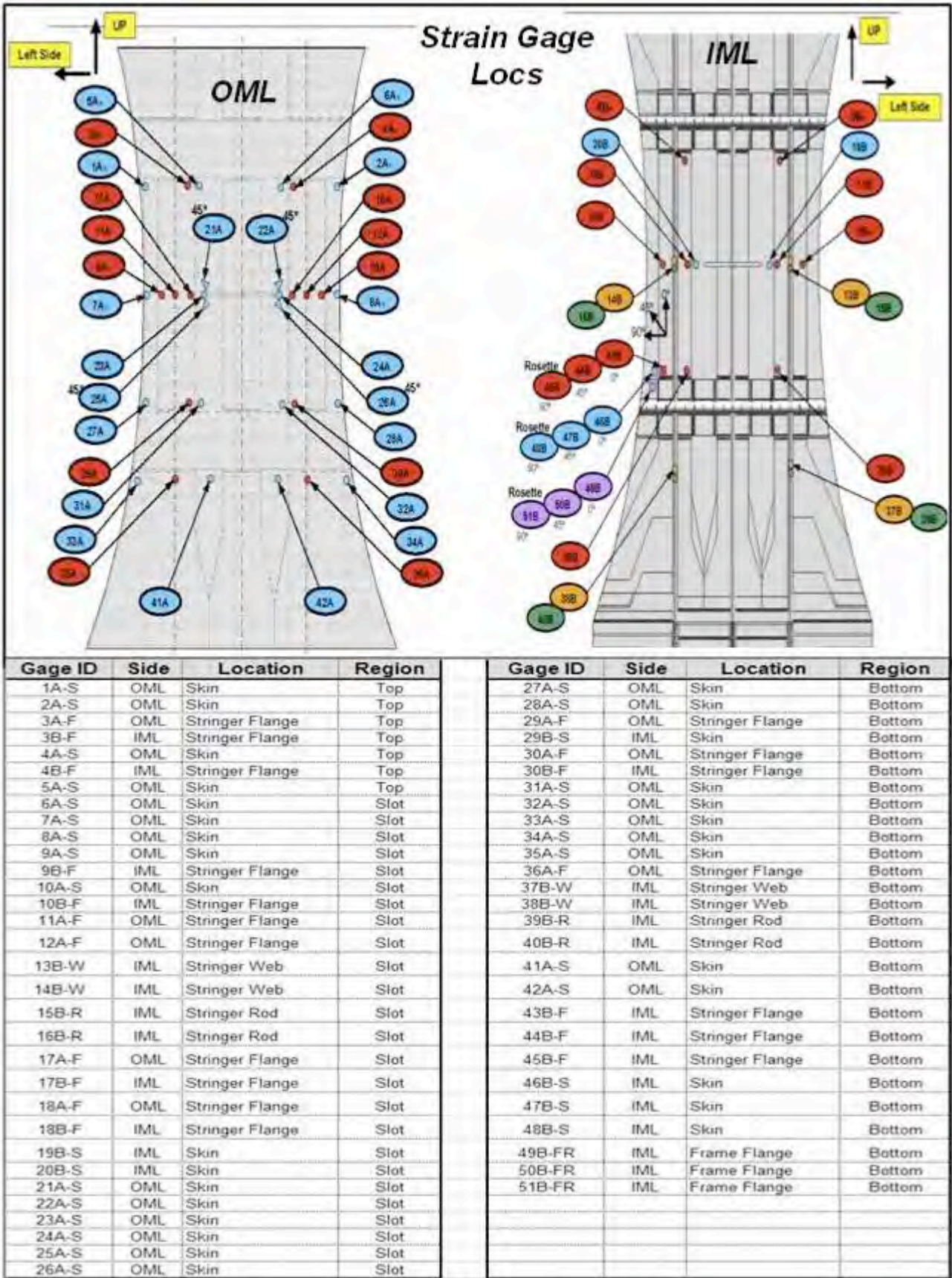


FIGURE 213. STRAIN IDENTIFICATION AND LOCATIONS

Strain Gage Data – Top Region

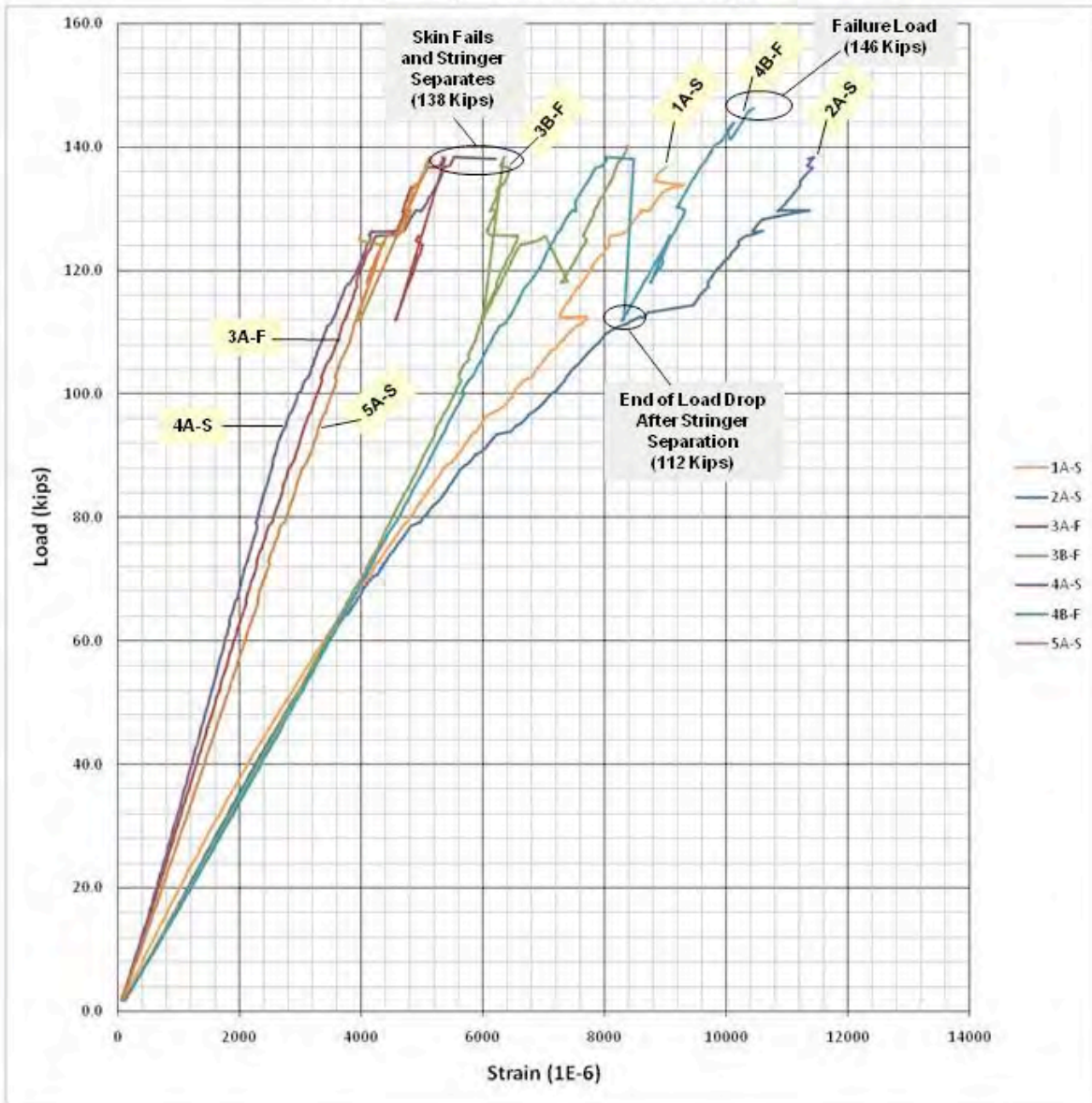


FIGURE 214. STRAIN GAGE PLOT - TOP REGION

Strain Gage Data – Slot Region 1 of 2

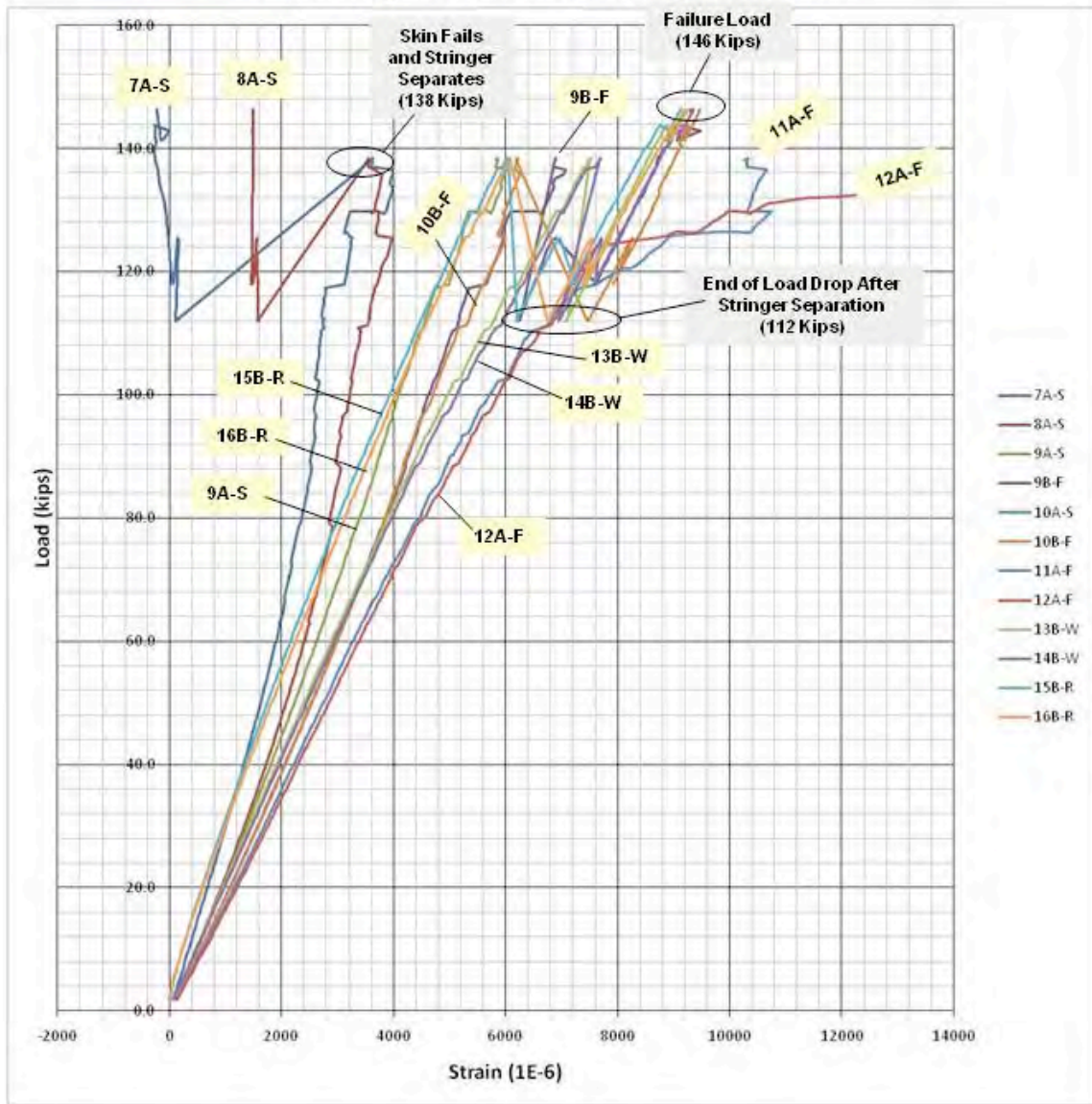


FIGURE 215. STRAIN GAGE PLOTS - SLOT REGION 1 OF 2

Strain Gage Data – Slot Region 2 of 2

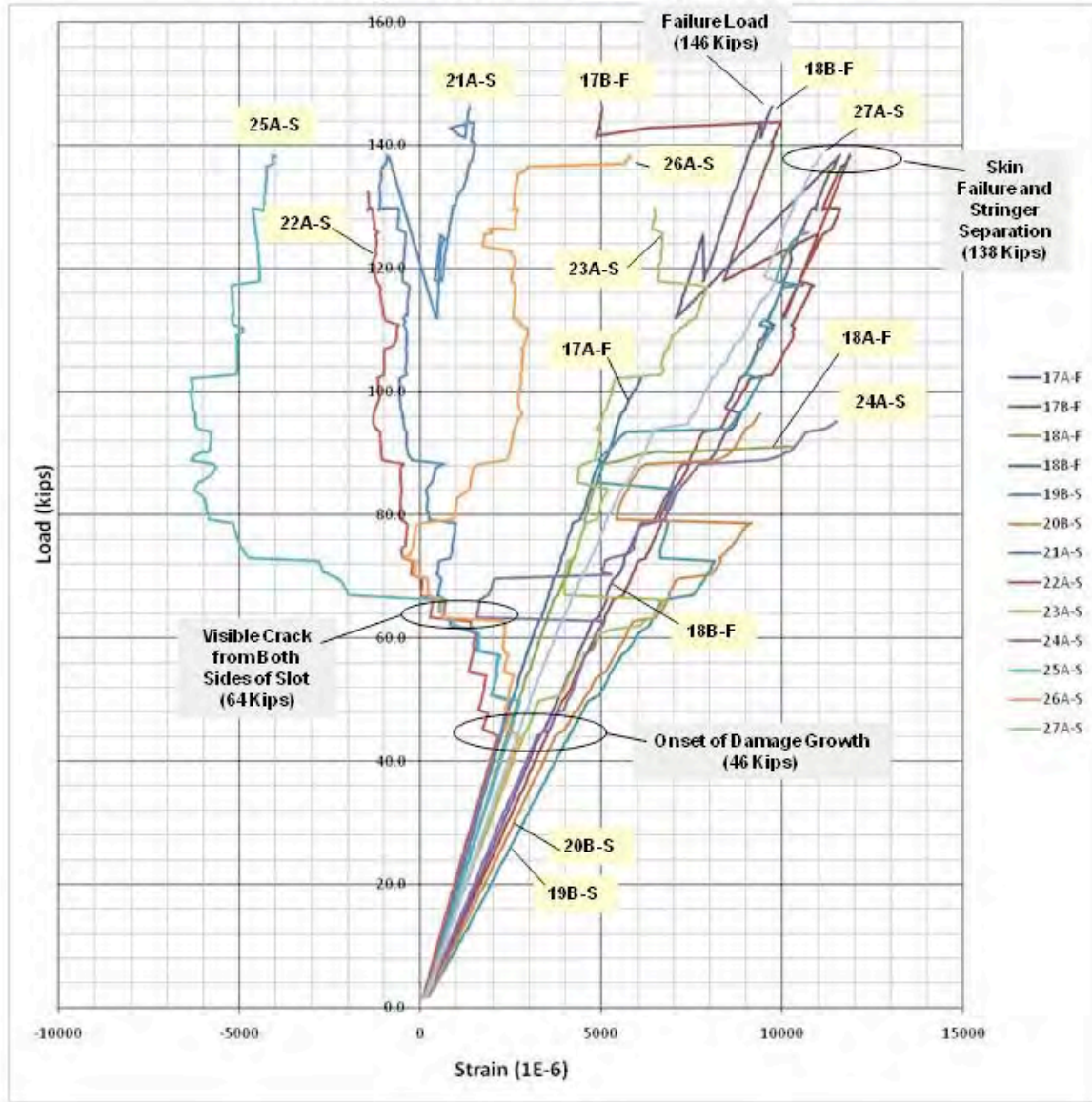


FIGURE 216. STRAIN GAGE PLOTS - SLOT REGION 2 OF 2

Strain Gage Data – Bottom Region 1 of 2

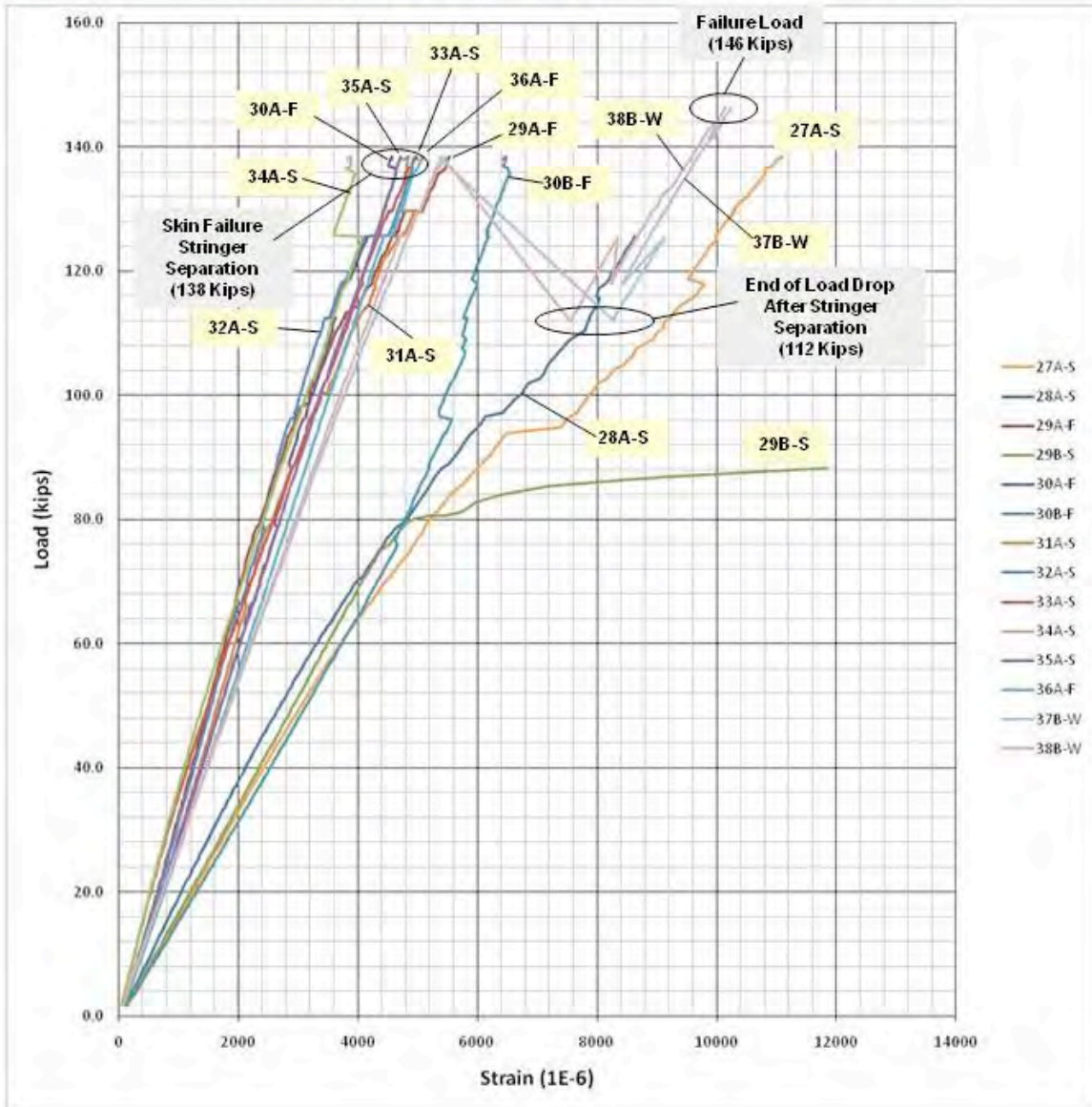


FIGURE 217. STRAIN GAGE PLOTS - BOTTOM REGION 1 OF 2

Strain Gage Data – Bottom Region 2 of 2

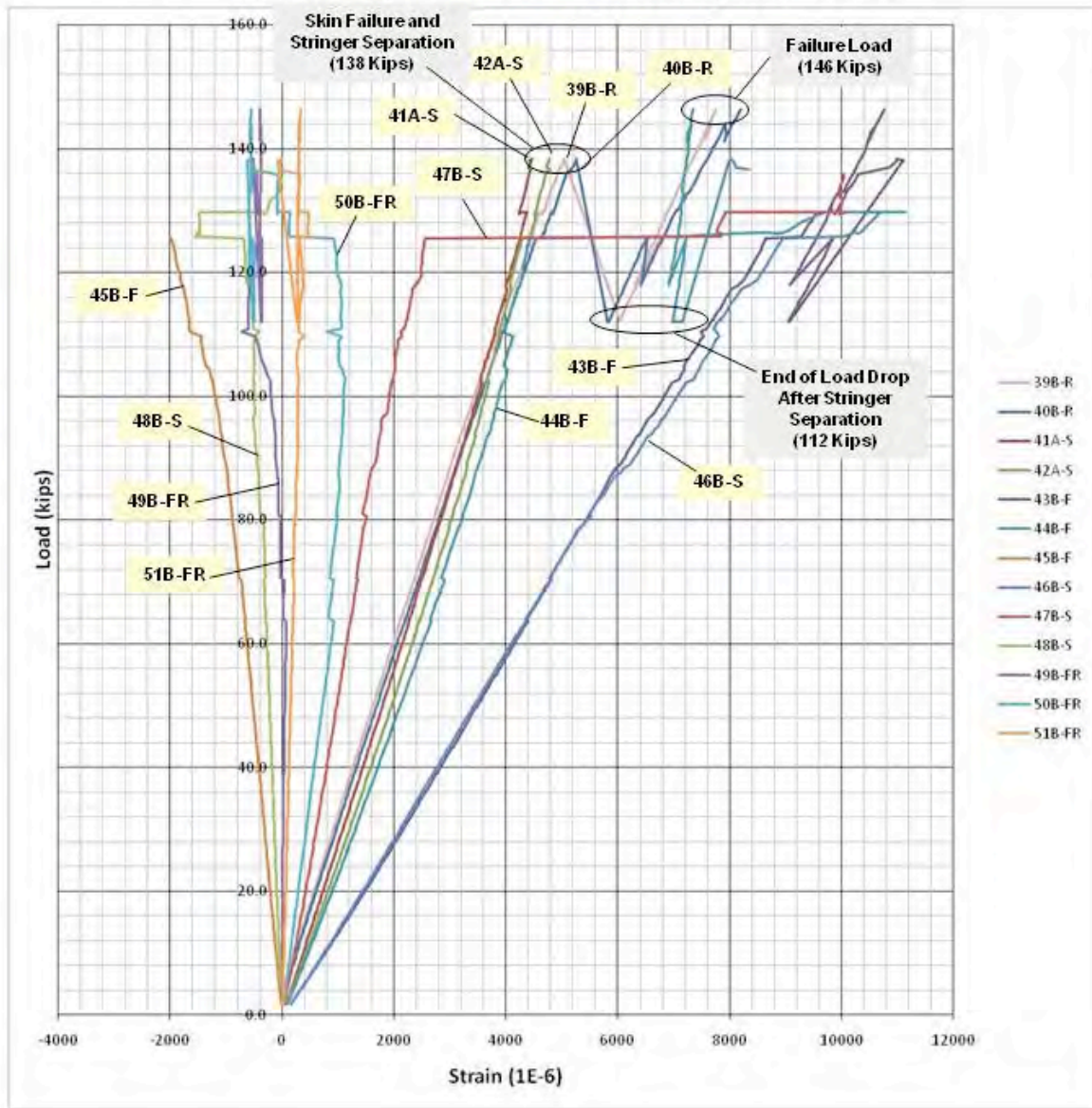
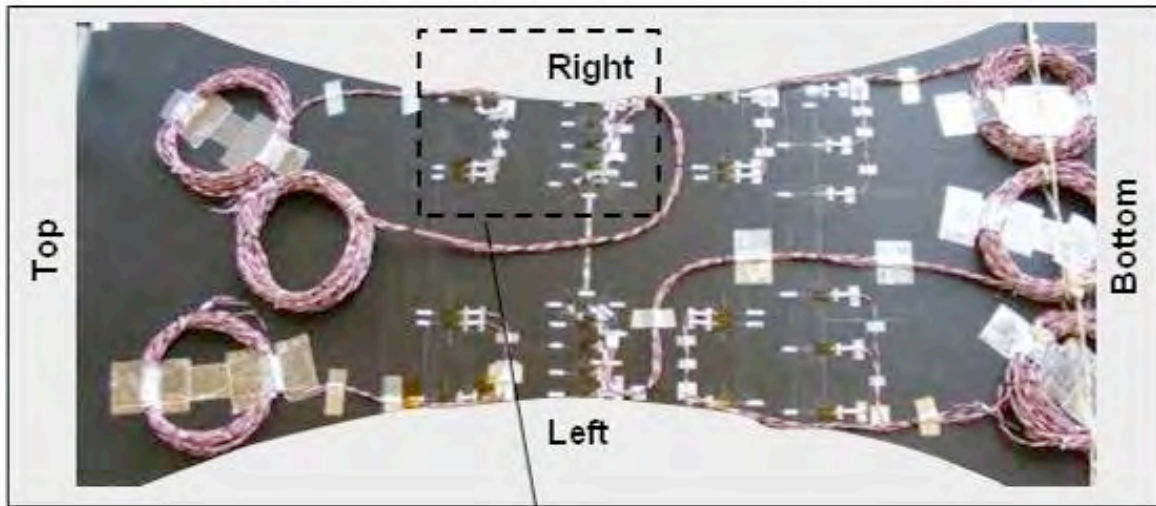
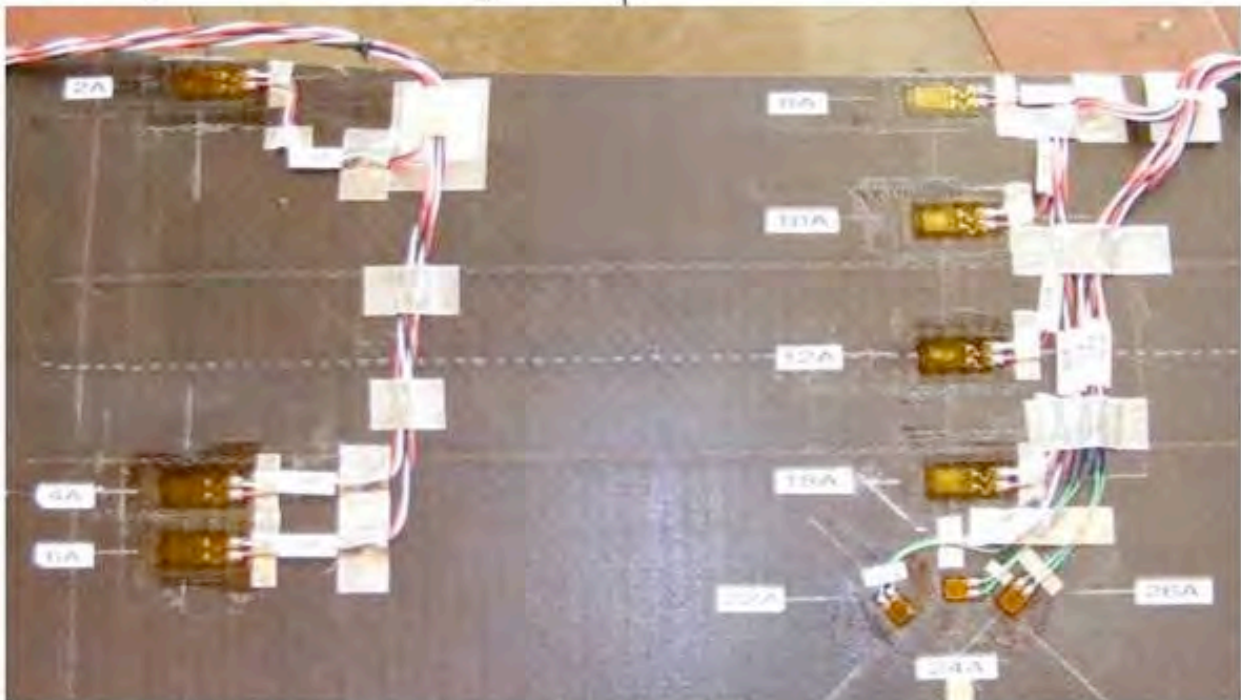


FIGURE 218. STRAIN GAGE PLOTS - BOTTOM REGION 2 OF 2

View Looking Down at OML Surface



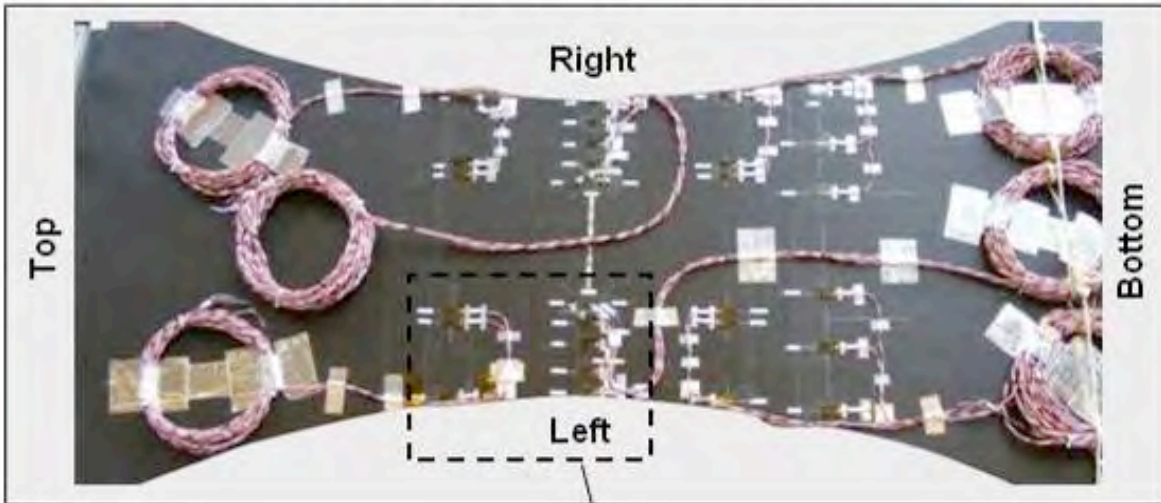
Enlarged Photo of Region



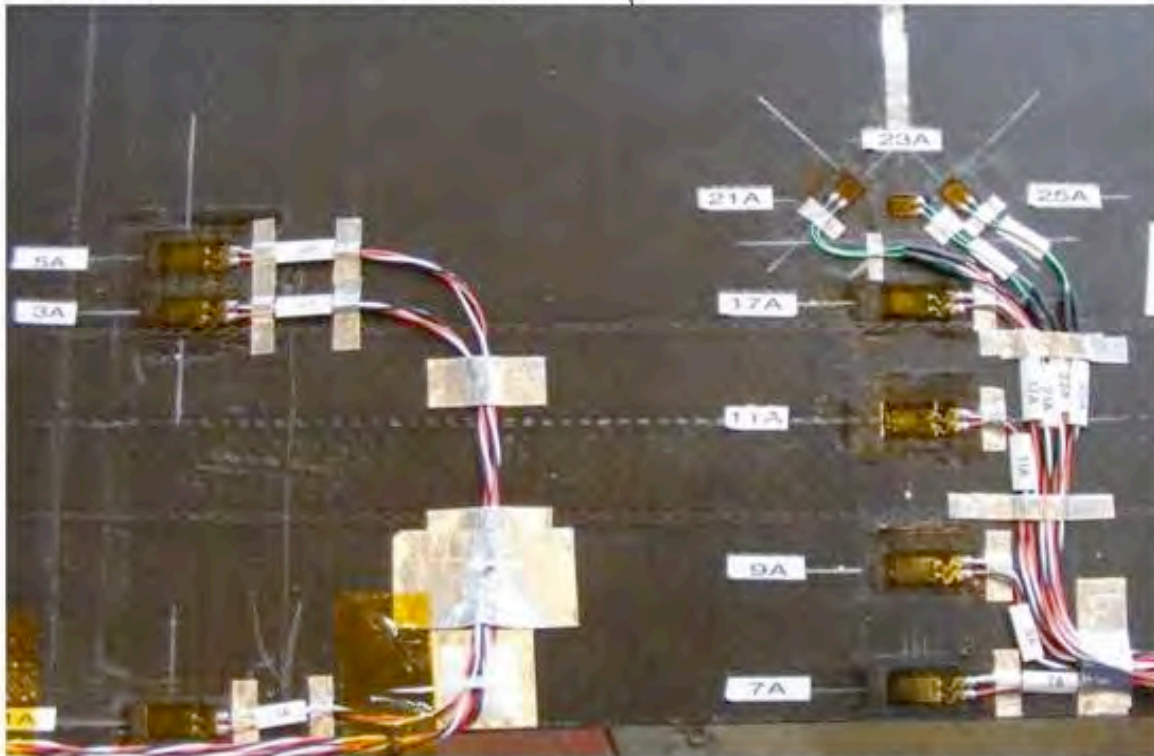
OML Strain Gage Locations

FIGURE 219. OML STRAIN GAGE PLACEMENT - 1 OF 4

View Looking Down at OML Surface



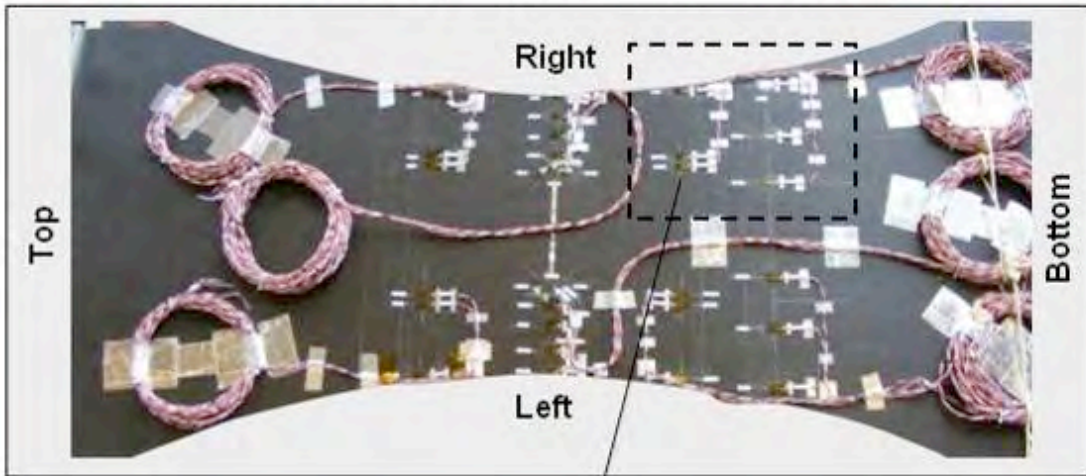
Enlarged Photo of Region



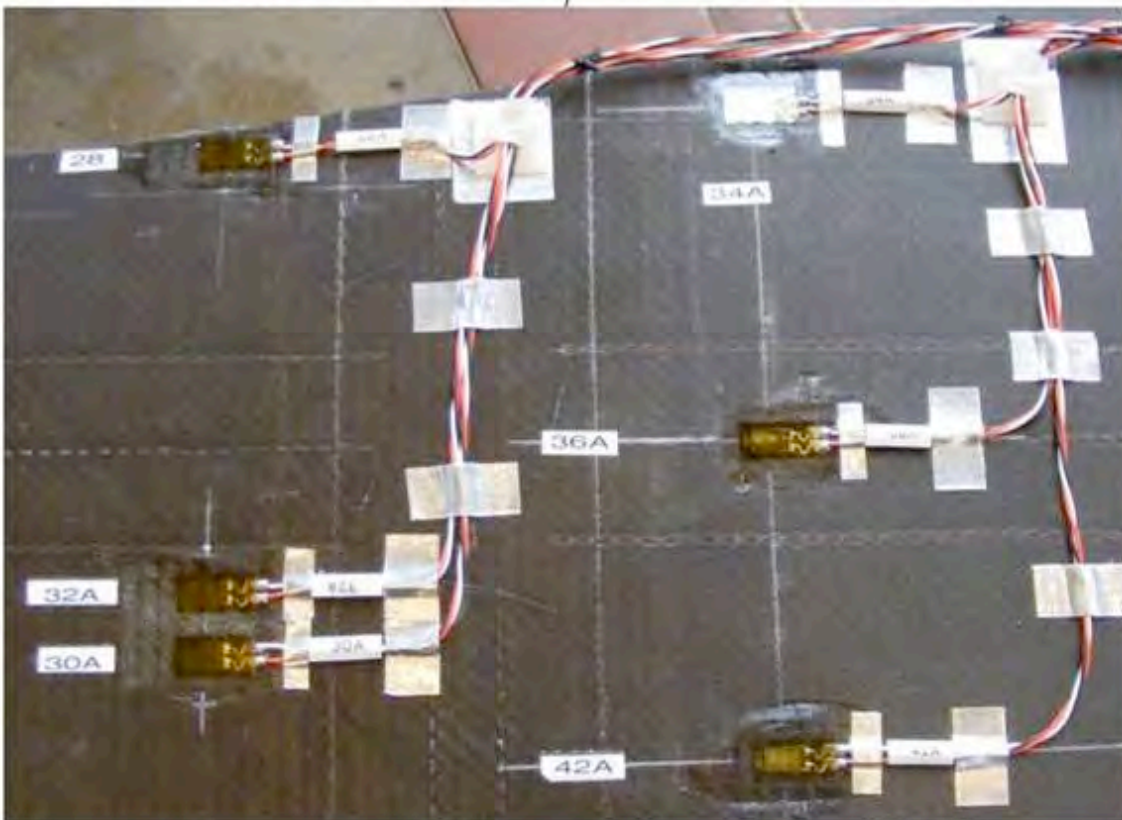
OML Strain Gage Locations

FIGURE 220. OML STRAIN GAGE PLACEMENT - 2 OF 4

View Looking Down at OML Surface



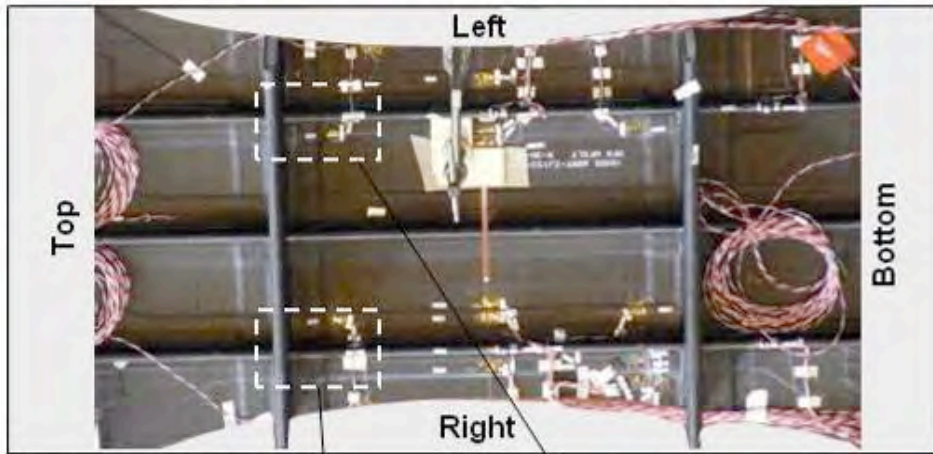
Enlarged Photo of Region



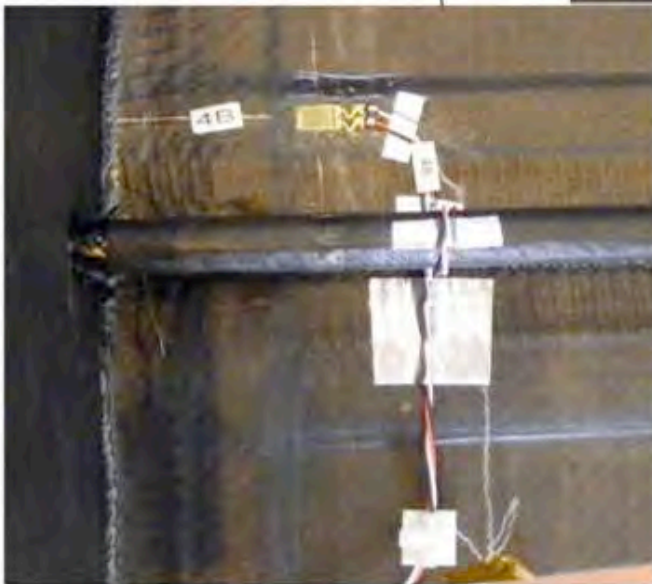
OML Strain Gage Locations

FIGURE 221. OML STRAIN GAGE PLACEMENT - 3 OF 4

View Looking Down at IML Surface



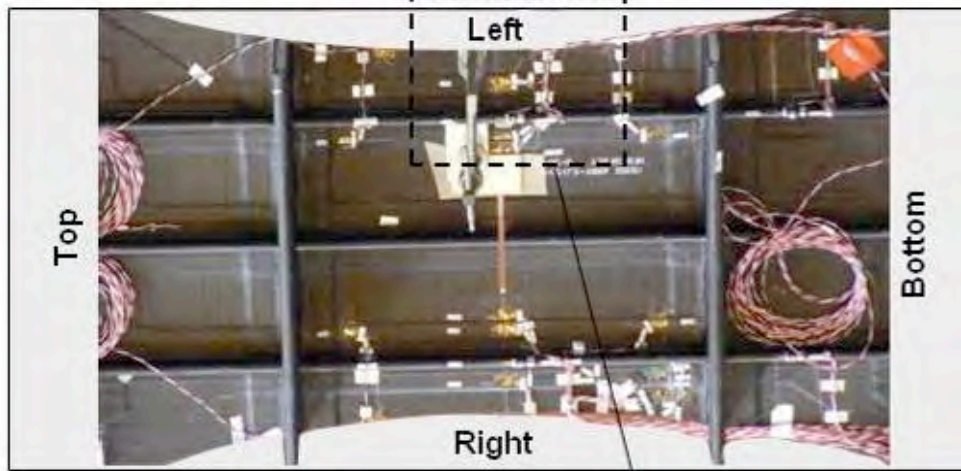
**Enlarged Photos
of Regions**



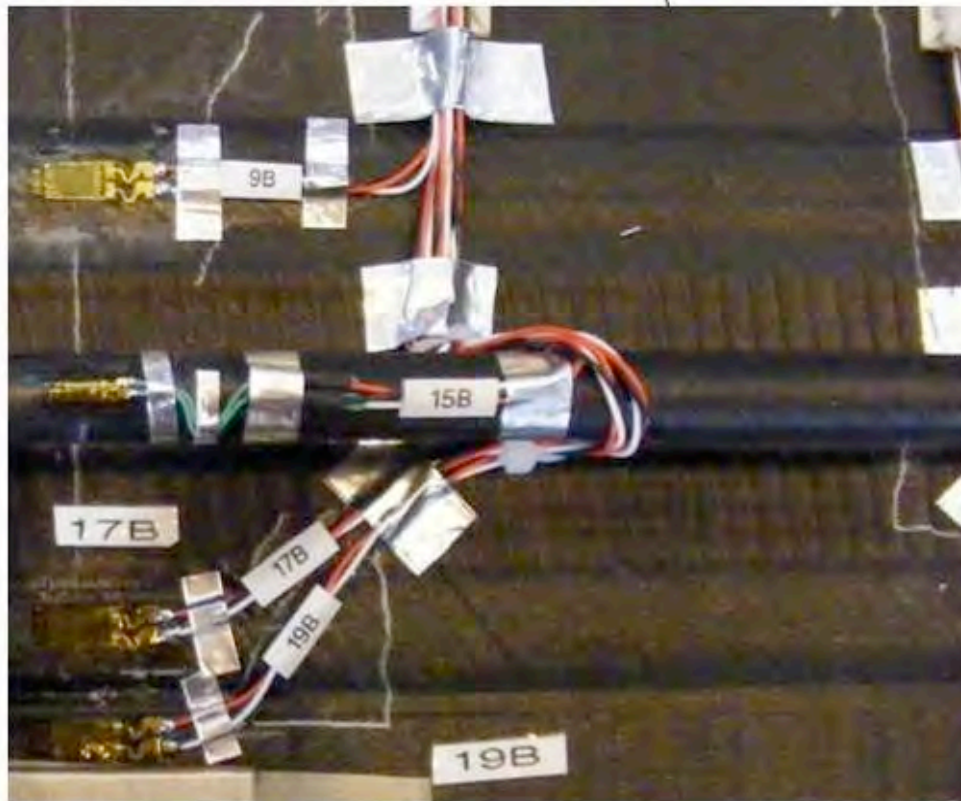
IML Strain Gage Locations

FIGURE 223. IML STRAIN GAGE PLACEMENT - 1 OF 5

View Looking Down at IML Surface



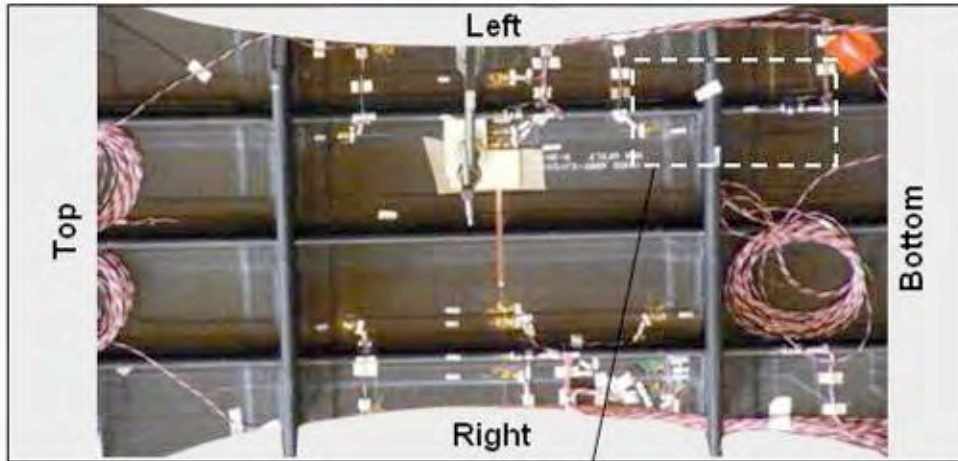
Enlarged Photo of Region



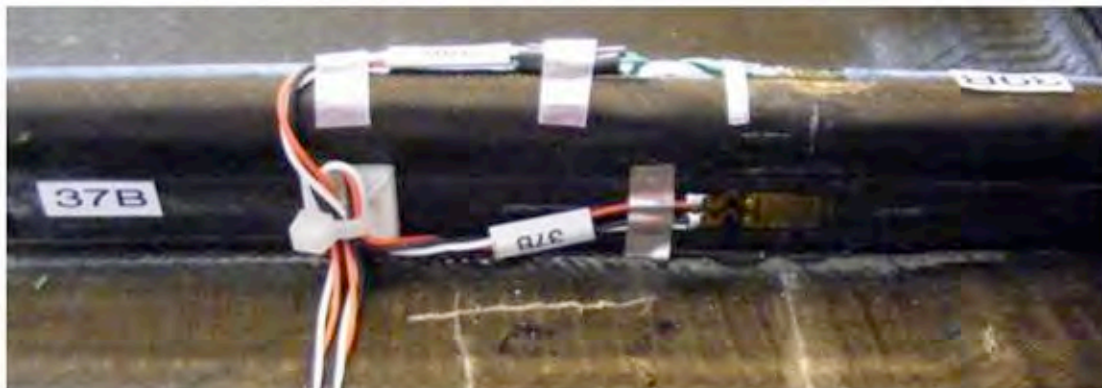
IML Strain Gage Locations

FIGURE 224. IML STRAIN GAGE PLACEMENT - 2 OF 5

View Looking Down at IML Surface



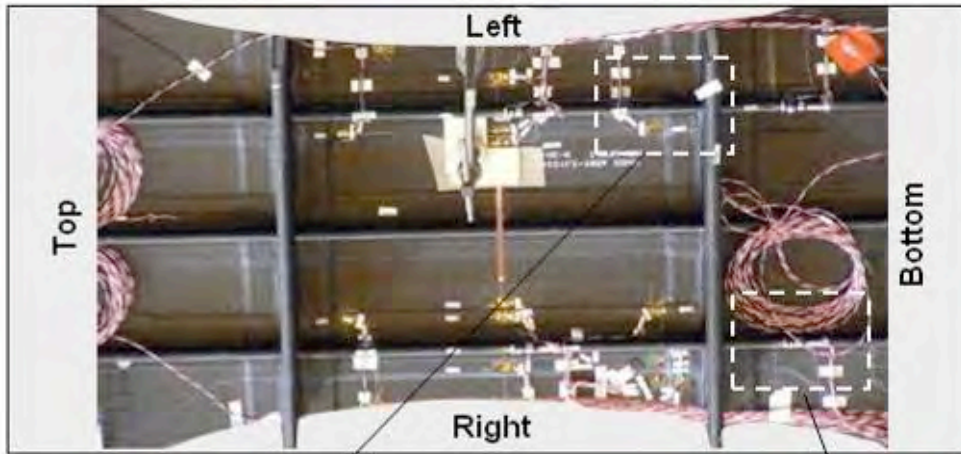
Enlarged Photo of Region



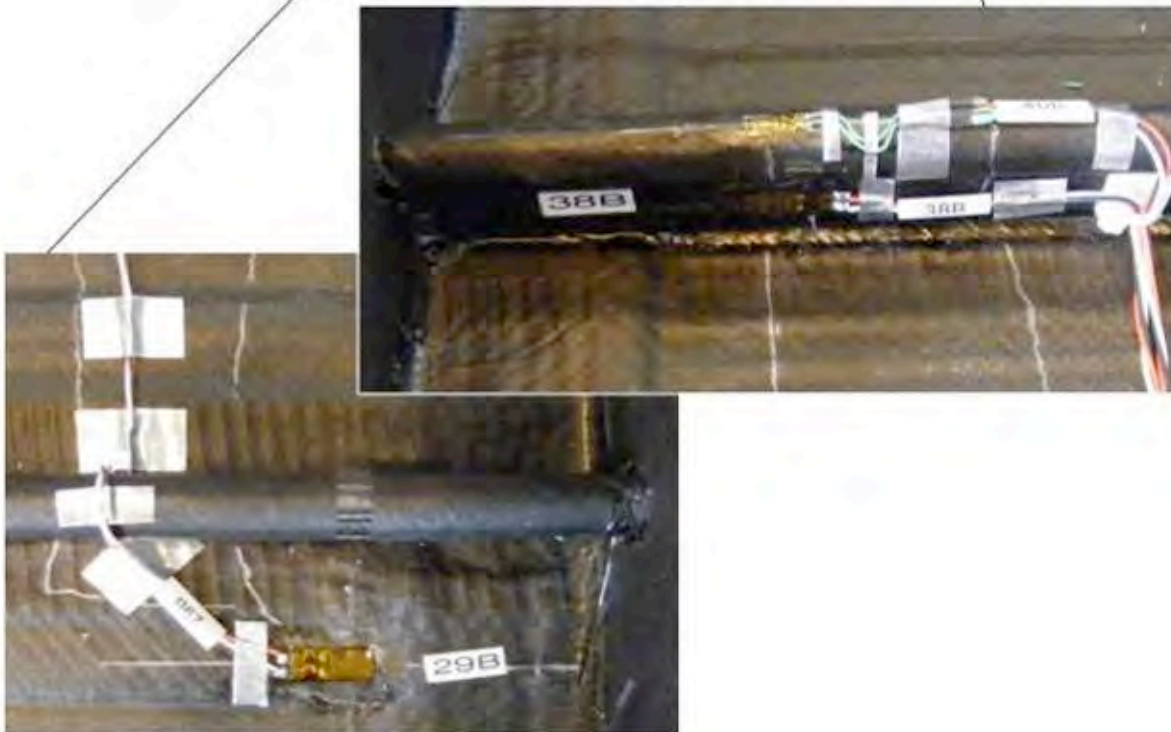
IML Strain Gage Locations

FIGURE 225. IML STRAIN GAGE PLACEMENT - 3 OF 5

View Looking Down at IML Surface



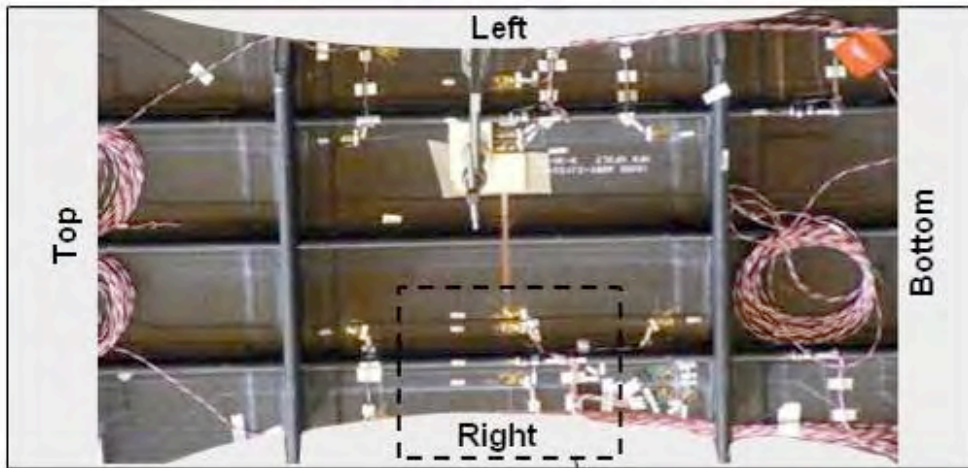
Enlarged Photos of Regions



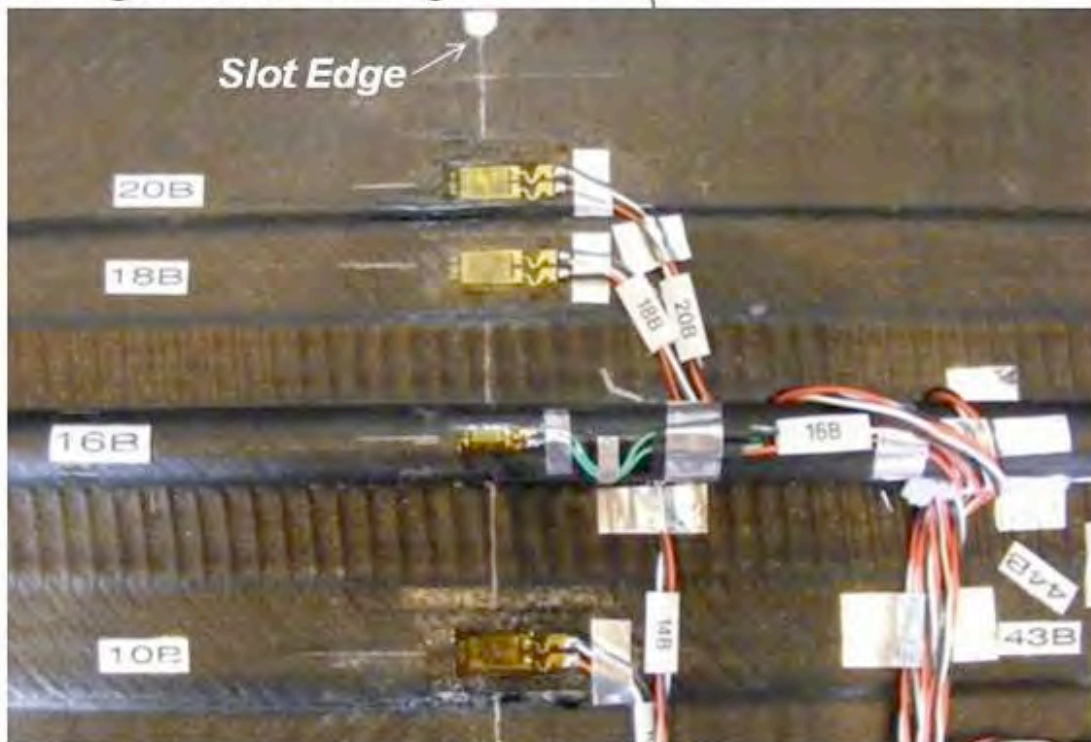
IML Strain Gage Locations

FIGURE 226. IML STRAIN GAGE PLACEMENT - 4 OF 5

View Looking Down at IML Surface



Enlarged Photo of Region



IML Strain Gage Locations

FIGURE 227. IML STRAIN GAGE PLACEMENT - 5 OF 5

APPENDIX C – SPANWISE COMPRESSION PANEL

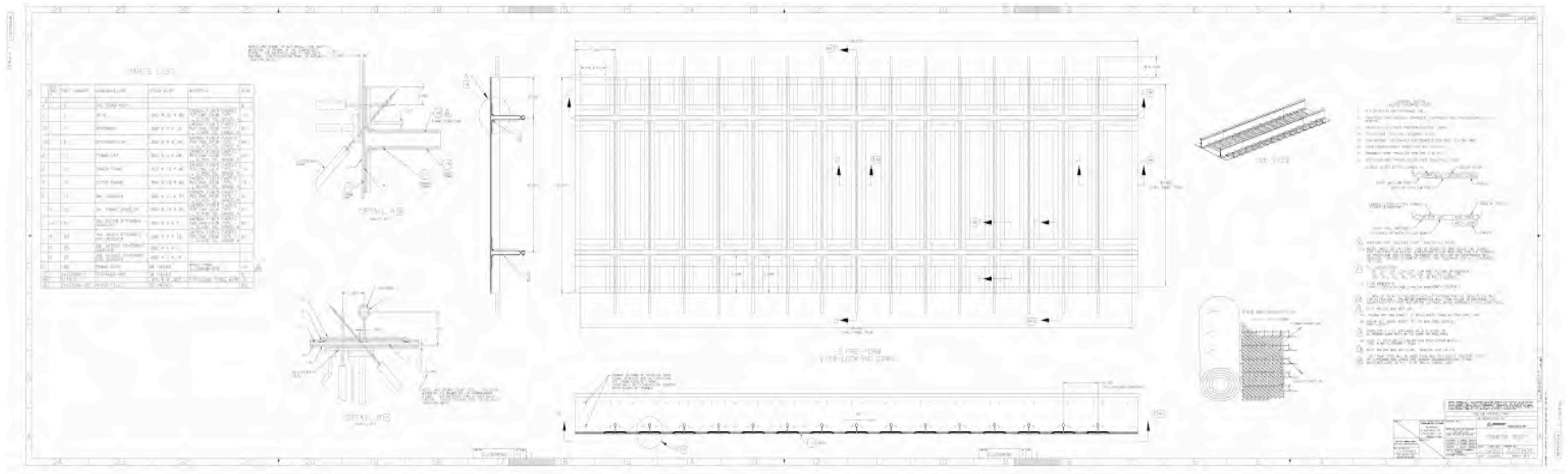


FIGURE 228. SPANWISE COMPRESSION PANEL DRAWING

APPENDIX D - HYPERSIZER USER INSTRUCTIONS

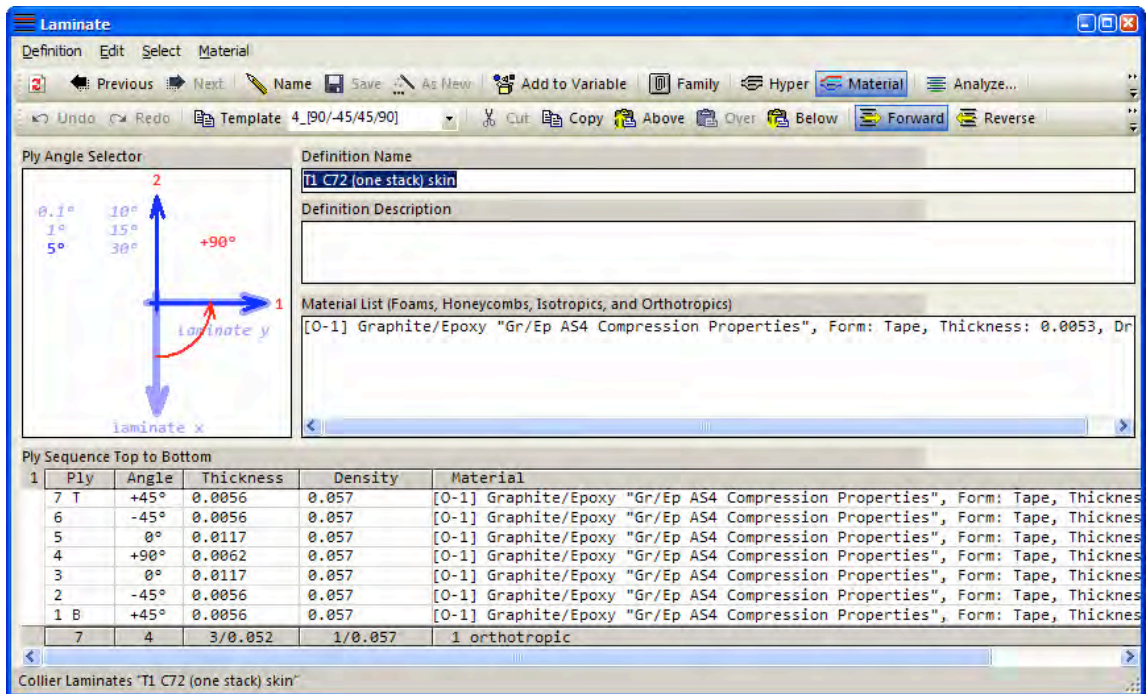
An example is used to demonstrate step-by-step processes for PRSEUS sizing. This is a seven-stringer flat panel with four frames. The stringer spacing is 6 inches and 20 inches for frame spacing. The overall dimensions of the panel are 80 inches x 42 inches (Figure 229).



FIGURE 229. SEVEN-STRINGER PRSEUS PANEL

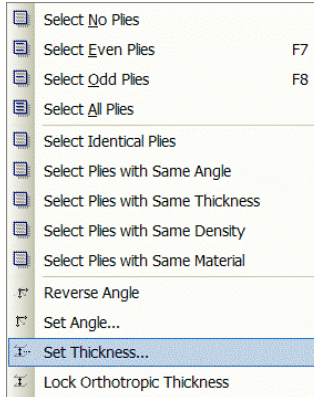
Begin by creating the primary PRSEUS laminate.

- 1a Create a $[+45/-45/0/90]_s$ laminate material named '*T1 C72 (one stack) skin*'. Apply the orthotropic material "Gr/Ep AS4 Compression Properties" to all plies in the laminate.

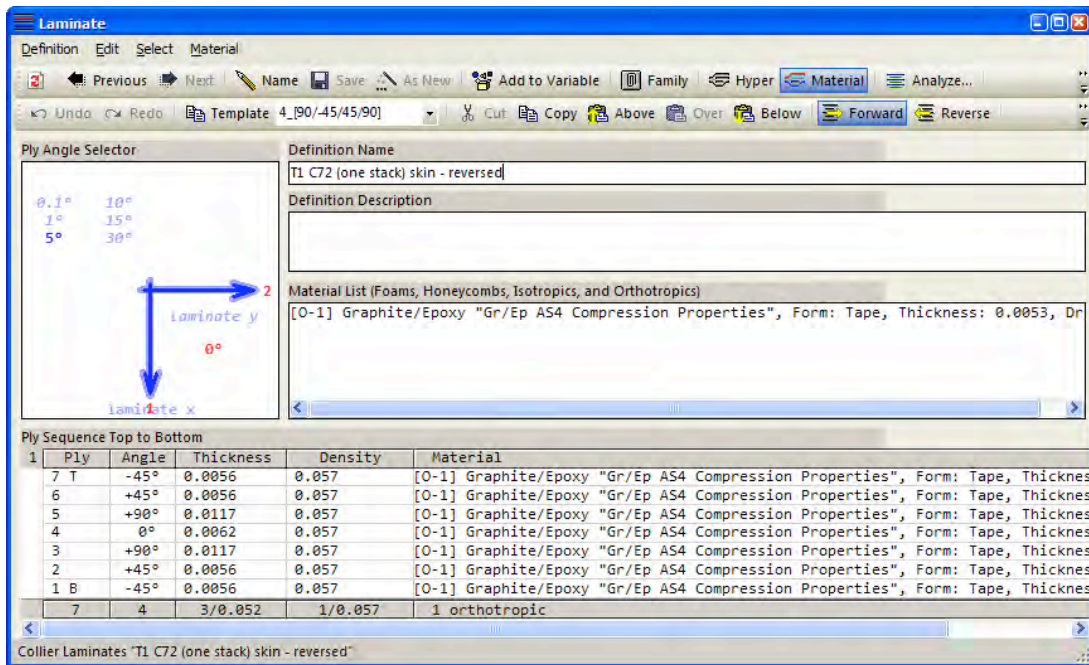


Notice when you apply the material to the plies, the material thickness (0.0053 in) and density (0.057 lb/in³) are automatically populated with the values stored for the material.

- 1b To modify the thicknesses right click on the individual plies and select '*Set Thickness*' then enter the corrected thickness. Repeat the process until the ply thicknesses are stored as shown in the laminate above.

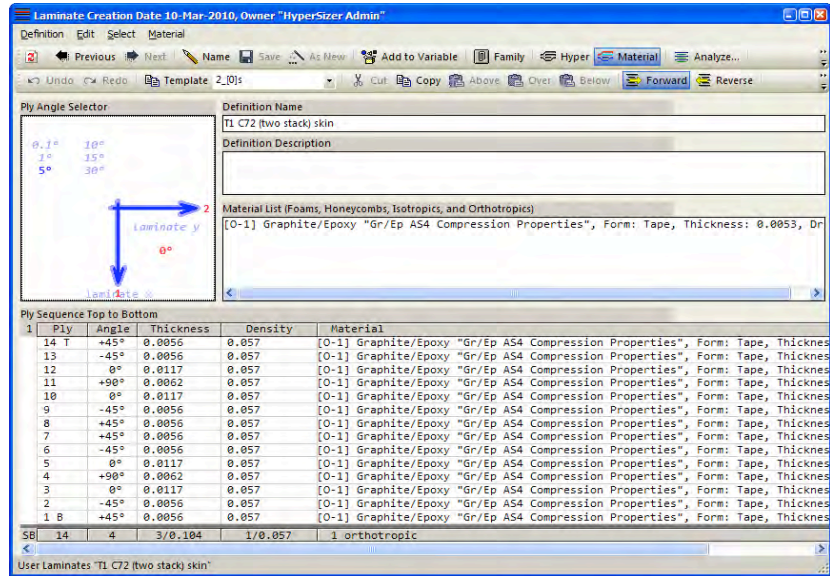


- 2a. Now create a $[-45/+45/90/_0]_s$ laminate material named '*T1 C72 (one stack) skin - reversed*'. Apply the same orthotropic material "Gr/Ep AS4 Compression Properties" to all plies in the laminate.



- 2b. Again modify the thicknesses by right clicking on the individual plies and select '*Set Thickness*' then enter the corrected thickness. Repeat the process until the ply thicknesses are stored as shown in the laminate above.

- 3a. Now create a $[+45/-45/0/90/0/-45/+45]_s$ laminate material named '**T1 C72 (two stack) skin**'. Apply the same orthotropic material "Gr/Ep AS4 Compression Properties" to all plies in the laminate.



- 3b. Again modify the thicknesses by right clicking on the individual plies and select '*Set Thickness*' then enter the corrected thickness. Repeat the process until the ply thicknesses are stored as shown in the laminate above.

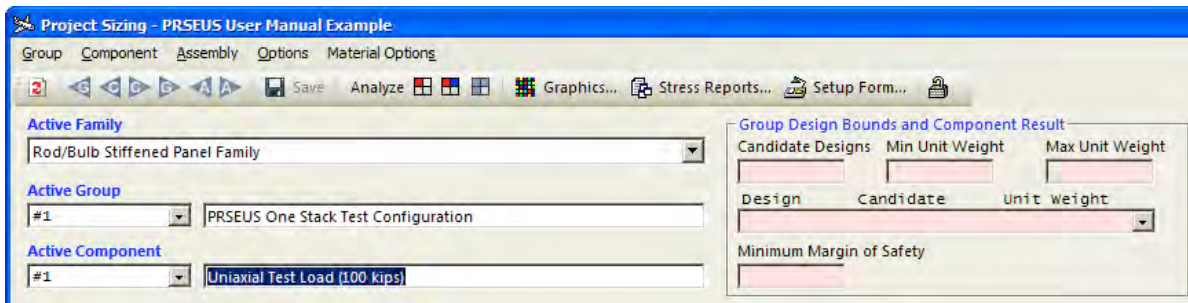
There should be 3 new laminates in your database, these laminates are listed below:

Laminate Name	Layup
T1 C72 (one stack) skin	$[+45/-45/0/_90]_s$
T1 C72 (one stack) skin - reversed	$[-45/+45/90/_0]_s$
T1 C72 (two stack) skin	$[+45/-45/0/90/0/-45/+45]_s$

D.1 Creating the Workspace

We will optimize the PRSEUS panels in the workspace environment using user-specified loads. First we should create a workspace and select the available materials.

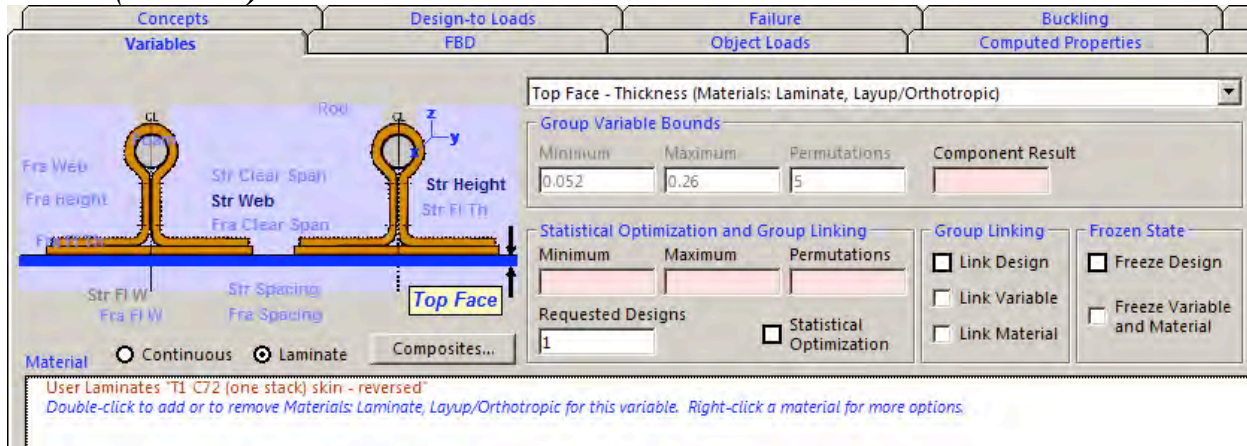
- 4a. Create a new workspace named '*PRSEUS User Manual Example*'
- 4b. Expand the database and right click on **Available Materials** and select the three laminates we just created to make them available for use in the new workspace.
- 4c. Now open the sizing form and browse to the '*Rod/Bulb Stiffened Panel Family*'. Create a new group named '*PRSEUS One Stack Test Configuration*'.
- 4d. Add a component to the group and name the component '*Uniaxial Test Load (100 kips)*'. The group/component definition in the sizing form should be the same as shown below:



D.2 Assigning Sizing Variables

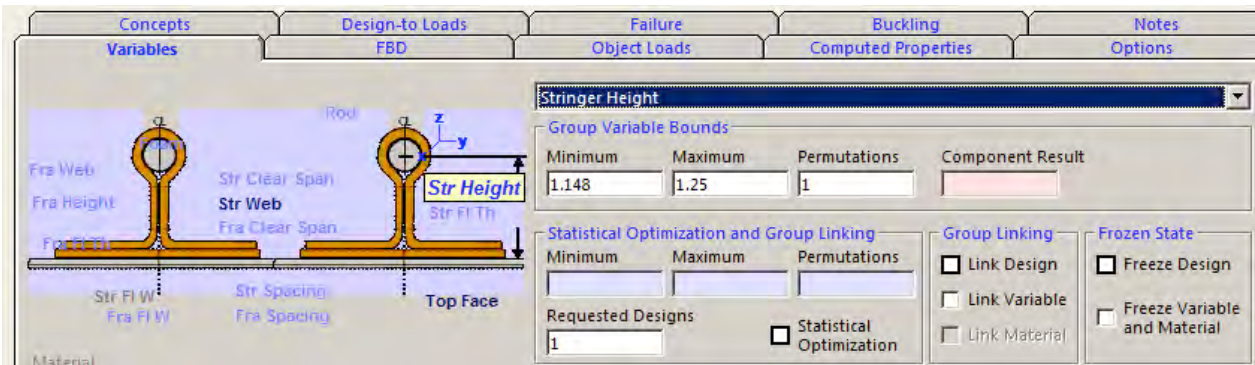
The PRSEUS panel concept has many variables to define. We will now assign materials, thicknesses and widths to all panel objects.

- 5a. Start with the top facesheet, select the '*laminate*' radial button and assign the '*T1 C72 (one stack) skin - reversed*' laminate to this variable.



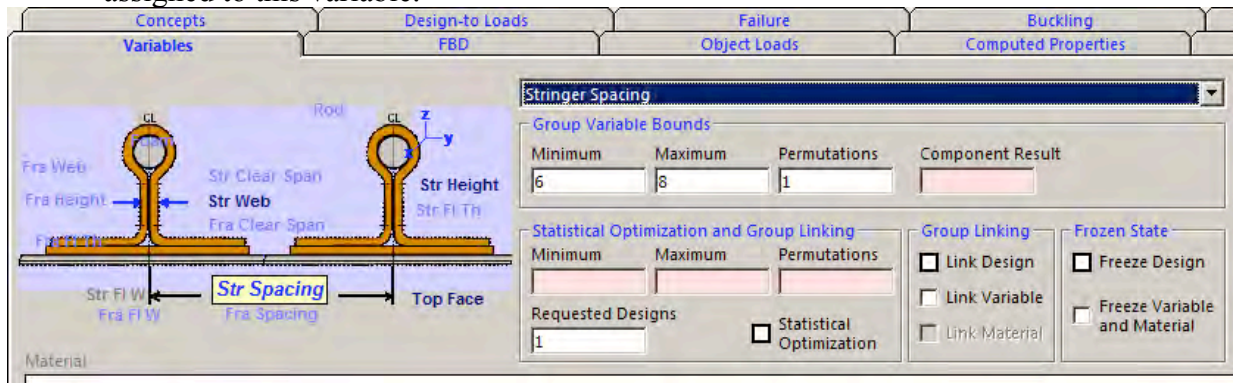
Note: The PRSEUS test panel drawings are configured with facesheet 0 degree fiber direction parallel to frames (transverse panel direction), which is 90 degrees different than of HyperSizer's reference, therefore the '*reversed*' panel T1 C72 laminate configuration is applied to this variable.

- 5b. Next enter the Stringer Height as 1.148in and enter 1 permutation. No material is assigned to this variable

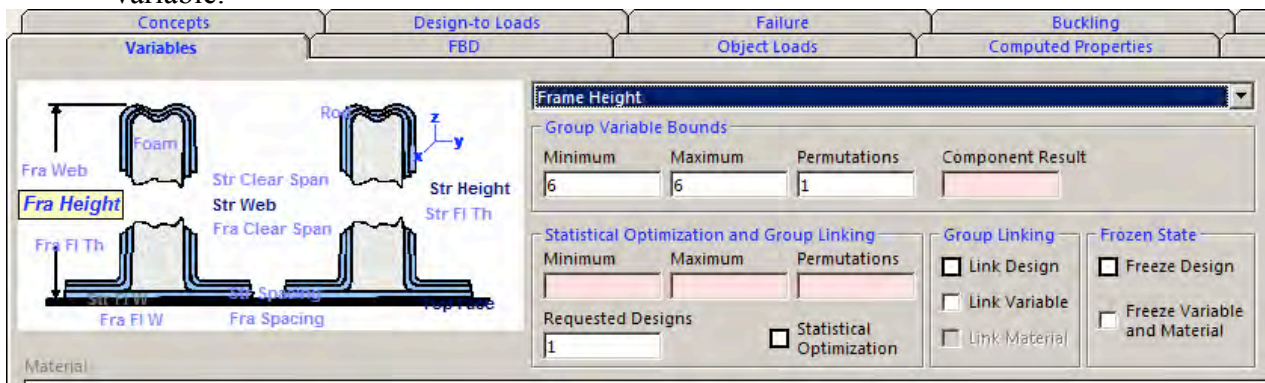


Note: The stringer height dimension in HyperSizer slightly different from the callout in original drawing. Remember in HyperSizer the stringer height dimension is measured from the IML of the facesheet to the center of the stiffener. In the original drawing the stiffener height is measured from the OML of the facesheet to the tip of the stiffener, which includes the thickness of the facesheet.

5c. Continue by assigning the stiffener spacing as 6in with one permutation. No material is assigned to this variable.

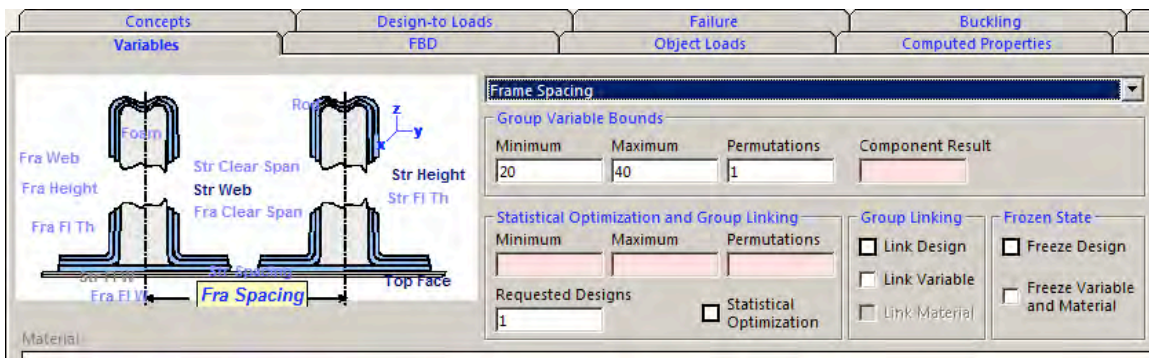


5d. Assign the Frame Height as 6in with one permutation. No material is assigned to this variable.



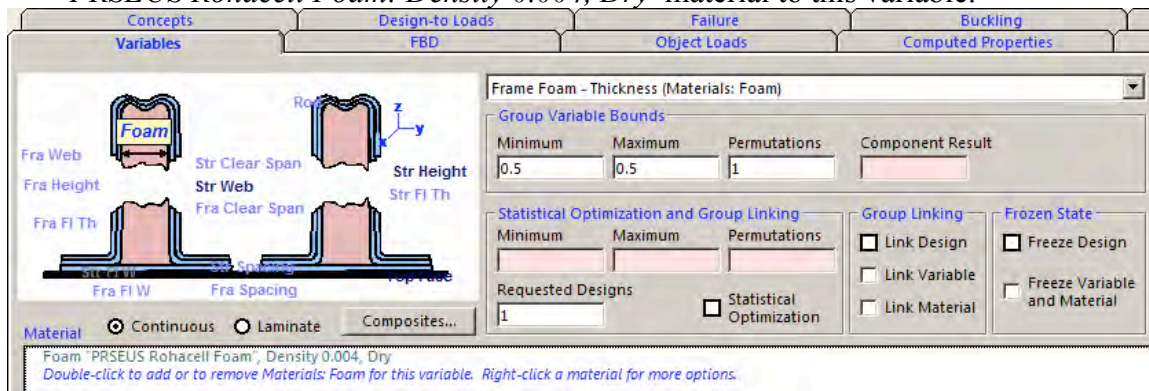
Note: The Frame Height variable is defined from the top facesheet to the top of the frame and includes the frame flange and frame cap thicknesses.

5e. Now define the frame spacing as 20 inches with one permutation. No material is assigned to this variable.

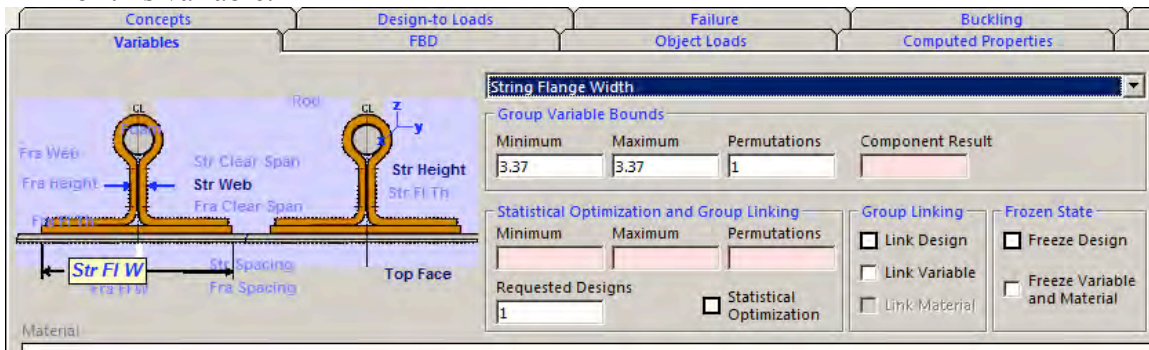


If the 'Frame Span Buckling failure methods are active, the Frame spacing defines the X-Buckling span for the panel.

5f. Now define the Frame Foam Thickness as 0.5in with one permutation. Also assign the 'PRSEUS Rohacell Foam: Density 0.004, Dry' material to this variable.

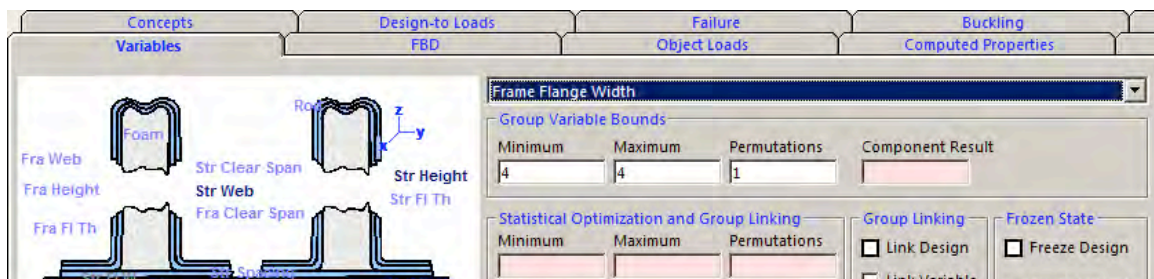


5g. Assign a Stringer Flange Width of 3.37in with one permutation. No material is defined for this variable.



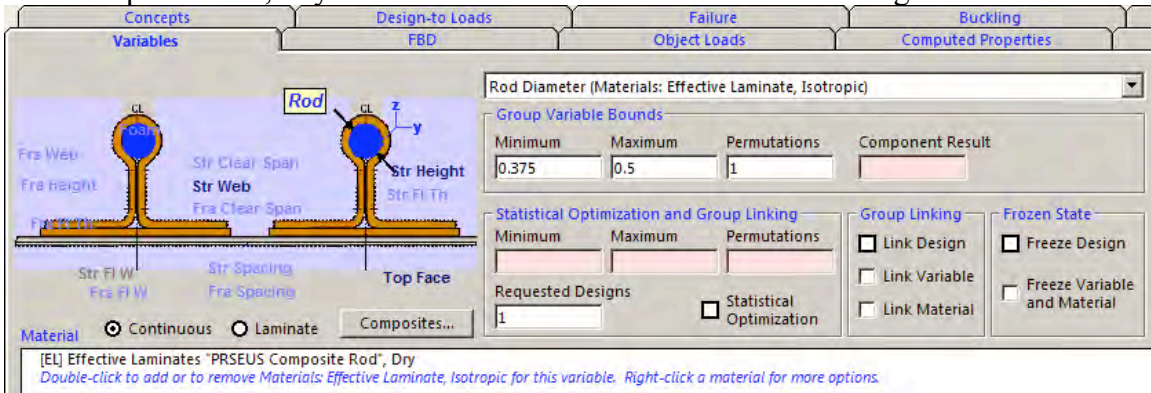
Note: The Stringer Flange Thickness is a dependant variable. Since the stringer web is defined with a HyperLaminate, the flange thickness is dependent on the stringer laminate definition.

5h. Define the Frame Flange Width as 4in with one permutation. No material is defined for this variable.



Note: The Frame Flange Thickness is a dependant variable. Since the Frame web is defined with a HyperLaminate, the flange thickness is dependent on the web material.

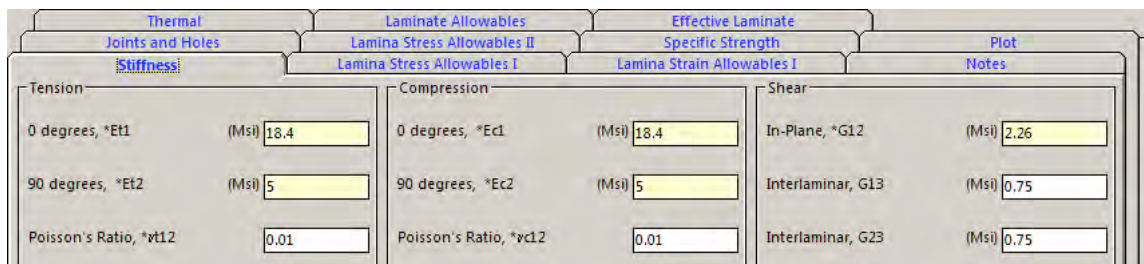
5i. Now define the Stiffening Rod material and Rod diameter. Assign the "PRSEUS Composite Rod, Dry" Effective laminate material to the stiffening rod.



Since the rod is defined as an orthotropic (continuous) material that represents a laminate with a set ply percentage, the diameter may be defined as a range like an isotropic material.

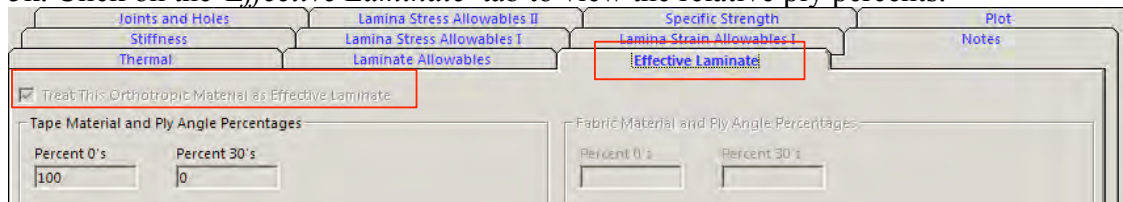
5j. Enter a diameter of 0.375in with one permutation.

To view the properties of this material, right click on the material in the available materials window and select 'Edit This Material...', the orthotropic material form will appear. The stiffness values entered for the rod material are shown below:



Notice the high stiffness in the 1 direction relative to the 2 direction.

5k. Click on the 'Effective Laminate' tab to view the relative ply percents.

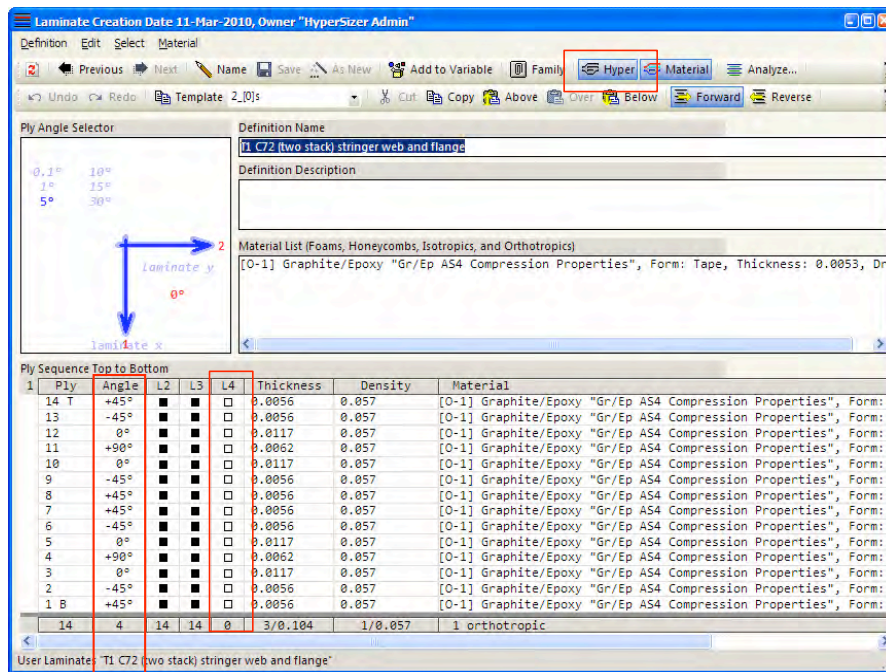


Notice the 'Treat this Orthotropic Material as Effective Laminate' option is toggled on. This option allows the user to treat this material as continuous and apply a user defined thickness variable.

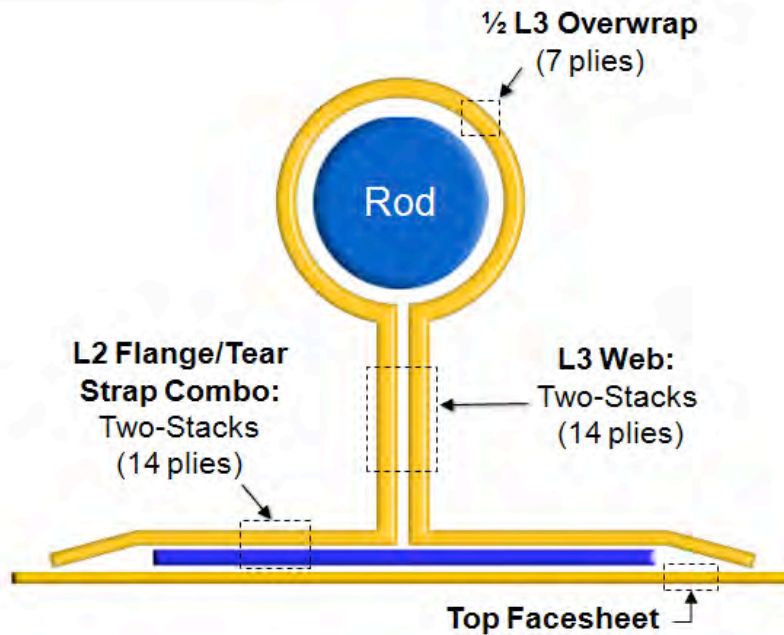
D.3 HyperLaminate for Stringer Web and Flange Material/Thickness

Now we will create a HyperLaminate based on the '*T1 C72 (two stack) skin*' laminate and assign it to the Stringer Web - Thickness variable.

- 6a. Open the '*T1 C72 (two stack) skin*' laminate, we will create a "HyperLaminate" based on the T1C72 stack.
- 6b. Press the '*Hyper*' button to activate this material as a HyperLaminate and expose the L2, L3 and L4 objects.
- 6c. Turn off all of the L4 objects and change the name of the laminate to '*T1 C72 (two stack) stringer web and flange*'.
- 6d. Press the "*Save As New*" button to save this as a new laminate definition.



Note: The objects L2 and L3 represent the Stringer Flange and Stringer Web objects respectively.



In this case the web (L3) consists of 14 plies which is two T1C72 stacks. The stringer flange is made up of a 7 ply tear strap, one T1C72 stack, added to 7 plies from the Stringer Web, a second T1C72 stack that is the left and right half of the flange.

This means when defining the HyperLaminate for the stringer web the flange object (L2) is also made up of 14 plies or two T1C72 stacks, which includes both the tear strap and stringer flange. So when turning objects on and off for the stringer web and flange laminate, all fourteen plies should be turned on for objects L2 and L3.

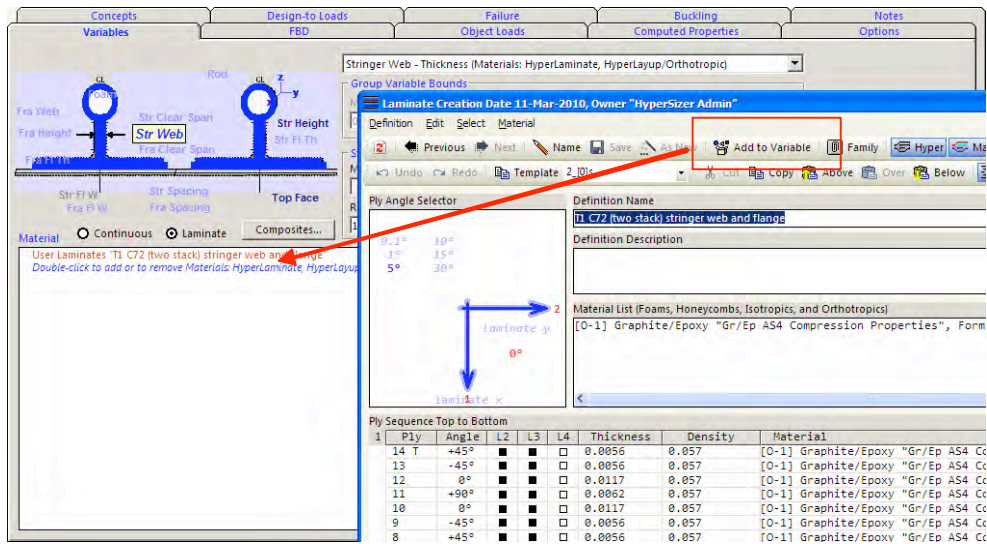
The L4 object is not currently being used for the PRSEUS concept. The stiffener rod overwrap is always assumed to be 1/2 the stringer web laminate.

- 6e. We will now add this material into our workspace available materials and then add this material into the '*Stringer Web - Thickness*' sizing variable.

Tip: A quick way to do this is to leave the Laminate Form open and return to the Sizing form. Then change the variable to the "Stringer Web - Thickness" variable and select the 'Laminate' radial option.

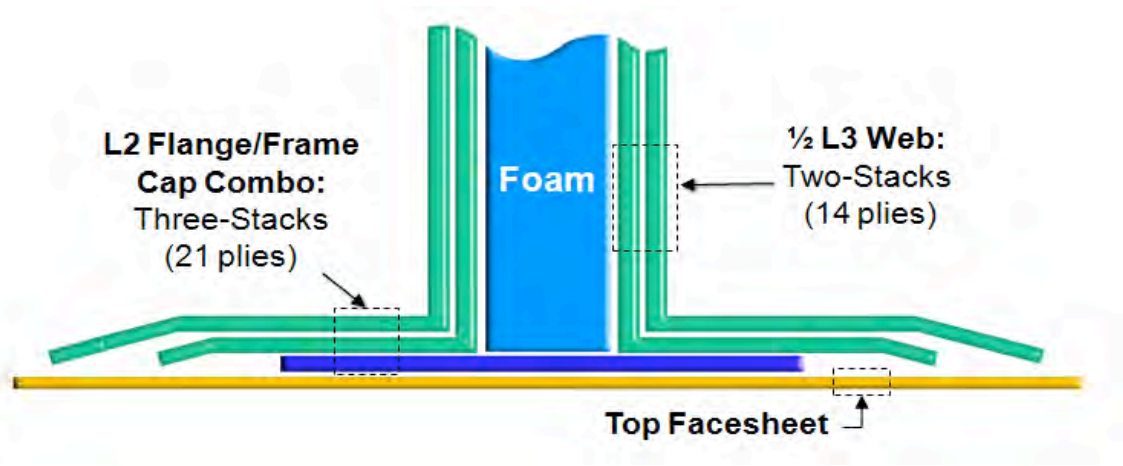
Now with the sizing form open return to the laminate form and press the '*Add to Variable*' button.

Pressing this button will add the material to the workspace available materials and add the material to the active variable on the sizing form in one step.



D.4 HyperLaminate for Frame Web and Flange Material/Thickness

Now we will define the Hyperlaminate for the Frame Web. The laminate for the frame web is the entire laminate representing the left and right halves of the frame (on either side of the foam).

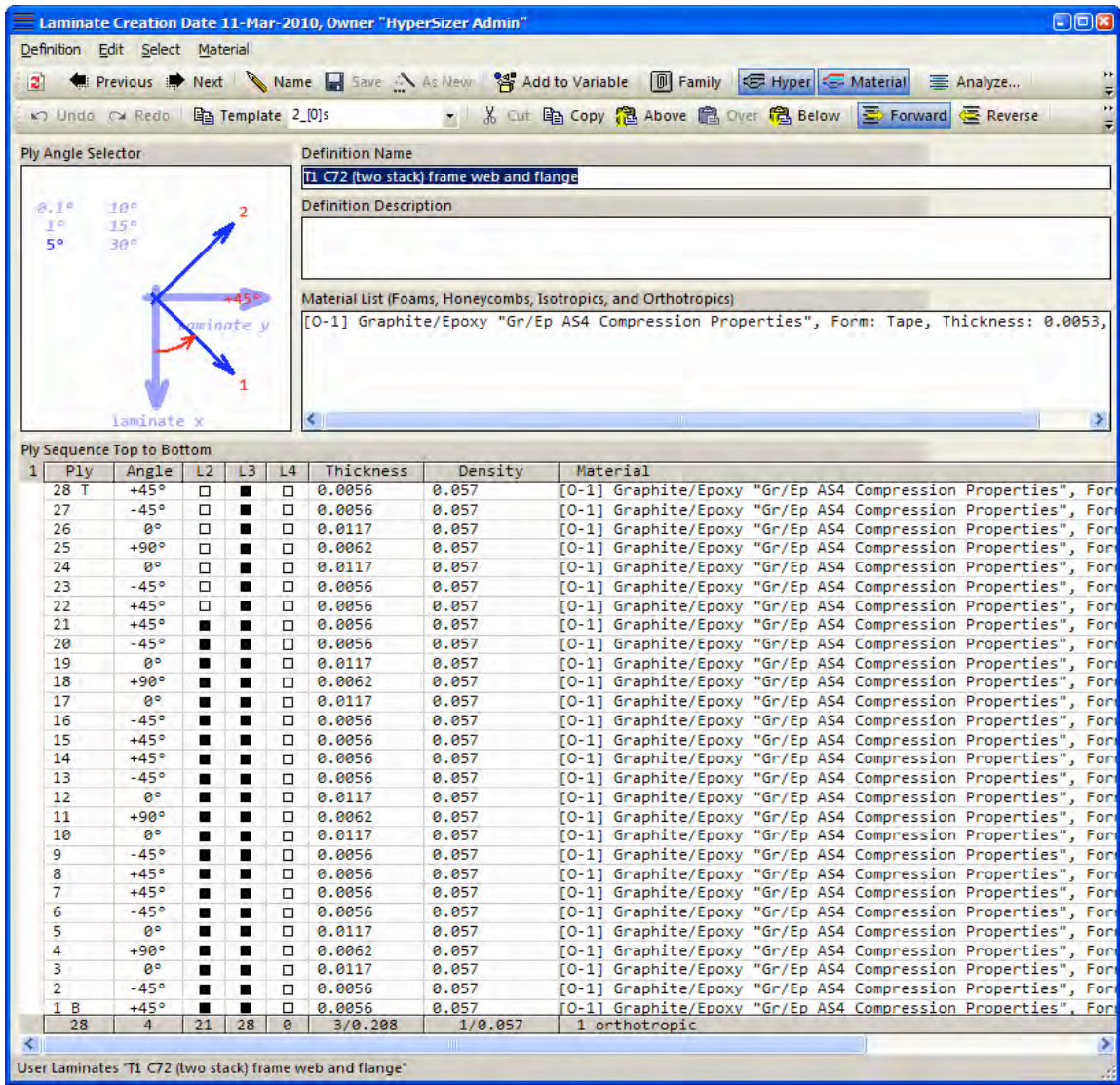


For the test setup, there are a total of 28 plies in the frame web (L2), 14 plies on either side of the foam. The flange (L2) is made up of one T1C72 stack (7 ply) frame cap bonded to two T1C72 stacks (14 plies) from the frame web, which totals 21 plies for the flange.

6f. Now to create the laminate for the frame web and flange, open with the laminate previously created for the stringer web, **'T1 C72 (two stack) stringer web and flange'**

6g. Copy the 14 plies and paste them over the 14th ply in the stack to create a 28 ply symmetric laminate.

6h. Now, turn off the L2 (Flange) object for the first 7 plies as shown below.



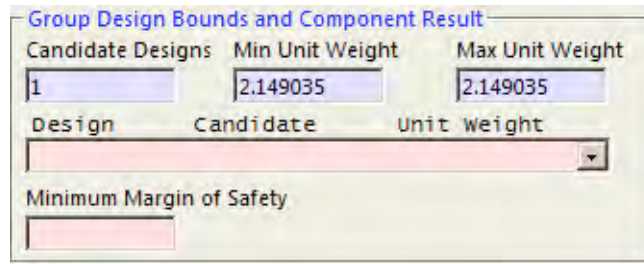
This leaves 21 plies for the flange object L2 (7 ply frame cap + 14 plies from the divided frame web) and 28 plies for the frame web object L3. Once again, the L4 object is not used for the PRSEUS panel.

- 6i. Change the name of the laminate to **'T1 C72 (two stack) frame web and flange'** and press the **"Save As New"** button.

Add this laminate to the Frame Web - Thickness sizing variable and be sure to select "Laminate" rather than "Continuous" as the material type.

- 6j. After all variables have been specified, press the **'Save'** button on the sizing form.

Note: If all materials and variables were entered the following in the Group Design Bounds. There will be a single candidate design with a unit weight of 2.149 psf.



If this is not what is shown in the Group Design Bounds and Component Result window, please review the variables entered for this group.

D.5 Mechanical Loads and Panel Dimensions

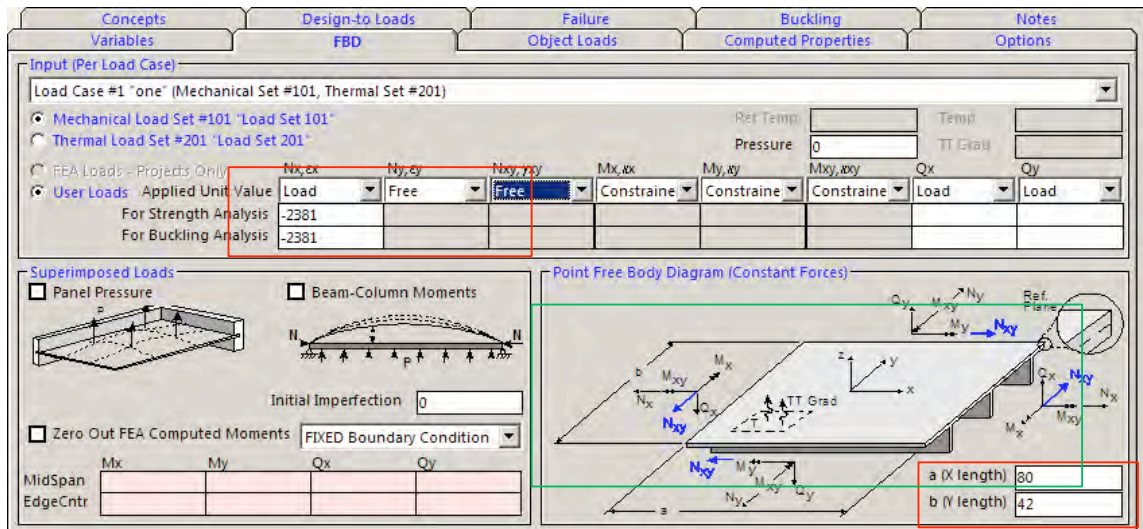
We will now enter the design-to loads and dimensions on the 'FBD' tab.

- 7a. For the a and b buckling length, enter the test panel overall dimensions of 80 inches and 42 inches respectively.

As a starting point, we want to enter a total panel compressive load of 100 kips. As a unit load, this is entered as $N_x = (\text{total load}) / (\text{width}) = (-100,000\text{lb}) / (42\text{in}) = -2381 \text{ lb/in}$.

- 7b. Enter -2381 for N_x .

- 7c. Then set N_y and N_{xy} to "Free" and leave M_x , M_y and M_{xy} as constrained.

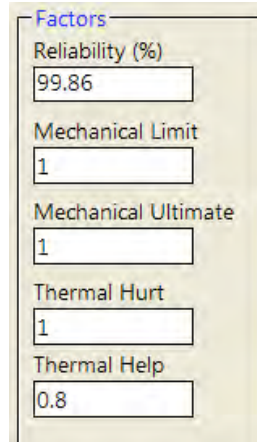


Setting N_y and N_{xy} to 'Free' allows the panel to expand . This eliminates Poisson's effect and no panel N_y loads will to be developed.

Note: The image portrayed in the "Point Free Body Diagram" frame is not specific to the Rod-Stiffened Panel Family. It is a generic picture that depicts the sign convention for overall panel loads. For example N_x is in the direction of the stringers and N_y is perpendicular to the stringers (in the case of PRSEUS, N_y is the overall panel load in the Frame direction).

Since this is a test analysis rather than a sizing, we want to set the Limit and Ultimate factors to 1.0 to ensure the design-to loads are not scaled up by any mechanical factor.

7d. Set the Mechanical Limit and Mechanical Ultimate factors to 1.0 on the Design-to Loads tab.



D.6 Active Failure Modes

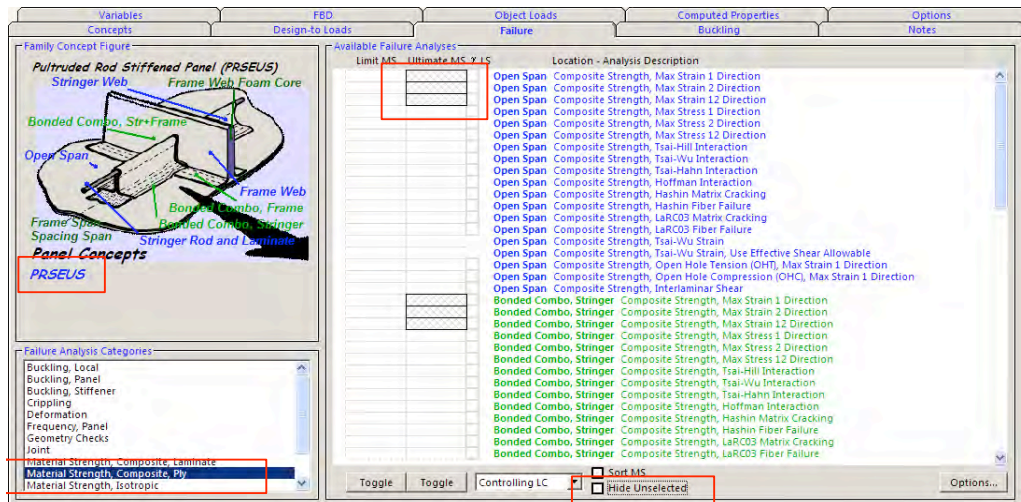
We will now specify the active failure methods in the Failure Tab. By activating the failure method you are prompting HyperSizer to return a margin of safety for that method during analysis.

We will start by turning off all composite failure theories except for Max Strain.

8a. In the Failure Analysis Categories section of the failure tab, select "Material Strength, Composite Ply"

If nothing appears in the Available Failure Analysis window, click on the text "PRSEUS" to activate all analysis objects.

8b. Turn off all of the composite analyses for every object using the "Toggle" button and then turn on max strain 1, 2 and 12 for every object.

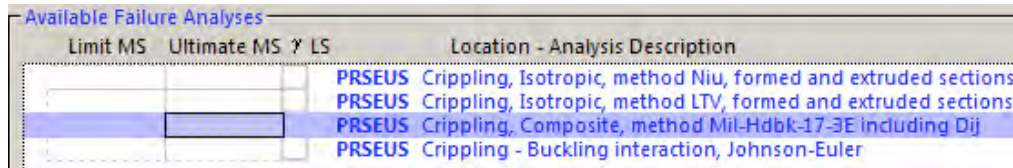


Make sure that you have the three max strain analyses turned on for all analysis objects.

Tip: Press the "Hide Unselected" button to hide all failure analyses that are not active. This will make the following steps easier by not showing the failure methods that are inactive.

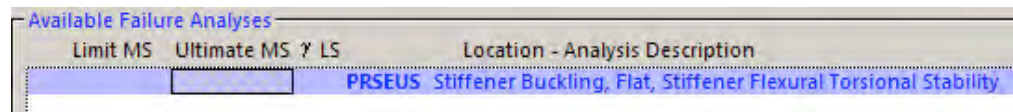
8c. Next click on "Crippling" under Failure Analysis Categories

8d. Turn off the isotropic crippling analyses and the "Johnson-Euler Buckling Interaction" margin of safety so that Crippling-Composite is the only active Crippling failure analysis.



8e. Now isolate the stiffener buckling failure analysis by clicking on "Buckling, Stiffener" under Failure Analysis Categories

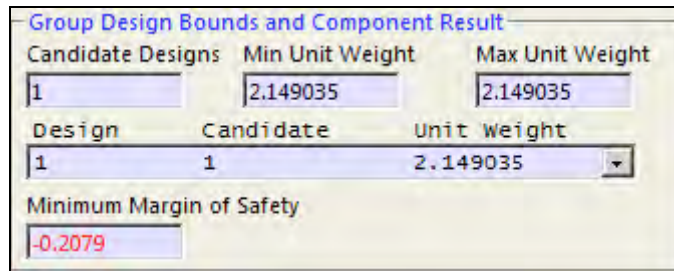
8f. Then turn on the "Stiffener Buckling, Flat, Stiffener Flexural Torsional Stability failure mode.



If no failure analyses are displayed, deselect the 'Hide Unselected' option.

D.7 Review the Analysis Results

9a. Press the "Analyze" button to analyze the PRSEUS panel.



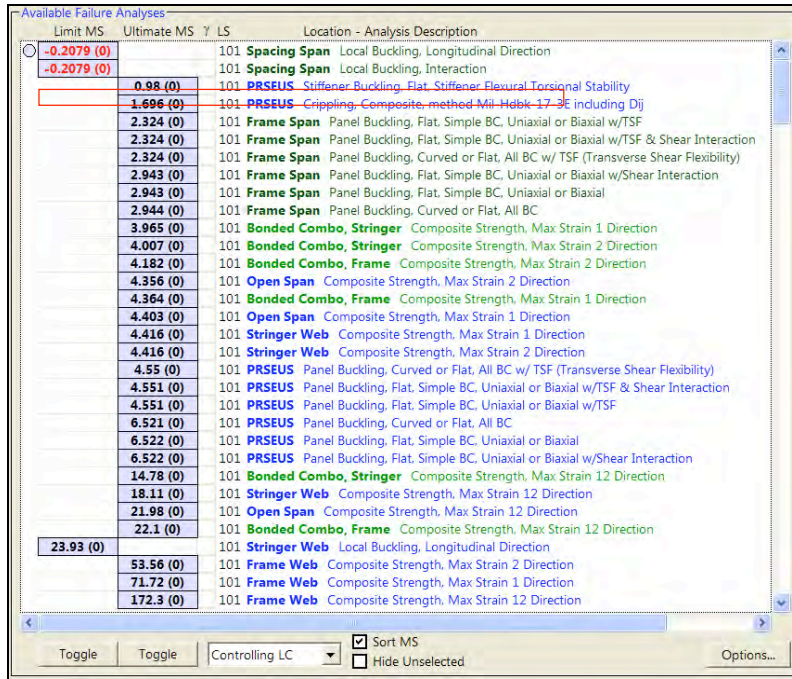
HyperSizer will return a minimum margin of safety of -0.2079, which is displayed in red on the Component results section of the sizing form.

This margin of safety indicates first failure at $(100 \text{ kips}) * [1 + (-0.2079)] = 79 \text{ kips}$. Although this shows up as a "failure", we will see that this is not actually a catastrophic failure, but rather it is local buckling of the "Spacing Span". Recall the spacing span includes both the facesheet and stiffener flanges.

With the PRSEUS concept, we expect the panel to exhibit substantial post-buckling strength. We will review HyperSizer's post buckling capability in the following pages.

9b. On the Failure tab, make sure that all of the margins of safety are visible by clicking all of the categories under Failure analysis categories.

9c. Next press the "Sort" margins checkbox to show the minimum margins of safety at the top of the window.



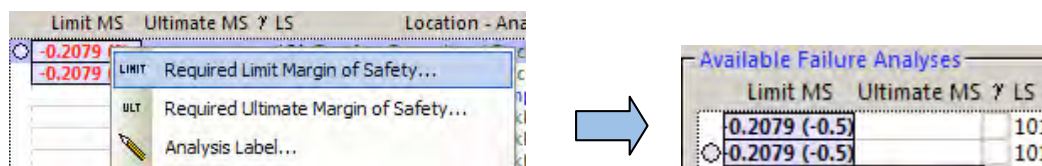
Since we know for PRSEUS that local buckling of the spacing span should not be considered a "catastrophic failure" we can enter a "required" margin for this failure mode so that HyperSizer will not consider it to be failure.

We will enter a required margin of -0.5. By entering this value, we are saying that local buckling of the spacing span is allowable up to 50% of the user entered limit load (if using an ultimate factor of 1.5, then local buckling would be allowed up to 33% ultimate load).

In this case, we are saying that local buckling is allowed for any load above 50 kips.

9d. Right click on the -0.2079 margin and select "Required Limit Margin of Safety".

9e. Enter a required margin of -0.5. Repeat this for both the Longitudinal and the Interaction failure modes.



Notice the margins of safety immediately turn blue indicating that this is no longer considered a failure. **If you do not specify a required margin, HyperSizer will consider any facesheet buckling margin below 0 to be a catastrophic failure and as described in the next section, no post-buckling analysis will be performed.**

To determine the final failure prediction(s), look at the other margins of safety returned on the Failure tab. Behind the two local buckling margins, the next lowest margin is the stiffener Flexural-Torsional stability margin of 0.98. This margin indicates torsional buckling or "rolling" of the stiffener. This failure mode is predicted at a load of:

$$\text{FT Buckling Load} = (100 \text{ kips}) * (0.98 + 1) = 198 \text{ kips}$$

HyperSizer Flexural-Torsional Stability is a new failure mode in HyperSizer and is described in detail in the HyperSizer Methods and Equations document: "AID 016 Stiffener Flexural-Torsional Stability.HME"

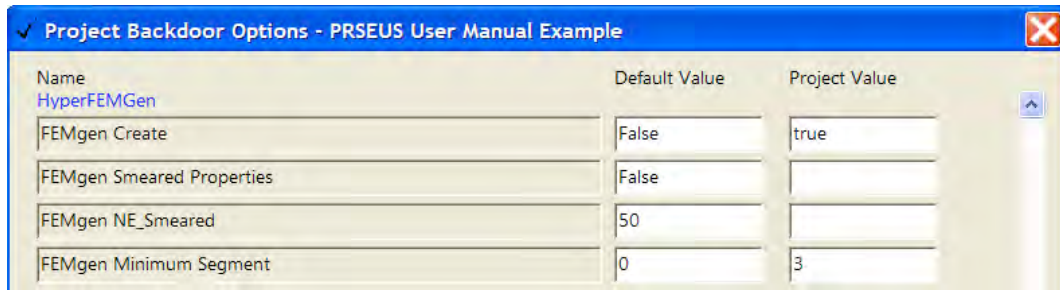
Additional Failure mechanisms are predicted at the following failure loads:

Failure Mode	Margin	Panel Load (kips)	Strain ($\times 10^6$ in/in)
Flexural Torsional Buckling	0.98	198	3291
Crippling	1.696	270	4480
Frame Span Buckling with TSF	2.324	332	5520
Frame Span Buckling w/o TSF	2.943	394	6550
Material Strength (Max Strain)	3.97	497	8250
Panel Buckling (full 80x42 panel) with TSF	4.551	555	9210

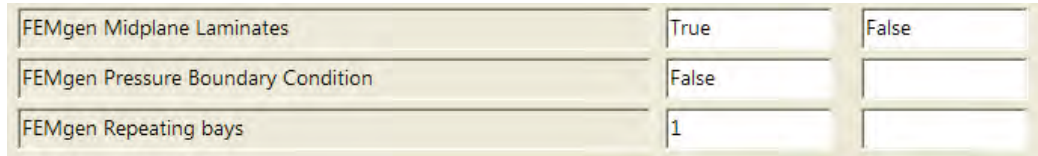
D.8 Generate a Local FEM using HyperFEMGen

Local FEMs with discretely meshed stiffeners and frames are used to verify HyperSizer's smeared load determination and local buckling results. By using HyperFEMgen these models are easily created with the correct boundary conditions and enforced displacements. For these verification models each panel object is represented with a PCOMP property where the layups are discretely defined so HyperSizer's smeared approach may be verified with FEA.

- 10a. To create the local model open the Backdoor Data file for this workspace.
- 10b. Set the FEMgen Create option to 'True'
- 10c. Also set the FEMgen Minimum Segment option to '3'



- 10d. To ensure the proper load eccentricity is captured from the property offsets, set the FEMgen Midplane Laminates to 'False'.



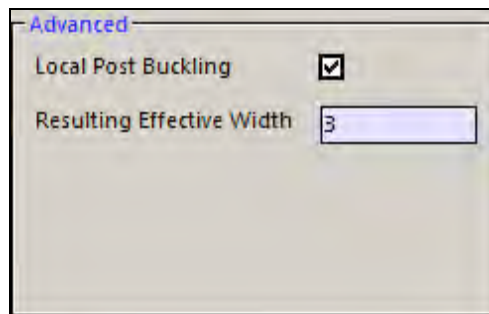
For a more detailed description of the HyperFEMgen options, ref: '0451_+HyperSizer-Training-HyperFEMGen_Discrete-Panel_FEM_Generation_2009-03-17.ppt'

D.9 Post Buckling Behavior

Note that the margins of safety that have been presented so far assume that the panel has a linear-elastic response to the loading, from the onset of local buckling up through the additional failure modes.

In reality, when local buckling in the spacing span occurs, a portion of the buckled spacing span becomes non-effective and will carry no additional load. HyperSizer can calculate this reduction in effective area with its local post-buckling capability.

- 11a. To activate this capability, go to the Buckling tab and select "Local Post Buckling" then re-analyze the component.



Notice the '*Resulting Effective Width*' that is returned as a result of the local post buckling analysis is displayed in this frame.

A look back at the failure tab reveals an increase in post-buckling load capability:

Limit MS	Ultimate MS	LS	Location - Analysis Description
0.2079 (-0.5)	LPB ON	101	Spacing Span Local Buckling, Longitudinal Direction
0.2079 (-0.5)		101	Spacing Span Local Buckling, Interaction
1.224 (0)		101	PRSEUS Stiffener Buckling, Flat, Stiffener Flexural Torsional Stability
1.874 (0)		101	PRSEUS Crippling, Composite, method Mil-Hdbk-17-3E including Dij
2.13 (0)		101	Frame Span Panel Buckling, Flat, Simple BC, Uniaxial or Biaxial w/TSF
2.13 (0)		101	Frame Span Panel Buckling, Flat, Simple BC, Uniaxial or Biaxial w/TSF & Shear Interaction
2.131 (0)		101	Frame Span Panel Buckling, Curved or Flat, All BC w/ TSF (Transverse Shear Flexibility)
2.634 (0)		101	Frame Span Panel Buckling, Flat, Simple BC, Uniaxial or Biaxial w/Shear Interaction
2.634 (0)		101	Frame Span Panel Buckling, Flat, Simple BC, Uniaxial or Biaxial
2.635 (0)		101	Frame Span Panel Buckling, Curved or Flat, All BC
3.6 (0)		101	Bonded Combo, Stringer Composite Strength, Max Strain 1 Direction
3.624 (0)		101	Bonded Combo, Stringer Composite Strength, Max Strain 2 Direction
3.705 (0)		101	Bonded Combo, Frame Composite Strength, Max Strain 2 Direction
3.806 (0)		101	Bonded Combo, Frame Composite Strength, Max Strain 1 Direction
3.822 (0)		101	Open Span Composite Strength, Max Strain 2 Direction
3.848 (0)		101	Open Span Composite Strength, Max Strain 1 Direction
3.85 (0)		101	Stringer Web Composite Strength, Max Strain 1 Direction
3.85 (0)		101	Stringer Web Composite Strength, Max Strain 2 Direction
4.487 (0)		101	PRSEUS Panel Buckling, Curved or Flat, All BC w/ TSF (Transverse Shear Flexibility)
4.487 (0)		101	PRSEUS Panel Buckling, Flat, Simple BC, Uniaxial or Biaxial w/TSF & Shear Interaction
4.487 (0)		101	PRSEUS Panel Buckling, Flat, Simple BC, Uniaxial or Biaxial w/TSF
6.318 (0)		101	PRSEUS Panel Buckling, Curved or Flat, All BC
6.32 (0)		101	PRSEUS Panel Buckling, Flat, Simple BC, Uniaxial or Biaxial
6.32 (0)		101	PRSEUS Panel Buckling, Flat, Simple BC, Uniaxial or Biaxial w/Shear Interaction
13.59 (0)		101	Bonded Combo, Stringer Composite Strength, Max Strain 12 Direction
15.85 (0)		101	Stringer Web Composite Strength, Max Strain 12 Direction
19.03 (0)		101	Open Span Composite Strength, Max Strain 12 Direction
19.43 (0)		101	Bonded Combo, Frame Composite Strength, Max Strain 12 Direction
23.93 (0)		101	Stringer Web Local Buckling, Longitudinal Direction
42.89 (0)		101	Frame Web Composite Strength, Max Strain 2 Direction
57.47 (0)		101	Frame Web Composite Strength, Max Strain 1 Direction
138.2 (0)		101	Frame Web Composite Strength, Max Strain 12 Direction

The critical failure mode is still Flexural-Torsional stability, but the margin of safety has increased to 1.22 for a total post-buckled load prediction of 222 kips.

REPORT DOCUMENTATION PAGE

*Form Approved
OMB No. 0704-0188*

The public reporting burden for this collection of information is estimated to average 1 hour per response, including the time for reviewing instructions, searching existing data sources, gathering and maintaining the data needed, and completing and reviewing the collection of information. Send comments regarding this burden estimate or any other aspect of this collection of information, including suggestions for reducing this burden, to Department of Defense, Washington Headquarters Services, Directorate for Information Operations and Reports (0704-0188), 1215 Jefferson Davis Highway, Suite 1204, Arlington, VA 22202-4302. Respondents should be aware that notwithstanding any other provision of law, no person shall be subject to any penalty for failing to comply with a collection of information if it does not display a currently valid OMB control number.
PLEASE DO NOT RETURN YOUR FORM TO THE ABOVE ADDRESS.

1. REPORT DATE (DD-MM-YYYY) 01-01 - 2011			2. REPORT TYPE Contractor Report		3. DATES COVERED (From - To) Oct. 2008 - Sept. 2010	
4. TITLE AND SUBTITLE Damage Arresting Composites for Shaped Vehicles - Phase II Final Report				5a. CONTRACT NUMBER NNL07AA48C		
				5b. GRANT NUMBER		
				5c. PROGRAM ELEMENT NUMBER		
6. AUTHOR(S) Velicki, Alex; Yovanof, Nicolette, P; Baraja, Jaime; Linton, Kim; Li, Victor, P; Hawley, Arthur, V; Thrash, Patrick, J; DeCoux, Steve; Pickell, Robert				5d. PROJECT NUMBER 4200208122		
				5e. TASK NUMBER		
				5f. WORK UNIT NUMBER 699959.02.08.07.02.02		
7. PERFORMING ORGANIZATION NAME(S) AND ADDRESS(ES) NASA Langley Research Center Hampton, VA 23681-2199				8. PERFORMING ORGANIZATION REPORT NUMBER		
9. SPONSORING/MONITORING AGENCY NAME(S) AND ADDRESS(ES) National Aeronautics and Space Administration Washington, DC 20546-0001				10. SPONSOR/MONITOR'S ACRONYM(S) NASA		
				11. SPONSOR/MONITOR'S REPORT NUMBER(S) NASA/CR-2011-216880		
12. DISTRIBUTION/AVAILABILITY STATEMENT Unclassified - Unlimited Subject Category 39 Availability: NASA CASI (443) 757-5802						
13. SUPPLEMENTARY NOTES Langley Technical Monitor: Dawn C. Jegley						
14. ABSTRACT This report describes the development of a novel structural concept, Pultruded Rod Stitched Efficient Unitized Structure (PRSEUS), that addresses the demanding fuselage loading requirements for the Hybrid Wing or Blended Wing Body (BWB) airplane configuration. In addition to the analytical studies, a three specimen test program was also completed to assess the concept under axial tension loading, axial compression loading, and internal pressure loading.						
15. SUBJECT TERMS Composites; Pultruded rod; Stitched composites; Unitized structure; VARTM; CAPRI; Resin infusion; BWB structure; Rod-stiffened; Warp-knit fabric; Self-supporting perform; Stiffened panel; Integrated structure						
16. SECURITY CLASSIFICATION OF:			17. LIMITATION OF ABSTRACT	18. NUMBER OF PAGES	19a. NAME OF RESPONSIBLE PERSON	
a. REPORT	b. ABSTRACT	c. THIS PAGE			STI Help Desk (email: help@sti.nasa.gov)	
U	U	U	UU	211	19b. TELEPHONE NUMBER (Include area code) (443) 757-5802	